POSITRON INTERACTIONS IN CONDENSED MATTER

M. MOUSSAVI-MADANI

B.Sc. (Tehran), M.Sc. (London)

A thesis submitted

for the Degree of DOCTOR OF PHILOSOPHY

in the University of London.

Department of Physics

Royal Holloway & Bedford New College

London 1986

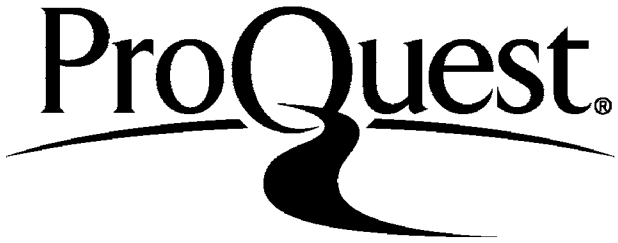

DEDICATED TO MY WIFE AND MY DAUGHTER, THEIR PATIENCE AND SUPPORT PLAYED AN IMPORTANT ROLE IN THE COMPLETION OF THIS WORK.

ACKNOWLEDGEMENTS

My special thanks are due to Dr. P. Rice-Evans whose inspiration and guidance at all stages of this research have been invaluable.

My thanks are also due to Dr. P. Fozooni and Messrs S. Creamer, D. Britton , K.U. Rao and N. Navazash for their helpfulness, willing cooperation and valuable discussions. I also wish to acknowledge the interest of Professor E.R. Dobbs in this work.

Dr. P. Pal and the staff of the computer center, Messrs P. Taylor, M. Datke, L. Nodes and Miss S. Marshall gave me advice in computing which was of great value to me. Also, Mr. R. Gol'Jawaheri kindly assisted in proof-reading this thesis.

Finally, I should like to thank my father, Abolfazl, and my wife, Fariba, whose moral and finacial support made the completion of this work possible.

ABSTRACT

Positron annihilation has been studied in a number of solids, and at some condensed monolayer surfaces. The bulk specimens, which included cadmium, tin, selenium, and graphite, yielded information on lattice defects and phase transitions. Two dimensional layers of condensed gases, including argon, nitrogen, oxygen and helium result in positronium formation suggesting the existence of positron surface traps.

The Doppler broadening method has been applied to these studies. The 511-Kev Gamma-rays resulting from the annihilation of positrons with electrons was detected by a Germanium detector with high resolution. The cadmium and tin specimens were plastically deformed at 77K and measurements with increasing temperature provided information on phase transitions, annealing processes and on the nature of the defects concerned.

The application of the positron trapping model provides values of the vacancy formation energy (enthalpy) and of the concentration of monovacancies and divacancies. The energy spectra were analysed, with Gaussian and Parabolic components convoluted with instrumental resolution function, to indicate the proportion of annihilation of positrons with core and conduction electrons.

An important result of the work on tin was the observation of the phase transition of white-tin to gray-tin at 240K.

Positron trapping at graphite surfaces, and the formation of positronium has been observed by introducing a parameter R, related to the positronium fraction in this work. The growth of monolayers of gases condensed on graphite has been observed in the changing of the

total area of the annihilation line shape spectrum, and also in the changing positronium fraction parameter. Estimated values of adsorption energies are discussed.

TABLE OF CONTENTS

ABSTRACT 1

TABLE OF CONTENTS 3

Chapter I Introduction to positron annihilation

1.1-General Introduction: 8

1.2-Positron sources 10

1.3-Positron thermalization 11

1.4-Positron annihilation 12

1.5-Positron wavefunction and annihilation rate 14

1.6-The experimental technique 15

1.6.1-Lifetime measurement 16

1.6.2-Angular correlation measurement 19

1.6.3-Doppler broadening measurement 24

Chapter II Defects study in metal by positron annihilation

2.1-Introduction 27

2.2-Characteristics of defects 27

2.2.1-Point defect 28

2.2.2-Line defect 28

2.2.3-Grain bounries 29

2.3-Equilibrium and non-equilibrium measurements. 29

2.4-Annihilation of positron with free and core electrons 30

2.5-Thermal effect 32

2.6-Trapping model and trapping rate 36

2.7-Self-trapping 39

2.8-Phase transitions 42

2.8.1-Definition 42

2.8.2-Phase transition in tin 42

Chapter III Positron annihilation at surfaces

3.1-Introduction 45

3.2-Positron beam study 46

3.3-Determination of the positronium fractions 50

3.4-Physical adsorption 52

3.4.1-Introduction 52

3.4.2-Van der waals force 53

3.4.3-Thermodynamics of physisorption 54

3.4.4-Langmuir monolayers 56

3.4.5-Boltzmann approximation 57

3.4.6-Gas adsorption on graphite 57

Chapter IV Instrumental details of experimental equipment.

4.1-Introduction 60

4.2-Electronical instruments 62

4.2.1-(ADC) and (MCA) 62

4.2.2-380Z micro-computer 62

4.2.3-Master temperature controller (MTC) 63

4.2.4-Digital temperature controller (DTC) 64

4.2.5-Stabilization of electronics system 64

4.3-Low temperature measurement (Cryostat) 66

4.4-High temperature measurement (Furnace) 70

Chapter V Data analysis

5.1-Introduction 72

5.2-F and W parameters 72

5.3-Background problem 75

5.4-Temperature dependence on line shape parameters 78

5.5-Line shape analysis 80

5.6-Positronium fraction parameter (R-parameter) 84

5.7-Zero-point motion 87

Chapter VI Positron annihilation in polycrystalline Cadmium

6.1-Introduction and method 90

6.2-Line-shape parameter 92

6.3-Line-shape parameter analysis 96

6.4-Line-shape analysis 101

6.5-Zero-point motion 110

6.6-Conclusion 110

Chapter VII Positron annihilation in annealed and deformed polycrystalline Tin

7.1-Introduction and method 117

7.2-Line shape parameter 118

7.3-Line-shape parameter analysis 120

7.4-Line-shape analysis 123

7.5-Conclusion 126

7.6-Positron annihilation in deformed tin

7.6.1-Introduction and method 127

7.6.2-Line-shape parameters 133

7.6.3-Line-shape analysis 136

7.6.4-Zero-point motion 137

7.6.5-Conclusion 141

Chapter VIII Positron annihilation in selenium

8.1-Introduction and method 144

8.2-Line shape parameters 148

8.3-Line shape analysis 151

8.4-Search for positronium 153

8.5-Conclusion 153

Chapter IX Positron annihilation in Grafoil

9.1-Introduction and method 155

9.2-Line shape parameters 160

9.3-Line shape analysis 164

9.4-Positronium fractions 166

9.5-Theoretical expression for R-parameter 167

9.6-Geometric orientation of the sample 169

9.7-Conclusion 171

Chapter X Positron annihilation with argon condensed on grafoil

10.1-Introduction and method 173

10.2-Line shape parameter 176

10.3- Positronium fraction (R-parameter) 178

10.4-Theoretical fitting on R-parameter 180

10.5-Line-shape analysis 182

10.6-Conclusion 184

Chapter XI Positron annihilation in the nitrogen condensed on surfaces of grafoil

11.1-Introduction and method 187

11.2-Line shape parameter 190

11.3-Positronium fraction parameter (R-parameter) 193

11.4-The dependence of coverage on Pressure 195

11.5-R-parameter fitting 197

11.6-Line-shape analysis 199

11.7-Conclusion 202

Chapter XII Positron annihilation in oxygen condensed on surfaces of grafoil

12.1-Introduction and method 205

12.2-Line shape parameter 207

12.3-Line-shape analysis 210

12.4-Fitting the F-parameter 217

12.5 Positron annihilation for helium on the grafoil surface

12.5.1-Introduction and method 220

12.5.2-Line shape parameter results 221

12.5.3-R-parameter 223

12.5.4-Line-shape analysis 226

12.6-Conclusion 226

APPENDICES 231

REFERENCES 239

Chapter I- Introduction to positron electron annihilation

1.1-General introduction:

The positron is an antiparticle, which was first predicted, theoretically by Dirac (1930). It was observed later experimentally by Anderson (1933) in cloud chamber photographs of cosmic radiation at Pasadena, California, and by Occhini and Blackett who were working on the construction of the counter-controlled cloud chamber in England. In fact the positron is an antielectron with the same rest mass, magnetic moment, and spin, but with opposite electric charge $e^{+}=-e^{-}$, and stability in vacuum. Positrons can be produced by the beta-decay mode of the isotope of an element, and also by interaction of Gamma-rays with the surrounding field of atomic nucleus of matter (pair production). The conservation of energy and momentum are violated in free space for pair production.

The first observation of annihilation of positrons with electrons "resulting two Gamma-rays in opposite directions" was found in angular correlation measurements by Beringer and Montgomery (1942). After that many experimental works have shown that positrons are not stable in matter, and they annihilate in less than a few nano-seconds, this is the lifetime of the positron. Recently experimental works on positron annihilation with electrons in matter have shown that this technique can be a good tool for the investigation of its electronic structure and concentration of defects and their temperature dependences (Siegel 1980). When the positron enters condensed matter, its energy is reduced to thermal energy (few ev) in a time of less than a nano-second, by ionization of the medium and then annihilates with core electrons or conduction electrons (free electrons). In an insulator positrons can capture an electron to form

positronium atoms (Hydrogen like), and then annihilate in different modes. Another process which is observed is trapping of positron at a vacancy in metals. The lifetime of positrons increased when they are trapped in vacancies. Recently scattering of positron beams with surfaces of metals has provided some information about electronic structure of the surface of metals. The annihilation of a positron with electrons is summarized in Fig(1.1.1)

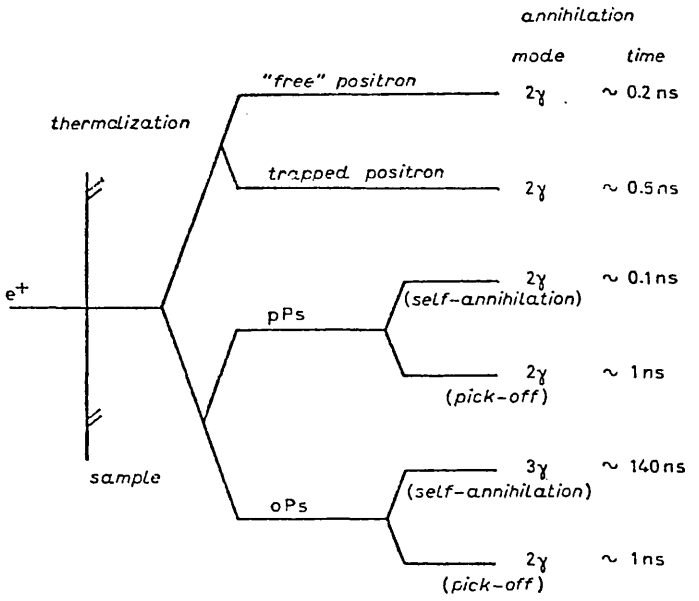

Fig(1.1.1) Positron in solids annihilate from different states with experimentally discernible annihilation characteristics.

The positronium state may decay by 3γ or 2γ emission from ortho-positronium or para-positronium respectively, but sometimes o-Ps atoms pick-off another electron and annihilate to two γ's in the shorter lifetime. This is because there is an overlap between the o-Ps wavefunction and spin-averaged electron wavefunction of the medium which gives rise to electron pick-off where the positron, bounded with an electron in an o-state, annihilates from a p-Ps with an electron of medium (Brandt positron solid state physics 1983).

Positron annihilation with matter can be categorised as:

a)positron annihilation in a metal gives information about the electronic structure of the metal, lattice defect concentrations and

enthalpy.

b)Positron annihilation at a surface gives information on electronic structure of the surface and adsorbed gases.

c)Measurement in annealed metals gives information about the momentum distribution of the electrons in metals and also the Fermi energy of the electrons.

d)Finally, positron annihilation is a technique to investigate phase-transitions in metals and alloys, such as the melting point, recrystallization, crystal transitions etc.(Doyama, 1979)

1.2-Positrons sources:

Positrons are emitted by the process of β-decay from a number of nuclei such as ^{19}Ne, ^{22}Na, ^{44}Ti, ^{58}Co, ^{64}Cu, and ^{68}Ge. The most useful source is ^{22}Na, for many experimental methods it is easier to obtain as well as being cheaper than the others. On the other hand, it has a long half life (2.58 y). It is used normally for lifetime measurement experiments because emission of the positron and the high energy gamma-rays occur simultaneously. This source is usually available as $^{22}NaCl$ solution. It vapourise at slightly above 600K, therefore it is not a good source for investigating vacancy formation for metals with high melting points such as Copper, Carbon, etc. The other useful source for positron annihilation measurements is ^{64}Cu which has a short lifetime but a high melting point. It is usually used for Doppler broadening and angular correlation measurements. ^{68}Ge and ^{58}Co are also used in measurement of positron annihilation studies. This is because ^{68}Ge has a relatively long lifetime and it gives rise to a very small background. All the positron sources and their properties have been arranged in table(1.2.1).

ISOTOPES	HALF-LIFETIME	MAXIMUM ENERGY OF POSITRON(Kev)	INTENSITY OF COINCIDENT γ-RAYS
^{19}Ne	17.48 S	2220	100%
^{22}Na	2.58 Y	545	90%
^{44}Ti	47.0 Y	1470	94%
^{58}CO	71.3 days	480	15%
^{64}Cu	12.9 h	650	0%
^{68}Ge	275.0 days	1880	1.5%

Table(1.2.1)

The disadvantage of ^{68}Ge source is its sample preparation, because it is rather difficult. The sample preparation for Doppler broadening measurement usually is direct evaporation of the source solution on the centre of specimen, and sandwiches together by wrapping aluminium or copper foils.

1.3- Positron thermalization:

When a positron enters condensed matter, it rapidly loses its energy in a time short compared to its lifetime by inelastic interaction with ions or electrons of the medium, and the positron becomes thermalised. The probability of thermalization of positron is given as:

$$P(x)=A \exp(-\alpha_{+}dx) \qquad (1.3.1)$$

where P(x) is probability of positron thermalizing between distance x and x+dx and α_{+}^{-1} is the reciprocal of the mean free path of the positron after thermalization, and is proportional to maximum energy of positron and the density of the metal. The mean free path (R) can be obtained from:

$$R=0.407XE_{max}^{n}/d \qquad (1.3.2)$$

where d is density and n=1.38 for $0.15<E_{max}<0.8$ Mev. Estimations of the mean free path for certain metals, including the range of samples studied in this work, are shown in table (1.3.4).

Metals	Zn	Cd	Graphite	Se	C	Sn	Pb
Maximum Range(μm)	248	203	1872	367	766	306	156

Table(1.3.3)

1.4-Positron annihilation:

Thermalized positrons interact with electrons and ions in the medium; this is in agreement with the laws of quantum electrodynamics (Berestetskii et al 1971). As a result of this, a positron-electron pair can be radiated in the form of electromagnetic energy. The amount of energy released in this process can be calculated from the conservation of energy;

$$E=2Xm_e c^2+E_k+E_b \qquad (1.4.1)$$

where E_k is total kinetic energy of positron-electron pair , and E_b is binding energy. All the positrons having survive the slowing down process, before being annihilated by electrons of the medium, their kinetic energy reduces to the order of a few electronvolts and this is much smaller than the total rest mass energy of the electron-positron pairs. If the bound state exists the binding energy is so small that the total energy $E=2m_o c^2$ is the energy of annihilation. The binding energy of the pairs is 6.8eV in free space and may be even smaller in matter (Ore and Powell 1949, Wallce 1960). From the total momentum and energy conservation at least two photons should be emitted by this process (Yong 1950). Annihilation to a single photon is possible only in presence of third body such as an electron or a nucleus which can adsorb the recoil momentum. If positron-electron pair is not free it can in certain cases bind together (known as positronium forms), which

are found in non-metallic elements and at the surface of materials. The decay mode of this process also obeys the electromagnetic laws, thus the energy, momentum, charge parity and spin charge must be conserved. If the initial state of annihilating pairs is well defined, so the effect of conservation laws on decay mode are easily demonstrated (Muirhead et al 1965). If the positronium is formed in the ground state (i.e. the total angular momentum L=0), then, the Ps atom depends on spin orientation. Therefore the Ps atom can either be in the singlet state ($^1S_0$) or triplet state ($^3S_1$) with total spin zero or one respectively. The charge parity must be conserved in positron electron interactions with final state. The total charge parity of system, given by Berestetskii et al (1961), is $P_c = P_i P_l P_s$, where P_i is intrinsic parity, and it is equal to "-1" for particle and "1" for antiparticle system. P_l is orbital parity and it is given by $P_l = (-1)^l$ and P_s is spin parity equals $P_s = (-1)^{s+1}$. Therefore the charge parity of the left side is;

$$P = (-1)(-1)^l (-1)^{s+1} = (-1)^{s+l} \qquad (1.4.1)$$

On the other hand the charge parity of a photon is negative, then:

$$P = (-1)^{s+l} = (-1)^n \qquad (1.4.2)$$

where n is number of the photon emission.

Therefore for the singlet state L+S=J=even it means n should be even. For J=0 two photons emission is usually observed. For L+S=J odd the n should be odd, hence one or three photon emission is possible, but about 90% three photon emission is observed. The case of singlet electron positron pairs is known as parapositronium (pPs) and triplet as orthopositronum (oPs). Statistically one-quarter of Ps decay to two γ-rays and three-quarter to three γ-rays. But Kerr 1974 showed that the annihilation of positrons in positronium formed in polymers was one-third pPs. That may be due to pick-off by

another electron and annihilation in a time shorter than oPs itself (in free space is 140 ns). Another posibility is that the spin exchange process may occur. It means that the triplet state ($^3S_1$) quenching to a singlet state ($^1S_0$), as is observed in oxygen monolayers on aluminum in room temperature (Lynn and Lutz 1980). It was also observed in adsorbtion of oxygen on grafoil at low temperature in this work.

1.5-Positron wave function and annihilation rate:

In 1950 (De Benedetti et al) suggested that the positron wavefunction was represented by single plane wave, identical to that of the one-electron wavefunction, $\Psi_+(r)$=constant, since k=0 at ground state. On the other hand, since Coulomb repulsion of the positron with nucleus is not included this does not accurately represent the wavefunction in the core region. Berko and Plaskett (1958) employed the Wigner-Seitz method, which approximates the cell by a sphere, to calculate the positron wavefunction in the core region for aluminium and copper, given by

$$\Psi_+(r)=R_+(r)/r \qquad (1.5.1)$$

where the $R_+(r)$ satisfied the schroedinger equation

$$(d^2/dr^2+E+2V(r))R_+(r)=0 \qquad (1.5.2)$$

where V(r) was taken to be the potential of the positive ion, together with a uniform charge distribution potential due to valence electrons.

The cross-section of the electron-positron interaction has been calculated by Dirac. The result for two-photons emission is;

$$\sigma(2)=\pi r_0^2/(\gamma+1)\{(\gamma^2+4\gamma+1)/(\gamma^2-1).\mathrm{Ln}[\gamma+(\gamma^2-1)^{1/2}]-(\gamma+3)/(\gamma^2-1)^{1/2}\} \qquad (1.5.3)$$

where $r_0=e^2/m_0c^2$ is classical radius and $\gamma=(1-v^2/c^2)^{-1/2}$. For v<<c and using $\gamma^2-1=(v^2/c^2)\gamma^2$ so the expression simplifies to:

$$\sigma(2)=2\pi r_0^2 c/v \qquad (1.5.4)$$

The annihilation rate is the number of positrons with velocity v annihilated by electrons and with density per unit volume n is given by

$$\Gamma_2 = \sigma(2)n.v \qquad (1.5.5)$$

The result of equation (1.5.2) gives the ground state wavefunction of positron and electron pairs (positronium) by

$$\Psi(r)=(\pi a^3)^{-1/2}\exp(-r/a) \qquad (1.5.6)$$

where $a=2\hbar^2/m_o e^2$ is the Bohr radius of positronium atom and r is relative coordinate. The electron density at positron is $n=|\Psi(0)|^2$ then substitute (1.5.4) to (1.5.5), so the decay rate of positronium is given as;

$$\Gamma_2=4r_o^2 c/a^3 \qquad (1.5.7)$$

The positron lifetime is inverse of decay rate therefore $t_{para}=123$ psec that is the parapositronium lifetime. It can be seen that the cross-section of positron-electron interaction resulting in two photon decays is dependent on the velocity of positron but that the lifetime is independent of that. The expression for the spin average cross section for three-photon annihilation has been found by (Berestetskii et al 1971).

$$\sigma(3)=4(\pi^2-9)r_o^2 c\,\alpha/3v \qquad (1.5.8)$$

where α is the coupling constant. The lifetime of orthopositronium is found $t_{orth}=140$ nsec about 1110 times greater than t_{para}. The three-photon annihilation rate can be investigated by a triplet coincidence technique or from a study of the energy spectra of annihilation photons (De Blonde et al, 1972; Gainotti et al, 1964).

1.6-The experimental technique:

The result of positron-electron annihilation is, in fact, photospectroscopy of photon emission. Consequently any information from the distribution of photon energy gives direct information about

the electron and its annihilation with the positron. There are three useful techniques in positron electron spectroscopy; lifetime, angular correlation and Doppler broadening measurements.

1.6.1-Lifetime measurement:

At the time $\delta(t)$ after positron injection into metals, the positron will annihilate with an electron, almost always, yielding two photons. One and three photons are also possible but rare. The positron annihilation spectroscopy measurement techniques integrate over a large number of annihilation events. The distribution of the $\delta(t)$ values for a number of these events, measured in a lifetime experiment yields information on the total electron density $\overline{\rho}(r)$ in the region of annihilation. This is because the positron annihilation rate λ is the reciprocal of positron lifetime, and is given by overlap integral of the positron and electron densities (Siegel 1980).

$$\lambda = \pi r_o^2 c \iint \rho_-(r)\rho_+(r)dr \qquad (1.6.1.1)$$

where r_o is classical electron radius, c is the velocity of light and $\rho_-(r)$ is electron density, $\rho_+(r)$ is positron density in the metal. The positron source used in this technique is ^{22}Na because of its long half lifetime, and also 90% of the intensity of positron activation includes 1.28Mev high γ-ray energy at the same time. The source should be sandwiched between two identical samples being investigated. The thickness of sample must be thick enough to stop all positrons. The schematic arrangement of the apparatus used in lifetime measurement is illustrated in figure(1.6.1.a). As is shown in the figure(1.6.1.a) two plastic scintillation counters were used with photomultiplier tubes. The two outputs of the detectors, one from the 511 keV death of the positron and the other from the 1.28MeV birth of the positron were fed to timing discriminators, the 511 keV one after being passed

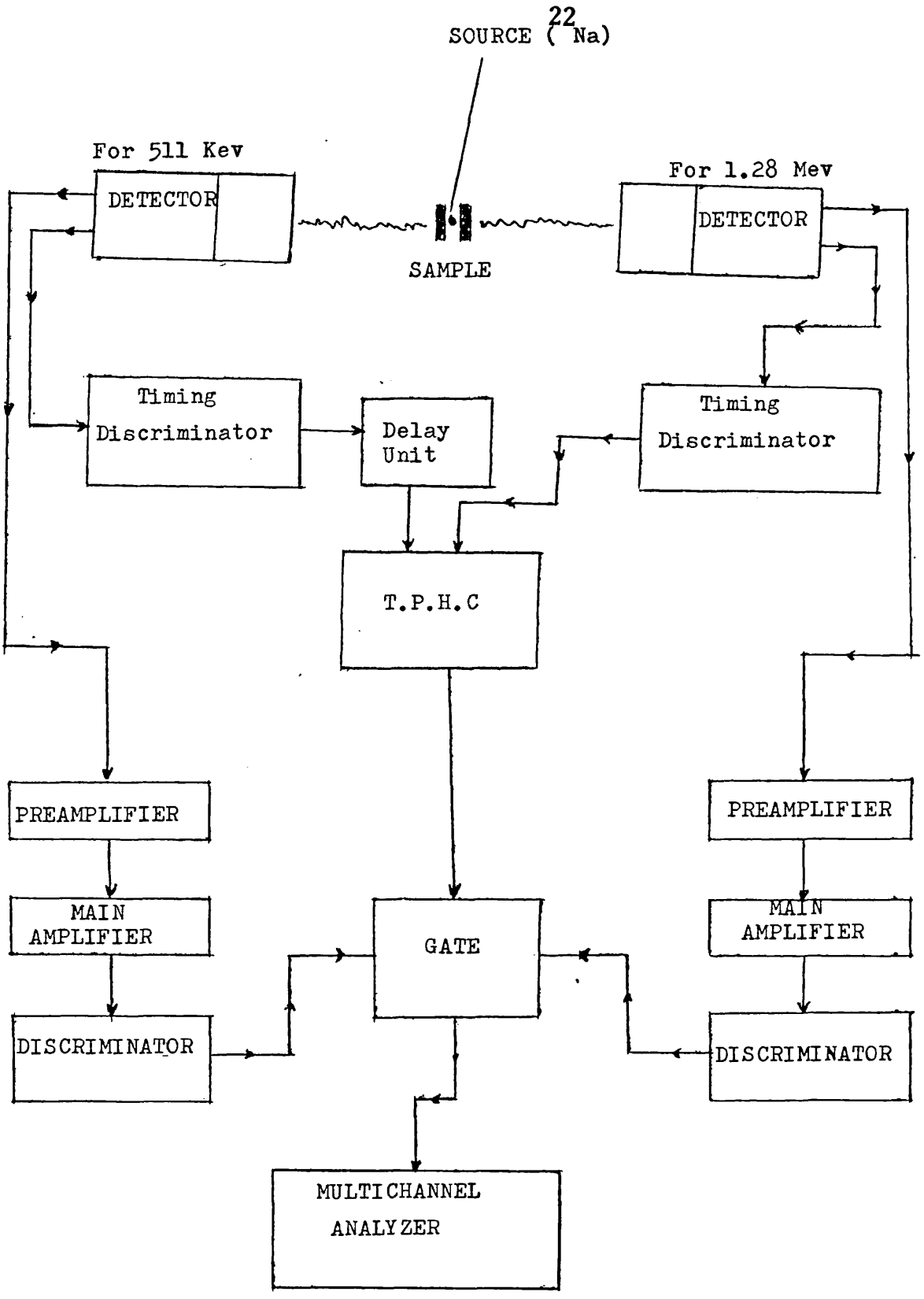

Fig(1.6.1.a) Schematic diagrams of typical Life-time measurement.

through the delay. Finally both outputs were fed to the time pulse height convertor (output pulse proportional to amplitude height). The delay time between the two γ-rays emission from annihilation and source is the lifetime of positron (τ). The fast channels are used to establish $\delta(t)$ as precisely as feasible, while the slow channels utilizing energy selection are used to drive linear gate to the multichannel analyser. This in principle, allows only correlated events to be stored in the collected lifetime spectrum. The slow outputs of detectors were fed to preamplifiers and, after being amplified, to discriminators, and to the gating unit passing the fast output from the T.P.H.C, and finally to the multichannel analyser to collect the spectrum. From the spectrum the lifetime of positron can be obtained, this lifetime for free positron annihilation lies between 100-250 psec and for the bulk or ionic annihilation between 100-400 psec but it is increased with respect to the free positron

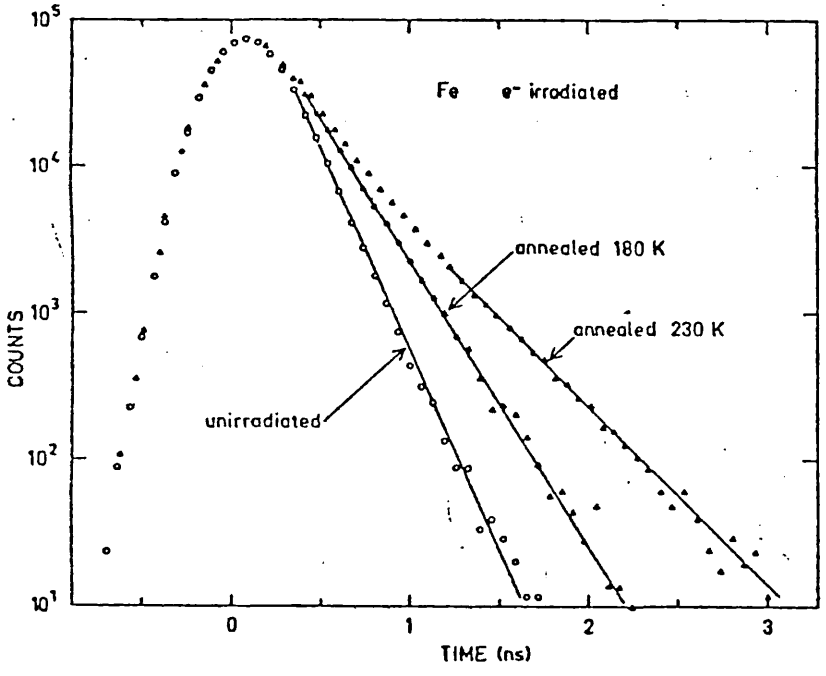

Fig(1.6.1.b) Positron lifetime spectra, after source-background subtractions in electron-irradiated high-purity α-Fe at the various stages.

lifetime when the positron is trapped by any defects (vacancies,

dislocations, etc.) in the metal (Siegel same paper 1980). Typical experimental lifetime spectra are shown in Fig(1.6.1.b) for well-annealed α-Fe and electron irradiation α-Fe. That shows the different spectra of irradiation α-Fe annealed at two different temperatures at 180K and 230K respectively (Hautojorvi, et al 1979). The spectrum should be fitted by;

$$N(t)=(1-I_2)\exp(-\Lambda_1 t)+I\exp(-\Lambda_2 t) \qquad (1.6.1.1)$$

convolution with the instrumental resolution function. Where $\lambda_t=\Lambda_2$ and $\lambda_b=[\lambda_t.I_2+\sum_j \sigma_j.C_j]/I_2$. C_j is the concentration of defects and σ_j is the positron annihilation rate. The results obtain the positron-electron lifetime and the intensities of free positron annihilation or trapping which are both temperature dependent. The intrinsic time resolution of lifetime system can be determined from the prompt curve of ^{58}Co (full width at half maximum of spectrum FWHM). Complete deconvolution analyses of the lifetime spectra can be carried out in order to find the positron lifetime, or lifetimes and relative intensities in cases in which distinguishable positron states occur. The large computer programs are necessary to analyse the lifetime data (Kirkegoard and Eldrup 1972, 1974).

1.6.2-Angular correlation measurement:

If both members of an annihilation electron-positron pair are at rest, the conservation of energy and linear momentum demands that in two-photon annihilation the two γ-rays are emitted with exactly the same energy, $E_\gamma=m_0c^2$, but in opposite directions with linear momentum $P_\gamma= m_0c$, where m_0 is rest mass of electron or positron. Since the annihilating pair has a nonvanishing linear momentum P, this symmetry is lost by a deviation angle from opposite direction, θ. Usually the angular correlation curve is $N(\theta)$ versus θ. Consider two photons from

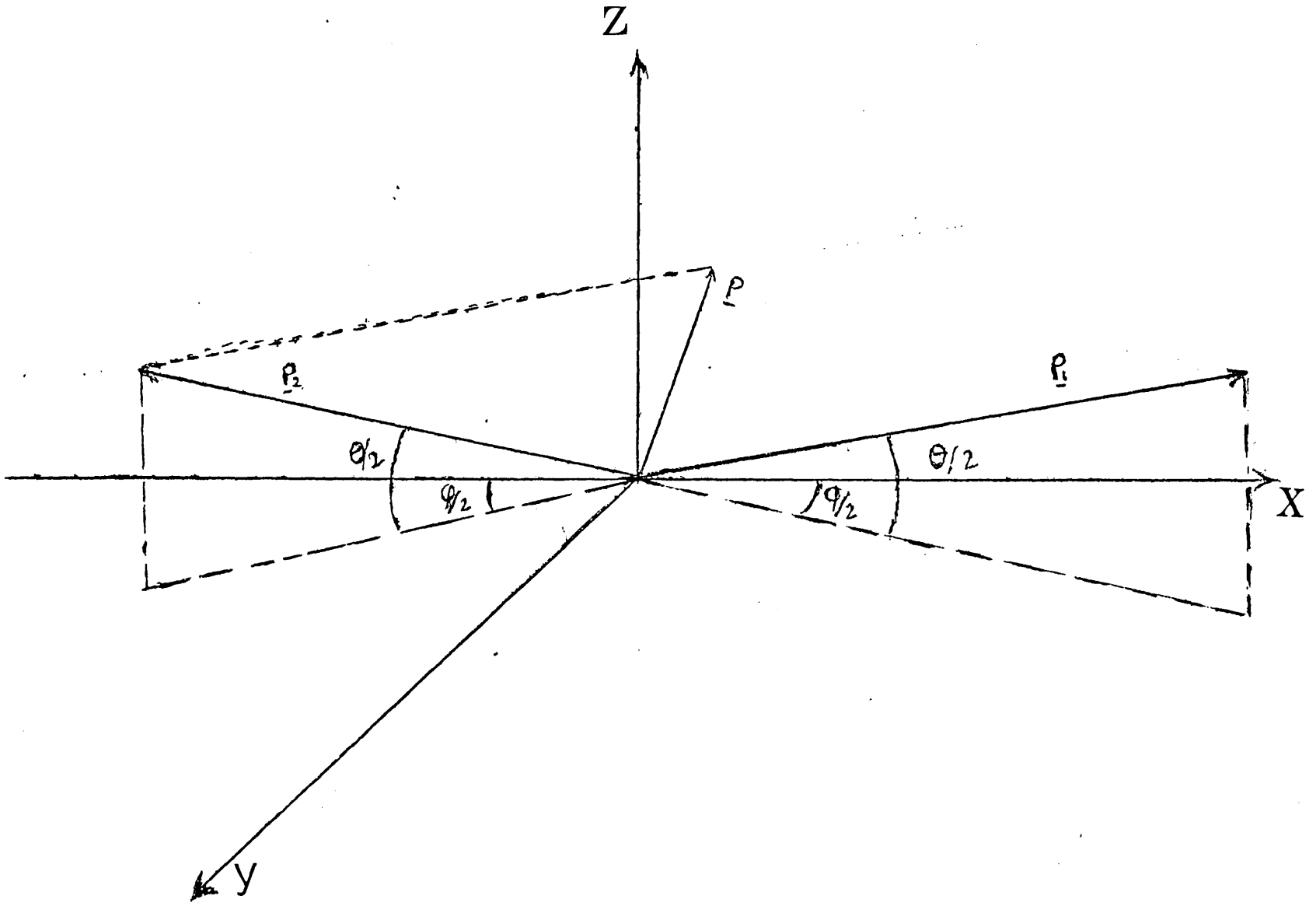

Fig(1.6.2a) The geometry of a two-photon angular correlation experiment for a typical positron-electron momentum P. Typically, angles θ and ϕ are a few milliradians.

the annihilation in opposite directions with angle θ/2 relative to the X-axis and with angle $\varphi/2$ relative Y-axis Fig(1.6.2.a). From conservation of momentum and energy it can be written

$$(|P_1| + |P_2|)c = 2m_o c^2 \qquad (1.6.2.1)$$

and conservation of momentum gives

$$P = (\underline{P}_1 + \underline{P}_2) \qquad (1.6.2.2)$$

where from fig(1.6.2.a) $P_y = |P_1|\sin(\theta/2) + |P_2|\sin(\theta/2)$ similarly for P_z, and P_x assuming that θ and φ very small so it can be written

$$P_z = 2m_o c\theta/2 \qquad (1.6.2.3)$$

$$P_y = 2m_o c\varphi/2 \qquad (1.6.2.4)$$

$$P_x = (|P_1| - |P_2|) \qquad (1.6.2.5)$$

If R(p) is the probabilty of positron electron annihliation "in the terms of independent-particle -model (IPM)" yields two γ-rays emission with total momentum P. Therefore the angular distribution of the gamma-ray emission is given by;

$$N(\theta_z) = \iint R(p)\,dp_x\,dp_y \qquad (1.6.2.6)$$

where $$R(p) = \pi r_o^2 c \sum_k n_k \iiint \left|\exp(-ip.r)\,\Psi_k(r)\,\Psi_+(r)\right|^2 dr^3 \qquad (1.6.2.7)$$

and $\Psi_+(r)$, $\Psi_k(r)$ are the positron and electron wavefunction respectively and n_k is Fermi function, k represents the electron wave vector and bound index. The angular correlation measurement is the distribution of momentum versus angle θ, and therefore gives information about linear momentum and velocity of the annihilating pair and also the Fermi energy. A typical schematic diagram of the apparatus for angular correlation experiment is illustrated in figure(1.6.2.b). In this experiment positron source usually are ^{64}Cu, ^{22}Na or ^{58}Co with greater activity (0.01-1Ci) sandwiched with the sample specimen. Two INa(Th) scintillation counters are used where one is fixed and the other moves with angle θ in the Z-axis direction. Both outputs from the counters were fed to the amplifiers and

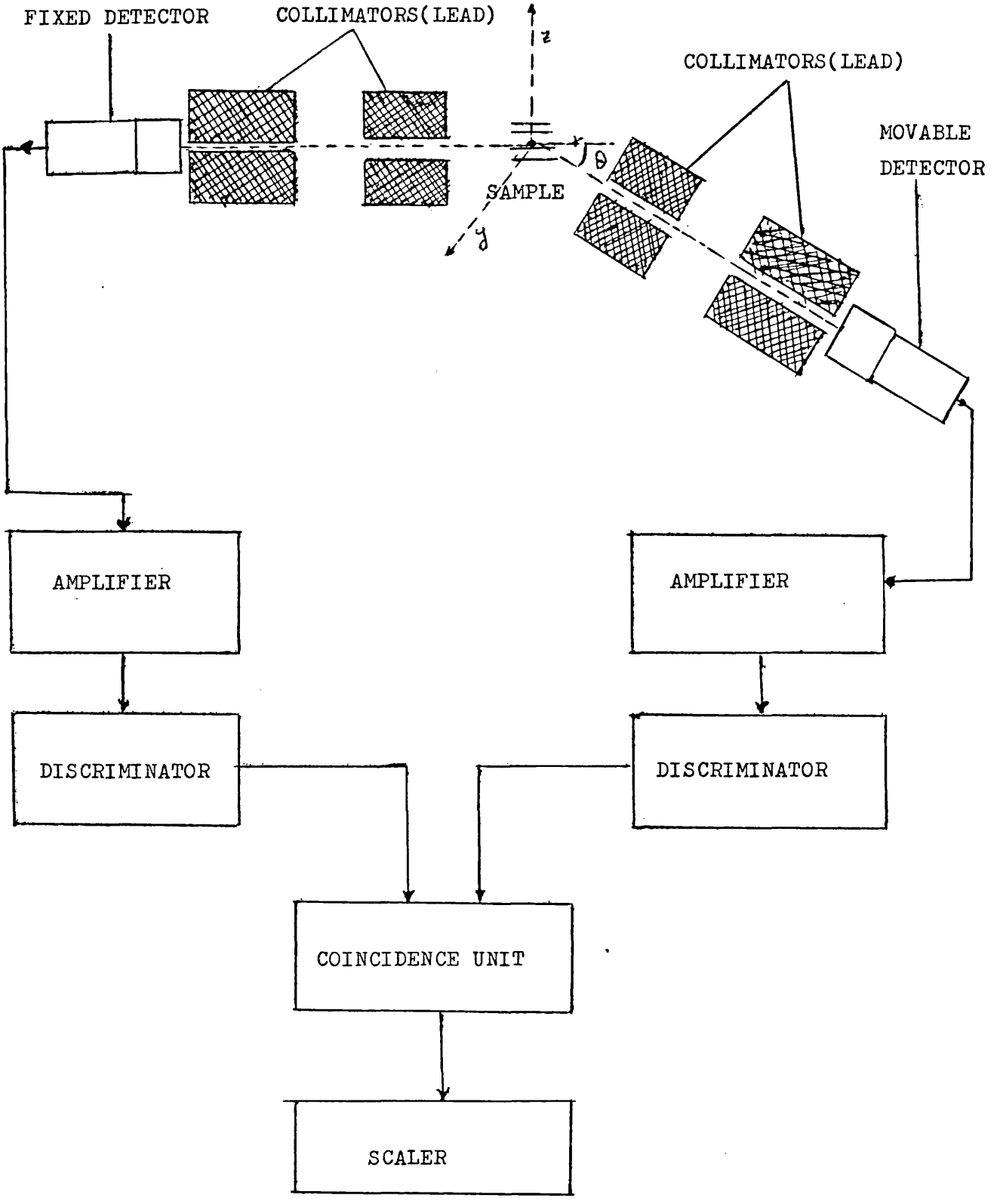

Fig(1.6.2.b) Typical diagram of apparatus for angular correlation measurement.

through discriminators to the coincidence unit. Finally the output from coincidence unit was fed to the scaler. The spectrum of experiment is counting rate verses angle θ. High angular resolution (so far ~0.2 mrad) can be achieved in such a system which uses narrow colliminator openings combined with large sample detector sep ration (Siegel 1980). The typical example of angular correlation measurement of positron annihilation in aluminum and copper is shown in fig(1.6.2.c), that is symmetry at θ=0 with axes (Hautojarvi 1972, 1973).

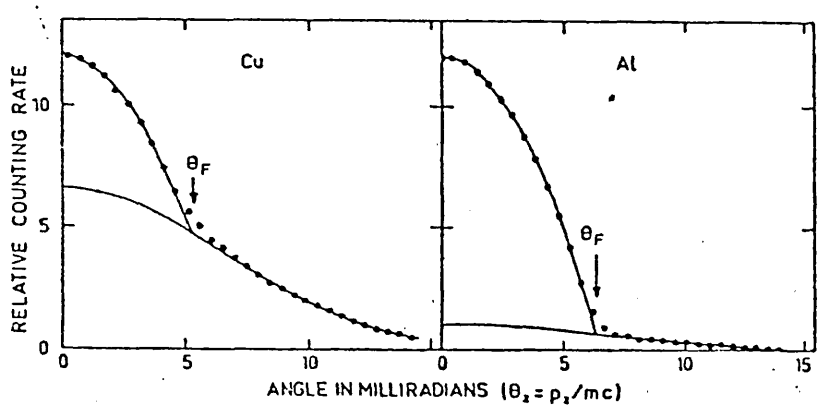

Fig(1.6.2.c) Angular correlation curves for (a)Cu and (b)Al obtained using along-slit detector geometry. Inverted parabola and Gaussian fitted to data corresponding annihilations with valance and core electron respectively. θ_F is Fermi-surface cutoff values.

If the positron annihilates with a gas of free electrons then N(θ) is calculated as

$$N(\theta)=N(0)[1-(\theta_z/\theta_f)^2] \quad \text{for } \theta_z < \theta_f \qquad (1.6.2.8)$$

and N(θ)=0 for elsewhere, where $\theta_f=\hbar k_f/m_0c$ is the Fermi cutoff angle that can be seen in fig(1.6.2.c). Experimentally it can easily be seen that an inverted parabolic contribution resulted from positron annihilation with conduction electrons superimposed with a much broader and slower varying background Gaussian contribution which resulted from the core electrons.

For orthopositronium three coincidence counters that were first

built by Berko and Mader in 1975, have the advantage of rapid data accumulation which aims to compensate for the loses due to the low counting rate.

1.6.3-Doppler broadening measurement:

The third typical experimental method for electron positron annihilation measurement is the Doppler broadening method. Because the velocity component of positron electron annihilation will lead to Doppler shifts in the energy of the annihilation photons, this will result in a broadening of the two γ-ray decay photon line at 511 kev. The result of the Doppler broadening spectroscopy of annihilation line is the distribution of number of photons vers.s energy. Therefore

$$P(\Delta E)=\iint R(p)dp_z\, dp_y \qquad (1.6.3.1)$$

where R(p) is probability of the annihilation, which is found from equation (1.6.2.7). From conservation of momentum and energy this can be written

$$P=h(\upsilon_2-\upsilon_1)/c \quad \text{and} \quad 2m_oc^2=2h\upsilon_o=h(\upsilon_1+\upsilon_2) \qquad (1.6.3.2)$$

and then

$$P=2h(\upsilon_2-\upsilon_o)/c=2h(\upsilon_o-\upsilon_1)/c \qquad (1.6.3.3)$$

is the momentum shift of the photons.

Annihilation of positrons at rest with electrons with the Fermi velocity V_F yield an annihilation energy distribution which is an inverted parabola centred $E_o=m_oc^2$ and extending for $E=E_o(1-V_F/2c)$ to $E=E_o(1+V_F/2c)$. The width of parabola is proportional to $(E_o.V_F/2c)$. In the metal the velocity of core electrons on average is larger than the velocity of conduction electrons. Therefore the energy distribution core electrons is much wider than conduction ones; similarly to angular correlation it is usually represented by a

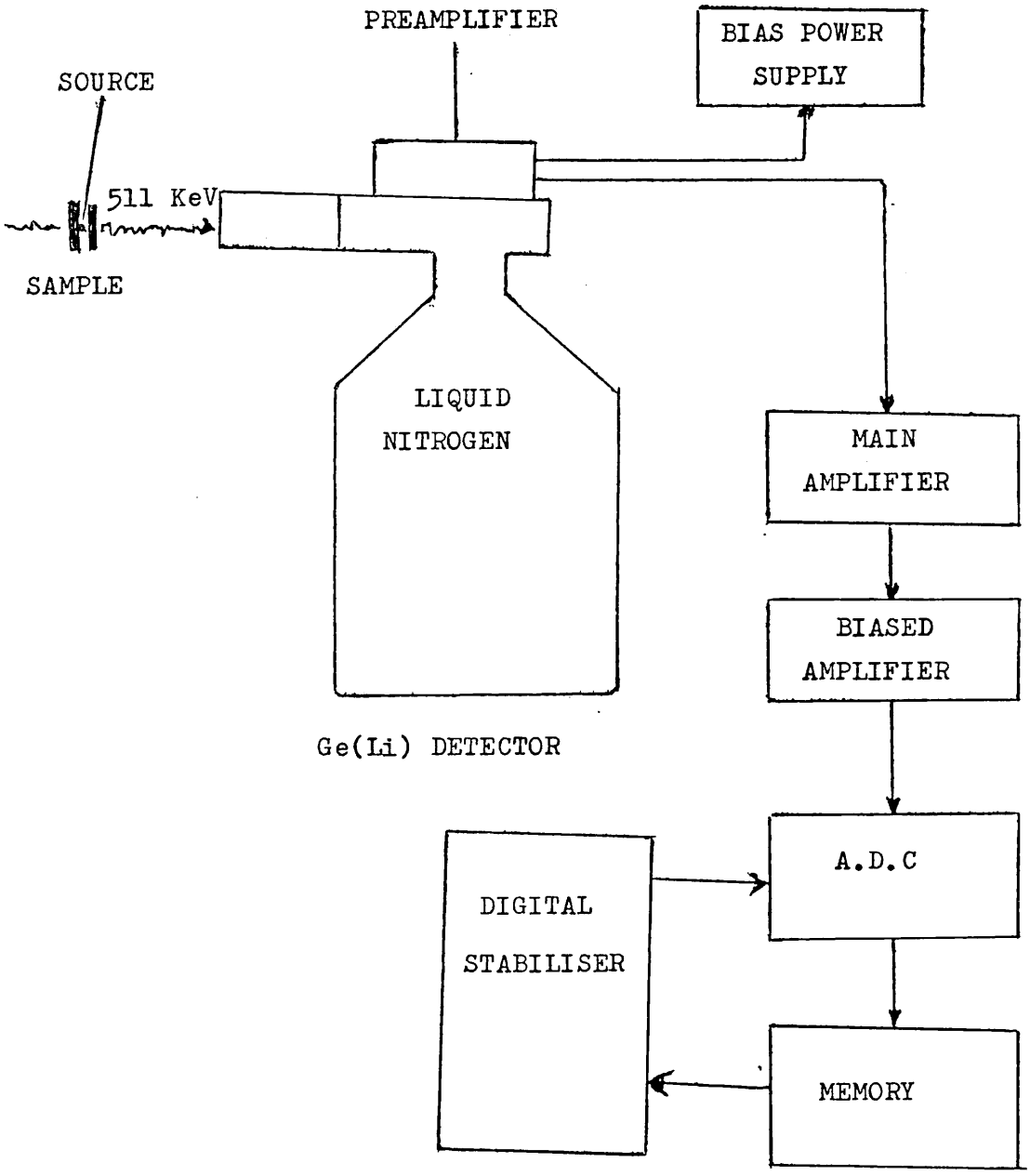

Fig(1.6.3.c) Electronic apparatus for Doppler broadening studies consisting of a Ge(Li) detector and a preamplifier in conjunction with a main and biased amplifier and a data storage system. The data storage system is a combination of an analog-to-digital converter and a memory unit, complemented with a digital stabiliser.

Gaussian function centred at E_0. This measurement needs a good detector, sensitive to the γ-rays resulting from annihilation of the positron with an electron and usually is a semiconductor detector Ge(Li) with resolution about 1Kev for 514 kev γ-rays. The useful sources for this experiment are ^{22}Na, ^{64}Cu, or ^{68}Ge because of high lifetimes and high melting points. Typical experimental equipment useful for this method has been illustrated in figure(1.6.3.a). The output from Ge(Li) detector is fed to preamplifier then through main amplifier going to the biased amplifier. The biased amplifier should provide sufficient expansion of the energy scale to allow many analyser channels to be encompassed by Doppler broadening curve whose width can be measured with great accuracy. Finally the output from biased amplifier was fed to an ADC (analogic-to-digital converter) and then into memory.

The energy shift given by expression (1.6.3.3) means for example for a 6 ev Fermi energy of the electrons the energy of the photons can be shifted by about 1.3Kev. The intrinsic resolution of a detector for ^{85}Sr at 514 kev is 1.15 kev which has recently improved the Doppler broadening measurement (Rice Evans et al 1978a) and it is just enough to allow a changing ratio between core and conduction electrons annihilation, to be detected by detector without any loss of information. Doppler broadening measurement is the most popular method to investigate defects in metals and also the concentration of defects (vacancy, dislocation, etc.).

Chapter II Defect study in metal by positron annihilation

2.1-Introduction:

When positron enters condensed matter it loses its initial kinetic energy rapidly to the thermal energy in a small time compared with its lifetime. These thermalized positrons can then be trapped by a kind of defect (e.g. monovacancies voids etc.) in metals. Finally the positrons will be annihilated with electrons in the medium (conduction and core). The annihilation process is only delayed as the result of trapping. This delay time depends on the concentration of the defects and temperature of the metal. Positron annihilation studies play an important role in understanding of defects in metals.

2.2-Characteristic of defects:

A defect in a solid is defined as any deviation from the perfect lattice structure. The simplest defect is a vacancy, which is a site in the crystal where atoms or ions are missing. The complementary defect to the vacancy is an interstitial, that is an extra atom or ion inserted into site where there is not normally an atom or ion of the regular crystal structure. These extra sites are called interstitials. The nature of the defects is fairly well understood for some solids. In thermal equilibrium a number of lattice vacancies are always created because the entropy is increased by the presence of disorder in the structure. The well known lattice defects can be broadly classified into a number of categories such as; point defects (zero-dimensional imperfections), line defects (one-dimensional imperfections) and grain boundaries (two-dimensional imperfections).

2.2.1-Point defect:

Defects that occupy only a few sites in lattice, such as vacancies, interstitials and dissolved impurity atoms are generally called point defects. Fig(2.2.1.1) shows the simple point defect in a crystal;

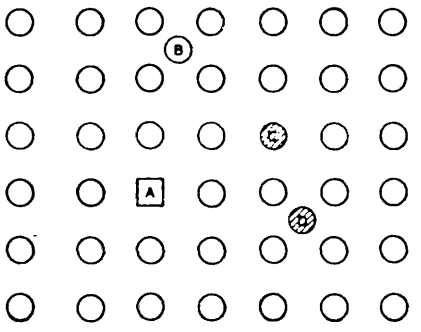

Figure(2.2.1.1)

A:vacancy, B:interstitial, C:substitutional impurity atoms, D:interstitial impurity atom. If the displaced atom moves to surface of the cystal the resulting vacancy is called a Schotty defect and if it moves somewhere within the crystal body it is called Frenkel defect. Impurities in solids may occupy subtitutional or interstitial sites. The defects which are made by impurities in a solid are called extrinsic and conversely vacancies and interstitials are called intrinsic defects.

2.2.2-Line defect:

Line defects are also known as dislocations. Line defects occur in all crystals in different forms. Two example of such dislocations are edge dislocation and screw dislocation. In an edge dislocation an extra half plane of atoms are inserted into the lattice structure and terminating at a particular plain (Hughes and Pooley 1975). The boundary between the slipped and unslipped regions is called slip. The neighbouring lattice planes bend to accomodate this half plain of atoms and as result introduce strain fields into the crystal. The strain field can be shown as Burgers vector. The magnitude of the

Burgers vector (b) represents the amount of strain and its direction indicates the dislocational properties of strain field. In a screw dislocation there is no extra plane of atoms but a shear dislocation is introduced parallel to the dislocation line so that the circuit around the line takes the form of a helix. A general dislocation is a mixture of line and screw dislocation which is normally seen in solids. Line defects are commonly produced in solids by plastic deformation and influences their mechanical properties.

2.2.3-Grain boundaries:

A grain boundary is formed by adjoining two edges of a single crystal of different orientations along a common planar surface. When this difference is small the boundary is referred to as low-angle grain boundary. The internal strain in these regions critically depends on the grain size. The tilt boundary is represented as an array of edge dislocations of spacing $D=b/\theta$, where b is the magnitude of the Burger's vector of the dislocation (Kittel 1971).

2.3-Equilibrium and non-equilibrium measurements.

Study of point defects is essential in determining many properties of solids. This study can be broadly classified in two categories; equilibrium and nonequilibrium measurements. In equilibrium impurities or vacancies will be distributed uniformly (Kittel 1971). In principle, any physical quantity influenced by point defects can be used to study their equilibrium concentration and its dependence on temperature and pressure. But in practice because of the background problems there are only a limited number of techniques which are useful (Seeger 1974), in the study of metals. Generally two techniques are valuable;

a)the comparison between rate of change of specimen length $\Delta l/l_o$ and

the relative change of X-ray lattice parameter $\Delta a/a_o$.

b)The measurement of the γ-radiation from annihilation of positrons which are trapped at vacancies.

The most common experimental ways of producing point defect concentrations in excess of the equilibrium concentration are bombardment with energetic radiation, plastic deformation, quenching from high temperature and quenching condensation on cold substrate. A principle advantage of equilibrium measurement over non-equilibrium measurement is that in former the temperature and pressure determine the point defect concentration, whereas in latter the specimen history is very important. It means that concentration of defects not only depends on temperature and pressure but it also depends on the size and shape of specimen.

2.4-Annihilation of positron with free and core electrons:

The thermalized positron annihilates with conduction and core electrons of the perfect metal. The higher rate of positrons may be annihilated with conduction electrons, because of the screening of the conduction electrons around positron. This results lead to an increase electrons density near the positron. Therefore a stronger overlap of the positron electron wavefunction give a higher rate of annihilation in conduction electrons according to the independent particle model (IPM) which agrees well with those measured in angular correlation experiments (Seeger A 1974). In order to find a positron annihilation rate with conduction electrons usually it is necessary to introduce many simplifying assumptions in order to make progress (Herman and Skillman, 1963). The annihilation rate is proportional to the expectation value of the electron density averaged over all the positron positions. The spin independent free electron states

wavefunction is given by;

$$\Psi(r)=V^{1/2}\exp(ik.r) \qquad (2.4.1)$$

define a spherical Fermi surface for $\underline{k} < k_F$ where k_F is the Fermi momentum, V is volume of normalization and at k=0, $\Psi(r)=V^{1/2}$.

The annihilation rate of the positron with wavefunction $\Psi_+(x)$ with the j-th electron in the metal, with wavefunction $\Psi_j(x)$ including two emitted photons having momentum between k and k+dk is given by (De Benedetti et al 1950 and West 1974);

$$\Gamma(k)d^3k=(\pi r_o^2 c/(2\pi)^3)\left|\int d^3x \exp(-ik.x)\Psi_j(x)\Psi_+(x)\right|^2 d^3k \qquad (2.4.2)$$

The total annihilation rate is obtained by summing over all occupied states and photon momenta.

$$\Gamma=\sum_j \Gamma_j(k).dk^3 \qquad (2.4.3)$$

The conventional long slit angular correlation apparatus measurement gives a quantity proportional to the distribution of the momentum component of γ-ray pairs with $p=\hbar k$.

$$N(p_z)\,dp_z=\int_{-\infty}^{+\infty}\int_{-\infty}^{+\infty}\Gamma(p)\,dp_x\,dp_y\,dp_z \qquad (2.4.4)$$

where $N(p_z)$ is proportional to the number of positron-electron annihilations. The total area under $N(p_z).dP_z$ is proportional to the total annihilation rate. That is provided a Fermi area relative to

$$N(p_z)=2\pi p_F^2\,(1-p_z^2/p_F^2) \qquad \text{for} \quad p_z<p_F \qquad (2.4.5a)$$

$$N(p_z)=0 \qquad \text{for} \quad p_z \geq p_F \qquad (2.4.5b)$$

In metals, like copper, the rate of positron annihilation with core electrons is higher, and the simple IPM is inadequate to describe them (Chaglar 1978). Furthermore this model is unable to provide correct lifetime predic tions (2.4.2). Therefore the many body interaction model has to be considered to obtain a reasonable agreement with experiment.

The positron can also be annihilated with core electrons, which are generally much more numerous than conduction electrons. On the other

hand the repulsive force between the positron and nuclei (or ions) is the reason that the positron has been kept out of the core region. This reduces the overlap of the positron and electron wavefunction. The core electrons will lead to broad tails in (p_z), because they are localized in space, being quite distinct from the conduction electron contribution. For the n,l atomic quantum number can be written;

$$\Psi_{n|mk}(x)=[1/N^{1/2}]. \sum_{v} \exp(ik.x)\ U_{n|m}(x-R_v) \qquad (2.4.6)$$

where N is total number of ions, n,l,m are quantum numbers. and R_v is the lattice positions in configuration space. $U_{n|m}$ is given as

$$U_{n|m}(x)=Y_{n|m}(x/r)P_{n|}(r)/r \qquad (2.4.7)$$

where $Y_{n|m}$ is a spherical harmonic function and $P_{n|}$ is the radial core electron function.

The annihilation rate is given as;

$$\Gamma_{n|m}(p)=\lambda/\Omega\ (4\pi(21+1)/\Omega_o)\delta_{m,o}\left|\int_0^{\infty} P_{n|}(r)\ \Psi_+(r)\ J_{|}(pr)dr\right|^2 \qquad (2.4.8)$$

where $\Gamma_{n|m}$ is positron rate per electron density, $\Omega=\Omega_0 N$ volume of the crystal and $J_{|}(rp)$ is the l-th spherical Bessel function. The annihilation rate decreases as the electron is near by nucleus. The distribution of the annihilation energy core electrons obeys a Gaussian and not a parabolic function.

2.5-Thermal effect:

As discussed in section 2.3 the experimental methods of equilibrium measurement can be classified as;

i)X-ray measurements the relative change in specimen length (macroscopic) compared to the relative change in lattice parameter (microscopic).

ii)Positron electron annihilation techniques.

The temperature depends on the vacancy concentration in both methods. The following quantitative consideration connects the measured

quantities and hence the difference between macroscopic and microscopic volume changes, with concentration of point defects. Suppose the crystal volume at temperature T is V, and the atomic volume at the same temperature is Ω. Because both are temperature dependent, the volume of crystal at temperature T is given as

$$V=N'\Omega \tag{2.5.1}$$

where N' is the total number of atomic sites, and $N'=N+n$, where N is the number of atoms and n is the number of defect which is positive for a vacancy and negative for an interstitial. Consider a crystal volume V_0 at a fixed temperature T_0 with atomic volume Ω_0 so

$$V_0=N\Omega_0 \tag{2.5.2}$$

The change in volume from T_0 to T, are:

$$\Delta V=V-V_0 \tag{2.5.3}$$

$$\Delta\Omega=\Omega-\Omega_0 \tag{2.5.4}$$

From relation of expression (2.5.3) to (2.5.4) we have

$$\Delta V/V_0=n/N+\Delta\Omega/\Omega_0+(n/N)\Delta\Omega/\Omega_0 \tag{2.5.5}$$

Therefore $$C_v-C_i=n/N=(\Delta V/V_0-\Delta\Omega/\Omega_0)/(1+\Delta\Omega/\Omega_0) \tag{2.5.6}$$

Because the values of $\Delta\Omega/\Omega_0$ are very small compared to unity, then they can be ignored in equation (2.5.6).

Therefore $$C_v-C_i=n/N=(\Delta V/V_0-\Delta\Omega/\Omega_0) \tag{2.5.7}$$

If $\Delta V/V_0$ and $\Delta\Omega/\Omega_0$ are small compared to unity, then relation are proportional with three times of relative $\Delta l/l_0$ macroscopic specimen length of crystal and $\Delta a/a_0$ microscopic lattice parameter respectively, because quadratic terms can be neglected. Therefore the concentration of defects is given as

$$C_v-C_i=3(\Delta l/l_0-\Delta a/a_0) \tag{2.5.8}$$

The final equation (2.5.8) gives information on whether vacancies or interstitials are dominanted at thermal equilibrium. In all metals so far investigated the interstitial concentration C_i is so small

relative to C_v, that it is negligible.

On the other hand the concentration of point defects has a dependence on pressure and temperatures in equilibrium measurement. Existence of point defect in a crystal at finite temperatures is governed by statistical thermodynamics. The Gibbs free energy of vacancy formation is given as

$$G^f_{1v} = (H^f_{1v} - T.S^f_{1v}) \qquad (2.5.9)$$

Where H^f_{1v} is the enthalpy of monovacancy formation, and is equal to the work done in the process at temperature T. S^f_{1v} is the entropy of monovacancy formation. Entropy represents disorder in the system due to the changes in the vibration spectrum of the crystal when the vacancy is created. In order to determine the total entropy the configurational entropy has to be computed. Consider N´ to be the total number of atoms in the specimen and N the number of the atom in sites at constant pressure then the number of point defects or vacancy sites is n=N´-N, giving the free Gibb´s energy of system:

$$\Delta G = (nG^f_{1v} - T.S_n) \qquad (2.5.10)$$

where S_n is the total entropy of vacancies. According to thermal equilibrium measurements, at a fixed temperature and pressure ΔG must be a minimum then,

$$\partial \Delta G / \partial n = (G^f_{1v} - T.\partial S_n / \partial n) = 0 \qquad (2.5.11)$$

By using Boltzmans statistical interpretation the total entropy for n vacancies is equal to

$$S_n = k.\ln(W_n) \qquad (2.5.12)$$

where W_n is the probability of formation of n vacancies in a crystal, and it is

$$W_n = N'!/(N'-n)!.n! \qquad (2.5.13)$$

By substituting (2.5.12) and (2.5.13) into (2.5.11), one obtains

$$G_{1v}^{F} - kT.\partial(\ln(N'!/(N'-n)!.n!)/\partial n=0 \qquad (2.5.14)$$

Therefore by the application of Stirling's theorem

$$\ln(x!)=x\ln(x) \qquad (2.5.15)$$

and differentiating relative to n the concentration of monvacancies is given by

$$C_{1v}^{F}=n/N'=n/N=\exp(-G_{1v}^{F}/kT) \qquad (2.5.16)$$

or
$$C_{1v}^{F}=\exp(S_{1v}^{F}/k).\exp(-H_{1v}^{F}/kT) \qquad (2.5.17)$$

The results of C_{1v} show that the concentration of the monovacancies depend on temperature. H_{1v}^{F}, S_{1v}^{F} are enthalpy and entropy of monovacancies respectively. As S_{1v}^{F} results from changes in the vibration spectrum of the crystal with the introduction of a vacancy it is necessarily positive, since on the average vibration frequencies near a vacancy will be lowered relative to an ideal crystal (Seeger 1973).

Sometimes, near the melting point of the specimen, vacancies in neighbouring lattice sites might bind together to form divacancies. Divacancies may take up different orientations in the crystal, depending on the coordination number. For instance in a crystal with coordination z there are z/2 different orientations possible. The total of vacancies is given by summing over all vacancies and divacancies, etc.

$$C_V=\sum_n nC_{nv} \qquad (2.5.18)$$

for a divacancy $C_V=C_{1v}+2C_{2v}$, the Gibbs energy and Gibbs binding energy is found as

$$G_{2v}^{F}=H_{2v}^{F}-T.S_{2}^{F} \quad \text{and} \quad G_{2v}^{B}=2G_{1v}^{F}-G_{2v}^{F} \qquad (2.5.19)$$

The divacancy concentration is calculated as

$$C_{2v}=z/2.\exp(S_{2v}^{F}/k).\exp(-H_{2v}^{F}/kT) \qquad (2.5.20)$$

The discussion above clearly shows that the concentration of any type of vacancy, for metal depends on the temperature.

2.6-Trapping model and trapping rate:

A simple rate theory, such as trapping (Seeger 1973) has been applied to describe the trapping of positrons in vacancies. This model has been a great success when applied to the results from experiments using lifetime, angular correlation and Doppler broadening techniques. The trapping model was first suggested by Gol'Danskii and Prokopev (1965), was applied to trapping in metals by Connors and West (1969). Consider the number of the untrapped (free) positrons to be n with decay rates λ_f. The thermalized positrons diffusing in metals are assumed to be trapped by various types of defects (labelled j) with annihilation decay rates λ_j and numbers of positrons trapped n , and also with trapping rates σ_j . If m be the different types of traps with atomic concentrations C_j, the general trapping model is given by

$$dn_f(t)/dt=-\lambda_f n_f(t)-\sum_{j=1}^{m} \sigma_j C_j n(t) \qquad (2.6.1)$$

where C_j is the concentration of the jth-type defect, and then

$$dn_j(t)/dt=-\lambda_j n_j(t)-\sigma_j \cdot C_j n(t) \qquad (2.6.2)$$

The solution of equation (2.6.1) substituted into (2.6.2), gives

$$n_f(t)=n_f(0)\exp(-\lambda_o t) \quad \text{where} \quad \lambda_o=\lambda_f+\sum_{j=1}^{m} \sigma_j C_j \qquad (2.6.3)$$

$$n_j(t)=[\sigma_j.C_j/(\lambda_j-\lambda_o)]n_f(0)\exp(-\lambda_o t)+[n_j(0)-C_j.\sigma_j/(\lambda_j+\lambda_o).n_f(0)]\exp(-\lambda_j t) \qquad (2.6.4)$$

The mean lifetime of the positron can be calculated as

$$\tau=(1/n_f(0))\int_o^\infty [n_f(t)+\sum_{j=1}^{m} n_j(t)].dt \qquad (2.6.5)$$

with the condition that there is no intial trapping of positrons in defects, i.e $n_j(0)=0$ for j=1,2,3,.....m. Then the mean lifetime is

$$\bar{\tau}=\tau_f.(1+\sum_{j}^{m} \tau_j \cdot \sigma_j C_j)/(1+\tau_f \sum_{j}^{m} \sigma_j \cdot C_j) \qquad (2.6.6)$$

An important quantity can also be calculated from equtions(2.6.3) and (2.6.4), this is the probability of the positrons annihilating in the free or trap state, and is given by

$$P = \int_0^\infty (n_f(t)/n_f(0)).dt = \int_0^\infty \exp(\lambda_f + \sum_{j=1}^{n} \sigma_j C_j)t.dt \qquad (2.6.7)$$

So that

$$P_f = \lambda_f/(\lambda_f + \sum_{j=1}^{m} \sigma_j C_j) \quad \text{and} \quad P_j = \sigma_j C_j/(\lambda_f + \sum_{j=1}^{m} \sigma_j C_j) \qquad (2.6.8)$$

where $P_f + \sum_j P_j = 1$.

Application of the trapping model to positron annihilation measurements is usually preformed in the following manner (McKee et al 1972a); Let F be a feature of the positron annihilation process, for example, a characteristic of the momentum or lifetime distribution. This fraction will be proportional to the fraction of the two different states; free state to trapped state. It is defined as

$$F = F_f . P_f + \sum_{j=1}^{m} F_j . P_j \qquad (2.6.9)$$

where F_F and F_j are the fraction of positron annihilating as free positrons and that as trapped positrons respectively. The complete expression for the F parameter will be written down in chapter five.

It is also very important to have a clear picture of the physical nature of the trapping rate and in particular its temperature dependence. As mentioned in preceding sections, the positron becomes thermalized in metals in a time small compared with its lifetime, that it then diffuses through the crystal until it annihilates or becomes trapped. This diffusion motion can be characterized from the theory of Waite (1975). The capture of the diffusing particle by a trapping centre may be described by rate equation of form (2.6.1). The capture cross-section is then given by

$$\sigma = 4\pi D r_o / \Omega \qquad (2.6.10)$$

where Ω denotes the atomic volume. At sufficently high temperatures the mobility of positrons is limited because of scattering by lattice vibrations. The thermalized positron obeys Boltzmann statistics, hence the mobility of the positron is given by

$$\mu = 2^{3/2}\pi^{1/2}\rho\, c_l^2 \hbar^4 / 3m^{5/2}\epsilon_d^2 (kT)^{3/2} \qquad (2.6.11)$$

where ρ is the density of the metal, c_l the longitudinal sound velocity, m_+ effective mass of the positron and ϵ_d the deformation potential constant. A uniform dilation θ changes the energy of the free positron ground state ϵ by $\delta\epsilon=\epsilon_d\theta$. Again since positrons obey the Boltzmann distribution, the diffusion constant can be calculated by the Nernst-Einstein relationship $D_+=kT\mu$. By substitution into equation(2.6.10) the trapping rate is found as;

$$\sigma=8\pi r_o\rho(2\pi)^{1/2} c_l^2 \hbar^4/3\Omega(kTm_+)^{1/2} m_+^2\epsilon_d^2 \qquad (2.6.12)$$

In deriving above equation Seeger made the following assumptions:

i)The temperature high enough then the positron mobility is limited by scattering from lattice vibration and may be treated as being elastic. The deviation from above equation to be expected at low temperature.

ii)The elastic scattering properties of the metal are assumed isotropic

iii)The Bloch wavefunction of ground state of the positron belongs to the wavevector k=0 (Seeger 1973).

There are two different ways to measure the temperature dependence of the trapping rate of positrons by vacancies:

1)Under the preceding conditions the quantity of $\tau_{1v}\sigma_{1v}C_{1v}$ is determined on quenched metal as a function of temperature, C_{1v} is constant, hence the temperature dependence on σ_{1v} is obtained.

2)The mean lifetime taken at a fixed temperature T as a function of quenching temperature T_q and compared with high temperature measurment of mean lifetime at temperature $T=T_q$.

In 1971 Conners et al found a temperature dependence of the trapping rate in angular correlation measurements on cadmium, which had been quenched quickly from 570K to liquid nitrogen temperatures. But using the assumption that the trapping rate depends on $T^{-1/2}H_{1v}^f$ changed by just .01eV, .02eV and .03eV at 300 K, 600 K, and 900 K respectively.

McKee et al in 1971 applied the $T^{-1/2}$ law to aluminium and found the expected value of H^f_{1v} to increase by .02ev. However, the temperature dependence of the trapping rate is rather weak compared with the exponential temperature dependence of the concentration of vacancies and ,hence, can probably be neglected. But Hoges (1970) treating the trap as a potential well found that the resultant trapping rate was independent of temperature a hypothesis which is supported by Bergersen and Taylor(1974)

2.7-Self-trapping:

The anomalous temperature dependence of positron annihilation in cadmium has been observed by Lichtenberger et al in 1975, observing a non-linear F-parameter rise in an intermediate temperature range. They argued that this non-linear rise could not be due to the vacancy trapping of thermalized positrons and neither to thermal expansion. Seeger (1974) concluded that the effect was not that of thermal expansion on the annihilation of "free" or "untrapped" positrons which is small, while the effect observed was relatively large. He argued that this anomaly may be due to lattice acoustic phonon interactions with the positron. According to this Seeger 1975 has given an alternative explanation for this effect. He shows that the anomalous temperature dependence in positron annihilation properties is a result of the existence of meta-stable states with respect to free positrons, in which the positrons become self-trapped.

In 1961 Toyozawa showed that, if the interaction between a charged particle in a metal with an acoustical phonon is included to the polaron theory, the polaron properties may change discontinuously as a function of coupling strength between the electric charge and acoustical phonons. This discontinuity in fact is associated with

the interaction of an electron or hole with the acoustical phonon being of short range, the interaction with an optical phonon is of large range. Because of the screening of electric field by a redistribution of conduction electrons the interaction between a phonon and a positive charge in a metal is of short range. If the coupling between positive charge and a phonon is sufficiently strong, two different configurations, associated with positively charged particles, are possible; i) interaction is weak in which charged particle remains in Bloch state. ii)an interaction corresponding to the self-trapping picture where there is a strong localized wavefunction. Following this argu ment Sumi and Toyozawa (1973), Seeger (1975) described the interaction between positron acoustical phonons through a coupling of electric dilation $\theta(r)$ with positron charge density $|\psi_f(r)|^2$. It can be written

$$\theta(r)=-\epsilon_d/C\cdot|\psi_f(r)|^2 \qquad (2.7.1)$$

where C is a combination of elastic constants and ϵ_d denotes the positron deformation potential Seeger (1975). Seeger found the energy function of this interaction by using expression (2.7.1) as

$$E(\Psi(r))=\hbar^2/2m_+\int[\Delta\Psi(r)]^2 dr^3 - \epsilon_d/2C\int[\Psi(r)]^4 dr^3 \qquad (2.7.2)$$

Here m is the positron bound mass and h is Plank's constant. He used a trial function for positrons, with an adjustable parameter k, that has a wave number dimension, giving

$$\Psi_+(r)=(2K^2)^{3/2}\exp(-\pi K^2 r^2) \qquad (2.7.3)$$

by substituting $\Psi_+(r)$ into (2.7.2) he obtained the energy of the system as function of K as

$$E(K)=3\pi\hbar^2/2m_f.K^2-(\epsilon_d^2/2C).k^3 \qquad (2.7.4)$$

equation (2.7.4) has two minima, one at K=0 representing free positron states (non-localized) and the second at $K=K_o$ due to an upper cut-off approximately equal to the reciprocal interatomic distance.

$$E(K_o)=3\pi\hbar^2 K_o^2/2m_+ - \epsilon_d K_o^3/2C \qquad (2.7.5)$$

where the maximum value of equation (2.7.2) is when

$$K_{max}=2\pi\hbar^2 .C/\epsilon_d^2 m_+ \qquad (2.7.6)$$

The second minimum corresponds to localized positrons and gives the rise in the positron annihilation line shape parameters. Now two possibilities may occur

i)$E(K_o)>0$ is positive so the self-trapping state is metastable relative to low-lying free positron states.

ii)$E(K_o)<0$ is negative so the self-trapping state is stable whereas the free positron states is metastable.

For the case of $E(K_o)>0$ temperature depends on the self-trapping of positron in intermediate temperature range. He also calculated the probability of annihilation which has now changed to two states one self-trapping P_{St} and other for a free positron P_f, where $P_{st}+P_f=1$, therefore

$$P_{St}=[1+B^{-1}.T^{3/2}\exp(E(K_o)/kT)]^{-1} \qquad (2.7.7)$$

$$P_f=[1+B^{-3/2}.T\exp(-E(K_o)/kT)]^{-1} \qquad (2.7.8)$$

where $$B=\Pi_i(\nu_i/\nu_i').(2\pi\hbar^2/mK)^{3/2}/\Omega_o \qquad (2.7.9)$$

and Ω_o is the atomic volume, ν_i, ν_i' are vibrational frequencies of the crystal with a free or self-trapped positron, and the product Π extends over all the lattice vibrational modes. Finally the F-parameter is improved with the addition of the self-trapping part to

$$F(T)=P_t F_t+[P_f F_f+P_{St} F_{St}](1-P_t) \qquad (2.7.10)$$

Hodges and Trinkaus in (1976) and Leung et al (1976) have concluded that the deformation potential in Seeger's calculation is too large to be realistic in metals, and for most of them positron self-trapping is not the same.

2.8-Phase transitions:

2.8.1-Definition;

In nature there are three phases of atoms: solid (eg. gold, iron etc.), liquid (eg. water alcohol etc.), and gas (eg nitrogen oxygen etc.). These phases are dependent on the pressure, temperature, and volume (Walton A,J 1980), Therefore at atmospheric pressure and almost room temperature all these three phases are stable. By varying the thermodynamic parameters however, the solid, liquid and gas phases can be made similar until they can no longer be distinguished at a tricritical point (tricritical point means at a certain temperature and pressure, in constant volume, the three phases co-exist). At certain temperature one phase changes to another, for example nitrogen in at mospheric pressure change to liquid at 77 K.

In the solid the atoms are held together at short range in order, like geometrical shape, cubic, tetragonal, hexagonal, etc. Some of the elements or alloys are transformed from one structure to the other structure at particular temperature, (eg. tin transforms from cubic structure to tetragonal structure at 13.2 ^{o}C). A transition from one (ordered) crystal structure to another, in which each atom moves relative to its near neighbours by an amount small compared with the unit cell dimensions, is called a displacive phase transition.

2.8.2-Phase transition in tin:

Tin is an element with melting point 510K and 3 or 4 valence electrons. Naturally tin has two or three allotropic structures, one is grey-tin or α-tin with a cubic structure, the second is white-tin or β-tin, the ordinary form of metal, and some authorities believe a form exists between 434.5K and melting point. The ordinary tin

(β-tin) is stable but grey-tin is transformed to the white-tin at 286.4K, and below this temperature is stable. The transition of tin is dependent on temperature and time. If the white-tin is cooled down from the high temperature the structure remain s the same. But by increasing temperature it will transfer to grey-tin after at least about 23 days at 240K (Puff W et al 1984). This transformation results in a 27% change in volume of tin. The transformed fraction is given by Avrami's equation as

$$1-f(t)=\mathrm{Exp}(-At)^{k}$$

where value of k varied between 1-3 (Burgers and Groen 1957).

The study of the kinetics of the transformation has been limited to observation and calculation of the temperature-dependence of the linear growth-rate of the phase transformation (Burges and Groen same paper).

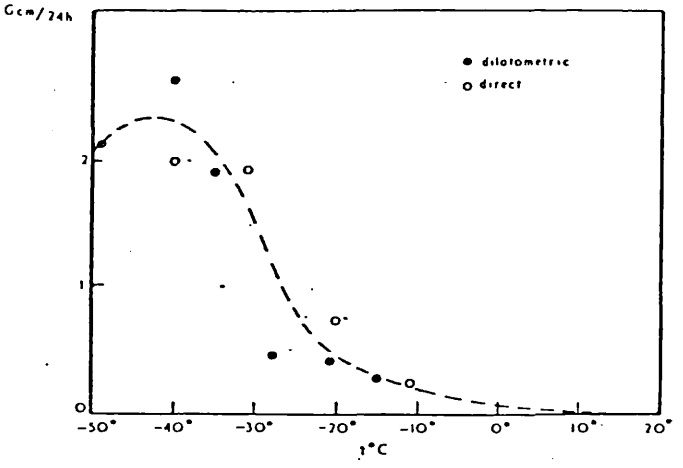

Fig(2.8.2.a) White to grey transformation. Linear rate of growth G at different temperatures for high-purity tin, as measured directly, and as calculated from dilatometer experiment.

They found that the growing rate of the grey-tin to white-tin is dependent on temperature (eg. .003mm/sec at 303K while the rate increases to .022mm/sec at 310K). They also reported the maximum phase transition occured from grey to white tin at 300K to 310K the whole transformation will complete. Cohen and Van Eyk observed that the transformation of β-tin to α-tin is accelerated if it is immersed

into a solution of pinksalt $(NH_4)_2 SnCl_6$. In our measurements it was observed the transformation also accelerates if the tin is plastically deformed. The rate of transformation of white to grey tin matrix measured by Tammann and Dreyer 1953, is illustrated in figure(2.8.2.a).They found the reverse transformation experiments, value for linear rate of growth α to β -tin is started at 303.3K and is increased at 310K and then transformation is completed figure (2.8.2.b). This transformation was clearly observed in our measurements which will be discussed in chapter seven. The process of the transformation divided the material; white filings

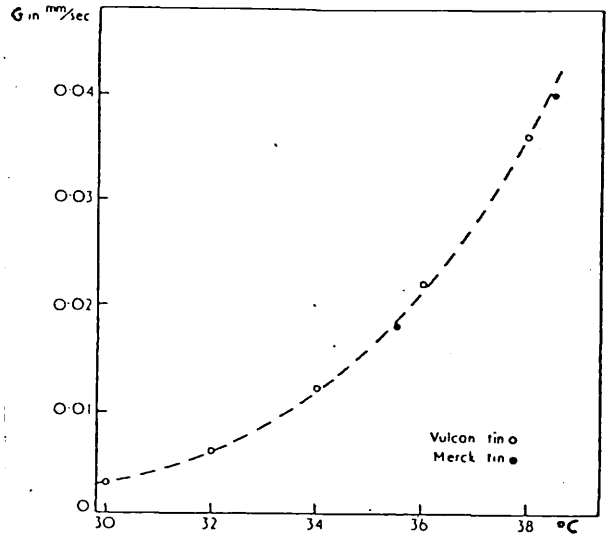

Fig(2.8.2.b) Grey to white transformation. Linear rate of the growth G at different temperature.

transformed into the grey powder, formed by transformation of a white bar, and the powder retransformed from grey to white.

Chapter III Positron annihilation at surfaces

3.1-Introduction:

The efficiency of a positron on a surface to form positronium (Ps) was a key factor in facilitating the spectroscopic studies of this basic quantum-electrodynamic system (Nieminen R.M 1983). The slow positron beam techniques have made it possible to investigate in detail the properties and structure of surfaces of matter under ultrahigh-vacuum conditions by the positron-surface interaction. At somewhat higher incident energies of positrons at the surface, the great majority of them thermalized during the implantation and slowing-down. Then following diffusion motion of the positrons, during which a substantial fraction may reach the entrance surface, if the initial penetration depth was not too long. At the surface several process will happen. If the positron work function for particular surface is negative then the positron may be re-emitted into vacuum with kinetic energy of the order of a few eV (Mills Jr. et al 1978a). While being emitted, the positron also has a considerable probability to pick up an electron from the surface and emerge as Ps in vacuum (Mills Jr. 1978b). Finally the positron may be captured in to the image-potential at surface (trapping at surface). The positron mean energy in the bulk with respect to the vacuum level is, by definition, the positron work function and thermal energy neglected is given by;

$$\varphi_{ps} = -D_{+} + E_{s} + E_{corr} \qquad (3.1.1)$$

where φ_{ps} is positron work function, D_{+} is electrostatic surface dipole barrier and E_{s}, E_{corr} bound shift and correlation energy respectively. The correct surface barrier D_{+} is potential difference between the vacuum and the electrostatic potential at the edge of a bulk

Winger-Seitz cell. The positronium energy work function can be calculated from the Born-Haber cycle as

$$\varphi_{ps} = \varphi_{+} + \varphi_{-} - E_b \qquad (3.1.2)$$

where E_b=6.8eV is the binding energy of the positron with an electron and φ_- is electron work function.

Low energy of positron beams colliding with solid target surface came first in 1974 when Canter et al reported that positronium is formed by a positron hitting a metal target in vacuum. Then the low energy positron beam technique was developed by focusing the positron from the source to the target through the magnetic fields.

3.2-Positron beam study:

When the low-energy positron beam is interacting with a solid target surface many interesting phenomena occur. These phenomena are quite sensitive to the target material, orientation, crystalline perfection and surface contamination. A typical schematic of this scattering has been shown in the figure(3.2.1).

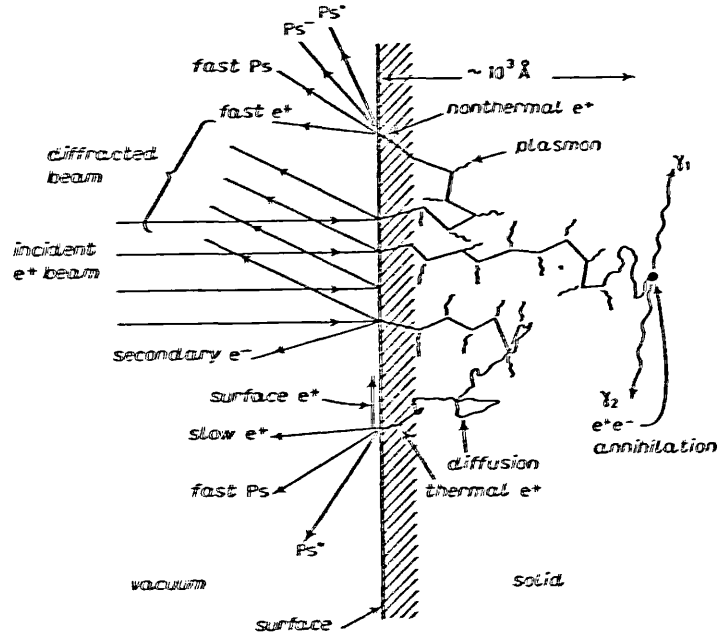

Fig(3.2.1)- Shows the result of slow positron beam intraction at surface

When the incident slow positron beam interacts at the surface of

matter two possible things will occur. Firstly some of them will scatter elastically from surface and become a diffracted beam, if the surface is single crystal. Secondly, a variety of inelastic processes will occur for the rest of the incident positrons which terminate when the positrons annihilate or are ejected from the surface. Before annihilation they diffuse back and may be trapped by vacancies or reach the surface and become bound in their "image" potential well at the surface or leave the surface as free particles, as positronium in its ground state or as one of its excited states or positronium negative ions (Mills Jr 1981).

Positrons are obtained with high kinetic energy from β-decay of radioactive nuclei. Normally in a metal these positrons lose their energy to be slowed down to thermal energy by interaction with ions or electrons, but in the slow-positron beam technique they are thermalised at one place and then transported to the target with monoenergetic form, in a controlled manner.

The idea of forming beams of thermal-energy positrons by moderating the energetic positrons from a radioactive source occured to (Madansky and Rasetti 1950). The positron beam experiment was then developed by Cherry in 1958, he succeeded in producing a slow-positron beam from ^{64}Cu source with yield relative to total positron $\epsilon=3.1X10^{-8}$. Following his success in producing a beam, Madey in 1968 and at the same time Groce et al also succeeded in forming a beam of few slow positrons per second which they were able to measure the total scattering cross-section of positrons in helium for the first time. The efficiency of the positron beam is mostly dependent on the type of elements that are used in moderators.

After developing slow positron beam production, it was useful to study metal surfaces. In the previous section we explained that a positron

at surface is bound by its image-potential or emission in vacuum by capture an electron to form positronium in the ground state and may be emitted from surface like a free positron in vacuum. The positronium will decay to two photons with short time ($\sim 10^{-10}$ s), when it is in the singlet state ($^1S_0$) and to three photons with a longer time ($\sim 10^{-7}$ s), when it is in the triplet state ($^3S_1$). The decay from the singlet state is to 2γ with energy $E_b+2m_oc^2$, but from triple state decays to three γ's with energy distributed between zero to m_oc^2. Therefore we have to attend to this problem of what fraction of the positrons have formed positronium. Suppose the counting rates measuring from R_2, R_2', R_3, R_3' for two γ's and three γ's annihilation for two different condition of sample respectively. Where total fraction of positron annihilation was equal sum of the three γ's fraction plus two γ's fraction $P=P_2+P_3$. Also consider $P_n=\epsilon R_n$, where ϵ is the counter efficiency then it is easy to find that

$$P_3=(1-R_2'/R_2)/(R_3'/R_3-R_2'/R_2) \qquad (3.2.1)$$

Because the angular distribution of the three γ's is mixed with two γ's rates therefore using (3.2.1) is not useful (Ore et al 1949). But Leventhal (1974) found a similar method for the positronium fraction f where they used the total area of spectrum as $T_t=f.T_o+(1-f)T_1$ and the area under the peak as $P_t=P_o.f+(1-f).P_1$, and then calcuated the fraction of positronium as;

$$f=[1+(R_t-R_o)/(R_1-R_t).(P_1/P_o) \qquad (3.2.2)$$

where $R_i=(T_i-P_i)/P_i$. The maximum energy need for positronium formation is

$$E_{Max.}=-\varphi_{ps}=-\varphi_+-\varphi_-+E \qquad (3.2.3)$$

where φ_{ps} is the positronium work function and it is negative for most of metals except Alkali metals (Hodges et al 1973). φ_+, φ_- are the positron and electron work functions respectively, and $E_b=6.8$eV is the

binding energy of electron-positron pairs.

Mills Jr in 1979 found the f positronium fraction probability thermally active. He measured the positronium fraction of positron beam interaction on copper and aluminium surfaces, his data fitted to expression as below

$$f=(f_o+f_\infty.\eta^{-1}.Z)/(1+\eta^{-1}.Z) \qquad (3.2.4)$$

where $Z=Z_o(T)\exp(-E_a/kT)$, η is temperature independent annihilation rate of surface bound positron, Z is the rate of occurance of the energetically forbidden desorption process, and E_a is the activation energy of the positronium by

$$E_a=E_s+\varphi_- -E_b \qquad (3.2.5)$$

where E_s is the binding energy of positronium on the surface. Jean et al in 1984 used just the exponetial part of equation (3.2.4), (Z) to fit their data for positron annihilation in grafoil (lifetime measurement). They found the activation energy is E_a=(0.22+0.02) eV and binding energy of positronium on the grafoil 2.58eV. The activation energy E_a is very sensitive to surface orientation and contamination. Z_o is temperature dependent if the positron forms a two-dimensional gas on the surface and positronium is formed with electrons from the bulk solid, then the constant rate is $Z_o=(8.335X10^{10}[K^{-1}]).T$ (Mills Jr 1980). If equation (3.2.4) is correct it can be expected that by lowering the electron wavefunction φ_- the E_a value will be negative. As electron wavefunction decreases the f will be increase, and thus it bring the surface positrons to desorb spontaneously without the need for thermal fluctuation (Mills Jr 1979).

3.3-Determination of the Positronium fractions:

In previous sections we discribed the behaviour of the slow positron interaction at surface of metals. The dominant processes occurring at a metallic surface can be categoried as:

i) localization of positron on surface state where it can either annihilate or be subsequently desorbed into the vacuum as Ps at sufficiently high sample temperatures (Lann and Lutz 1980, Mills Jr 1979).

ii) direct re-emission of the positron from the metal in vacuum with a negative positron work function (Mills Jr et al 1978a).

iii) re-emitted into vacuum as positronium where Ps state is formed while escaping from surface.

iv) reflection of the positron wave from the surface potential back in to the metal. Other processes like positronium in an excited state and Ps^- negative ions have also been observed, but are less probable. On the other hand Positronium formation has two possibilities to be formed, parapositronium (pPs) singlet state $^1S_0$ and a triplet state $^3S_1$ orthopositronium (oPs). Statistically there is a three-quarter probability of oPs being formed and one-quarter for pPs. The pPs state decays to two photons each with energy of mc^2, and a decay rate $8.1X10^9\ s^{-1}$. If we assume that no pick-off or spin exchange processes, oPs decays to three photons with a decay rate $7.09X10^6\ S^{-1}$ and producing a continuous energy distribution approximately between region 0 and mc_o^2. The methods used to measure the three photon annihilation process (ortho-positronium) are;

i) A coincidence ratio between decaying three photons to two photons annihilation.

ii) Measurement of lifetime spectra.

iii) Angular correlation measurement of two photon annihilation.

iv)A three-photon coincidence measurement with large angular acceptance.

v)Measurement of the changes in the photon spectrum by single detector.

The single detector method provides a high counting rate method for measuring F. F is fraction of positronium formation and depends on the relation of the peak area of the spectrum over the total area of the spectrum. For example figure(3.3.1a) shows the difference between spectra of positron interactions on aluminum target with different incident energies (Lynn 1980).

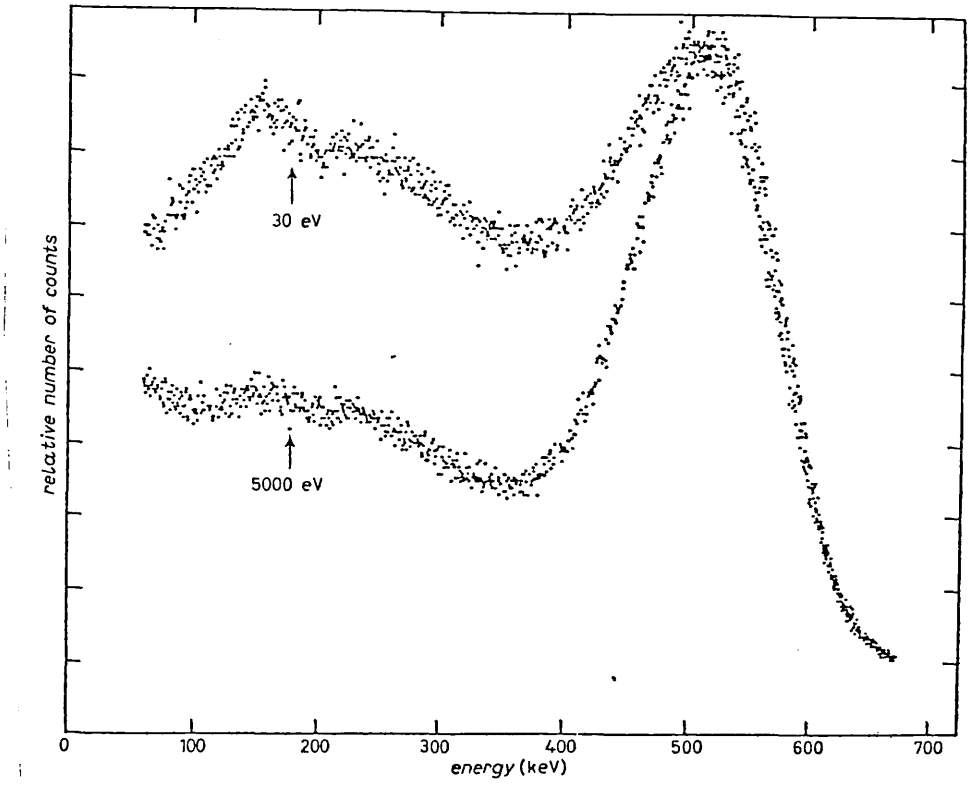

Fig(3.3.1a)

This fraction is calibrated between 0 and 1 for no positronium formation and 100% positronium formation at target surfaces by using incident positrons with high energy above 20KeV and zero energy respectively. The relation of the total area and peak area with positronium fraction is:

$$P_f = N_a(1-F)g_p + F.N_o.g_o + F.N_p.g_p \qquad (3.3.1)$$

and

$$T_t = N_a(1-F)h_p + F.N_o.h_o + F.N_p.h_p \qquad (3.3.2)$$

where N_a, N_p and N_o are the number of the counts per unit area for the direct annihilation of the positron in the metal or surface state, the pPs and oPs annihilation respectively. The quantities of g_o and h_o are the average probability of oPs decay to the three photons in the peak or the full energy spectrum. The g_p and h_p the same as above for pPs. By using ratio $R_i=(T_i-P_i)/P_i$, and substituting in 3.3.1 and 3.3.2 thereby eliminating the variations in the beam current between 0 and 100% which the result is same as equation (3.2.2).

3.4-Physical adsorption:

3.4.1-Introduction:

Films on surfaces are created when the particles are held by van der Waals force on the cooled surface of the substance (substrate). This processes has been called adsorption, and the particle has been called adsorbate.

In the ideal state at absolute zero temperature there is no vibration and all particles will be adsorbed. But in the equilibrium state positions of the atoms on a space lattice are more stable and regulary repeating. As temperature increase the atoms vibrate more vigorously around their location and then start to move out from their positions (Dash 1975). When gases cool down they tend to be adsorbed as thin films on the surfaces of a substrate under van der Waals forces, rather than condense into droplets or crystals (Dash 1980). The thickness of the films depend on pressure and temperature of the gases. Therefore by the control of the pressure and temperature it would be possible to control the thickness of the film layers. For instance at very low temperature (helium temperature) all the gases

with boiling points above that temperature become adsorbed. This means that the thermal energy of the gases is lower than the surface binding energy and van der Waals force is quite high to bind the molecules on the surfaces.

In physisorption the atoms and surface are not strongly perturbed from their isolated states, this fact and the lack of specificity might suggested that the properties of the physisorbed films can be understood without any detailed knowledge of the nature of the adsorbing surface. But this is not the case, the interactions between substrate atoms and films (adatoms) are important, and also interactions between atoms-atoms (Dash 1975). Therefore the study of adsorbed films give properties of the uncovered substrate and their intraction with individual atoms. The experimental studies of this subject usually are nuclear magnetic resonance, neutron irradiation and electron diffraction on surface etc. In this work, in fact from interaction of positrons with surface atoms, we investigate the adsorption of gas molecules on graphite.

3.4.2-van der Waals force:

The lower energy or force needed to hold nonpolar neutral molecules together are the so-called London dispersion force or van der Waals type. As two atoms or molecules are brought together their charge distributions gradually overlap, thereby changing the electrostatic energy of the system. The only general statement that can be made is that the potential has a minimum at a seperation r and it rises at less than this separation. At sufficiently close separations in the region of strong overlap, the repulsion increases very rapidly because of the Pauli exclusion principle. Although there are no expressions valid over the entire range, one of the most traditional forms is

Leonard-Jones potential

$$U(r)=4.\epsilon\,[(\sigma/r)^{12}-(\sigma/r)^{6}] \qquad (3.4.2.1)$$

where U(r) is simple summation of pair intractions, that is the intractions between neutral non-polar atoms and the surface of a van der Waals solid.

$$U(r)=\sum_i U_i(\,r-r_i\,) \qquad (3.4.2.2)$$

where r_i represents the location of atoms of the solid. U(r) is binding energy of gas molecules with distance r from substrate atoms. The life time of the adatoms on the substrate is not long because of the adatom trying to escape from its site to neighbouring sites. This migration happens even at absolute zero temperature by tunneling through the potential barriers between sites.

3.4.3-Thermodynamics of physisorption:

The theoretical formula of adsorption developed from thermodynamics began with Gibb's great work on the equilibrium of Heterogeneous substances. In the equilibrium system of adsorption the exchange of particles between films and vapour is constant and energy between substrate and adsorber is minimum. Consider a substrate which is a relatively stable solid with surface area A containing some adatoms adsorbed is a mixture of film and vapour. The mixture of three states substrate, films, vapour having minimum energy E_0 and high level energy E_i with energy density $\Gamma(E)$. In thermal equilibrium of adsorption system at temperature T the probability of each states with energy E_i is given by

$$W_i=\exp(-E_i/kT)/\sum_i \exp(-E_i/kT) \qquad (3.4.3.1)$$

where

$$\sum_i W_i=1 \qquad (3.4.3.2)$$

For simplicity of the calculation we assume three states only substrate (s), films (f) and vapour (v). The numbers of the sites of

substrate is N_s, and numbers of the atoms or molecules in film is N_f, and number of the vapour atoms or molecules is N_v. The fixed number of the particles in the system is Z which it is given as

$$Z=\sum_i \exp(-E_i/kT)=\int_{E_o}^{\infty}\exp(-E/kT)\,\Gamma(E)dE \qquad (3.4.3.3)$$

and defined $Z=Z_f.Z_s.Z_v$. The total energy of the system has been calculated by summation over states as

$$E=\sum_i W_i.E_i=\sum_i E_i.\exp(-E_i/kT)/\sum_i \exp(-E_i/kT) \qquad (3.4.3.4)$$

The expression above can be re-written as

$$E=-(d\sum_i \exp(-E_i/kT)/d(1/kT))/Z=-d(Ln(Z))/d(1/kT) \qquad (3.4.3.5)$$

where $E=E_s+E_f+E_v$. From thermodynamic properties the total energy of system is

$$S=-k.\sum_i Ln[(W_i)!]=-k.\sum_i W_i Ln(W_i) \qquad (3.4.3.6)$$

where $S=S_s+S_f+S_v$ and therefore it can be calculated simply by

$$S=E/T+k.Ln(Z) \qquad (3.4.3.7)$$

similarly we can write

$$S_s=E_s/T+k.Ln(Z_s),\quad S_f=E_f/T+k.Ln(Z_f),..etc \qquad (3.4.3.8)$$

The Helmholtz free energy is given by

$$F=-k.T.Ln(Z)=E-T.S \qquad (3.4.3.9)$$

From the first law of thermodynamics we have

$$dE=dQ-\sum_\alpha X_\alpha dx_\alpha \qquad (3.4.3.10)$$

using other properties of thermodynamics like enthalpy and Gibb's free energy of the system and finally find out

$$S_v=-(dF_v/dT)_{N_v,V}=N_v.k.Ln(e^{5/2}V/N\lambda^3) \qquad (3.4.3.11)$$

$$P=-(dF_v/dV)_{N_v,T}=N_v k.T/V \qquad (3.4.3.12)$$

$$\mu_v=(dF_v/dN)_{T,V}=-k.T.Ln(kT/P\lambda^3) \qquad (3.4.3.13)$$

where μ_v is chemical potential of vapour and $\lambda=h/(2\pi mkT)^{1/2}$, and it was assumed that the vapour behaves as ideal gas if substrate interactions are absent. Finally the vapour pressure can be calculated from expression (3.4.3.12), and (3.4.3.13) as the following

expression

$$P=(2\pi m/h^2)^{3/2}.(kT)^{5/2}\exp(\mu_v/kT) \qquad (3.4.3.14)$$

For more details of the above calculations see appendix I of this thesis.

3.4.4-Langmuir monolayers:

In this model consider the fixed number of identical sites (N_s) with each site capable of adsorbing one atom of gas with binding energy ε_o. Assuming that all the atoms are completely localized on the separate distance sites, and obey Boltzmann statistics, therefore the Z calculated by

$$Z_f = \sum_i \exp(-E_i/kT)=Q(N_f,N_s)\exp(-E(N_f)/kT) \qquad (3.4.4.1)$$

and $Q(N_f,N_s)=N_s!/(N_s-N_f)!.N_f!$. The Helmholtz free energy given by

$$F_f=-kTLn(Z_f)=-kTLn[N_s!/(N_s-N_f)!.N_f!.\exp(-\epsilon_o/kT) \qquad (3.4.4.2)$$

and by using Stirling's approximation we can write

$$F=N\epsilon_o-kT[N_s Ln(N_s)-N_f Ln(N_f)-(N_s-N_f)Ln(N_s-N_f)] \qquad (3.4.4.3)$$

In previous sections we explained the chemical energy relative to partial derivation of Helmholtz energy as $\mu=(dF_f/dN_f)_{T,Ns}$, also by substituting (3.4.3.13) can be written

$$(N_s/N_f-1).P=(2\pi m/h^2)^{3/2}(kT)^{5/2}\exp(-\epsilon_o/kT) \qquad (3.4.4.4)$$

where $N_s/N_f=x$ is called coverage of the monolayer on the substrate and it is easily carried out from above expression as

$$x=[1+(2\pi m/h^2)^{3/2}(kT)^{5/2}\exp(-\epsilon_o/kT)/p]^{-1} \qquad (3.4.4.5)$$

This means the coverage with assumption of localized atom on the substrate sites depends on the vapour pressure and temperature of adsorber and substrate. Then by controlling the temperature in an isothermal measurement it is possible to find a relationship between pressure and coverage. Most of the experimental measurement which has been done so far has been for the isothermal case.

3.4.5-Boltzmann approximation:

In the Langmuir monolayer the assumption was that the localization of the adatoms on the site of substrate without any movement. But if the adsorption is to be as a fluid it is not possible to use the above expression (3.4.4.5) for the coverage of the layer. In this case the Boltzmann approximation is useful to use for the coverage of the layer. Consider a uniform smooth attracting substrate of area A and N_S particles are adsorbed with binding energy ϵ_o of each particle relative to surface-normal motions. The film particles can translate freely in the x,y surface-parallel directions. Therefore the energy function of the film is

$$E(p,r)=-N_f(\epsilon_o)+\sum_i^N (p_i^2/2m) \qquad (3.4.5.1)$$

at sufficiently high temperature and low density this approximation can be used under condition $n\lambda^2<<1$, and $n=N_f/A$ is number of the films atoms or molecules divided area of substrate or unit area. In this case the Z calculated as

$$Z=(1/N_f!).[A\exp(\epsilon_o/kt)/\lambda^2]^N \qquad (3.4.5.2)$$

The Helmholtz energy is given by

$$F=-N_f[\epsilon_o+kTLn(Ae/N_f\lambda^2) \qquad (3.4.5.3)$$

and

$$\mu_f=(dF_f/dN_f)_{T,A}=-\epsilon_o+kTLn(n\lambda^2) \qquad (3.4.5.4)$$

Then

$$P=(n/\lambda^2).kT.\exp(-\epsilon_o/kT). \qquad (3.4.5.5)$$

where $\lambda=h/(2\pi mkT)^{1/2}$. In this work both formula have been used to fit the data which we will explain later.

3.4.6-Gas adsorption on graphite:

The adsorption of gases on the surface of the graphite has been investigated for many years by different methods such as low energy electron diffraction (LEED), Neutron diffraction on the surface, heat capacities measurements, calorimetric measurements etc. The graphite,

carbon black or exfoliated graphite, known commerically as grafoil, is a good substrate for studies of adsorption of gases. This is because some properties of graphite, such as, large surface area, energetically uniform surface area, and finally it can be removed any impurities on the surface easily by putting it at high temperature under high vacuum.

The gases, such as argon, nitrogen, oxygen, and helium adsorbed on graphite have been studied by many methods. The physical properties of the adsorption of these gases on the graphite surface are completely different and all depend on the vapour pressure and temperature. Furthermore higher vapour pressure is associated with higher temperature at monolayers coverages of the gases on substrate (Kjems et al 1984). The surface area of substrate can be found by adsorption of the gases on the surface, as monolayers registered on the surface, by two methods;

1)By the amount of the gas adsorbed on the graphite surface (e.g; 415 CC of nitrogen on 60.5 gr of graphite gives a surface area 1815 m^2 considering the molecule occupies 16.4 $\mathring{A}^2$)

2)Determination of the quantity of the gas registered on the surface $(\sqrt{3} \times \sqrt{3})$.

The adsorption of nitrogen and argon on graphite carbon black was investigated by Rouquerol et al (1976). They observed in vapour pressure measurements jump at nearly complete coverage at 12 torr for argon and at 8.5 torr for nitrogen. Where later it was reported as order dis-order transition of the nitrogen (Larher 1978). They also reported the area of the occupation of nitrogen molecules coveing three hexagons of graphite 15.7 $\mathring{A}^2$ and for argon molecules 12.5 $\mathring{A}^2$.

At very low temperature the gas molecules on the surface is like solid with binding energy ϵ_o. This binding energy was calculated for

nitrogen on graphite by Steele (1978) ϵ_0=1110 K which was latter improved by Bruch in 1983. He found ϵ_0=1159 K for nitrogen on the graphite by addition of the quadrapole-quadrapole interaction to London-Jones potential. The oxygen binding energy was calculated by Patrykijew et al in 1983, ϵ_0=1050 K. Recently the transitions of structure of solid layers was observed for oxygen on graphite at very low temperature 11.3 K from antiferromagnetic to ferromagnetic, or $\alpha-\sigma$ and $\sigma-\beta$ etc by Stephens et al 1980, and Toney et al 1984. The transition of order to disorder structure of nitrogen was observed above 50 K by Kjems et al 1976 and later by Larher 1978. He reported the transition of solid to fluid nitrogen at 80 K and it was 10 K above the value reported by Chang and Dash. But in 1983 the tricritical points of the nitrogen on graphite was reported at 85.34 K by Miner et al. The tricritical point is the end point of the commensurate-solid-fluid coexistence region near the monolayer.

Recently, positron annihilation experiment (lifetime measurements) was used to investigate the monolayer experiment of nitrogen and argon on the graphite by Jean and Zhuo 1985. They observed that maximum positronium was emitted at half coverage of the gas at 77 K. They observed the transition temperature of the monolayer solid to liquid and gas, for nitrogen and argon.

The light gases like helium and hydrogen, also adsorbed on grafoil, at low temperature were measured by (NMR) and (NDM). Dash has mentioned that there is no experiment, so far to show the monolayer of helium above 100 K.

Chapter IV Instrumental details of experimental equipment.

4.1-Introduction:

The system which is usually used in Doppler broadening spectroscopy is contained of a high resolution semiconductor detector as it was mentioned in the previous chapter. The intrinsic germanium planar detector that was employed in this study was supplied by Princeton Gamma-Tech (PGT), with active volume of 200mm^2 (16mm diameter and 9.2mm thickness). A preamplifier the heart of which is a field-effect transitor is incorporated with detector and is mounted at the end of a cooling system (cryostat). The detector should be cooled by filling the cryostat with liquid nitrogen twice a week. The power supply to the detector was 2000 volts, by a Tennelac TC941 high voltage power supply. The preamplifier uses optical feed back and there is a reset pulse (8 microsecond rise time) that is generated periodically to compensate for (a) leakage current in the detector and (b) detector currents caused by observed radiation. The output pulses from the preamplifier are of positive polarity. These pulses are then amplified to about six volts amplitude with less than 100 microsecond rise time, by the means of a main amplifier (Tennelac TC205 amplifier). The resolution of the detector was found to be 1.12keV at full width of half maximum (FWHM) for the single Gamma-ray ^{85}Sr of 514kev energy.

A typical schematic diagram of the system is shown in figure(4.1.a). It can be seen that our system consisted of three parts: i)electronic circuits, ii)low temperature system (cryostat), iii)high temperature system (furnace).

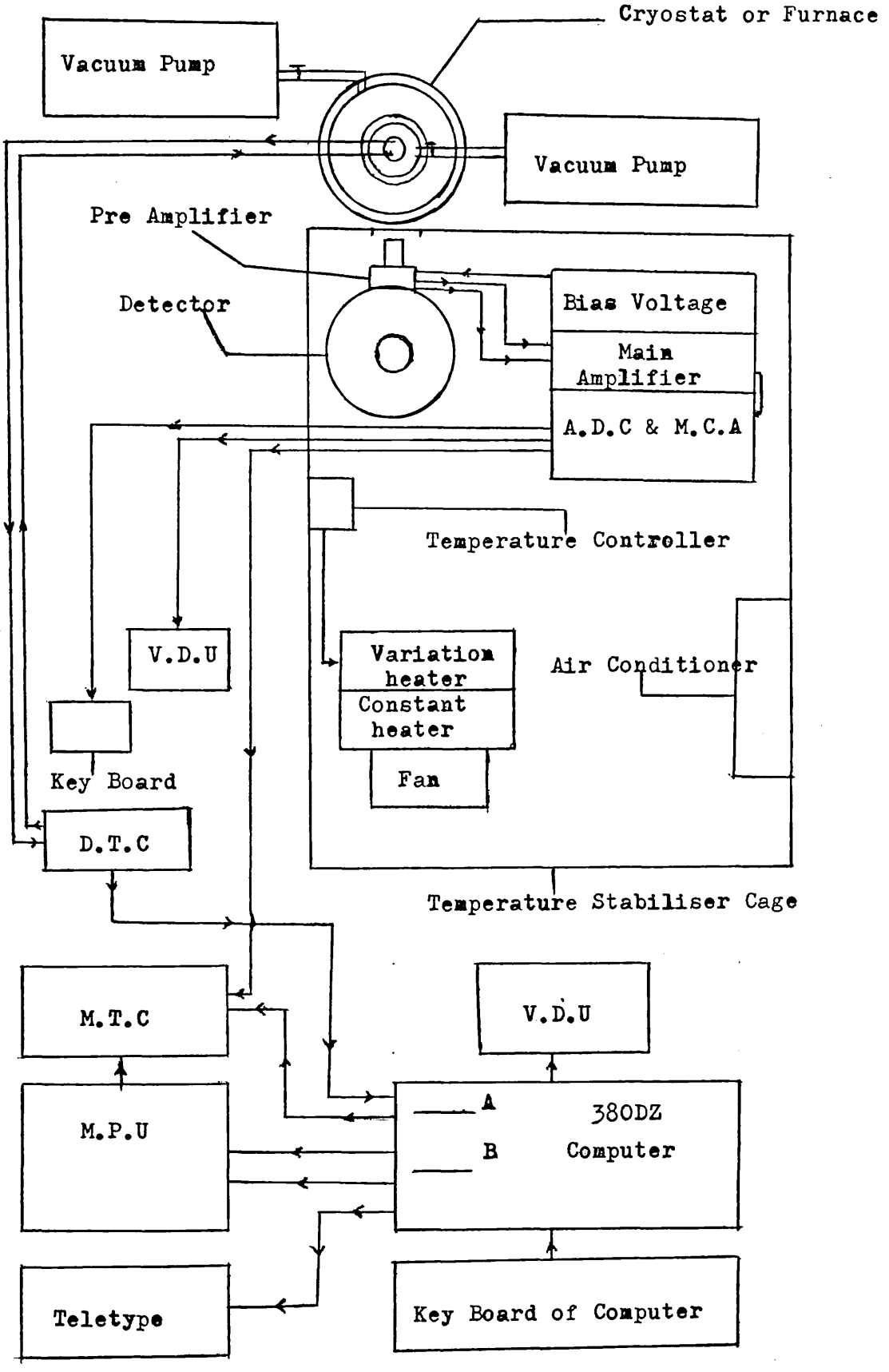

Fig(4.1.a) The schematic illustration of the Doppler-broadening system, employed throughout the work.

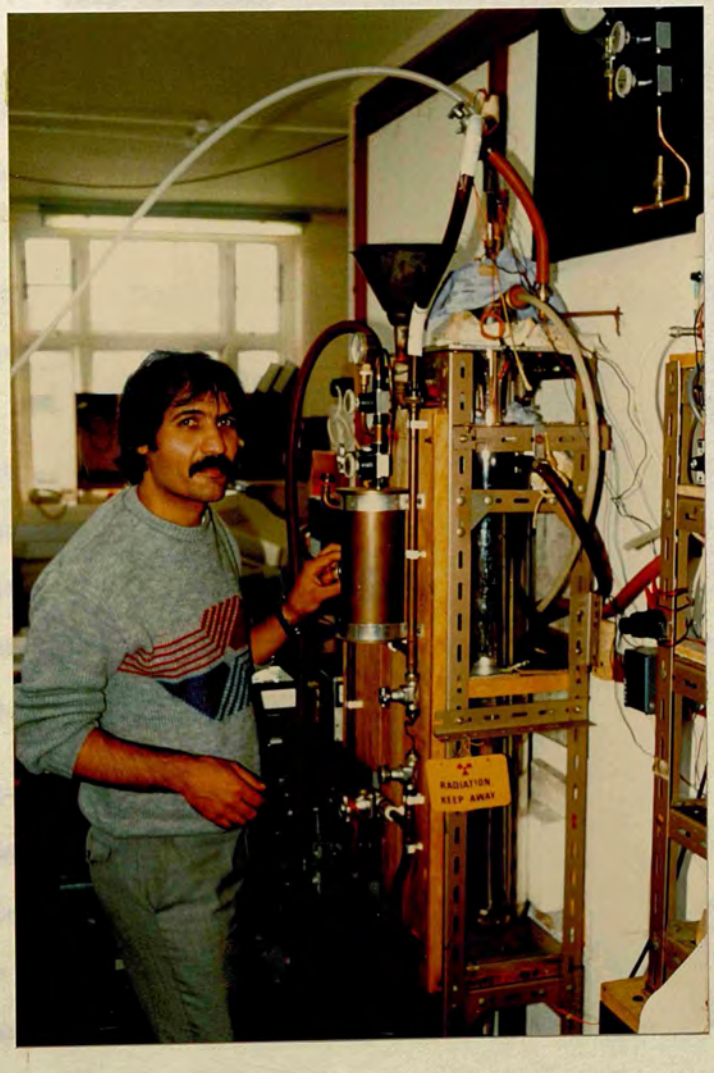
RADIATION
KEEP AWAY

4.2-Electronic instruments:

The electronic systems were used in this work are: a Laben 8215 analouge-to-digital convertor(ADC), a Multichannel analyser with memory (MCA Link system), a Digital temperature controller (DTC), a master temperature controller (MTC), and a 380DZ micro-computer incorporated with a Microprocesser unit, and a V.D.U.

4.2.1-(ADC) and (MCA):

Unipolar output pulses from the main amplifier were fed to the (ADC), with a fast converter time about 4.5 microsecond plus pulse rise time. These pulses were digitised linearly according to their amplitiude. Then the output from (ADC) was fed to the analogue input of a multichannel analyser with 4096 channels. Practically only half of the channels were used by off-setting the MCA. We were able to obtain gamma-ray energy distribution of about 93.5ev per channel. The data obtained by the detector were stored in a Nova-2 computer with 8K memeory, supplied by Link-system Ltd. Then the output data were typed by a teletype and kept on the disk drive of a 380DZ computer. These data were collected after two hours run while a total of 355 channels were used. For some measurements in this work we added about 200 channels, in the 340keV region of the whole spectrum, to the data of each run. One V.D.U was connected to (MCA), so that it was possible to see the whole spectrum of the annihilation lines on the screen.

4.2.2-380DZ micro-computer:

The 380DZ double density disk with 85K memor y was used, incorporated with the electronic system to control the whole system during the data accumulation. First of all a programme, which was written and developed by Umar Rao, was loaded into the memory. There

are some information which are asked for by the programme such as starting temperature, final temperature, title, etc. must be supplied by the user. There are also some output pulses provided by the programme which can do the following functions. The required temperature can be obtained by sending one of above output pulses, designed for this purpose, to MTC. Having obtained the required temperature the MTC is stopped by another output pulse. One output pulse sent by computer erases the previous data of MCA and another one starts it for a new run. At the end of the run the MCA would stop by another output pulse. Finally the collected data are stored on the provided disk and then printed out by the teletype. A sample of the output spectrum is appended in the appendex II.

The same process was repeated for the next run after the temperature of the new run had stabilized at the set temperature. The only disadvantage of this process is that the memory of the computer is not enough to collect the whole spectrum data, if necessary. This problem was fortunatly solved later by using another 380Z computer incorporated with the main one. The adventage of this computing system is that the experiments can be per formed automatically with more accuracy.

4.2.3-Master temperature controller (MTC):

The functions of the spectrometer of the MCA are controlled by MTC. There are two operation on MTC, one is manual and the other is automatic. If the manual operation is used, every thing should be controlled by the user. But in the automatic operations the MTC is operating by the use of a programmable cycle controller. The pulses which are fed from 380DZ to MTC controls the interval time between every two successive runs, the increment temperature of the sample and

erase the MCA to make the system ready for a next run. The MTC is in series with 380DZ computer, microprocesser unit, and DTC.

4.2.4-Digital temprature controller (DTC):

Another electronic system and a very important one is DTC which reads the temperature of the sample by means of a thermocouple input (mV). The output power of the DTC is fed to the heater wire of sample holder. This output is proportional to sample temperature. The temperature was calibrated with liquid nitrogen or helium temperature references. The calibration data was given to the computer as initial information, which was stored in the memory of the computer, Now any reading from DTC can be compared with the calibration data and converted to the temperature unit (K or ^{o}C). The wire heater of the sample holder had a resistance of 70 ohm and was supplied by the manufacturer with maximum temperature effect of 250 ^{o}C. At temperature equilibrium the output power supplied from DTC to the heater will remain constant, provided, when, there is no difference between the setting and reading on the DTC.

4.2.5-Stabilization of electronics system:

It is necessary to reduce the electronic noise and also the drift on position of the spectrum, which is affected by temperature fluctuation of the surrounding environment and main electric power. The best idea was to design a cage temperature controller and use a magnetic stabilizer to fix any fluctuations in the frquency and voltage from the main power to the system. The cage temperature controller is shown in figure(4.1a). It is consist of an air conditioning system to keep the cage cold, a constant heater, a fan, and finally a variable heater control switch (on or off) which works by mercury-to-glass thermometer. All these instruments are incorporated

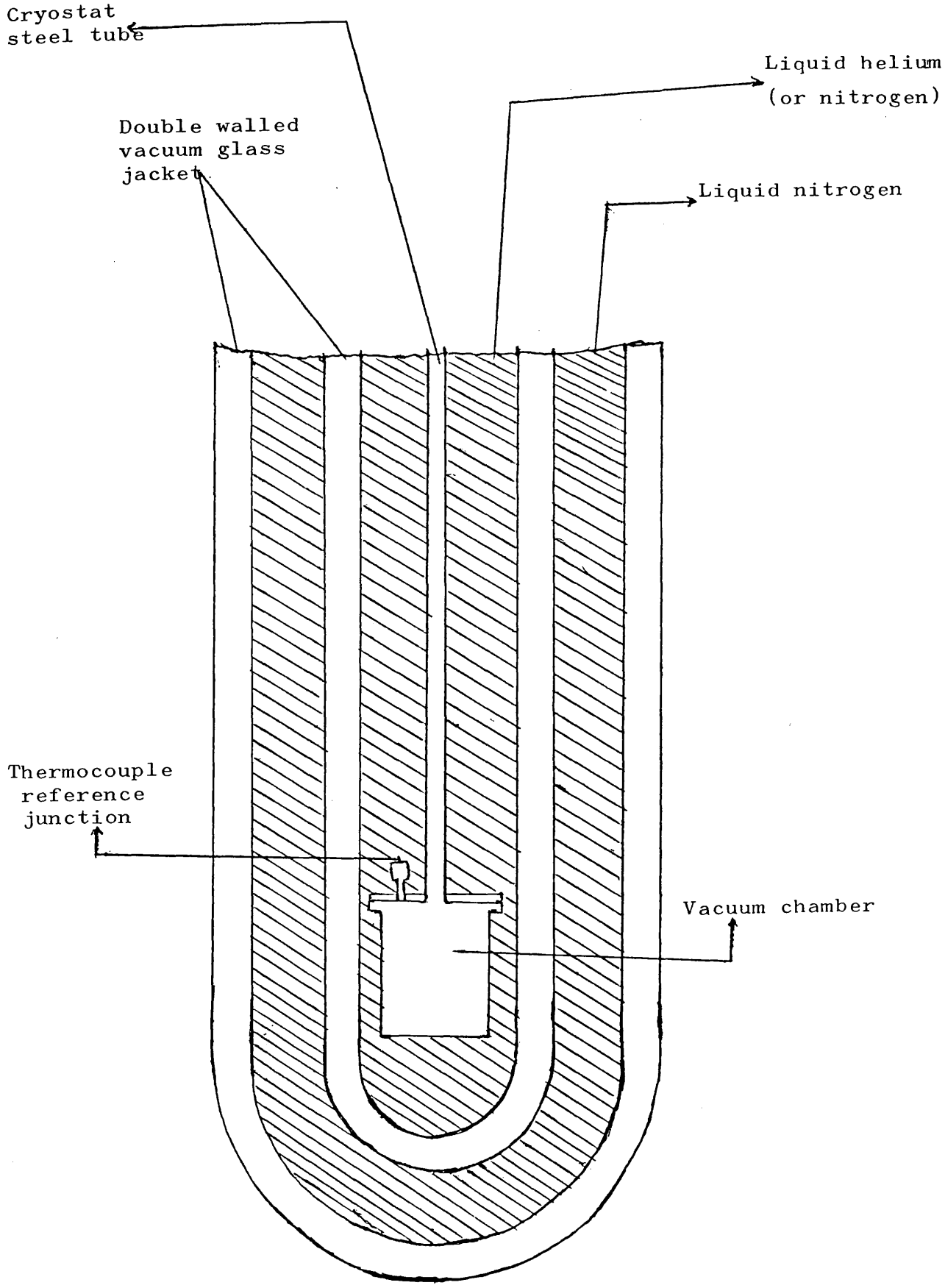

FIG(4.3.1a) Cross-section of the pyrex liquid nitrogen or liquid helium dewar.

together to keep the temperature of the cage constant at 21.5 ^{o}C. The walls of the cage are covered by 5cm thick polystyrene thermal insulator. The MCA, amplifiers, DAC and detector were kept in the cage. The detector was mounted in the corner of cage in front of the aluminum foil window.

In most of our measurements the single Gamma-ray radiation from ^{103}Ru with energy of 497keV was used. The significance of this source is that it introduces a new parameter as G-parameter which shows any drift in the position of the line shape of the peak. The G-parameter supposes to be stright line as a function of temperature therefore any points above or below the G value more than 1% correspond to the line shape (F-parameter) which is not reasonable and should be omitted from the analysis.

4.3-Low temperature measurement (Cryostat):

To investigate the positron annihilation in a large temperature range of 4.2K to 480K, it is necessary to design a low temperature cryostat. A schematic diagram of the cryostat is shown in figur(4.3.1a). This containes two concentric pyrex dewar vessels having outer diameters of 15cm and 9mm respectively. The sample holder has been mounted in the inner dewar, and both dewars have a double wall jacket evacuated by vacuum pump. The outer dewar was filled with liquid nitrogen and the inner one filled up gradually by liquid nitrogen or helium.

The sample holder is mounted in a brass vacuum chamber which is thermaly insulated from the sample holder. It is made from 99.99% copper with two grooves on the top and bottom as can be seen in figure(4.3.1b). The heater wire was wound around these grooves, with total resistance of 70 ohm. In between these grooves the sample

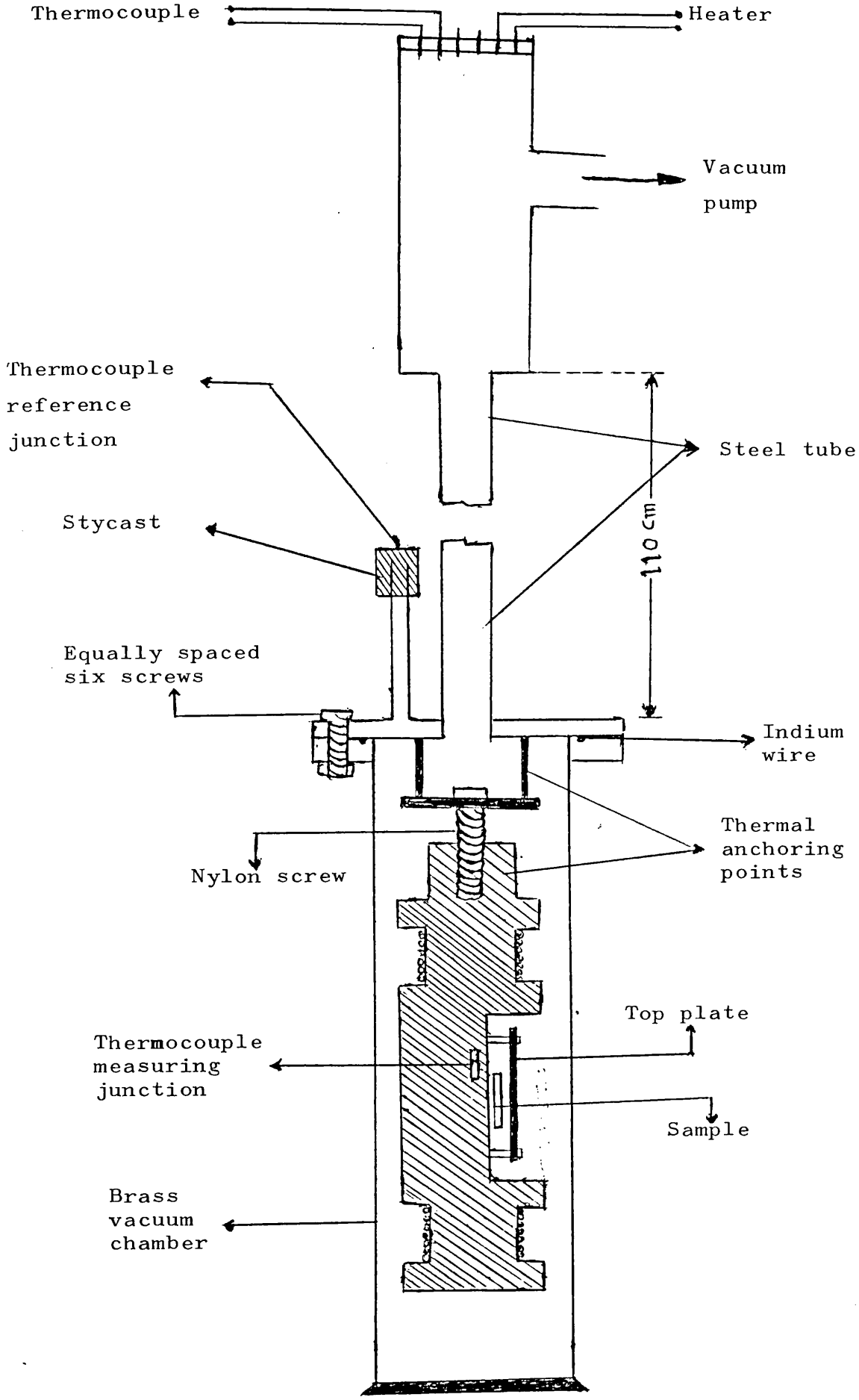

FIG(4.3.1b) A schematic drawing of the low temperature cryostat.

specimen is mounted, and it is held by a sheet of aluminium, which is screwed up to the sample holder. The Au+.03% Fe thermocouple is used to measure the temperature of the sample, and as it shows in the figure the measuring junction of thermocouple is screwed to the sample holder and the reference junction goes out of chamber, which is covered by stycast. There is a shallow groove on the top edge of the brass chamber which filled by an indium seal as washer, that is fixed on the chamber lid with six screws. The brass chamber is usually kept under vacuum better than 10^{-6} torr at room temperature before measurement for at least twenty four hours. Two output and input wires were connected to the top of a steel tube for temperature measuring and heating of the sample.

The process for cooling down the sample is as follow; first of all the double walled vacuum glass jacket and chamber must be evacu ated at room temperature for one day. Then the outer dewar of the cryostat was filled up with liquid nitrogen and the inner dewar filled up gradually. After at least five hours the temperature of sample became 80 K. To reach the liquid helium temperature (4.2 K) it is important that the system first be cooled down to 77.3 K and then the liquid nitrogen is blown out and replaced by liquid helium. A small amount of the helium exchange gas was used to speed-up the cooling of the sample from room temperature and maintain the sample temperature at low temperatures (77 K or 4.2 K).

Heat leak through the thermocouple and heater wires is a problem. A good temperature stability at the lowest temperature requires the elimination of this heat injection to the sample, and was best done by thermal anchoring of wire before they reached sample holder.

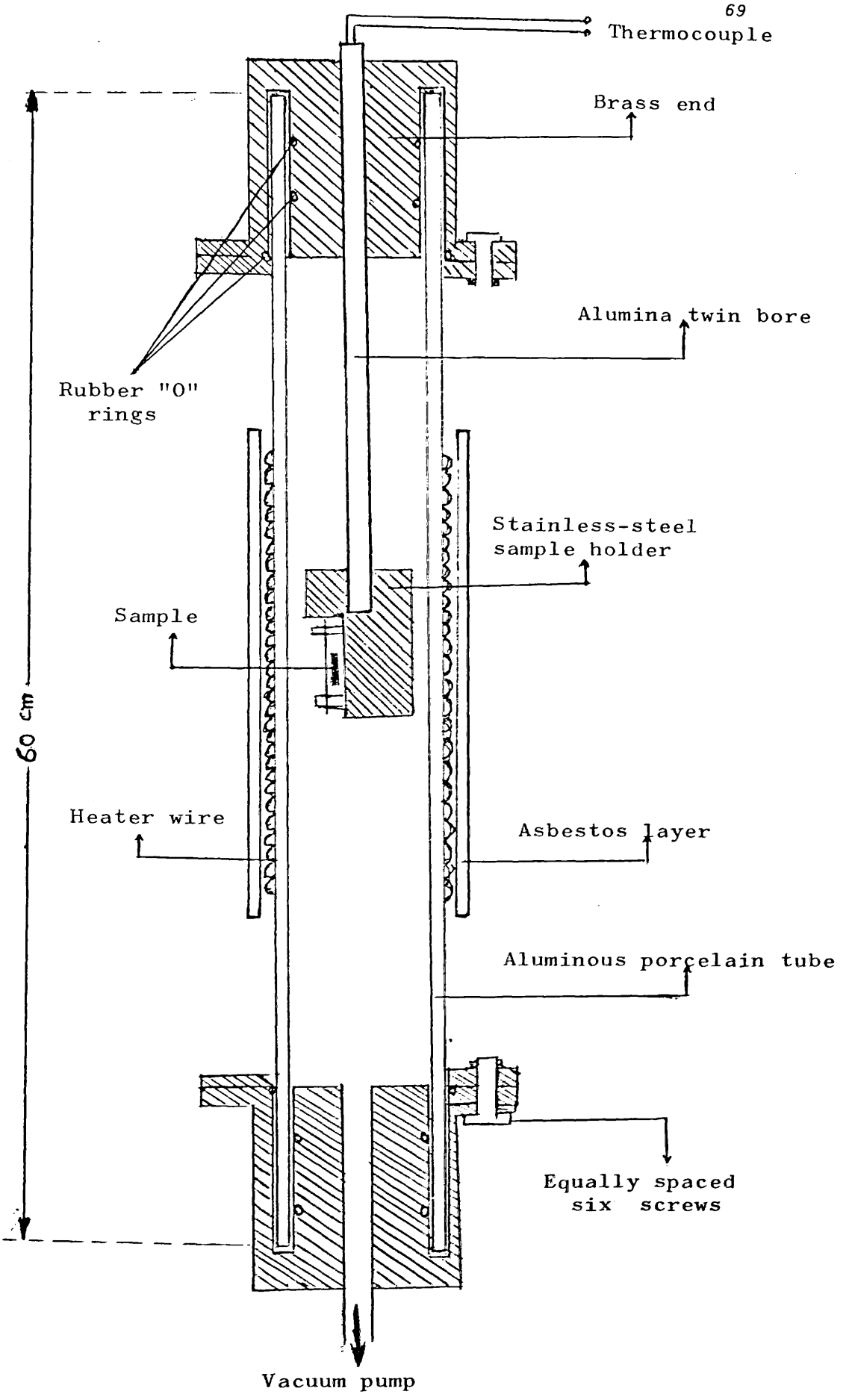

FIG(4.4.1a) A schematic drawing of the high temperature furnace.

4.4-High temperature measurement (Furnace):

In order to study positron annihilation from room temperature up to the melting temperature of the specimen, it is necessary to design a tubular high temperature furnace. This furnace is made from a thermal aluminous procelain tube and is 60cm long with a nominal bore of 2.25cm shown in figure(4.4.1a). A piece of stainless steel sample holder, was attached to the end of the 30cm alumona twin bore of 3mm diameter to maintain a fairly homogeneous temperature distribution in the sample. Aluminous porcelain was used because of two adventages, firstly it is a good electrical insulator but not thermal insulator, secondly it dose not outgas appreciably which may contaminate the sample at high temperature. Both of the tubes were held by two brass hats,which were fitted by rubber "O" rings.

Most metal specimens oxidise at high temperature, which may contaminate the sample, by a small amount of oxygen. Therefore it is essential to heat the metal under high vacuum conditions better than $5X10^{-7}$ torr. As shown in figure(4.4.1a), one end of the brass hat was connected to the high power Edwards E02 diffusion pump. The other end of the brass hat holds the alumina twin bore. The bottom end of the twin bore holds the sample holder where the measurring junction is connected to the sample holder. From the top end of the twin bore the chromel-alumel thermocouple, wires have come out. The referance junction go to the zero point cooler system and the output go to DTC-2. The top end of the twin bore is open to the atmosphere and sealed with araldite. Due to the high vacuum inside the tube, the temperature stability was better than 0.5K.

A high power 40 ohm nichrome heater wire was wrapped directly around the center zone of the aluminous porcelain tube for 20Cm and covered by an insulating asbestos layer, providing a hot zone at the position

of sample, which can safely go up to 1900 ^{o}C. Electrical power to the heater was provided by a power supply which can be controlled by a digital temperature controller (DTC-2), supported by Oxford Instruments External High Power unit. The whole furnace was covered by 1 Cm thick aluminum enclosure.

Chapter V Data analysis

5.1-Introduction:

The characteristic change in the Doppler broadening line-shape of the positron annihilation is representing the behaviour of the positron in matter. It is convenient to introduce a line shape parameter to illuminate this change in Doppler broadening line-shape. The first suggestion was the full width of half maximum (FWHM) of 511kev spectrum by Mackenzie in 1969. But this parameter was found incapable of providing a quantitative description of the physics involved. After that in 1970 Mackenzie et al, introduced another parameter S, which is relating to the integration of the central area of the spectrum over the whole area of the spectrum. It is therefore a parameter that relies on the fact that the line shape narrows as the defect concentration increases regardless of why it becomes narrow. One motivation for S or F parameters definition is their superposition property.

In this work the same parameter was introduced as (F-parameter). Similar to this parameter (N-parameter) used by Schultz et al (1980), and the parameter derived from the running Integrated Difference Curves used by Coleman C.F 1979.

5.2- F and W parameters:

In low temperatures for annealed specimens it is assumed that all the positrons annihilate freely with electrons of the medium. Since the positrons are trapped at high temperature in defects, the trapping fraction is different from the free annihilation fraction because the density of the electrons becomes less at high temperature. Therefore the energy distribution of the annihilation varies with the density of the defects, and the density of the defects depends on temperature

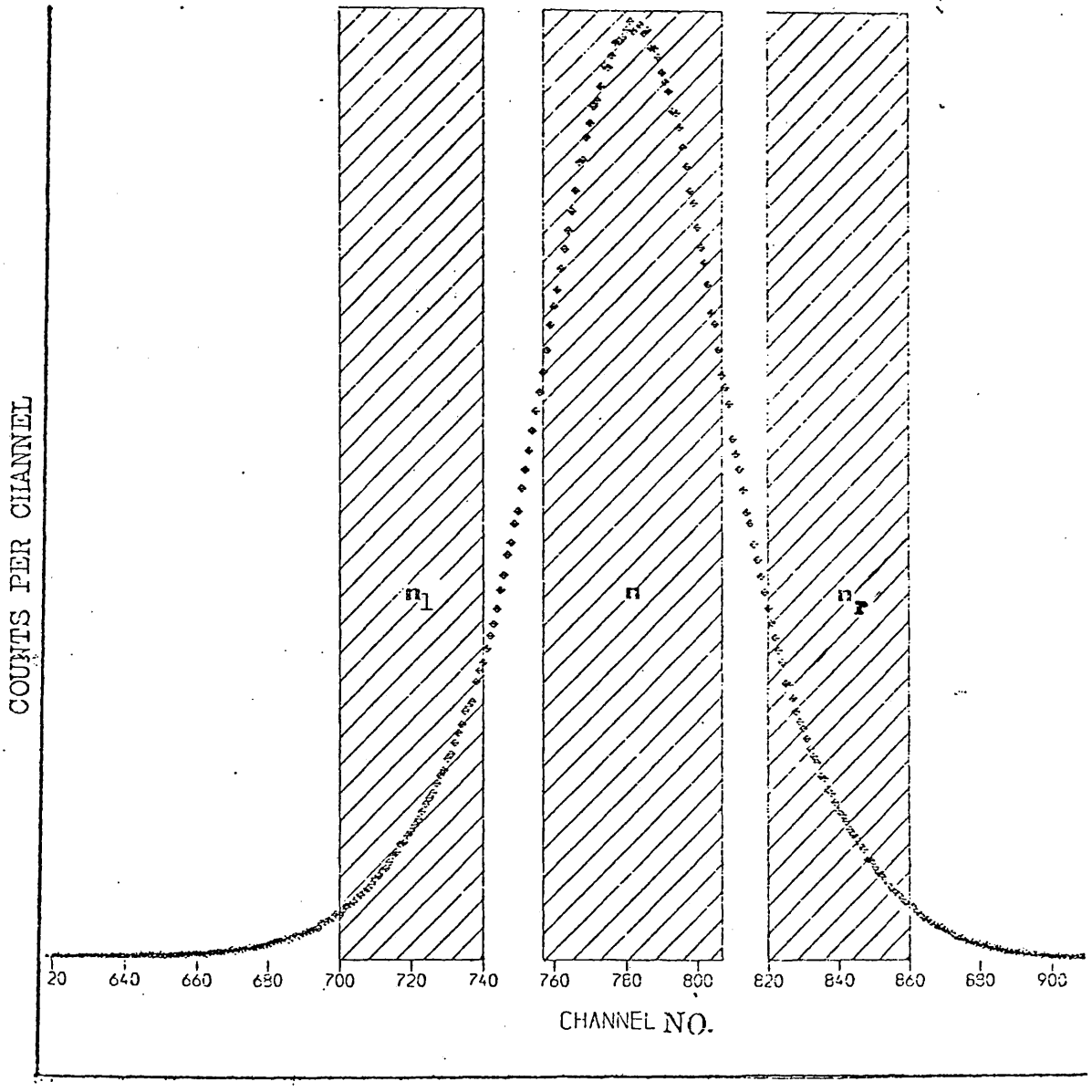

Fig(5.2.1a) The F and W parameter definitions when $n' = n_l + n_r$.

(Campbell et al 1977). As defects are created, the 511kev line-shape becomes narrow. This is primarily reflected, by more annihilations of positrons with free electrons (conduction electrons) and less with high momentum core electrons. The possible narrowest line shape is caused at time of saturation trapping (Schultz et al 1980). Therefore it is convenient to describe this effect on the positron annihilation distribution by a line-shape parameter (F-parameter). As was mentioned above, the F-parameter is defined as the ratio of the center integration counting rate of the line-shape to the whole integration of the line-shape. Thus as the annihilation line becomes narrow the F-parameter increases. If we divide the spectrum of the annihilation line into three regions as illustrated in figure(5.2.1a), N for total area, n for center area and n′ where $n' = n_l + n_r$, for the both wings of spectrum. Then we can define

$$F = n/N \qquad \text{and} \qquad W = (n_l + n_r)/N = n'/N \qquad (5.2.1)$$

The study of Doppler broadening of annihilation radiation involves the distribution of positron momentum, with data accumulation throughout the entire momentum range. Therefore it is convenient to use a similar parameter instead of the F-parameter which is called the W-parameter. The W-parameter is known as tail or wings parameter, and is obtained from the sum of the two symmetrical wings of the annihilation spectrum over total area of the spectrum as shown in figure(5.2.1a).

The modification of F-parameter by considering a different type of annihilation to occur with frequncy f_i, is a linear combination of frequency multiplied by F of the same type of annihilation as

$$F = \sum_i f_i F_i \; / \; \sum_i f_i \qquad (5.2.2)$$

where F_i is the line-shape parameter of each mode of annihilation with

frequency f_i. Since the value of F=n/N=P lies between zero and one, 0<F<1, the statistical properties of the F-parameter are determined by the binomial distribution (Campbell 1979). Therefore we can write

$$P(n)=N!/(n!.(N-n)!).P^{n}(1-P)^{N-n} \qquad (5.2.3)$$

where n=1,2,3.....N and 0<P<1

The variance in the measured central intensity n is given by

$$V(n)=N.P.(1-P) \qquad (5.2.4)$$

and the standard deviation of the line shape is calculated as

$$\sigma(F)=(n.(N-n)/N^{3})^{1/2} \qquad (5.2.5)$$

For a typical value of F=0.5 the standard deviation is $\sigma(F)=0.5/\sqrt{N}$. This is very small compared with the result from the invalid addition of independent counting error in n and N (Campbell et al 1979). The F-parameter reflects the fraction of total annihilation of positrons with conduction electrons. It is increased as the defects density increases in a crystalline solid, and means more positrons are trapped. Therefore the increament in F-parameter is associated with the decrement in W-parameter.

5.3-Background problem:

In Doppler broadening gamma-ray peak shape analysis, any variation in the shape of the annihilation line is relatively small but the line shape parameters which are chosen are highly sensitive with respect to these variation. In such analysis it is expected that the underlying background of the 511kev spectrum to be removed (Chaglar et al 1981). The gamma-ray peaks obtained by semiconductor detector are usually asymmetric and have generally a non-linear underlying background. This background is created, firstly becauce, of compton scattering of high energy Gama-rays (1.28Mev) of ^{22}Na, secondly by incomplete charge collection and photoelectric escape from the active volume of the

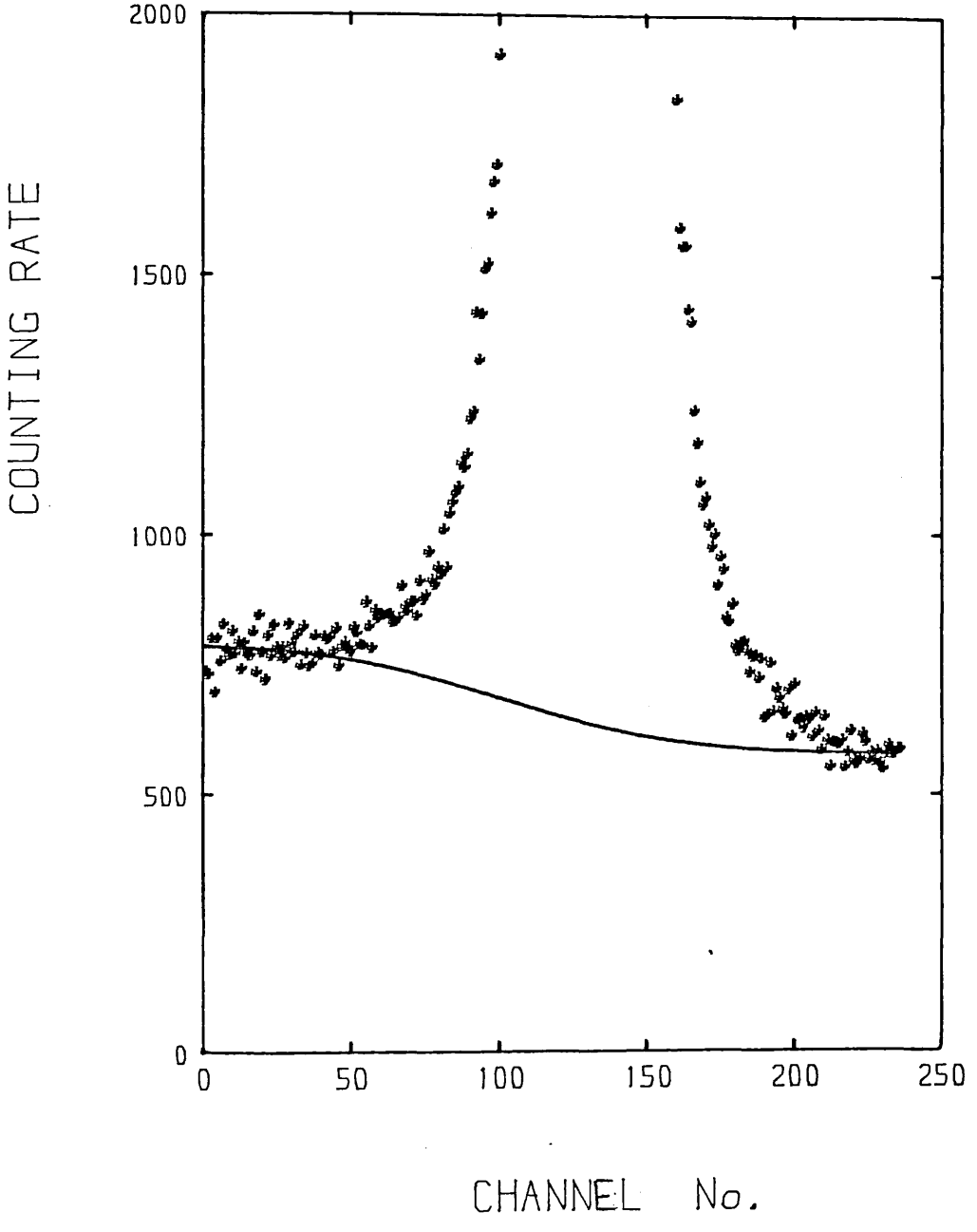

Fig(5.3.1a) Annihilation line shape with non-linear part of the underlying (error function) background.

detector.

Various attemps have been made to define the underlying background of monoenergetic gamma-rays, Kern (1970) used step function, Jorch et al (1976) used linear or polinomial background. For annihilation line shape, Jackman et al (1974) used the following method to define the underlying background. Firstly a background which shows a linear respons to energy was subtracted from the complete annihilation line shape. On the left hand side of the spectrum a straight line was fitted to the region from 486keV to 497keV, and this line was extrapolated to an energy of 503keV with positive slope. Similary on the right hand side of the spectrum another straight line was fitted to the region from 534keV to 542keV and was extrapolated to an energy 518keV. Finally the extrapolated limits were then joined by a straight line to give an underlying background. Some people used polynomial background, and Chaglar et al (1981) used erf(error function) background for underlying background of annihilation spectrum. They found the line shape parameter 25% increase after background subtraction in cadmium data.

In most experiments data were collected from liquid helium temperature up to the melting point of the specimen. Three different cases are distingu ished: a)liquid helium in the cryostat, b)liquid nitrogen in the cryostat, c)furnace run. Consequently two splits can be observed in the F-parameter calculation without any background subtraction from spectrum. It is necessary that the F-parameter to be normalized for these cases. There are two ways to solve this problem either by useing a third order polynomial with constant background, or use error function (erf) with constant background. The erf background is calculated by

$$B(i)=H/2[1-erf((i-i_o)/flhm)]+C \qquad 5.3.1$$

where C is constant background and it is extrapolated from high energy side of spectrum line-shape, i.e subtracted from whole line-shape; H is the average of differences between low energy side (left) and high energy side (right) of the spectrum, i represents the channel numbers, and i_o is the peack position. Figure(5.3.1a) shows the erf background of the line-shape of cadmium specimen at room temperature. The advantage of the erf background over polynomial background is that a smoothly curve of F and W parameters is obtainable.

5.4-Temperature dependence on line shape parameters:

In previous chapter, in trapping model section, it was mentioned that consentration of the defects depends on the temperature. In section (5.2) of this chapter we also mentioned that the F-parameter directly depends on the density of the defect. Therefore it is convenient to say that the line-shape parameters depend on defect concentration, and obviously on temperature. The application of trapping model in Doppler broadening method is discussed in chapter II equation (2.6.9) by assuming that two states of annihilation is occured, it can be rewritten as;

$$F=F_f . P_f + F_t . P_t \qquad (5.4.1)$$

Where P_f and P_t are probabilities of positron annihilation with electron, for free and trapped positron respectively where $(P_f + P_t = 1)$, and F_f, F_t are fractions of the free positron and trapping positron annihilating respectively.

By substituting equations (2.6.8), and (2.5.16) in (5.4.1) it can be shown that;

$$F= \frac{F_F + F_{1v} . A_{1v}^F . \mathrm{Exp}(-H_{1v}^F / kT)}{1 + A_{1v}^F . \mathrm{Exp}(H_{1v}^F / kT)} \qquad (5.4.2)$$

where $A=(\sigma / \lambda).\mathrm{Exp}(S_{1v}^F / k)$, in which, σ is annihilation rate

(assumming temperature independence) and λ is decay rate of free positron. S^F_{1v} and H^F_{1v} are entropy and enthalpy of the monovacancy formation respectively. A small linear rise was observed in F-parameter at low temperature up to room temperature. This is due to thermal expansion of the lattice (Lichtenberger et al 1974), (Rice. Evans et al 1978a). Therefore it is reasonable to say that the F_F and F^F_{1v} are lineary temperature dependents and substitute $F_F = F^o_F(1+\beta T)$ and $F_{1v} = F^o_{1v}(1+\alpha T)$, in expression (5.4.2) and rewrite it as,

$$F = \frac{F^o_F(1+\beta T)+F^o_{1v}(1+\alpha T).A^F_{1v}.\mathrm{Exp}(-H^F_{1v}/kT)}{1+A^F_{1v}.\mathrm{Exp}(H^F_{1v}/kT)} \qquad (5.4.3)$$

Later an anomalous temperature dependence was observed in positron annihilation of cadmium at intermeddiate temperature. It was suggested that this anomaly can not be only due to thermal expansion of the lattice (Lichtenberger et al 1974). Soon the self-trapping modle was suggested by Seeger (1975). By taking this effect into account the F-parameter formola was improved to,

$$F = \frac{P_F.F^o_F(1+\beta T)+F^o_{1v}(1+\alpha T).A_{1v}.\mathrm{Exp}(-H^F_{1v}/kT)+F_{St}(1-P_{St})}{1+A^F_{1v}.\mathrm{Exp}(H^F_{1v}/kT)} \qquad (5.4.4)$$

where $P_{St}=[1+B\,T^{-3/2}\mathrm{Exp}(-\varepsilon(K_o)/kT)]^{-1}$, ε ,B are already described in (2.6).

The expression (5.4.1) can be extended for three states annihilation phenomena. Then form (2.6.9) we have

$$F = F_F.P_F + F_{1v}.P_{1v} + F_{2v}.P_{2v} \qquad (5.4.5)$$

where F^o_{2v} is charactersting of saturation trapping in divacancies. By substituting (2.5.18),(2.5.19) and (2.5.16),(2.6.8) in (5.4.5) the expresion will be more complet as

$$F = \frac{F^o_F(1+\beta T)+F^o_{1v}(1+\alpha T).A_{1v}.\mathrm{Exp}(-H^F_{1v}/kT)+F^o_{2v}(1+\gamma T).D.\mathrm{Exp}(-H^F_b/kT)}{1+A.\mathrm{Exp}(H^F_{1v}/kT)+D.\mathrm{Exp}(-H^F_b/kT)} \qquad (5.4.6)$$

where H^F_b is divacancy and monovacancy binding energy formation, and it

is equal to $(2H^{F}_{2v}-H^{F}_{2y})$. The above expressions are also useful for the W-parameter instead of F-parameter.

5.5-line shape analysis:

The analysis of the gamma-ray spectrum obtained by Ge(Li) detector is very complicated. Various functions were used to analyses 514keV monoenergy gamma-ray specta of ^{85}Sr such as Sampo program by Routti and Pressin (1969), the Kern's functions including step function background, and Mc Neless and Campbell (1970 and 1975). In 1976, Jorch and Campbell used one Gaussian function to be convoluted with a distortion function plus one third order polynomial and a step function background to analyse the single gamma-ray spectrums.

In the case of the positron annihilation line-shape spectrum, the line-shape is broader than pure gamma-ray spectrum. Figure(5.5.1a) shows the difference between ^{85}Sr gamma-ray and positron annihilation line-shape, "both normalise to the same height". In principle the information derived from study of Doppler broadening of annihilation radiation is the same as angular correlation measurement, with relatively poor resolution (Jackman et al 1974). The observed annihilation spectrum is not the true distribution of the gamma-ray of the annihilation radiation, but a spectrum convoluted with the responce function of the detector system which is

$$A(E)=\int_0^{\infty} T(E')R(E-E')dE' \qquad (5.5.1)$$

where E is energy of radiation and it is corresponded to channel number of the spectrum. The problem of how to remove the finite spectrometer resolution function from the experimental points is very difficult. The first attempt was suggested by Hotz et al. He tried to correct the detector resolution function by matrix equation

$$S=X.R \qquad (5.5.2)$$

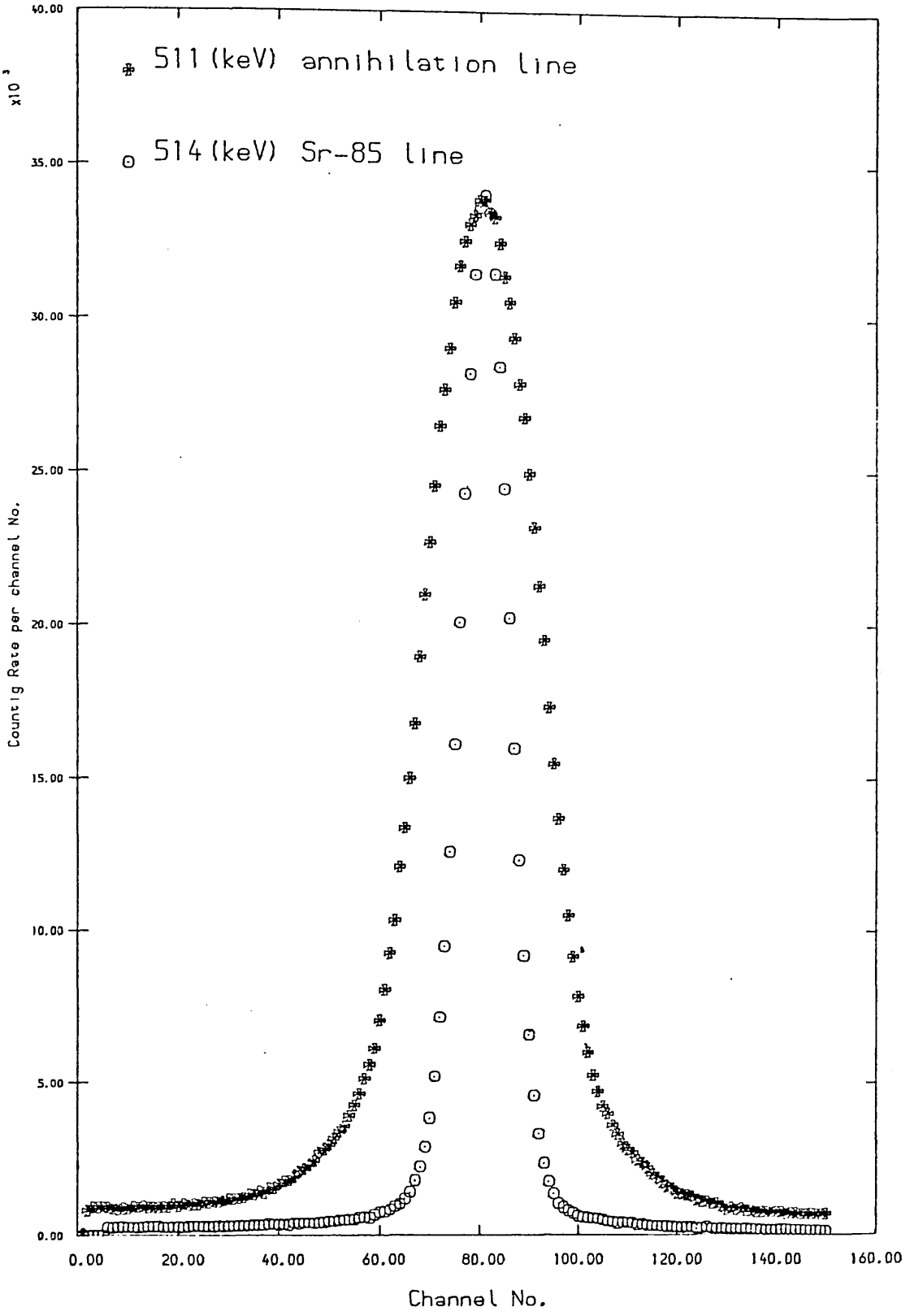

Fig(5.5.1a) Annihilation line in annealed tin compared to 514 keV gamma-ray line ^{85}Sr " normalize to the same height ".

Where S is synthetic spectrum and X is ideal spectrum, and R is resolution spectrum. The synthetic spectrum produces the value of X as

$$X^2 = \sum_i (S_i - A_i)^2 / A_i \qquad (5.5.3)$$

where A_i is experimental data points. Jackman et al (1974) suggested convoluted and deconvoluted method. They first subtracted the background from the spectrum by extrapolation of two linear background, from the both side of the spectrum, to 503kev on the left and 518kev on the right of the center. The extrapolated limited were joined by a straight line. They used the 514keV line of ^{85}Sr as resolution function deconvoluted from data and compared it with a Gaussian and an inverted Parabola. In convolution method the addition result of the Gaussian and an inverted parabola is first convoluted with the resolution function, and then a plus ploynomial background is added to convoluted result to be compared with respect to experimental data by least-squares minimization routine.

Rice Evans et al (1978a) used the convolution method and obtained their result as;

$$Y(i) = \int_{-\infty}^{+\infty} \mathrm{Exp}\left[-\frac{(i-i_o)^2}{2\sigma_g^2}\right] . R(i-i')di' + \int_{-\sqrt{2}\sigma_p}^{\sqrt{2}\sigma_p} \left[1 - \frac{(i-i_o)}{2\sigma_p^2}\right] R(i-i')di' \qquad (5.5.4)$$

where R(i-i′) is resolution function and i represents channel number. The program used for fitting of the experimental points is called Curfit in which the Nag routine of the least-squares minimization method is utilized. The Curfit program is briefly appended (see appendix III). The expression (5.5.4) is simplified for programs as;

$$A(i) = H_g \mathrm{Exp}[-(i-i_o)^2/2W_g^2] + H_p[1-(i-i_o)/2W_p] \quad \text{for } i-i_o < 2.W_p \qquad (5.5.5)$$

and $$A(i) = H_g \mathrm{Exp}[-(i-i_o)/2W_g^2] \quad \text{for } i-i_o > 2.W_p \qquad (5.5.6a)$$

or $$A(i) = 2H_g \mathrm{Exp}[-(i-i_o)/2W_g^2] \quad \text{for } i-i_o > 2.W_p \qquad (5.5.6b)$$

(Note the expression (5.5.6b) take from Berry and Khangi theses)

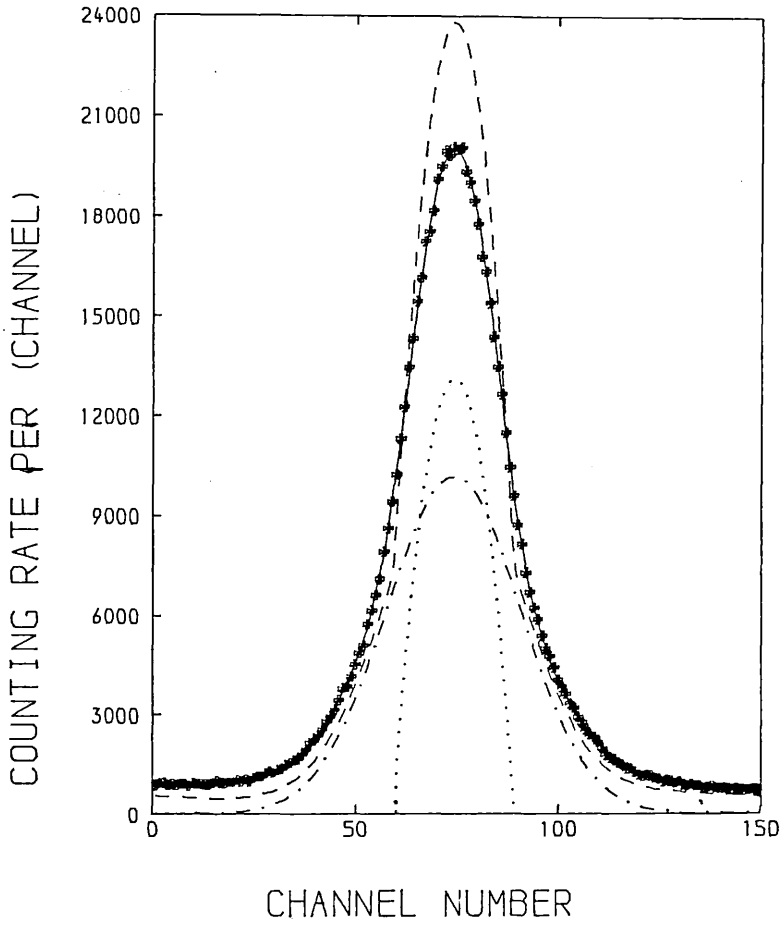

Fig(5.5.1b) Application of the convolution technique to seperate the two components, parabola (dot line), Gaussian (dot-dash line) of the annihilation gamma-ray line in cadmium at room temperature. The dash line is additional of the Gaussian and parabola plus background and the solid line is the convolution result.

where H_g, H_p, W_g, W_p are Gaussian and parabola height and width respectively. The value A(i) was then convoluted with resolution function (514keV line of ^{85}Sr), plus background. The result is given as;

$$y(i)=(1/N)\sum_{j=1}^{m} A(i).R(i-j)+B(i) \qquad (5.5.7)$$

where $N=\sum_{i=-n}^{n} R(i)$, and B(i) is the third order polynomial or error function background. That is y(i) has been compared with experimental data points and then minimized. This minimization means that the χ^2/υ (chi-squared) should be equal to one for the best possible fitting of the data. The chi-squared is given by;

$$\chi^2/\upsilon = 1/(M-N).\sum_{i=1}^{m} (y(i)-C(i))^2/y(i) \qquad (5.5.8)$$

where C(i) is experimental data points, M is number of the points and N is number of the variable parameters used. The value of chi-squared usually lies between 0.9 and 1.5 for positron annihilation in metals (in the case of no trapping). Figure(5.5.1b) shows the result of fitted data for positron annihilation in cadmium with χ^2/υ =1.2. The parabolic contribution generally shows an increase, similar to that shown by F-parameter, as the trapping probability increases.

5.6-Positronium fraction parameter (R-parameter):

As it was mentioned in chapter three, the positrons are implanted at the surface of solid targets. They are penetrated in solid and annihilate in bulk or trapped in deffects after thermalisation. However before this phenomena happens some of them may be diffused back to the surface and bound at surface in image potential (Mills Jr 1983), or leave the surface by capturing an electron from surface to form positronium (singlet or triplet). Statistically one-quarter of bounded positron in singlet state form parapositroniums (pPs), and then annihilate, in short time of about 10^{-10} seconds, to two

gamma-rays with energy of $E_{2\gamma}=mc_o^2$. The other three-quarter of bounded positrons in triplet state form orthopositroniums (oPs), and annihilate in a longer time (about 140 nanosecond) to three gamma-rays with energy of $E_{3\gamma}=2.mc_o^2/3$. Sometimes oPs pick-off either another electron and annihilate to two gamma-rays with shorter lifetime or it annihilates as pPs by spin exchange process (e.g. like positron annihilation in oxygen see chapter 12). In the case of no pick-off or spin exchange processes, the oPs annihilation energy is distributed between zero and mc_o^2. The measured photon energy spectrum of these positrons annihilating from the oPs state is markedly different from the two photons process obtained when positrons decay either in a metal or from the pPs state. There are several manner to determinate the oPs fraction, one of them is measurement of the changes in the photons energy spectrum or total area of line shape by a single detector (Lynn 1983). Mills.Jr and lynn et al in 1980 and 1984 used f(T) for positronium fraction of positron beams interaction on the surface of the specimen, which is calibrated between 0 and 1. They calibrated f(T) by using high energy beam of 25keV interaction on the cold surface of target for zero and low energy beam of a few ev for 1. They observed that f(T) is temperature dependent. In this work a similar parameter to f is introduced. This is taken to be the ratio of total area of the 511keV line-shape spectrum (A), to total area of a part of spectrum in the compton region around of $2mc_o^2/3$ (B). This is obtained as

R=total area(A)/integration over 200 channels or more(B)

In fact the R-parameter is represented as the relation of two photons decay to three photons decay of oPs. The appliction of this parameter is clearly shown in chapter nine, ten, and eleven.

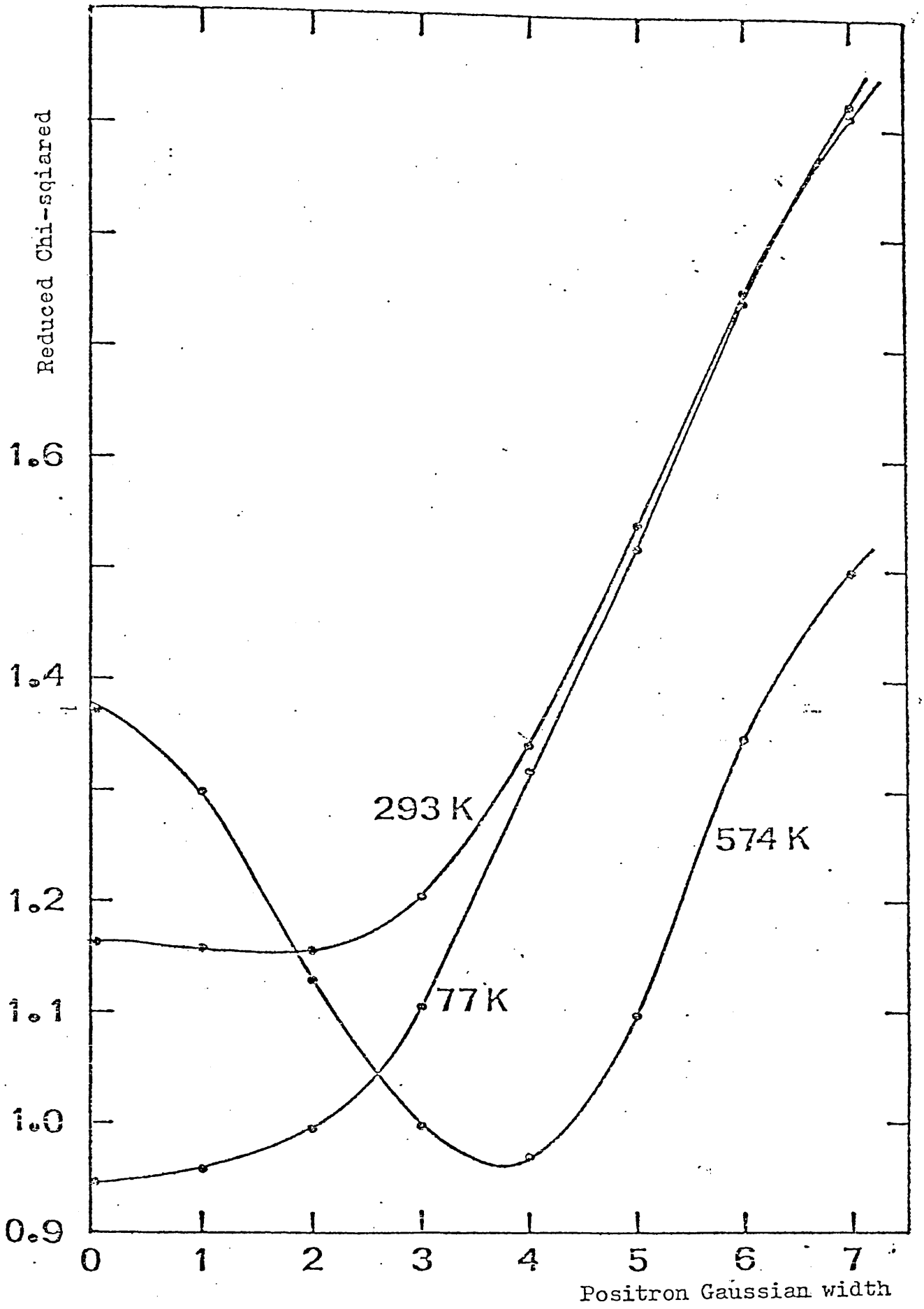

Fig(5.7.1a) The reduced chi-squared against positron Gaussian width in Single Crystal Cadmium.

5.7-Zero-point motion:

It was observed that by applying the convolution method in the metals like cadmium which show strong trapping effects, the goodness of the fitting (chi-squared) becomes worse, as the trapping probability increased. The model of inverted parabola and Gaussian convoluted with resolution function is applicable at best when dealing with completly annealed metal samples in which positrons are not trapped. When the positrons become trapped at vacancies or dislocations in defective samples, the momentum of trapped positron will contribute significantly to the momentum of annihilation pair. This effect is precisely due to zero-point kinetic energy of positron at trapped potential well which is created by defect. Since the trapped positron contributes appreciably to the centre of mass momentum, an effect excluded in the simple superposition of Guassian plus parabola. Therefore an additional a narrow width Gaussian function was introduced into the convolution procedure, reflecting effectively the zero-point kinetic energy of the high localized trapped positron (Jackman et al 1973). This employed Gaussian function with width σ_b, is added to the parabola-Gaussian model and convoluted with resolution function and then compared with experimetal data. Rice Evans et al (1979) found the width of the respond Gaussian for the positron annihilation in single crystal of cadmium to be σ_b=3.6 channels (at 94 ev/channels), where the chi-squared is minimised at this point (figure(5.7.1a)). The zero-point energy expression is given as

$$E = 2X\sigma_b^2/m_o c^2 \qquad (5.7.1)$$

They found the corresponding zero-point kinetic energy of trapped positron to be E =0.4ev.

In addition to the improvement in the reduced chi-squared the initial Gaussian becomes wider but this causes futher narrowing of the parabola

and an increase in the parabola percentage. This narrowing of the electron parabola seems to indicate that the conduction electrons density and local Fermi momentum seen by the positron at the trapping site are smaller than in the regions of the perfect lattice.

According to the trapping model of positron at high temperature (near melting point of the specimen). There should be a saturatiopn region for F-parameter. Rice Evans et al (1978b) consider that at saturation region of the F-parameter of positron annihilation in cadmium, 100% of positrons are trapped, and at low temperature below 100 K there is a zero percent positron trapped (100% untrapped). By this consideration it is convenient to improve the convolution process to a double convolution in two stages. In the first step the resolution would be convoluted and in second step the zero-point energy would be contributed. Therefore the new model of convolution is given as;

$$[P_t\,(\text{parabola+Gaussian})*g + (1-P_t)(\text{parabola+gaussian})]*R \qquad (5.7.2)$$

where * means convolution, P_t is denoted as trapping percentage probability, g is additional Gaussian according to zero-point motion, R is resolution function, and t and f represented trapping and free positron annihilation state respectively. If a third order degree polynomial background parameters is added to the expression above, then all together fourteen variable parameters are used for the fitting of line-shape. This is very difficult to find a satisfactory result. In practice the variable parameters calculated have mostly unphysical meaning (e.g. negative height or width etc) when chi-squared is satisfactory. When the reasonable parameters are obtained the chi-squared is unsatisfactory, which means poor minimization. The obvious advantage of this method, if applied successfully, is that it will provide a reliable means of correlating the F-parameter curve with parabola percentage. However it can be shown how the intensities

of the various analytic function behave as the trapping probability changes, thus establishing a characteristic of defect involved in the trapping process.

Chapter VI Positron annihilation in deformed and annealed cadmium

6.1-Introduction and method:

The annihilation line-shape parameters in many metals in equilibrium show that there are two temperature dependent regions. Firstly there is a linear slope at temperatures below the vacancy trapping region, and secondly there is an exponential increase in positron trapping in vacancy region. The prevacancy effect is known to vary widely between metals. But in cadmium measurements extended to liquid nitrogen temperatures and below by Lichtenberger et al 1975, Kim and Bauyer in 1976 and Rice-Evans et al 1978b show a linear region with a sharp slope above 230 K up to room temperature.

Originally this effect was thought to be due to the thermal expansion of the lattice (Mc Gervey and Triftshauser 1973). But because it was a sharp slope above 230 K and disappeared below 200 K, Lichtenberger et al in 1975 suggested that it could not be thermal lattice expansion. In 1975 Seeger suggested the effect was due to the acoustic interaction of lattice phonons with positrons, and was described as positron self-trapping (see section 2.5).

A variety of defects can be probed with positrons. In the event of 100% trapping a particular defect will be associated with characteristic values of the line-shape parameter (F-parameter) in the Doppler broadening measurements, and the lifetime of the positron in lifetime measurements; e.g. in a deformed sample at low temperature this value is greater than in an annealed sample at the same temperature. In 1967 Mackenzie et al observed that the lifetime in deformed aluminium was 20-30% greater than in annealed aluminium. Similary F-parameters in deformed cadmium are greater than in annealed cadmium at low temperatures.

Method:

Two discs of polycrystalline cadmium with purity 99.9999% and diameter 8mm with thickness 4.5mm, supplied by Koch-light Laboratories Ltd, were used to prepare the specimen. The discs were compressed in a hydraulic press resulting in an average diameter of 11.0mm and a reduction in thickness to 2.2mm. The specimen was then annealed at 500 K for 24 hours under vacuum better than 10^{-6} Torr. After etching the specimen in 35% nitric acid, approximately 150 micro-curies of carrier-free ^{22}NaCl solution was evaporated directly onto centre of each disc. These two discs were sandwiched together and then encapsulated in a wrapping of thin aluminium foil. The specimen-source was again deformed by the hydraulic press at room temperature with approximately a 21% reduction in thickness, after which it was mounted in the cryostat.

Annihilation spectra were then recorded at temperature increments of 10 K between 4.2 K and 409 K, with temperature stabilty better than $\pm$0.1 K. After this set of experiments the specimen-source was maintained at 409 K for 18 hours, then cooled down to 77 K and returned to the hydraulic press immersed in a bath of the liquid nitrogen, compressed further to reduce the thickness by approximately 34%. The specimen-source was mounted on the cryostat at the same temperature (77 K), and then the temperature was taken down to 4.2 K after which the spectrum was recorded from 10 K to 410 K with increments of 10 K. The procedure for sample mounting explained by A.A.Berry (1982 thesis). His data has been reanalysed with more detail in this chapter.

6.2-Line-shape parameter:

The F-parameter was the result of integration over the counting rate of 15 channels of the centre of the spectrum divided by the integration over the whole area of the spectrum. The W-parameter was the sum of the integration of two wings of the spectrum, each wing covering 20 channels, divided by the whole area of spectrum. Initially the error function background was sub tracted from the spectrum, and it was found that the benefits of such a subtraction were outweighed by enhanced fluctuation caused by the background subtraction. The result with background subtracted of positron annihilation in polycrystalline cadmium is illustrated in figure(6.2.1), this fluctuation is clearly shown in figure(6.2.1). Therefore it was decided to employ no background subtraction through this study. Figures(6.2.2) and (6.2.3) show the F and W parameters of the line-shape spectrum. The F-parameter changes about 11.8% at 80 K in the deformed sample compared with the annealed one (the star symbole in the figure 6.2.2), and 5.7% change in the deformed sample at room temperature (triangle on the curve). Deformed cadmium annealed out rapidly at about 150 K to 250 K Rice-Evans et al 1978b. This idea is also supported by our data as can be seen from the curve. The points A,B,C on the curve were backward (cooling the sample) points taken immediatly after 101K,158K, and 219K respectively. This means that the defect concentration remained the same or we can say the defect is frozen in the specimen when it is cooled down suddenly. The detrapping of positrons from defects shows the recrystalization of the specimen after plastic deformation. The specimen was annealed above 340 K, because the point D at 80 K on the curve has been taken immediately after 348K. As can be seen from the curve point D is about 5% down from the original point. The behaviour

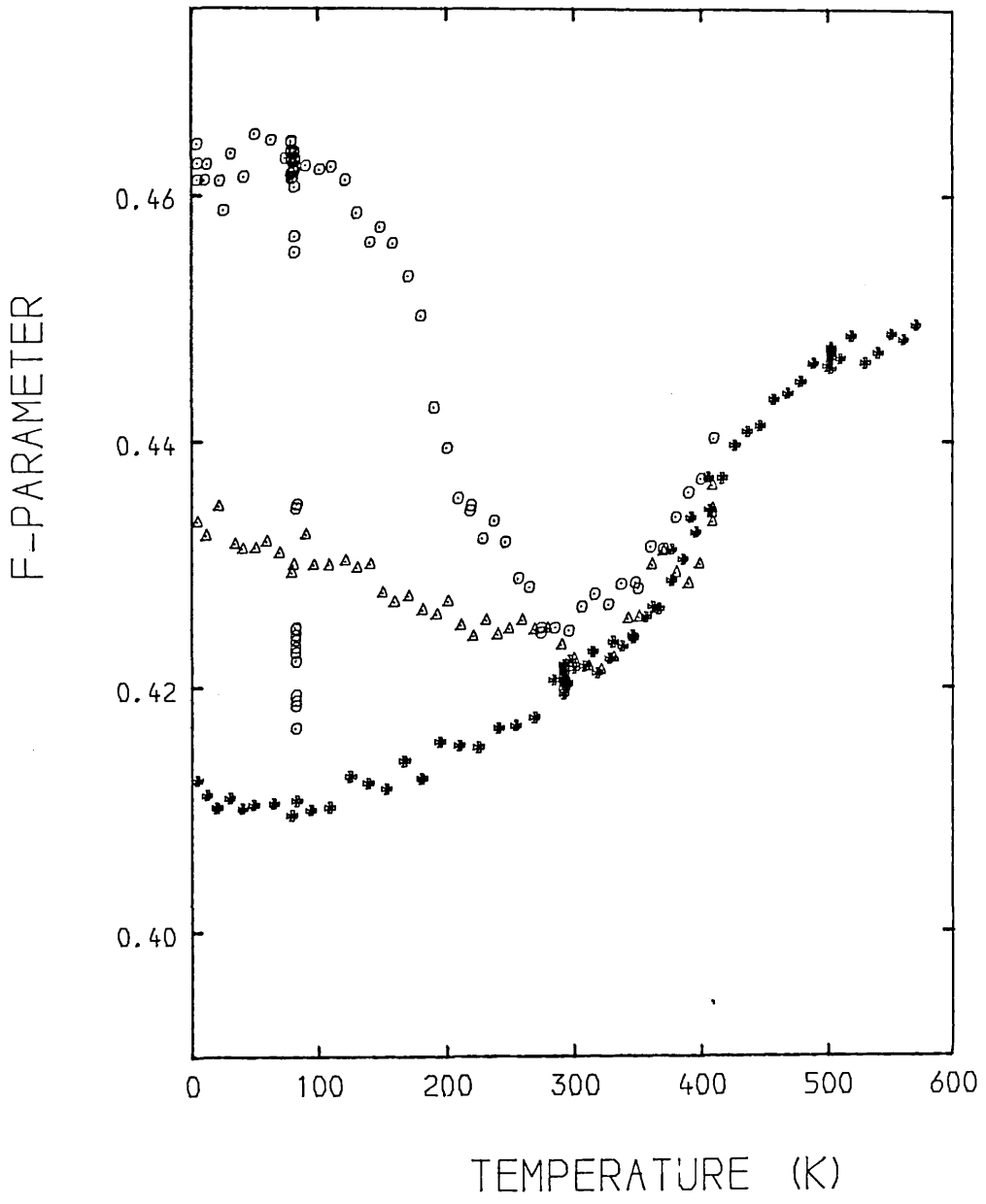

Fig(6.2.1) shows the F-parameter as a function of temperature of positron annihilation in deformed and annealed cadmium, with error function background subtracted. Standard deviation of the F-parameter is ±0.0008.

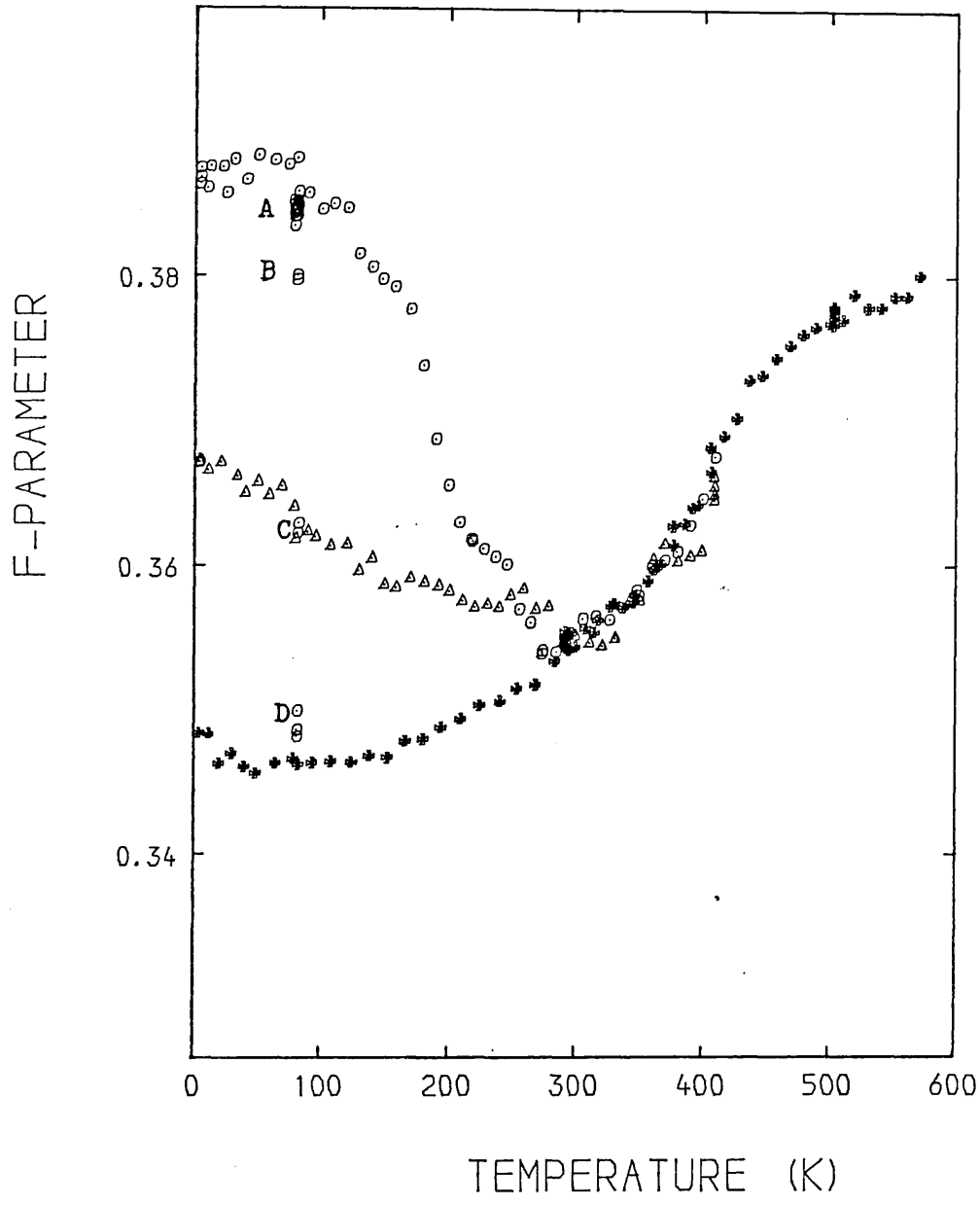

Fig(6.2.2) shows the F-parameter as function of temperature of positron annihilation in plastically deformed cadmium at liquid nitrogen temperature (circle), and at room temperature (triangle), and annealed cadmium (star), without background subtracted. The standard deviation of F-parameter is $\pm$0.0003.

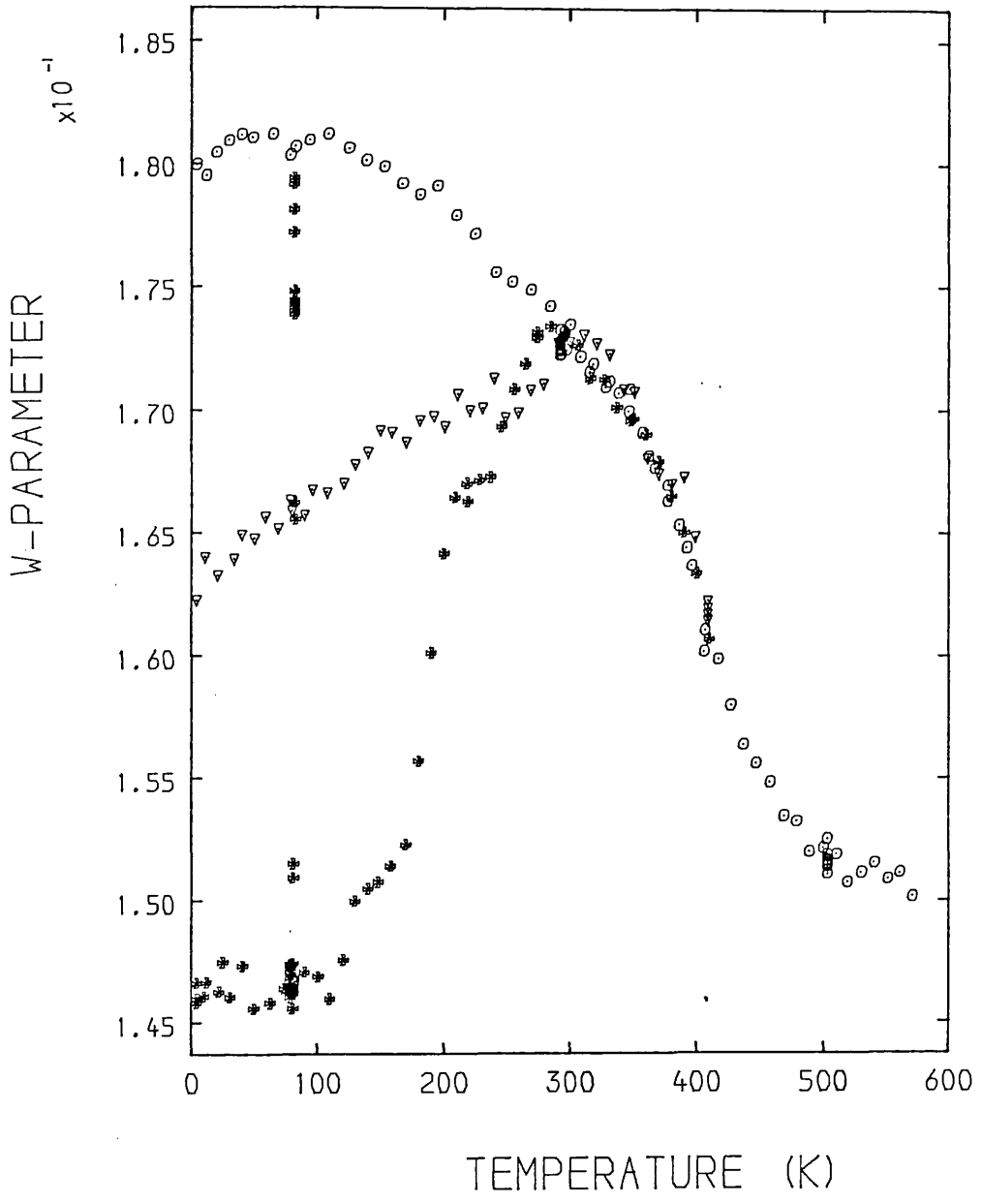

Fig(6.2.3) shows the W-parameter as function of temperature of positron annihilation in deformed and annealed cadmium, without background subtracted. The standard deviation of the W-parameter is $\pm$ 0.0002.

of the specimen after room temperature is the same as the annealed specimen. The specimen then kept 18 hours at 503K, the sample completly annealed at this temperature. After that the sample was cooled down again to 77 K and then to liquid helium temperatures. Below 50 K the F-parameter rises and this was also observed by Herlech et al in 1977 and Rice-Evans et al in 1978b. They suggested this rising occurs because the positrons are trapped "in shallow deep" by grain boundries and thermal detrapping occurs. Apart from the low temperature range, above 50 K the F-parameter is flat up to 150 K, and from 150 K to 230 K rises linearly because of the thermal expansion of the lattice. From 230 K tO 350 K it rises with a sharp slope and it was observed also by Lichtenbrger et al in 1975, Kim and Bauyer 1976 and Rice-Evans et al in 1978b. Above 350 K there is an exponential increase because of the creation of vacancies in the specimen and effect of trapping of positrons in the vacancies. A Saturation effect was observed near the melting temperature of cadmium that suggested the positrons were trapped in monovacancies (100% trapping).

6.3-Line-shape parameter analysis:

On the basis of the trapping model the line-shape parameter data from this study was analysed in terms of the three different models as:

(a)The "linear rise" model with $\alpha=0$ and $\beta\neq0$ in equation (5.4.3)

(b)The "self-trapping" model with $\alpha=0$ and $\beta=0$ in equation (5.4.4)

(c)The "three states" model with $\alpha=0$ and $\beta=0$ $\gamma=0$ in equation (5.4.6)

Each case was fitted to the data by means of a least square minimization routine. The result of these three cases including case b which applied to the W-parameter data (bw), is shown in table(6.3.1a). The value of H_{1v}^{F} the enthalpy (energy formation of

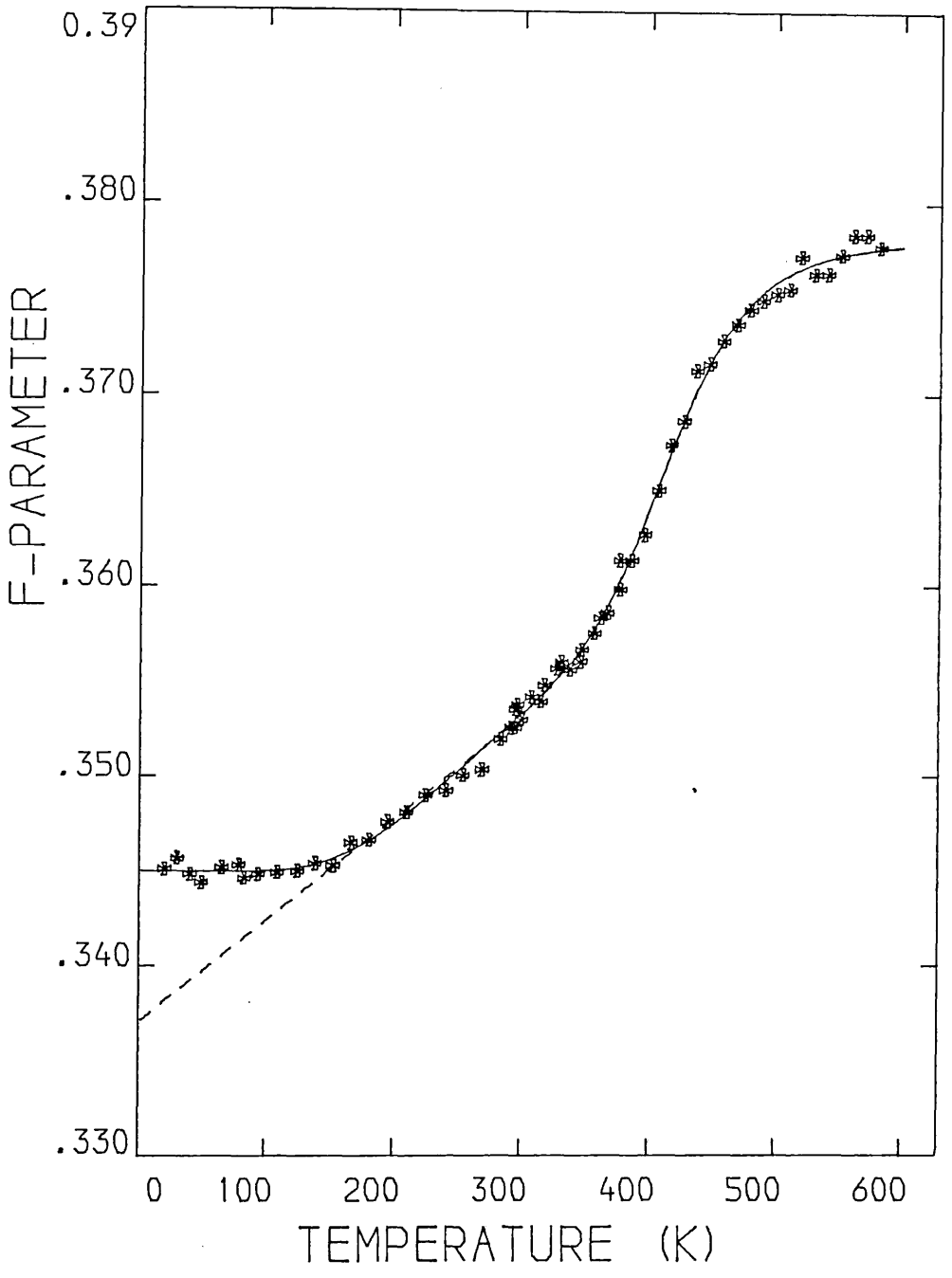

Fig(6.3.1) Theoretical fitting to the F-parameter for the annealed specimen of cadmium. The dash and the solid lines correspond to the cases where F_f is taken linearly to rise with temperature, and to fit Seeger's self-trapping model, respectively.

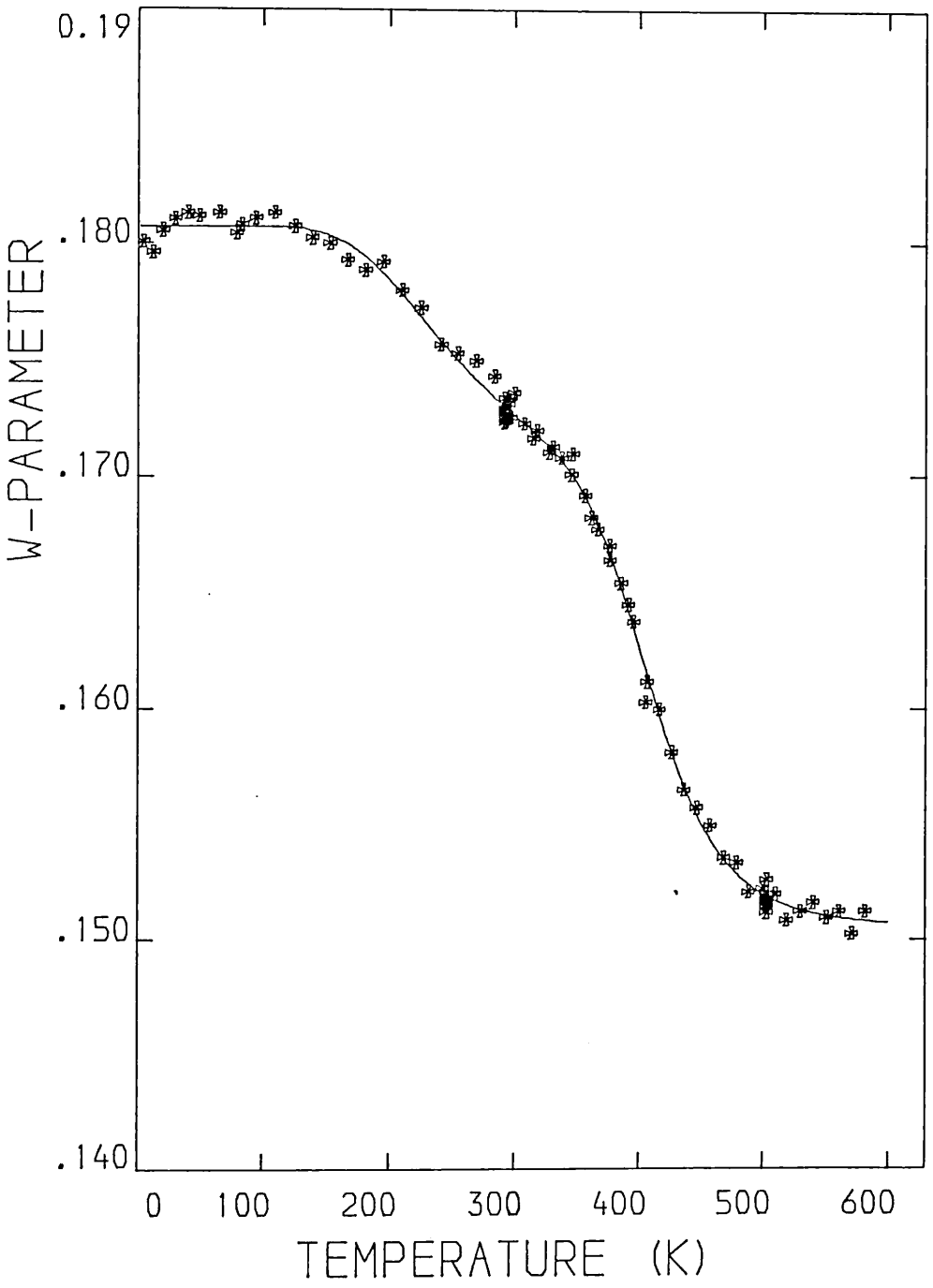

Fig(6.3.2) The self-trapping fits to W-parameter for annealed cadmium to compare with the F-parameter.

Modes	H_{1v} (ev)	H_{2v} (ev)	$E(K_o)$ (ev)	β $X10^{-5}$	A $X10^{5}$	B	F_f	F_{1v}	F_i	X^2/ν
(a) Monovacancies plus linear rise above 150K $\alpha=0$	o.46 $\pm$o.o3	—	—	1.59 $\pm$o.6	2.53 $\pm$o.3	—	o.337 $\pm$o.ooo6	o.378 $\pm$.ooo5	—	1.3
(b)Monovacancies plus self-trapping above 20K, $\alpha=\beta=0$	o.47 $\pm$o.o4	—	o.o98 $\pm$o.oo3	—	3.86 $\pm$o.8	o.28 $\pm$o.o5 $X10^{5}$	o.345 $\pm$o.ooo6	o.378 $\pm$o.ooo5	o.419 $\pm$o.ooo4	1.o8
(bw) Monovacancies plus self-trapping all points, $\alpha=\beta=0$	o.51 $\pm$o.o3	—	o.132 $\pm$o.o4	—	17.3 $\pm$1.2	1.24 $\pm$o.92 $X10^{5}$	o.181 $\pm$o.ooo3	o.151 $\pm$o.ooo5	o.167 $\pm$o.ooo7	1.55
(c) Monovacancies plus divacancies above 20K, $\alpha=\beta=\gamma=0$	o.52 $\pm$o.o3	o.o79 $\pm$o.oo4	—	—	38.8 $\pm$1.5	21.9 $\pm$o.2	o.345 $\pm$o.ooo3	o.364 $\pm$o.ooo6	o.378 $\pm$o.ooo7	1.o24

Table(6.3.1a)

Where i=st, in the cases (b) and (bw), and i=2v in the case (c)

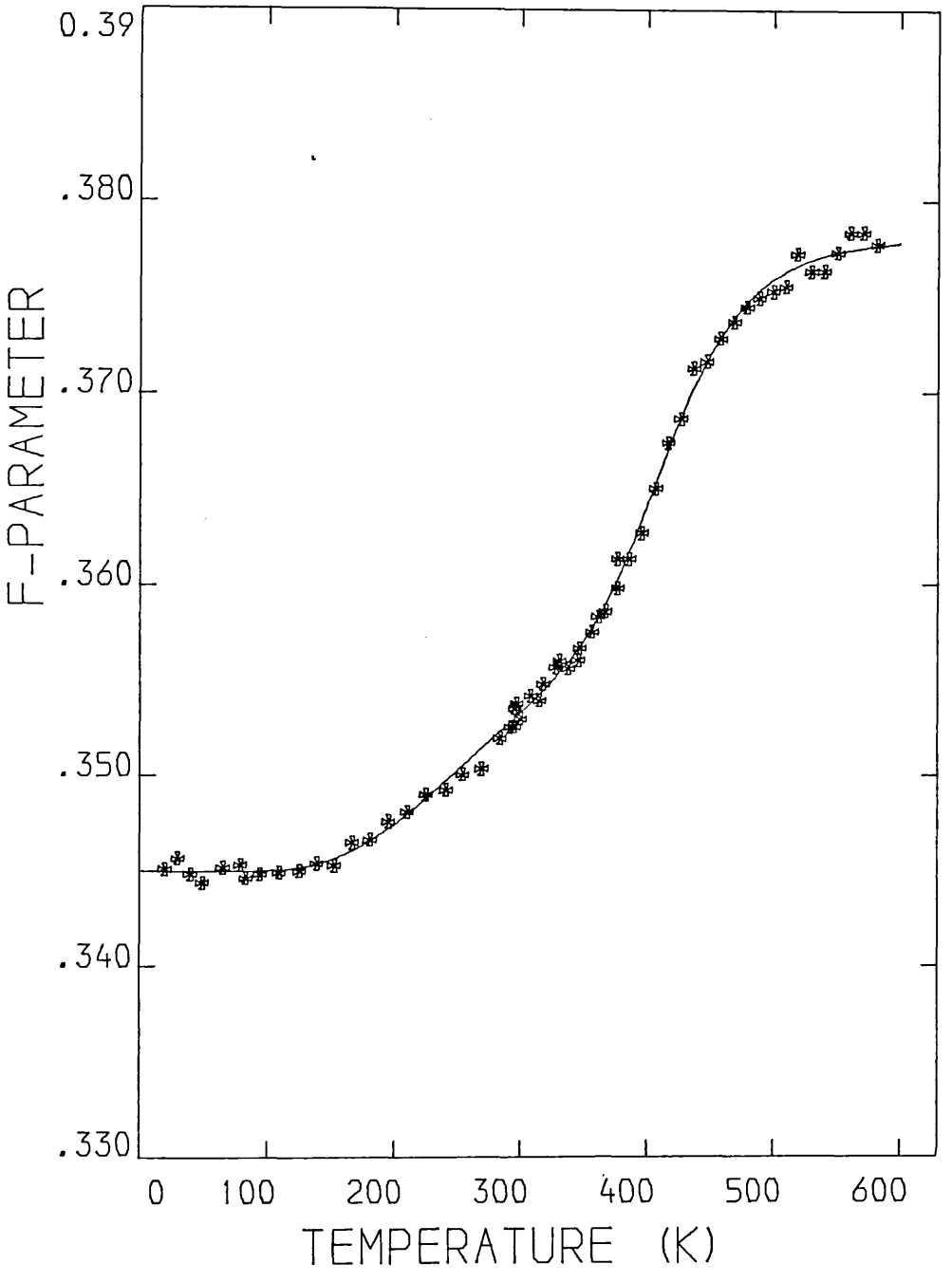

Fig(6.3.3) The divacancies fitting to F-parameter for the annealed specimen of cadmium.

monovacancy) was in good agreement with the value found by Sigh and West 1976 in lifetime measurements $H^F_{1v}=(0.52\pm0.05)$ev. The value is far from the value which has been found by Jackman et al 1973 and Segeer 1974, (0.40 ± 0.02)eV and (0.39 ± 0.03)eV respectively. The best chi-square value on the fitting of our data was in cases (b) and (c) with $H^F_{1v}=(0.47\pm0.04)$eV and (0.51 ± 0.03)eV in good agreement with other groups (Sigh and West, Conners et al 1971). The result of fitting or (a) and (b) cases is illustrated in figure(6.3.1), where the solid line represents self-trapping model and dashed line represents linear ris mode . The (bw) and (c) cases are also plotted and are illustrated in figures(6.3.2) and (6.3.3) respectively. Herlach et al in 1977 found the lifetime of annihilation of free positrons in cadmium to be 190 Picosecond and Hood and McKee in 1978 reported the positron annihilation rate in metal as $5X10^{14}\ S^{-1}$. By using this value and our result the concentration of monovacancies has been calculated for the three cases as $(3.13, 3.93 \text{ and } 18.0)X10^{-4}$ at 590 K respectively. Then the entropies can also be found for these cases 0.98k, 1.4k and 3.7k respectively, where k is Boltzman constant.

The F_{st} value associated with the self-trapping fit indicates that the trapping depth of the positron self-trapping is deeper than monovacancy trapping, and it is inconsistent with the interpretation of self-trapping at intermediate temperatures. Therefore it is concluded that this fit is not physically meaningful. While in case of W-parameter fitting this F_{st} (W_{st}) value is resonable apart from the chi-square value. Our results show that about 97% of positrons are trapped at 590 K in case (a) and 99% in the other cases.

6.4-Line-shape analysis:

The line-shapes of the annihilation spectrum for both annealed and deformed polycrystaline cadmium, were fitted with Gaussian and an inverted parabola equations (5.5.5) with (5.5.6b) after convolution with instrumental resolution function, by a least square minimization routine in the Curfit program (see appendix III). The result of fitting for one spectrum is illustrated in figure(6.4.1a). The result of the deformed sample at 77 K is shown in figures(6.4.1) and (6.4.2). It is shown that the Gaussian width is increased from 19.5 channels at 100 K to 22.6 at 300 K, with approximately one channel change in parabola width. The parabola percentage is 68.3% at 80 K and declines to 58.5% at 300 K and then increases. This satisfies the correlation between the parabola percentage and F-parameter. In the case of the deformed sample at room temperature the result of the spectrum analysis is illustrated in figures(6.4.3) and (6.4.4). As can be seen the Gaussian width changes from channels 21.5 at 80 K to 22.4 channels at 300 K, and the parabola percentage from 63.6% to 58.6% at 300 K. The parabola percentage in deformed sample is not in good agremment with Jackman et al 1973.

The fitting of the annealed cadmium has been shown in figures(6.4.5) and (6.4.6). The Gaussian width is silghtly flat arround 23.0 channels up to 330 K, but above 330 K decrease to 19.3 channels and this is in good agreemet to show that the trapping of positrons in vacancies by the narrowing the line-shape spectrum. The parabola percentage also increased from 57% at 100 K to 59% at room temperature (300 K) and increases to 65% at near the melting point. The percentage of the parabola was not in good agreement with Chagler 1978, and Khangi in 1980, and also with Jackman et al 1974, 1973. They found 38% or 40% at 77K respectivley. The average of the

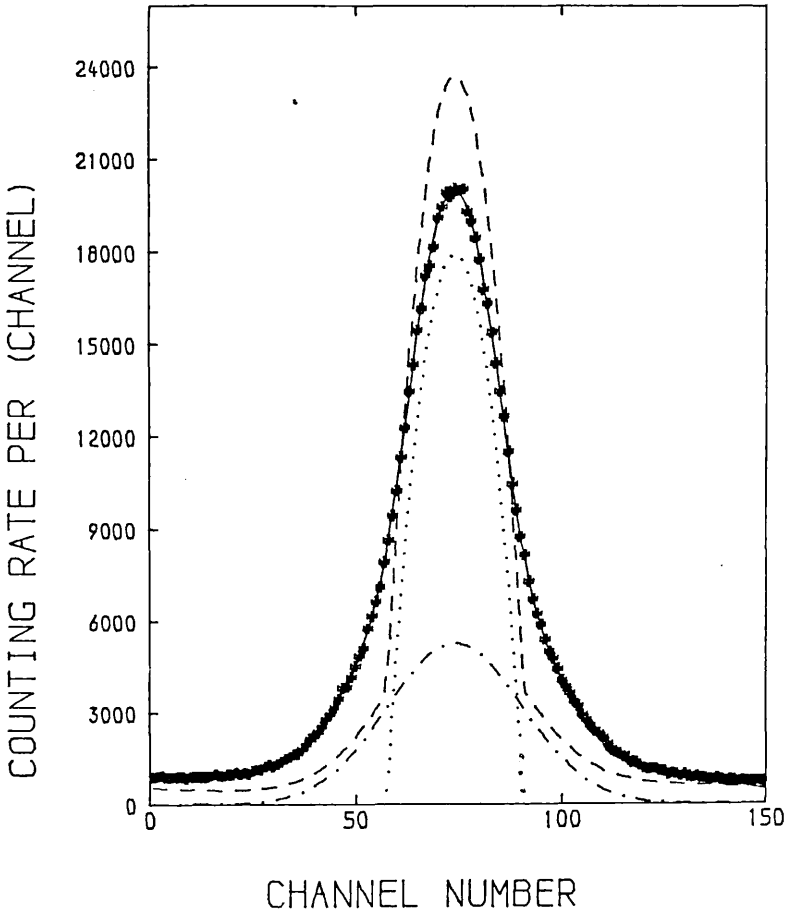

Fig(6.4.1a) Application of the convolution of a Gaussian and an inverted parabola for annealed cadmium, using equations (5.5.5) and (5.5.6b).

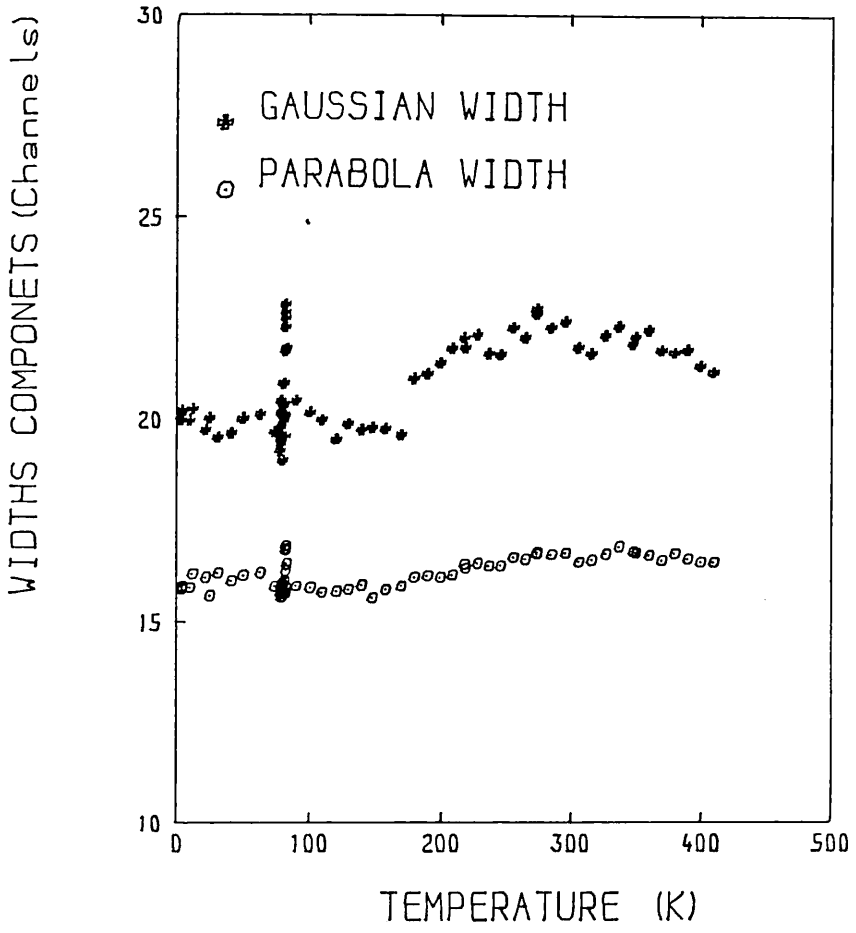

Fig(6.4.1) The variation of the width parameters of the Gaussian and the parabolic components with temperature for deformed cadmium at 77 K.

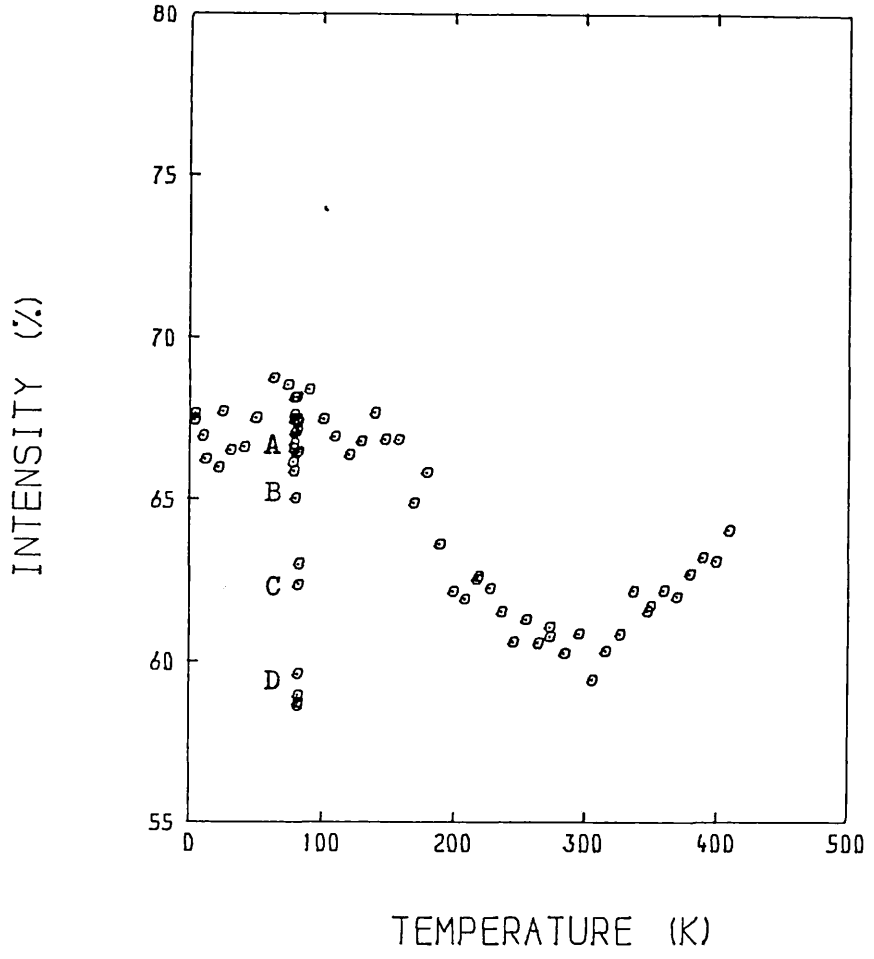

Fig(6.4.2) The variation of the parabolic percentage with temperature in deformed cadmium at 77 K. The standard deviation is estimated to be $\pm 1.6\%$.

parabola width was 16.4 channels which is about two channels greater than the value reported by Chagler and Khangi.

Because the inverted parabola represents the annihilation of positrons with free electrons then the parabola width is proportional to the Fermi energy of the electron, and this proportionality is given by the relation below

$$E_F = 1/2.m_o v_F^2 = 4\sigma_p^2/m_o c^2$$

Thus the Fermi energy of the cadmium was calculated to be about 9.1eV and this is 30% greater than value reported by Jackman et al 1974. The disagreement of the line-shape spectrum analysis with other groups was found because the ncorrect expression was used (5.5.6b), which is written in Khangi and Berry theses 1980, and 1982 respectively. Therefore some of the spectrums were also chosen and fitted again with expression (5.5.5) and (5.5.6a). The result of parabola percentage change from 38% at 100 K to 46% at melting point (509 K) which is in good agreement with the results of others groups were mentioned above. The Gaussian width was the same as above analysis but parabola width was found 14.7 at 100 K to 14.9 at 580 K, On average the parabola width was observed not temperature dependence and about 14.8 channels that gives us the Fermi energy 7.54ev. Where this value is in agreement with value 7.4eV calculated by Ashcrof and Mermim 1976 and Kittel 1976. Therefore it proves that expression (5.5.6b) is not right, in fact factor 2 infront of the Gaussian expression was not necessary. The Chi-square of the degree of freedom versus temperature in the case of the annealed sample is shown in figure(6.4.7). As can be seen the value of chi-square is approximately flat up to room temperature which is roughly arround 1.2 to 1.3, and this value increases to 2.4 at near melting point (509). This increase in chi-square suggested becase the zero-point motion of the

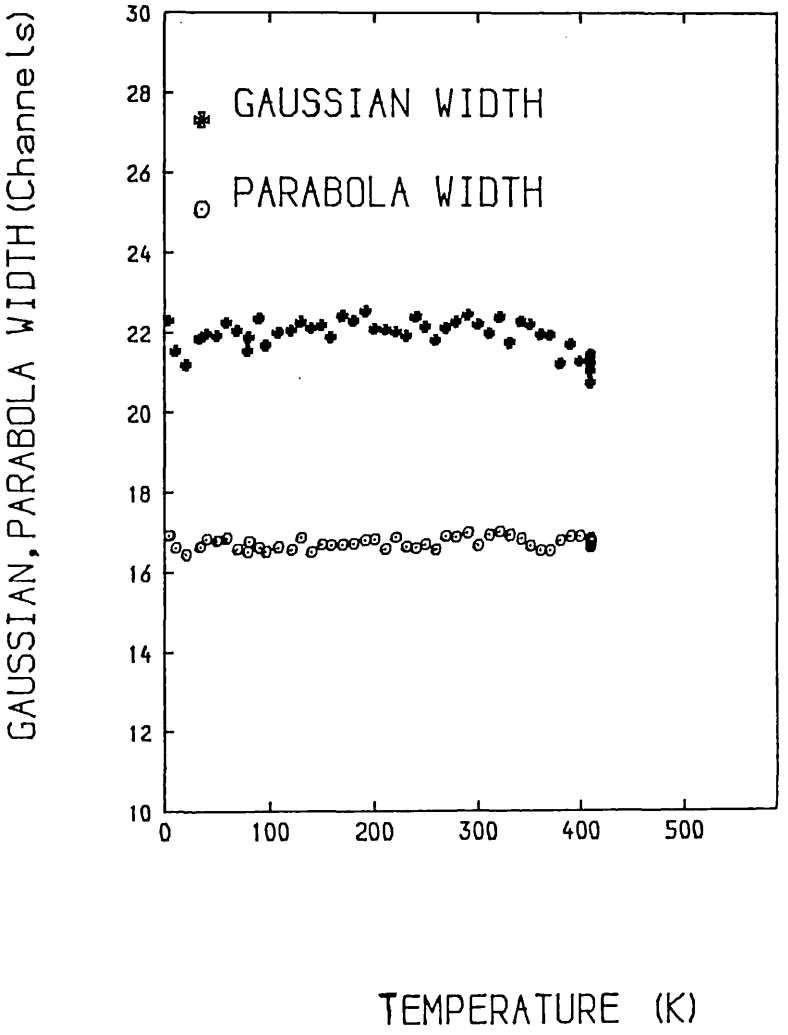

Fig(6.4.3) The variation of the width parameters as function of temperature for deformed cadmium at room temperature.

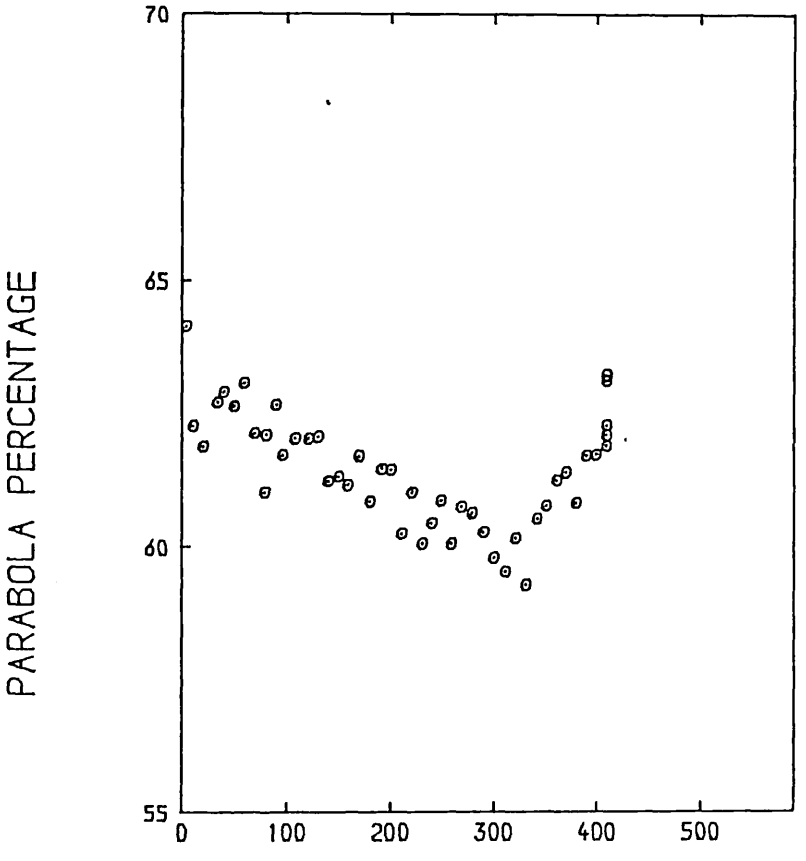

Fig(6.4.4) The variation of the parabolic intensity as function of temperature for deformed cadmium at room temperature. The standared deviation is estimated ± 2%.

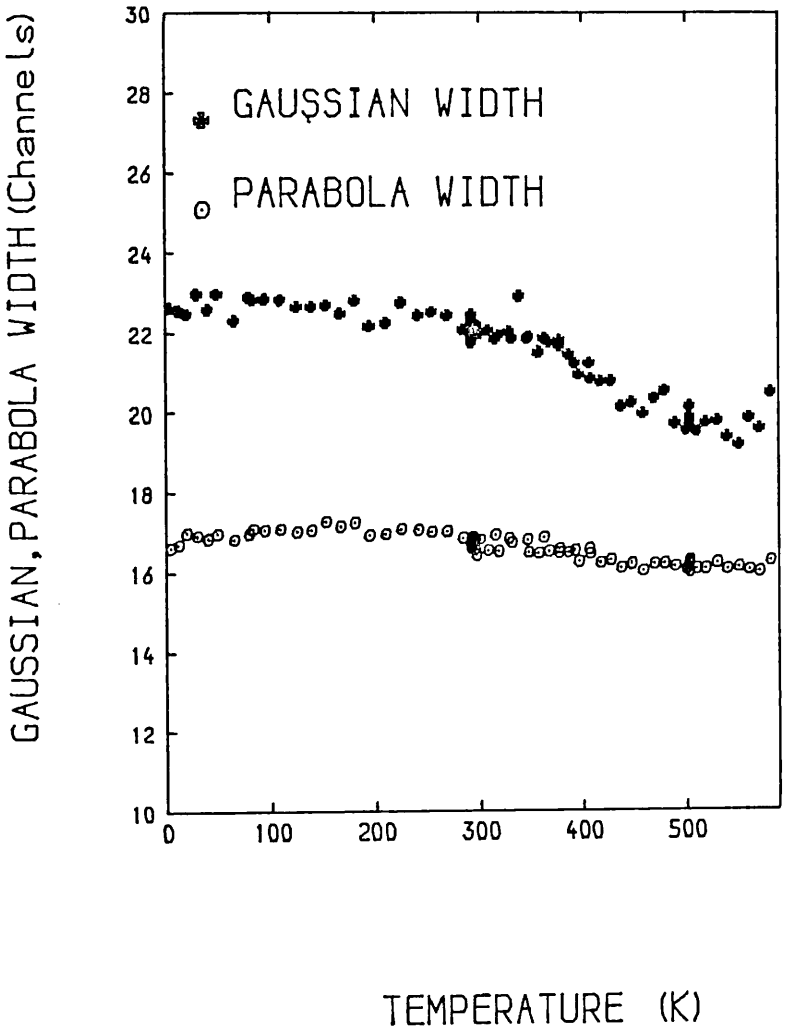

Fig(6.4.5) The variation of the width parameters of the Gaussian and the Parabolic for annealed specimen cadmium, with temperature.

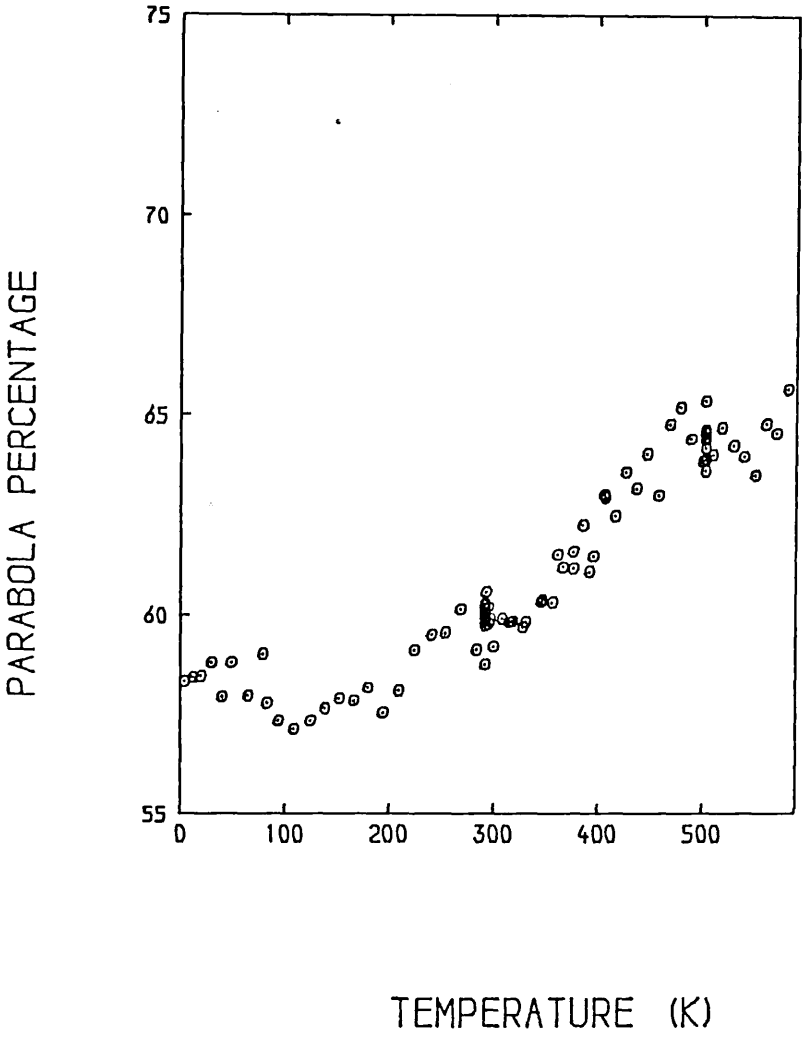

Fig(6.4.6) The variation of the parabolic percentage as a function of temperature for annealed specimen of cadmium. The standard deviation is estimated as $\pm$ 1.6%.

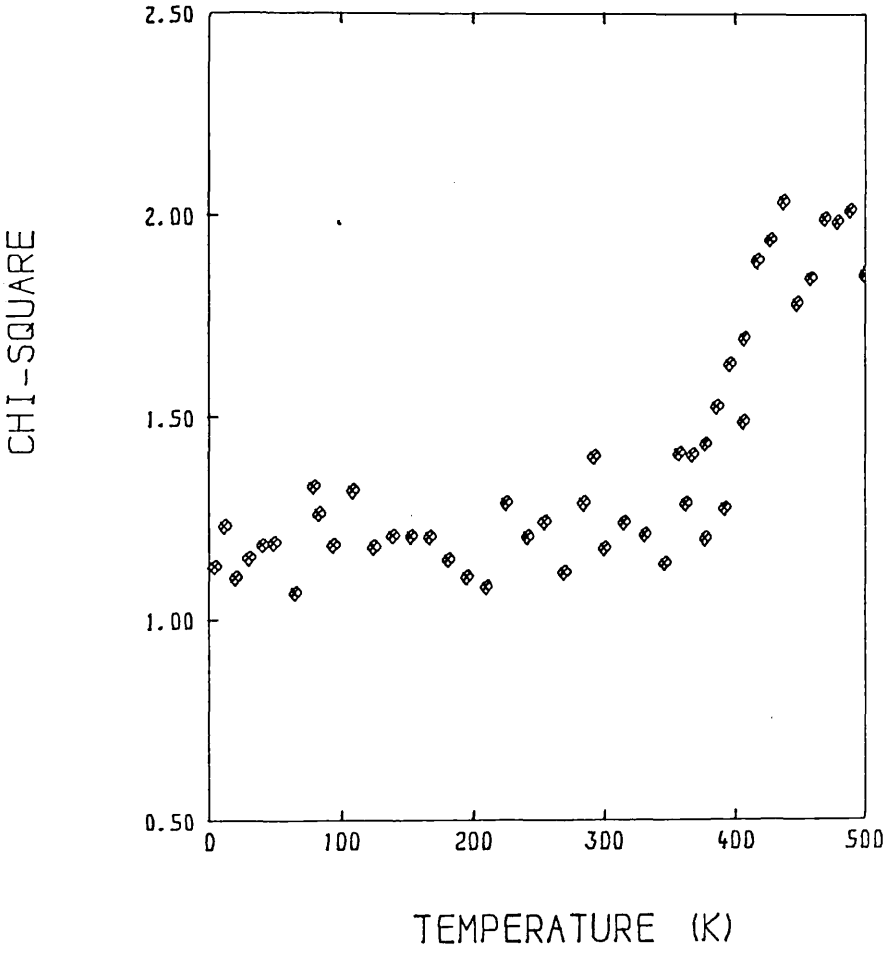

Fig(6.4.7) The variation of the chi-squared (X^2/υ) as a function of temperature for annealed cadmium.

positron trapped in vacancies or dislocation etc.

6.5-Zero-point motion:

The nature of a particular defect may be described by the trapping of a positron in a potential well which will have a physical size and certain depth. The wavefunction of the positron is localized in the vicinity of the defect and consequently a zero-point kinetic energy is expected (Rice-Evans et al 1981). They found the chi-square will be minimised with respect to σ_b which is the width of the extra Gaussian addition to the convolution expression. They found this value to be σ_b=3.8 for single crystal cadmium, and the zero-point kinetic energy of positron at trapping state to be 0.4ev.

The increasing value of the chi-square at high temperature figure(6.4.7) "in the trapping of positron in monovacancy region" is because the zero kinetic energy of the positron trapped was ignored it means σ_b=0. While this is not zero therefore the chi-square will be minimised by chosing the value of σ_b=4, figures(6.5.1) and (6.5.2) for the annealed sample at different temperatures.

It is clearly observed that the chi-squred minimised at σ_b=4.0 as was found by Berry. The chi-square is also minimised at the same value of σ_b for deformed cadmium (at 77 K) see figure(6.5.3) for two spectrums at same temperature. The kinetic energy of the positron at trapping for polycrstalline cadmium is 0.55ev. It is in good agreement with 0.4eV from the single crystal cadmium results that have been reported by Rice-Evans et al 1978.

6.6-Conclusion:

From the result of F-parameter versus temperature it is conculded that the line-shape spectrum of positron annihilation in the polycrystalline cadmium is temperature dependent. In the case of

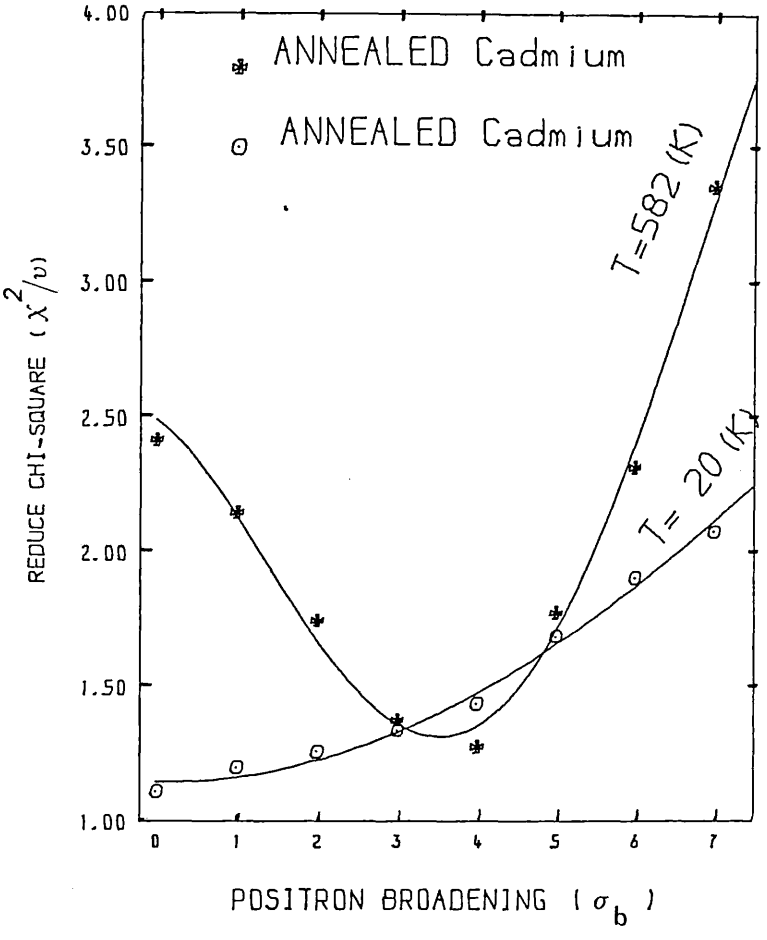

Fig(6.5.1) The variation of the reduced chi-squared with positron Gaussian width in annealed cadmium at different temperatures.

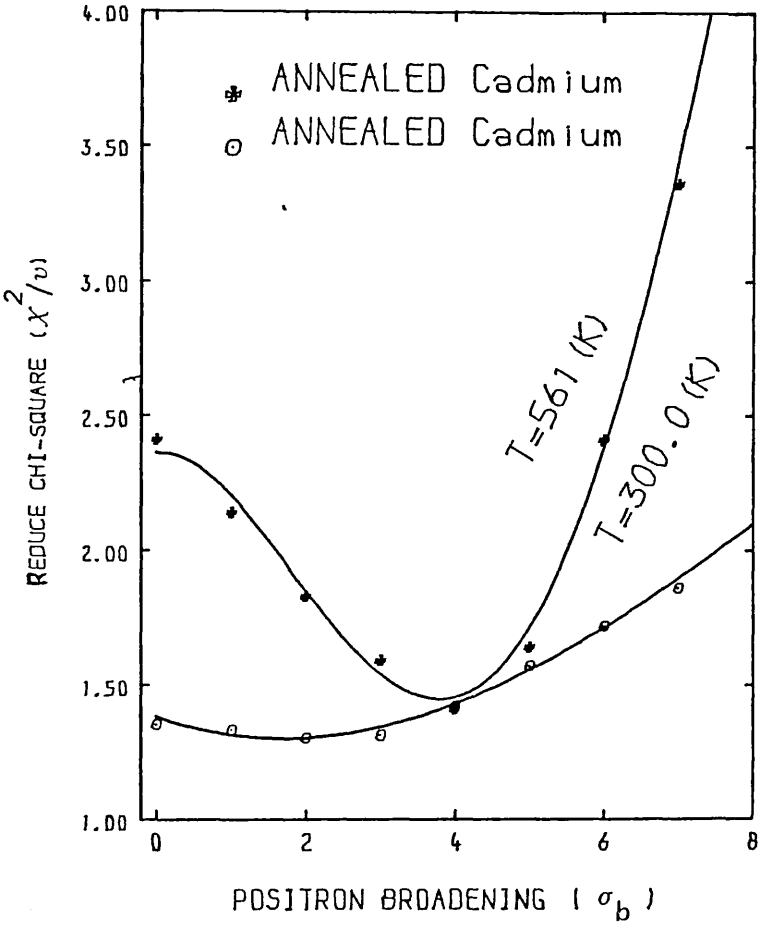

Fig(6.5.2) The variation of the reduced chi-squared with positron Gaussian width in annealed cadmium.

deformed cadmium at (77 K) the F-parameter was about to be 2% greater than the annealed sample at near melting point, that may be due to frozen dislocations, production of 30% reduction in thickness, which was also observed in deformed aluminuum. The recrystallization of the deformed cadmium was observed more clearly in this study, and it occurs rapidly between 150 K and 250 K as is reported by Rice-Evans et al in 1978. The annealing temperature of the sample is 350 K and above this tem perature vacancies will be created and positrons will be trapped. The trapping of positrons in monovacanc ies and possibly divacancies were .observed and it was in good agreement with Lichtenberger et al (1975). Apart from low temperature (below 50 K) the line-shape parameter is flat up to 150 K and it started to rise linearly with small slope because of thermal lattice expansion, and then from 230 K it increases by a sharp slope to 350 K (prevacancy region) because of self-trapping of the positrons (Segeer A. 1976). The saturation at high temperature suggested that 100% of the positrons were trapped.

The anomalous behaviour below 50 K is obvious since this effect also was observed by other groups (Herlach et al 1977 and Kupca et al 1980). But this effect was also observed in zinc and gold as well by (Rice-Evans et al 1978)and (Herlach et al 1977). Herlach suggested that during the slowing-down process, positron rejected from the sample via crystallographic direction and annihilate with helium gas or on the surface of the sample. But Kapce et al claimed in their lifetime measurement that, the lifetime of positron annihilation in polycrystalline cadmium at low temperatures (4.2 K) is 230 psec which is similar to the positron lifetime in deep traps . They prefer an explanation that involves indirect trapping into deep traps via shallow traps, grain boundaries, then thermal detrapping will occur.

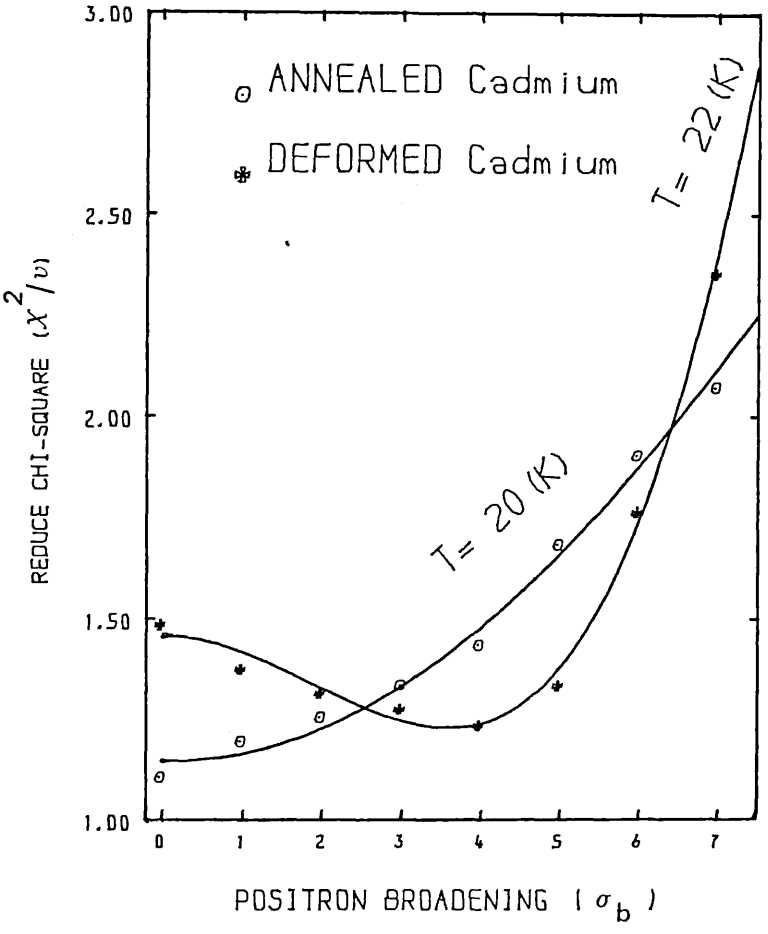

Fig(6.5.3) The variation of the reduced chi-squared with positron Gaussian width in annealed and deformed specimen of cadmium at very low temperature.

This effect has been not observed in the single crystal cadmium and zinc(p. Rice-Evans et al 1979).

The energy formation of monovacancies is also calculated for three different theories were (a) $H^F_{iv}=(0.46\pm0.03)eV$, (b) $H^F_{iv}=(0.47\pm0.04)eV$, (c) $H^F_{iv}=(0.51\pm0.03)eV$ which are in good agreement with Siagh and West 1976, Conner et al 1971. The parabola percentage and Fermi energy in the first try of fitting the line-shape spectrum was not in good agreement with other groups because the expresion (5.5.6b) was not correct which is written in the Berry and Khangi theses (1982,1980). But the result of parabola percentage and Fermi energy was in good agreement with respect to other groups when expression (5.5.5) with (5.5.6a)was used. The model of trapping expression (5.7.2) also tried to fit the spectrum line-shape but the result was physically meaningless when chi-squrare was good and when the result was physically meaningful chi-square was found to be worse (no minimization).

Chapter VII Positron annihilation in annealed and deformed polycrystalline Tin

7.1-Introduction and method

Much work has recently been done to investigate vacancy formation in metals. The resulting Doppler broadening line-shape of the annihilation process is very sensitive to positron trapping at vacancies, dislocations, and voids. Trapping of the positron in vacancies have been observed for many metals such as In, Au, Cd, etc. (Rice-Evans et al 1978b), (Kusmiv and stewart 1967), and (Makenzie et al 1964).

Seeger (1973) claimed that positron trapping in a metal near the melting point temperature, dependS on three factors, namely monovacancy formation volume, valance electron, and the size of the ions cores. He mentioned that the reason why trapping of positrons was not observed in the alkali metals, was because of narrow ion cores, unity valance, and small monovacancy formation volume.

The investigation of the positron annihilation in tin (white-tin) has already been measured by many groups (Badoux et al 1967, Dedoussis et al 1977, Mackenzie et al 1980, and Puff et al 1983). Dedoussis et al in 1977 suggested by their measurements (lifetime and Doppler broadening) of positron annihilation in tin, that the threshold temperature of annihilation at a vacancy site is 390 K. Balzer and Sigvaldaron calculated that the vacancy concentration in tin at the melting point is less than $3X10^{-5}$, using a thermal expansion experiment. Seger et al in 1980 observed a very small change in line-shape parameter, (about 2.1%), in the temperature range of 10 K to 490 K. But non of them observed the transition of the tin clearly in their measurements. In 1983 Puff et al mentioned that the increase

in the mean lifetime of the positron in tin above 230 K was due to thermal lattice expansion. In addition they mentioned a transition in tin at 230 K.

Method:

In the present work we observed no sign of the transition of white tin to gray tin (and vice versa) in the annealed sample, but it was observed in the deformed specimen. The annealed specimen was made by two pieces of 99.999% purity tin with dimensions 15X15X1mm spark erusion cut from a rod supplied by Koch-Light Laboratories Ltd. The two pieces are etched in a mixture of nitric acid and alcohol. approximately 0.1 mCi of carrier-free $^{22}NaCl$ solution was evaporated directly on the central region of the surfaces. The pieces were then arranged in a sandwhich configuration and encapsulated in a wrapping of thin aluminium foil. The specimen-source was then mounted in furnace under vacuum (of less than 10^{-6} torr), and subsequently annealed at a temperature of 450 K for 15hours. The specimen-source was cooled down to room temperature and then mounted in the cryostat which was cooled down to liquid nitrogen temperature, and then down to 4.2 K in a vacuum better than 10^{-6} torr. After a stable equilibrium temperature was acheived, data was accumulated from 4.2 K to 500 K with a temperature increament of 10 K. The preparation processes were preformed by Khangi.

7.2-Line-shape parameter:

The F-parameter was calculated after error function background was subtracted (as was mentioned in chapter five). Figure(7.2.1) illustrates the F-parameter variation as a function of temperature. It appears flat to above 220 K and then rises with a small slope above room temperature, 390 K, due to thermal expansion. From 390 K it

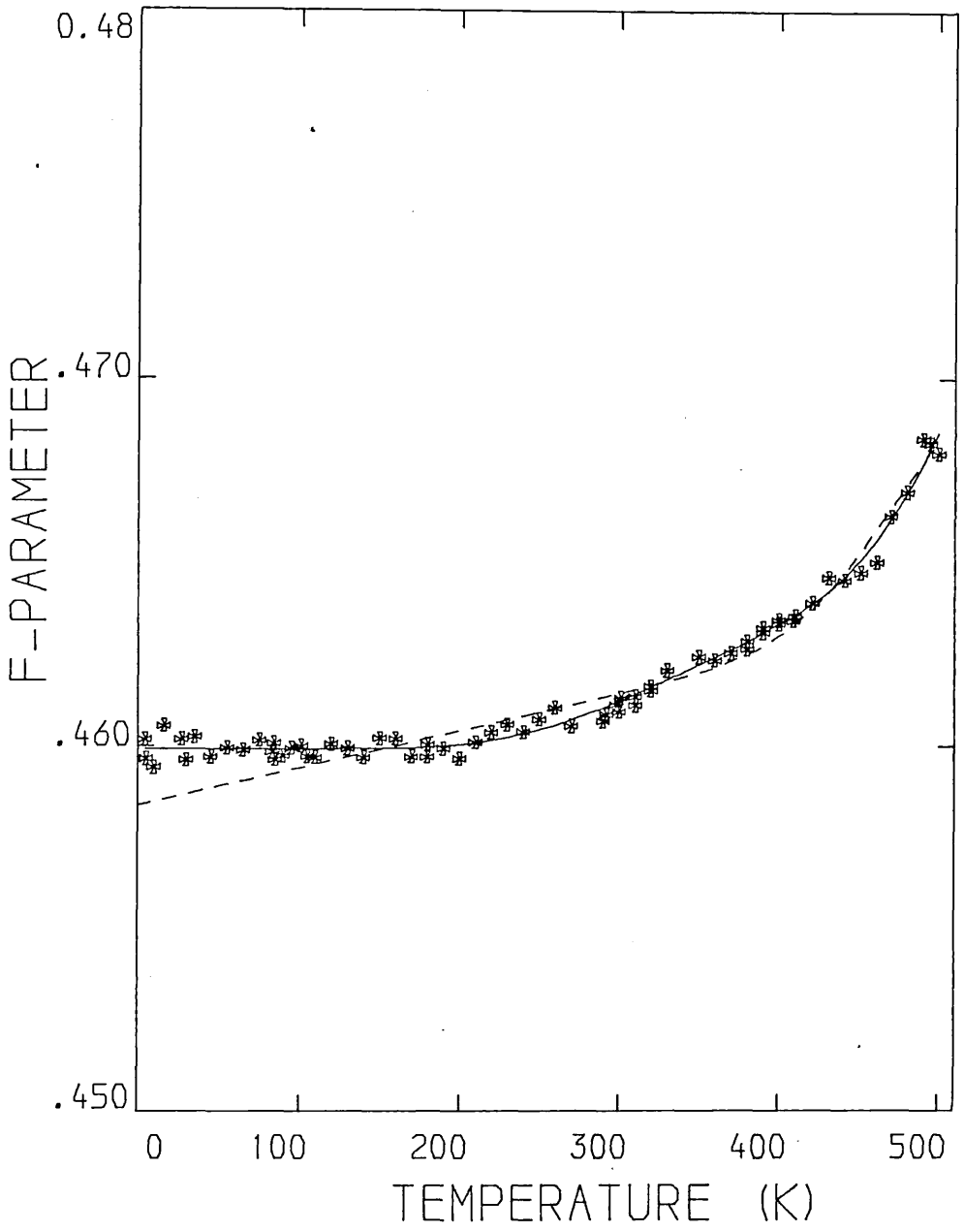

Fig(7.2.1) The variation of the F parameter as a function of temperature for anneald tin, the solid line resulting of the self-trapping model case (b), and dash line of linear rise model case (a). The standard deviation of F is $\pm$ 0.0004.

increases with sharp slope to 500 K near the melting point, at which point saturation was not indicated as was observed in cadmium and indium (Chaglar 1978 and Khangi 1980). The increase in F-parameter value from a low temperature up to 500 K is 2.2%, the same value as was observed by Segers et al 1980. They found the threshold temperature for tin was 403 K, but in our work as shown by the curve, it occurs at 390 K (the monovacancy creation temperature). They suggested that three lines should be fitted through their data with three different slopes. This is in accordance with our results, but not with Puff et al (1983) in which their lifetime measurements indicated four different regions, low temperature to 220 K, from 220 K to 370 K, from 370 K to 420 K, and finally trapping region from 447 K to 500 K. They believed that the threshold temperature is 447 K, rather than 390 K or 403K. Their explanation was not actually in good agreement with our results, which divided into three different regions rather than four. It is evident from the data that the line-shape parameter change in annealed tin as function of temperature is small. Nevertheless, the regions are quite distinguishable, so it is not possible to attribute them to electronic instabilties alone, a fact supported by the values of G-parameter which was described in a previous chapter (see 4.2.5), this data being found satisfactory.

7.3-Line-shape parameter analysis:

Two cases of trapping model were applied to the data, and fitted by using the least-square minimization method:

(a) "linear rise" equation (5.4.3) with α=0.

(b) "self-trapping" model equation (5.4.4).

The results are illustrated in table (a),(b) and the line fitted to data is shown in figure(7.2.1), "the solid line for case (b) and dash

line for case (a)". From the linear rise results, (table(a)), the probability of positron trapping was

$H^F_{1v}=(.56\pm0.02)$ev	$F_F=(.4576\pm0.0005)$
$A_{1v}=(8.3\pm0.7)X10$	$F_{1v}=(.4712\pm0.0007)$
$\beta=(29.0\pm3.1)X10$	Chi-squared=1.64

Table(a)

calculated as 65% at 500 K, while it was calculated as 63% by Khangi. Dedoussis et al (1977) found a value of vacancy formation energy for tin $H^F_{1v}=(0.5\pm.01)$eV by lifetime measurements and $H^F_{1v}=(0.51\pm0.05)$eV by Doppler broadening measurements, while a similer value $H^F_{1v}=(0.51\pm.02)$eV was found by Seger et al (1980), by threshold temperature method and $H^F_{1v}=(0.54\pm0.03)$eV by the trapping model. At the same time Mackenzie et al found $H^F_{1v}=0.57$eV by the threshold temperature method. This value was also recently found by Puff et al 0.58eV by the same method. Our results however show that this value is nearer to the value which was found by Mackenzie et al and Puff et al for the case (a) while it is near the other groups for the case (b).

$H^F_{1v}=(0.52\pm0.01)$ev	$E(K_0)=(0.143\pm.007)$ev
$A_{1v}=(2.95\pm0.65)X10^5$	$B=(7.25\pm.93)X10^5$
$F_F=(0.4596\pm0.0003)$	$F_{1v}=(0.4735\pm0.0008)$
$F_{st}=(0.4647\pm0.0004)$	Chi-squared=1.11

Table(b)

The result of table(a) and table(b) was also found by Khangi (1980), where he used the F-parameter calculation without a background subtraction. The lifetime of a free positron annihilating in tin was computed by Dedussis et al as $215X10^{-12}$ sec. and by Puff et al as $(199\pm1)X10^{-12}$ sec. Therefore the trapping rate and entropy exponetial factor, A_{1v}, has a value $3.9X10^{14-1}$ S in case (a) and $1.3X10^{15-1}$ S in case (b). This can be compared with $1X10^{15-1}$ S obtained by Dedoussis et al.

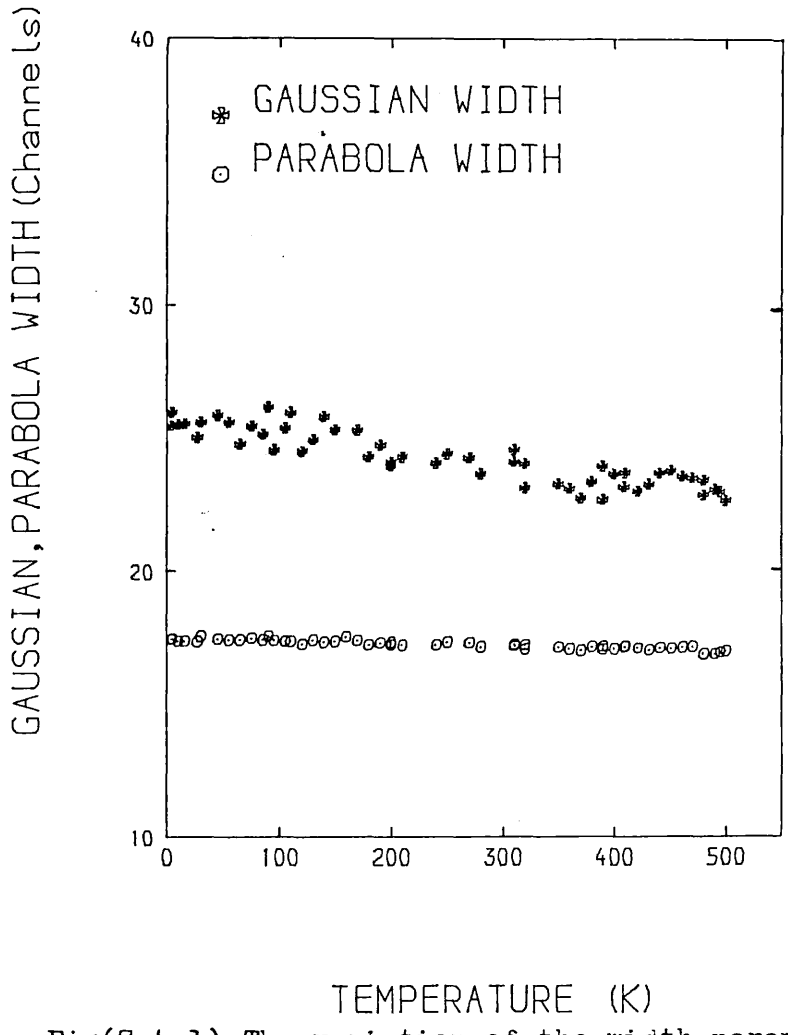

Fig(7.4.1) The variation of the width parameters of the Gaussian and the parabolic components of the polycrystalline annealed tin.

The entropy of monovacancy formation was obtained by Balzer et al (1974) as 1.7k from a thermal expansion experiment, where k is Boltzmann constant. By using this entropy, the concentration of monovacanc was obtained at 505K as $1.4X10^{-5}$ and $3.5X10^{-5}$ for case (a) and (b) respectively. This is in good agreement with the value they found. The monovacancy concentration in tin at the melting point is about two orders of magnitude smaller than in other metals. It is for this reason that Seeger classified tin as a metal that "melts too early".

7.4-Line-shape analysis:

The superposition of a Gaussian and an inverted parabola convoluted with the intrinsic resolutin function was applied to fit the line-shape spectrum in annealed tin. The parabola and Gaussian width is illustrated in figure(7.4.1) and parabola percentage in figure(7.4.2). The parabola width does not change appreciably as a function of temperature, but the Gaussian width changed about 2.3 channels from low temperature region relative to high temperature region. This small change in Gaussian width compared with cadmium also showns the signs of a weak trapping effect in tin.

The percentage change of the parabola was not as much as in cadmium and other metals above vacancy region. It can be seen from figure(7.4.2) this amount almost stayed constant within the statistics of the data and also shows no clear rise near the melting point. An average value of 67% parabola intensity is 10% less than the value obtained by Jackman et al (1973), who obtained 77%. But Jackman et al reported again in 1974 a new value of parabola intensity for tin of 70.4% at room temperature, and this value is not so different from our result. The result of fitting a spectrum taken at room temperature is

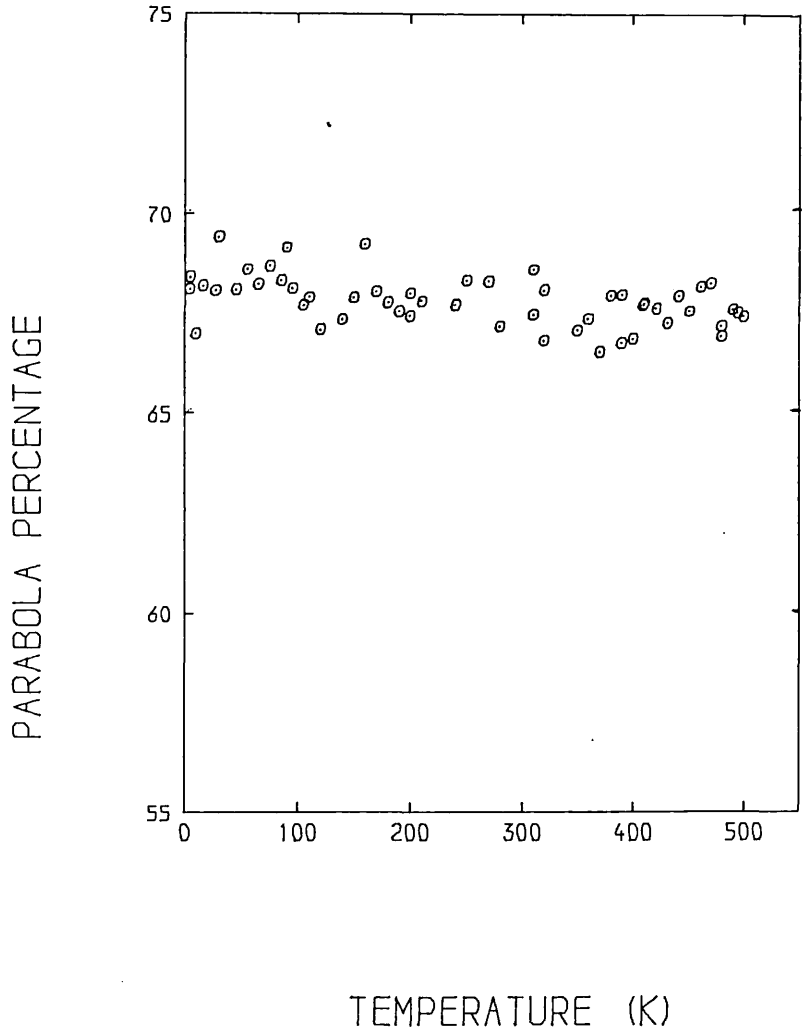

Fig(7.4.2) The parabolic intensity versus temperature for polycrystalline annealed tin. The standard deviation is $\pm$ 1.5%.

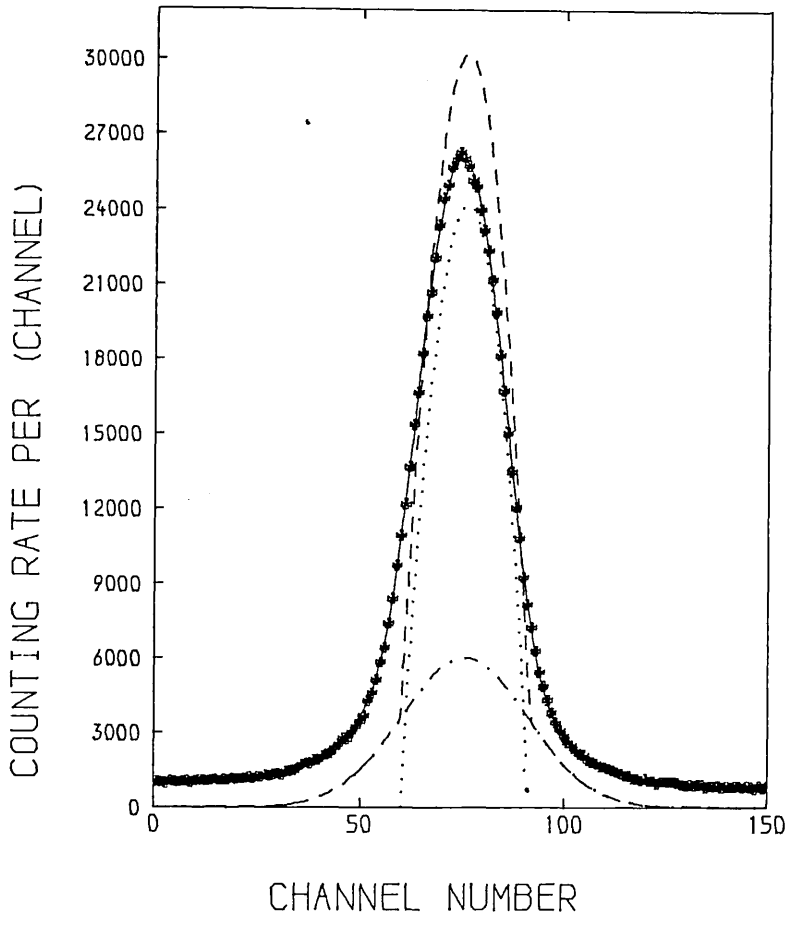

Fig(7.4.3) Application of the convolution technique to separate the two components of the annihilation gamma-ray line in polycrystalline annealed tin, at room temperature.

shown in figure(7.4.3). The solid line is the convoluted result of a Gaussian and an inverted parabola (dashed line) with the intrinsic resulotion function (^{85}Sr single gamma-rays). The fit is considered satisfactory by the value of chi-squared (between 0.95 and 1.3).
The Fermi energy was obtained from the avrage value of parabola width was equal to 17.2 channels at 0.0935keV per channels dispersion, giving E_F=10.12ev. This is in good agreement with Kittel but 15% greater in value than that obtained by Jackman et al (1973). The Fermi momentum was also obtained by Badoux et al (1967) as $P_F=6.32X10^{-3}Xm_o c$ and by Dedoussis et al (1977) as $P=6.3X10^{-3}Xm_o c$, from angular correlation and broadening measurements respectively. The Fermi energy derived from these momenta is in good agreement with our result.

7.5-Conclusion:

Although the F-parameter was fitted by the trapping model method and a value of enthalpy and probability of trapping was obtained, trapping was nevertheless weak. It could be said that no sign of trapping was observed compared to other metals (eg; Cd, Al, Au, In ,pb etc.). Seeger (1973) quotes the radius of Sn^{4+} ions as 0.71 $\mathring{A}$ which is small compared with half interatomic distances (1.40$\mathring{A}$ and 1.51$\mathring{A}$). Therefore Sn^{4+} is considered as narrow core metal similar to Pb^{4+} ion with a radius of 0.84$\mathring{A}$ and half an interatomic distance of 1.75 $\mathring{A}$. Both metals have the same "tetravalent" structure. Despite this, trapping effect has been observed in Pb (Rice-Evans et al 1978), but not in tin. A qualitative explanation for the weak trapping effect in tin has been reported by Seeger (1973). He reported that while some of the properties of tin and lead are the same, the monovacancy volume of tin is 0.25 which is almost the same as alkali

metals but smaller than the 0.4 monovacancy volume of lead. Another explanation is a strong vacancy relaxation implies that for a monovacancy in tin if the neighbouring ions core relaxes inward, they actually reduce the charge to be screened by the conduction electrons, thus resulting in a shallow trapping potential and a small positron-vacancy binding energy. This effect counteracts the formation of a positron bound state. Seeger mentioned (1973) "from the Hodeges calculations(1970)" the trapping potential and positron vacancy binding energy for tin as 5.2 and 1.4 eV respectively by assuming no vacancy relaxation at all. They are calculated in the "rigid" vacancy model.

The monovacancy formation energy in tin obtained in this work is in good agreement with other gruops. The calculated Fermi energy of the electron in tin was also satisfactory compared with other groups. In the case (a) the slope of thermal expansion was very near to value which obtained by Shah et al (1984), their value was $\beta=(32.+2)X10^{-6}$. They observed a remarkable rupture in the F-parameter above 505K the melting point of tin, they belived that is because of the phase transition from the solid to liquid.

7.6-Positron annihilation in deformed tin:

7.6.1-Introductions and method:

Tin has two allotropic forms, first gray-tin or (α-tin semiconductor) which has cubic (diamond) structure with density 5.76 gr/cm^3 and it is stable below 286.4K. Second, white-tin or (β-tin metal) which is ordinary tin and has tetragonal structure, is stable and has a density 7.29 gr/cm^3. At 286.4 K gray-tin changes to white-tin, which is stable above room temperature. The white-tin in the low temperature (230+10)K change to the gray-tin in at least 23

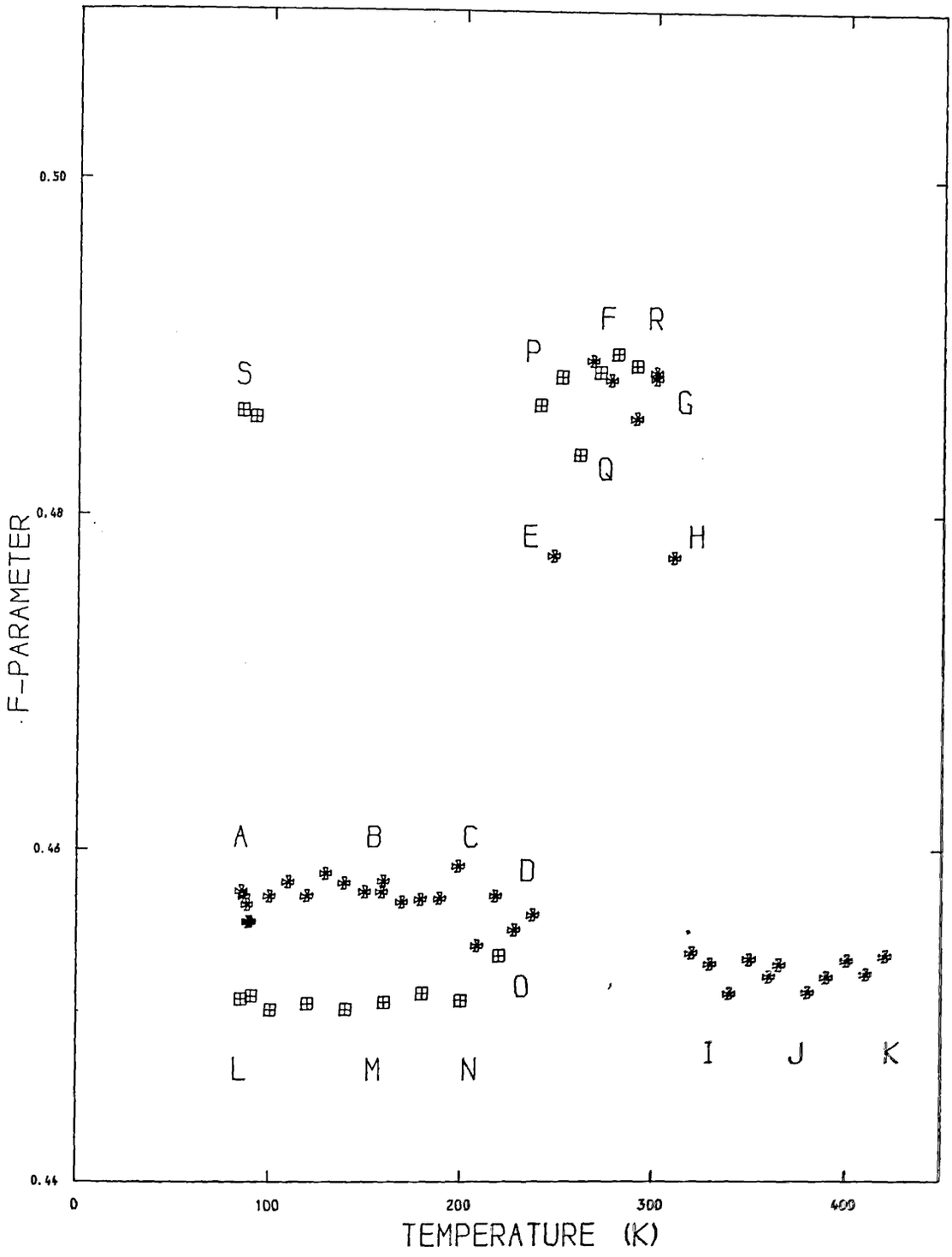

Fig(7.6.2.1) The variation of F-parameter as a function of temperature for polycrystalline tin plastically deformed at 77K. The measurements are indicated scquentially A to S. The standard deviation is ± 0.0005.

days(Puff 1984). This transformation was first reported by Erdiman in 1951. The transformation is accompained by 27% volume change after which a bar of white-tin becomes a powdery mass of gray-tin (Burger and Groen 1957). We explained more about this transformation in chapter two. Puff and Mascher (1984) mentioned that typically the transformation from β-tin to α-tin occured in 23 days, where after a few days (three days) the great mass of the β-tin changes to the α-tin and the rest change in remaining days. The transformation back to the β-tin took place in a shorter time.

Busch and Kern 1960 claimed that transformation from β to α-tin requires two process; first the phase formed at nucleation time t, second this nucleation time is followed by spherical growth of each nucleus with a linear rate of L, where both time and linear rate are temperature dependent. Traditionally, this transformation has been obtained by (a) dilatometric measurements and change of volume, (b) direct observation of the motion of the physical boundry. Recently modern techniques have been used, such as X-ray interaction technique (Burger et al 1957), mossbauer isomeric shift (Nikolaov et al 1973), positron lifetime measurement (Puff 1984) and Doppler broadening measurement (Rice-Evans et al 1985).

Method:

Two pieces of the tin with dime sion 1.5x1.5x.2cm, spark erusion cut from a rod with 99.999% purity supplied by Koch-light Laboratories Ltd. The pieces then was etched in nitric acid and cleaned up by alcohol, then 0.5 mCi of carrier-free ^{22}NaCl solution was evaporated directly onto central region of the surfaces of the two pieces. The estimated diameter of activation area was 0.2cm. The two pieces then put together as a sandwich configuration and wrapped in thin aluminium foil. The source-specimen was then placed in a bath of liquid

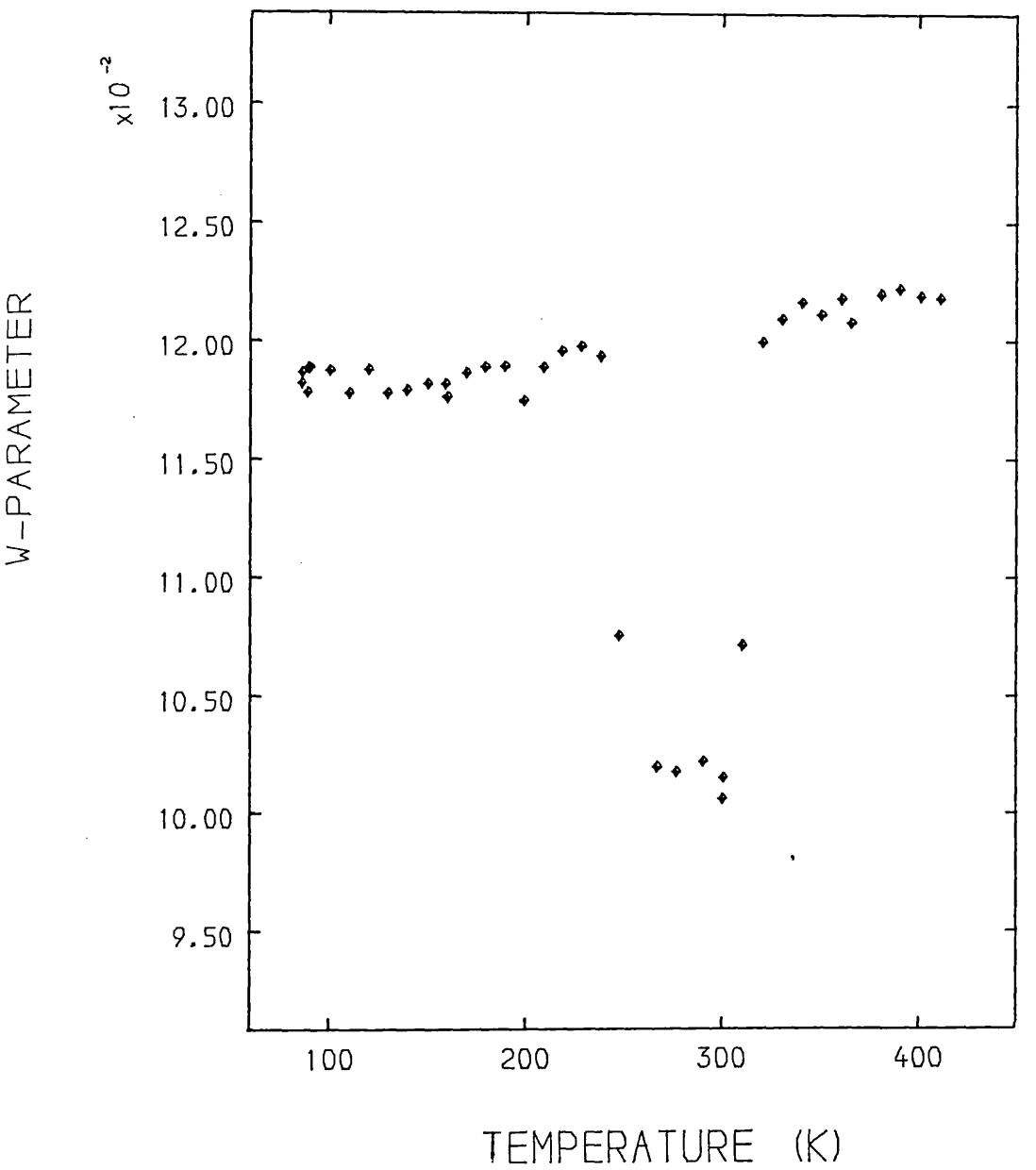

Fig(7.6.2.2) The variation of W-parameter as a function of temperature for polycrystalline tin plastically deformed at 77K.

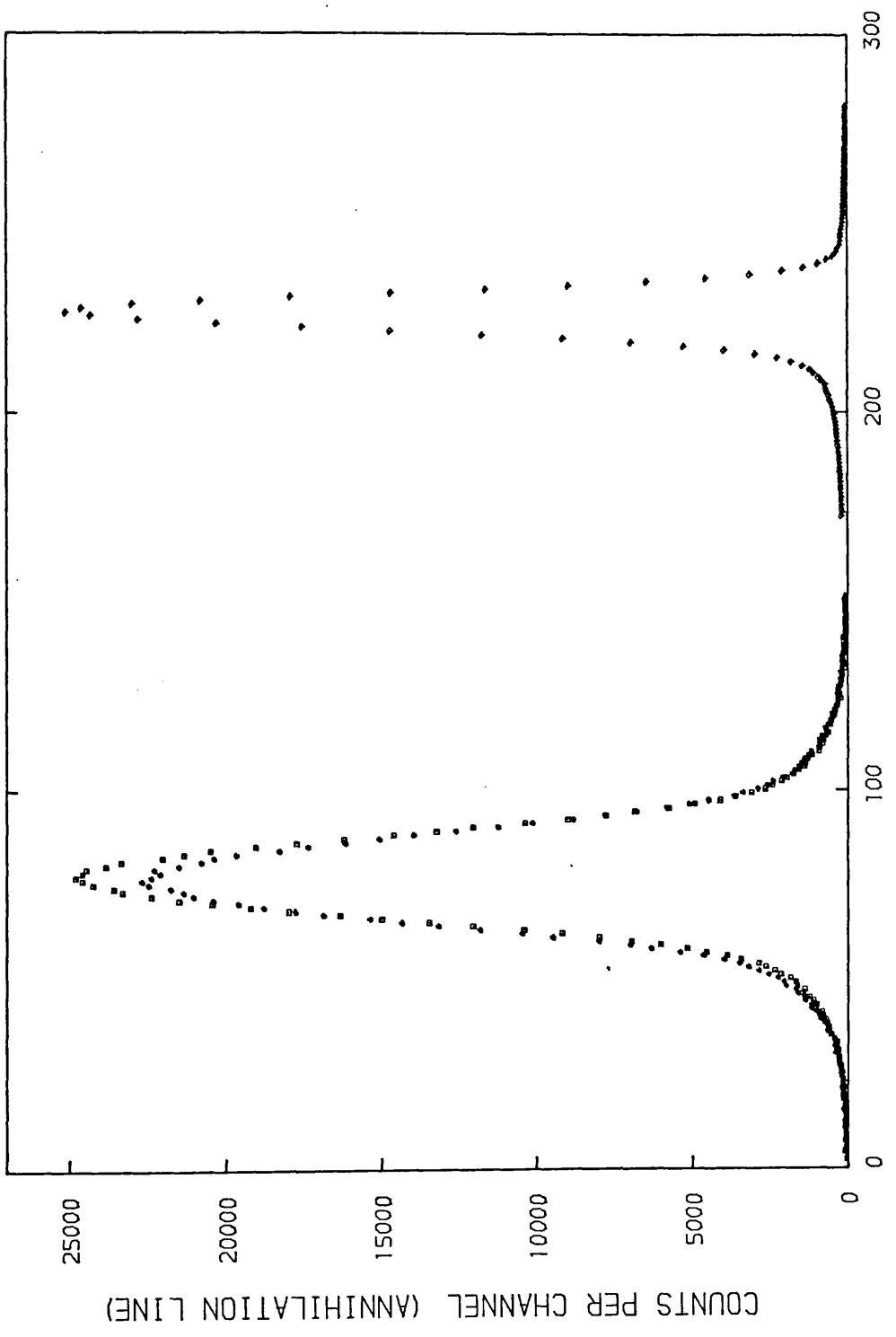

Fig(7.6.3.1) Examples of line shapes. To the right is the response of the photon detector to monochromatic gamma-ray at 514kev. To the left are two Doppler-broadened 511kev lines for white tin and grey tin.

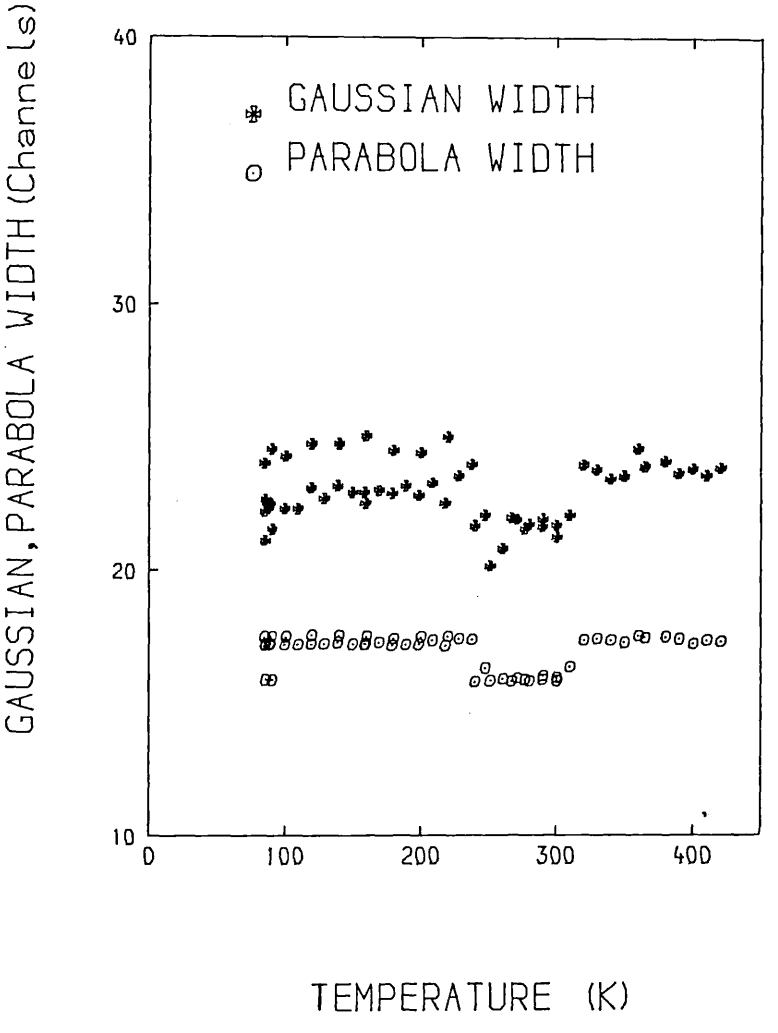

Fig(7.6.3.2) The temperature dependance of the width parameters of the Gaussian and parabolic components of individual lines for polycrystalline deformed tin.

nitrogen which lay between the jaws of a hydraulic press. The application of 10 tons pressure on the specimen resulted in the reduction of its thickness to approximately 50% at 77K. The source-specimen was then immediatly transffered to the cryostat under a bath of liquid nitrogen So that the temperature of the sample did not rise above 110 K. After mounting the specimen in the cryostat, the temperature of sample was kept at 80 K at equilibrium with a stability better than 0.5K. Data accumulation started in range 80 K to 420 K with increment of 10 K. The vacuum of the chamber during the measurement was better than $1X10^{-5}$ torr and the total counting rate was $7X10^{6}$ in two hours.

7.6.2-Line-shape parameters:

The annihilation radiation provides detailed information of the electron density in metals sampled by the positrons. Following the extensive theoritical work on positron electron annihilation (West 1979, Nieminen and Manninen 1979), it is known that the lifetime and line-shape parameters of positron annihilation are proportional to the average density of the electrons during annihilation. Therefore the analysis of line-shape parameters is suitable not only for the identification of the structure of the defect but also for the study of phase transitions. The line-shape parameters F and W-parameter versus temperature are illustrated in figures(7.6.2.1) and (7.6.2.2). As it can be seen the F-parameter is plotted as a function of temperature and is indicated alphabetically, to make the identification of each stage a little easier. Each point reprsents a two hour run starting at 80 K with incre ment of 10 K.

It shows that no change has been observed in the F-parameter by increasing the temperture up to 230 K (A-B-C-D on the curve). Above

230 K the F-parameter rises to 4.8% to point E in less than 3 hours and then again about 2% to point F. This demonstrated the rapid transition of the white-tin to gray-tin in about 5 hours which is coresponding to the reduced metalic density from 7.29 gr/cm^3 to 5.76 gr/cm^3. The F-parameter remains constant up to 300 K, this represented that the sample stays at constant structure (α-tin). The gray-tin was then changed to the white-tin again after approximately 4.5 hours (G-H-I) on the figure(7.6.2.1). It remained white-tin all the way up to 420 K (I-J-K), the small rise above 390 K indicates monovacancy creation for the annealed β-tin (see section 7.2). The sample was then cooled down from 420 K slowly to 80 K and again process repeated in an interval of 20 K up to 220 K (L-M-N-O). It is found that the F-parameter is significantly lower than for the deformed sample. This difference (of about 1.7%) demonstrated the recrystallzation process of the deformed β-tin from a high concentration of defects (A-B-C) to a low concentration for the annealed sample (L-M-N). The white-tin again transfer to the gray-tin at 240 K in 2 hours time and remained gray-tin at 290 K (P-Q-R). But unfortunately runs were not continued above 290 K because the heating wire of the sample holder was damaged at that temperature. But after it was cooled down, two more points were taken at low temperature (80 K), S point on the curve. It was clearly shown that the sample remained in α-tin as was expected from the properties of the element. Finally the sample was extracted from the cryostat and the metal discovered to have been reduced to a fine powder. The above process demostrated that the white-tin was transformed to gray-tin at (230$\pm$10)K and retransformed to the white-tin at (300$\pm$10)K, and process occured in short time because of plastic deformation. This was observed by Puff et al in lifetime measurements in 1984 after our measurements.

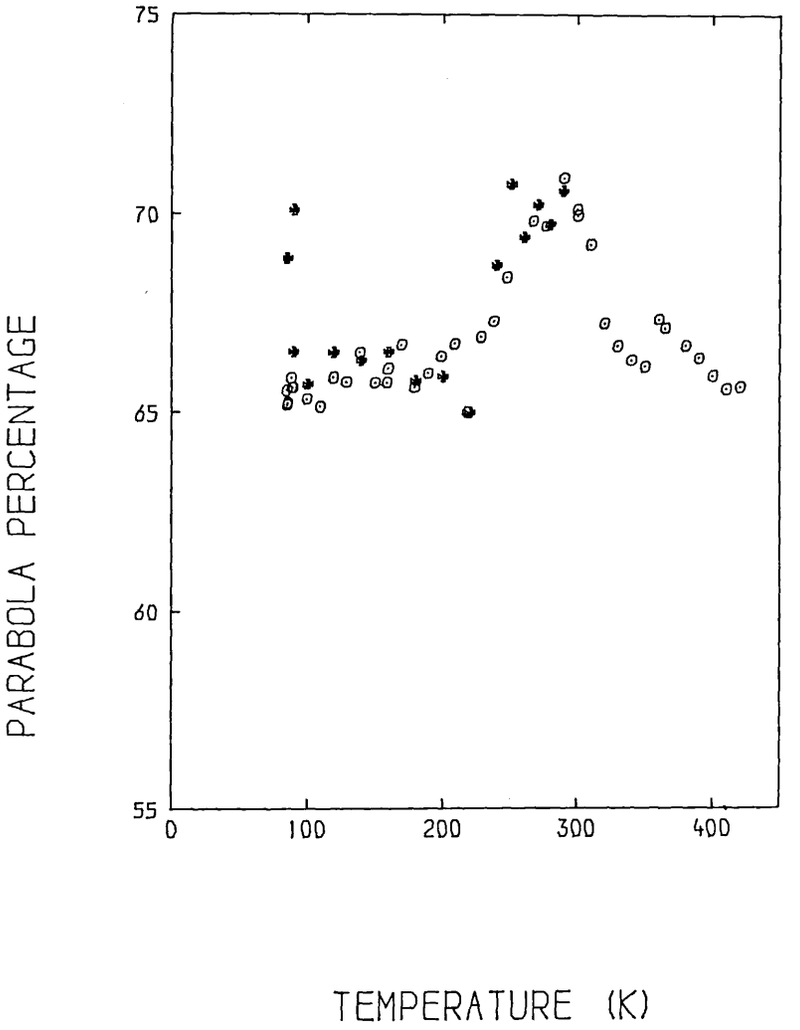

Fig(7.6 .3.3) The temperature dependence of the proportion of the annihilation contributing to parabolic component of line shape of the polycrystalline deformed tin (circle),and polycrystalline annealed tin (star). The standard deviation is ± 1.0%.

7.6.3-Line-shape analysis:

The application of the superpositon Gaussian and an inverted parabola convoluted with the resolution function has been applied to analyse the line-shape spectrum. Figure(7.6.3.1) is shown that the difference between spectrum of positron annihilation in α-tin and β-tin on the left of the figure, and on the right of the figure the mono-energetic Gamma-ray spectrum of ^{85}Sr (response function) normalized to the same peak height. The result of the convolution was illustrated in figure(7.6.3.2) and (7.6.3.3). The Gaussian and parabola width's vary with temperature, figure(7.6.3.2). There is a sharp drop and rise in Gaussian and parabola width's around the transition temperatures. The significant change in Gaussian width from 23 channels to 25 channels in average at low temperature shows the weak trapping of the positron in β-tin in deformed sample with respect to annealed β-tin. The parabola width for both deformed and annealed cases was remained constant versus temperature, on average 17.2 channels, the same as computed in the annealed sample as explained in section 7.4 of this chapter. But the parabola width as it could be seen from the curve was dropped about 1.2 channels at 240 K and stayed same as transition occured then back to the 17.2 channels. The Fermi energy then calculated for β-tin from 17.2 channels at .0935eV per channel 10.12 eV, is the same as before and for α-tin also calculated as 8.76ev. This compared with the value obtained by Badoux et al in 1967 from angular correlation measurements and was in good agreement.

Figure(7.6.3.3) shows the parabola percentage intensity in annihilation line-shape and it can be seen the correlation of the parabola intensity with F-curve in the case of the transition was satisfactory. But the intensity of parabola in annealed and deformed

was not the same as we expected like cadmium result (the star symble on the curve). The parabola percentage r se from 66% to approximately 70% at transition for β-tin and α-tin respectively.

7.6.4-Zero-point motion:

As we discussed in section 7.4 the trapping of the positron in β-tin was not like that in noble metals, where it is trapped in a deep potential well. Therefore no significant changes were expected in chi-squared by addition of an extra Gaussian to the convolution analysis because the effect of zero-point kinetic energy is not the same as for cadmium (Rice-Evans et al 1978b). But eight spectra have been chosen from the different cases (annealed, deformed, and transition), at different temperatures and then analysed by addition an of extra Gaussian to the convolution process as is explained in chapter five.

The results of these analyses are illustrated in figures(7.6.4.1, 7.6.4.2, 7.6.4.3, and 7.6.4.4). It can be seen that the chi-squared was reduced to the minimum value approximaty at σ_b=2 channels for the case of the deformed sample relative to the annealed sample at 100 K. The same happended for β-tin at a temperature of 160 K. In the case of the annealed β-tin sample at high temperatures (400 K) and low temperatures (100 K) also, there was a minimum point at σ_b=2, which is very weak compared to polycrystal cadmium and single crystal cadmium (Rice-Evans et al 1978b). Finally two spectrums at 290 K for α-tin and 110 K for β-tin were also shown in figure(7.6.4.4) which the chi-squared minimised at approximately the same σ_b . This might be another reason to show that the trapping of the positron in tin is very weak as compared to other metals.

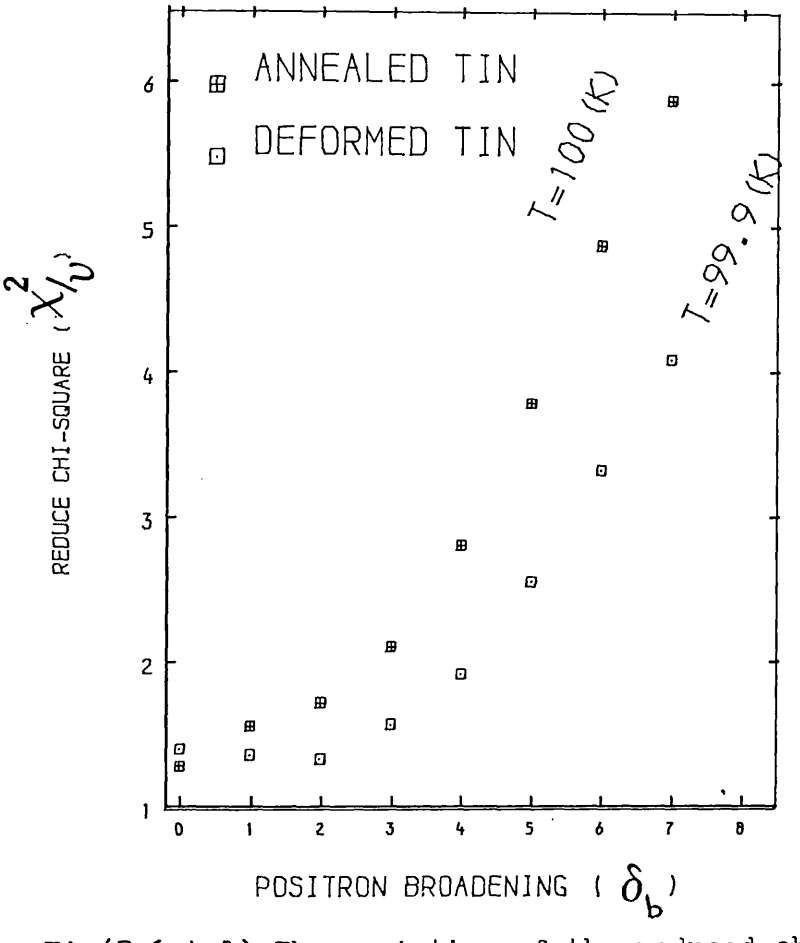

Fig(7.6.4.1) The variation of the reduced chi-squared with the positron Gaussian width in polycrystalline deformed and annealed tin at the same temperature.

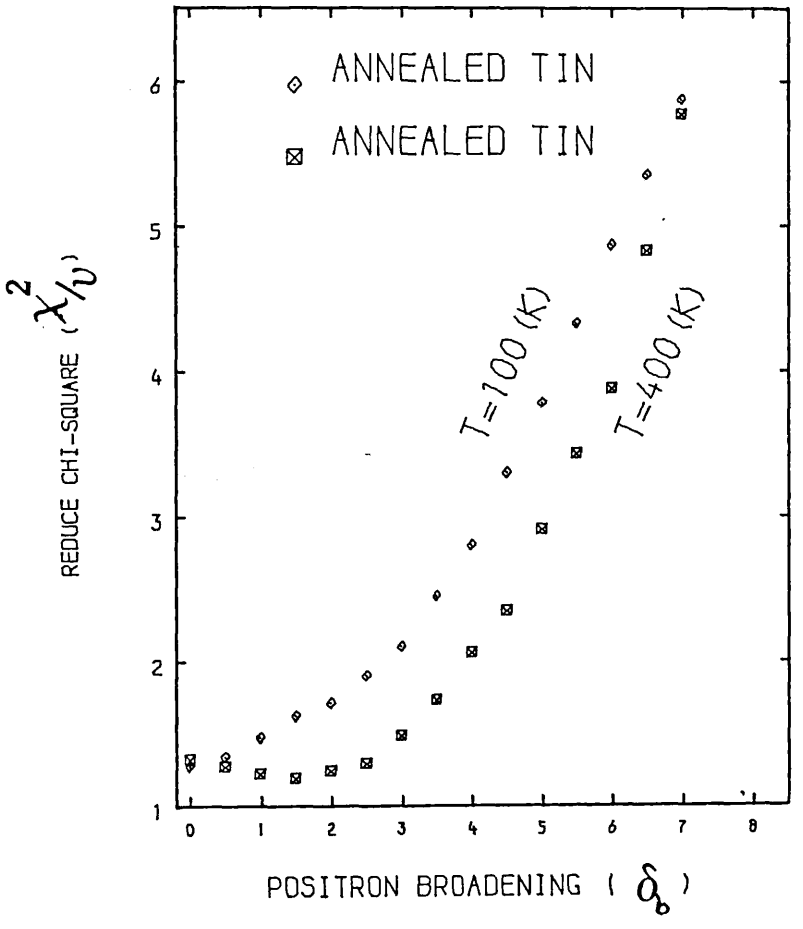

Fig(7.6.4.2) The variation of the reduced chi-squared with the positron Gaussian width in polycrystalline annealed tin at two different temperatures.

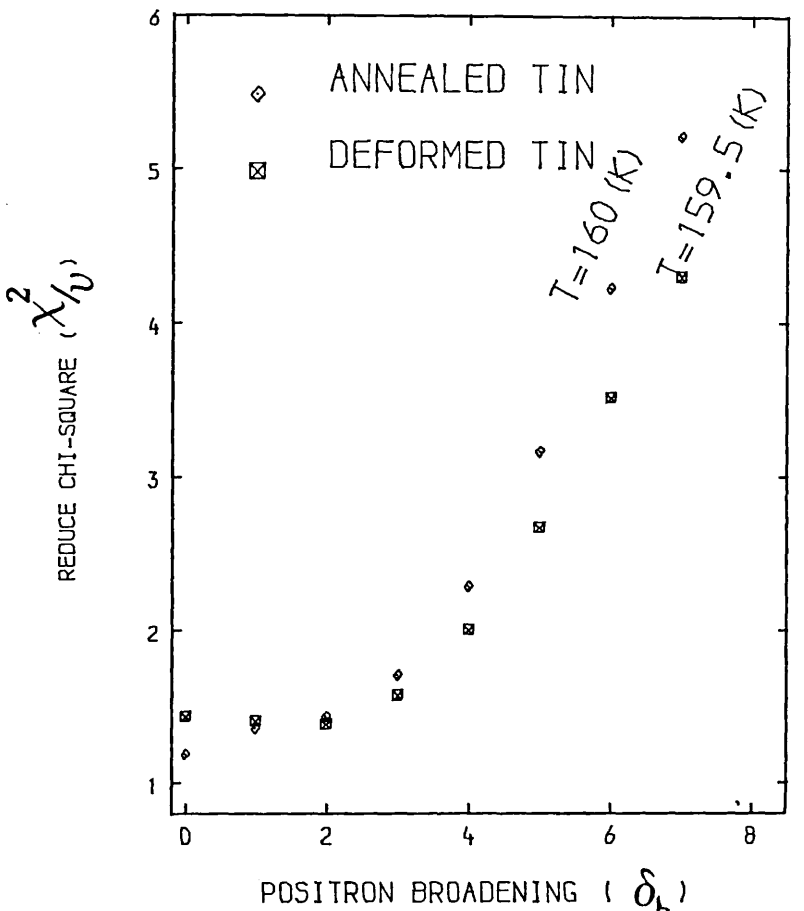

Fig(7.6.4.3) The variation of the reduced chi-squared with the positron Gaussian width in polycrystalline deformed and annealed tin at the same temperature.

7.6.5-Conclusion:

As mentioned by Bush and Kern (1960), a necessary requirement for the occurence of transition is the existence of the α-nuclei in the metallic phase. After nucleation the transformation starts near the surface of the sample, and the growth rate is strongly dependent on temperature and impurity content. This transformation occured in at least 23 days where 85% of the annealed sample change in at least three days and rest of that in more than 20 days Puff et al (1984). The principle of the transition of β-tin to α-tin and vice versa was in good agreement with Puff et al, but the transformation time is completely different from their results. We believe from our results that about 70% of the β-tin was transformed to the α-tin at (230±10)K in approximately 2.5 hours and the rest transformed in another 2.5 hours, while they obtained a complete transformation in 23 days. Therefore it is obvious that deformation of the tin or high concentration of defects promotes the transition. That is reasonable because it is also mentioned by Lohberg and Presche (1968), where undeformed white-tin do not transform even after considerable time in the absence of contact with grey-tin or with isotopic phases, incubation time may be reduced to less than one hour by deformation. The other method to accelerate the transformation was observed by Cohen and Van Eyk (1899). The transformation of white-tin to gray-tin will be accelerated if sample was immersed into a solution of pinksalt $(NH_4)_2SnCl_6$. The sample configuration changed from the bar to powder, possibly because of the 27% change in volume which accompanied the transformation from β-tin to α-tin.

The Fermi energies of white-tin and gray-tin which were calculated in this work, 10.12 eV and 8.76eV respectively, were both satisfactory when compared with other groups. The transformation temperature at

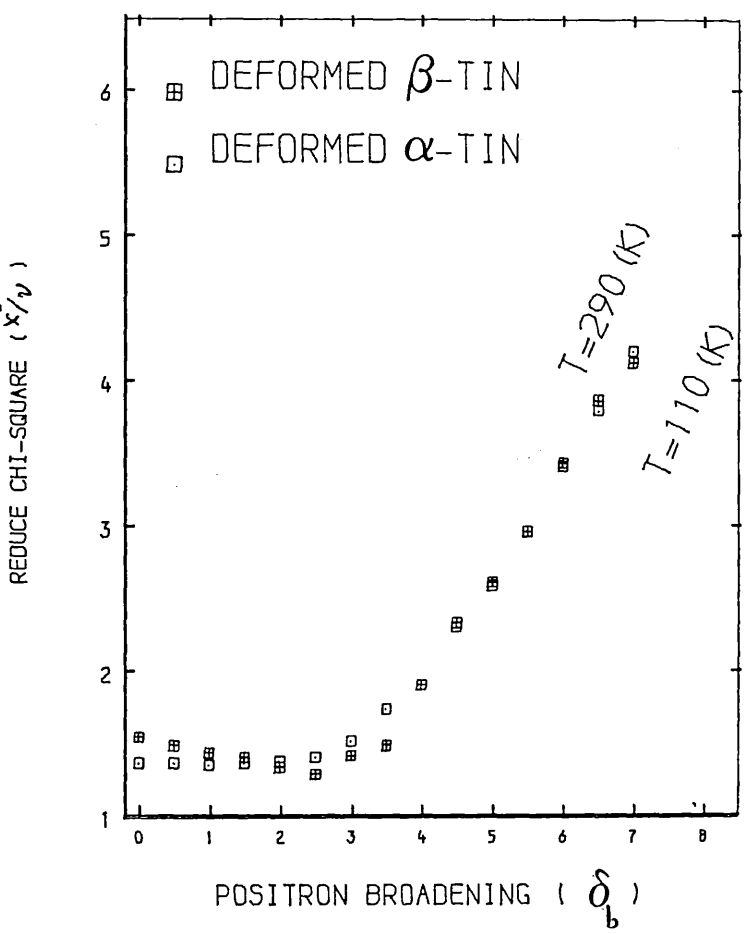

Fig(7.6.4.4) The variation of the reduced chi-squared with the positron Gaussian width in polycrystalline white and grey tin at two different temperatures.

(230±10) K β-tin to α-tin was also satisfactory when compared to Bursh and Kern 1960 and Puff et al 1984 and vice versa.

Chapter VIII Positron annihilation in selenium.

8.1-Introduction and method:

Selenium is a very complicated substance and very little is known about its basic properties (Chizhikoz et al 1968). Selenium has several alltropic structure forms. The more stable one is grey with a trigonal structure. It can be produced with either an amorphous or crystalline structure. The colour of amorphous selenium is red in powdery form and black in vitreous (glassy like) form. The structures of the three principle crystalline allotropes of selenium, namely α-monoclinic, β-monoclinic, and trigonal are well documented. The amorphous selenium with a density 4.28 gr/cm^3 transfers to hexagonal structure at 333.15 K. In fact the lattice of trigonal selenium consists of screw-like spiral chains which are arranged in hexagonal symmetry.

Positron annihilation studies of selenium have been already reported in the literature. Most of the experimental measurements using positron annihilation in selenium reported, so far, have used angular correlation measurements and the results compared with other semiconductors such as silicon, and germanium (Hautojarvi and Jauho 1967). An angular correlation measurement in different types of selenium was reported by Baskova et al (1961). They reported that the angular correlation curve for crystalline selenium is wider than for amorphous and a narrow component of the angular distribution was observed in black and red amorphous selenium representing positronium formation. However, Hautojarvi and Jauho reported that the behaviour of a positron in selenium was more like that in an insulator. The lifetime of positrons in polycrystalline selenium was measured by Brandt and Oremland in 1976. They reported that the recrystalization

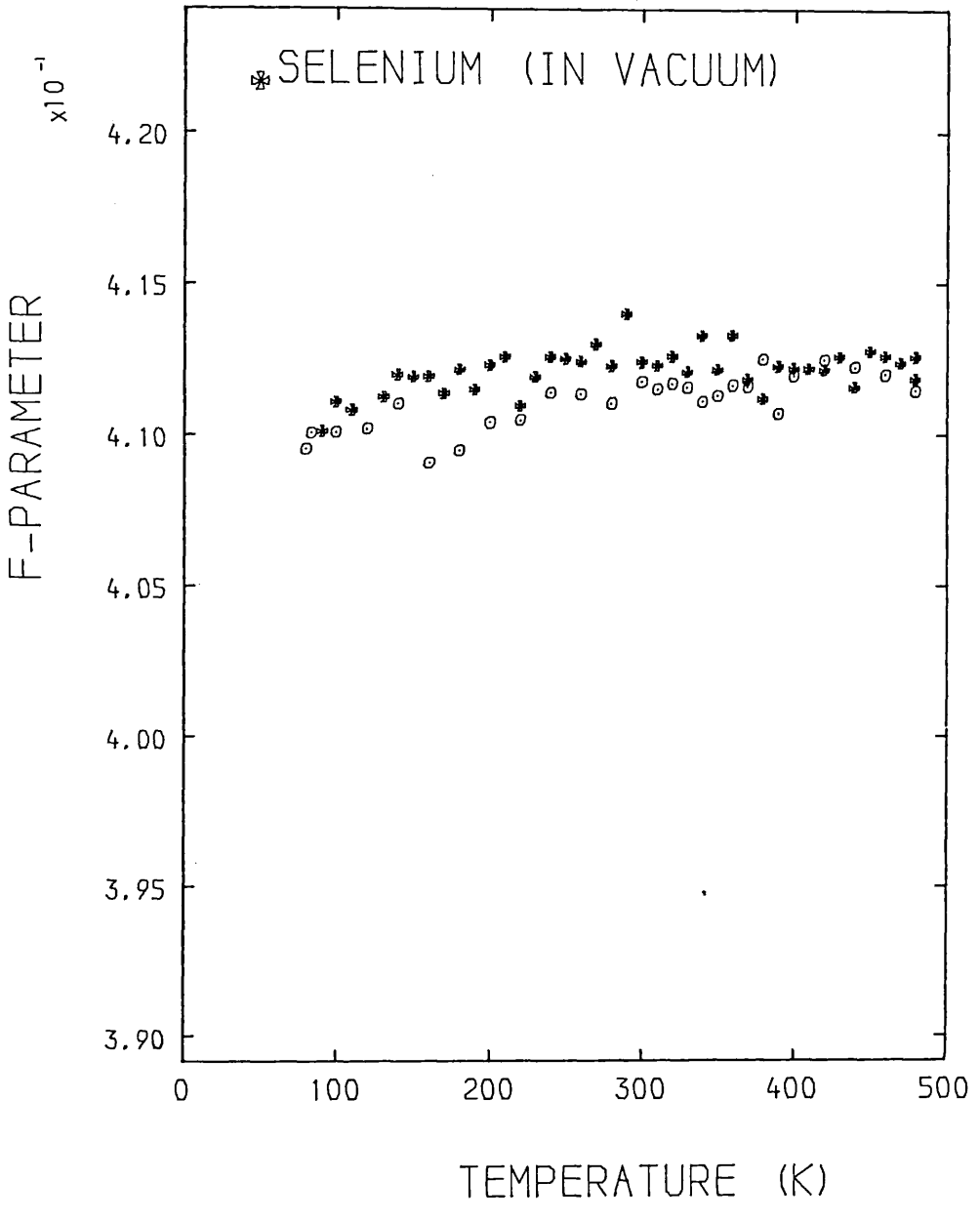

Fig(8.2.1) The variation of F-parameter with temperature for selenium sample. The standard deviation is estimated to be ± 0.0005. Star is for heating the sample and circle is for cooling the sample.

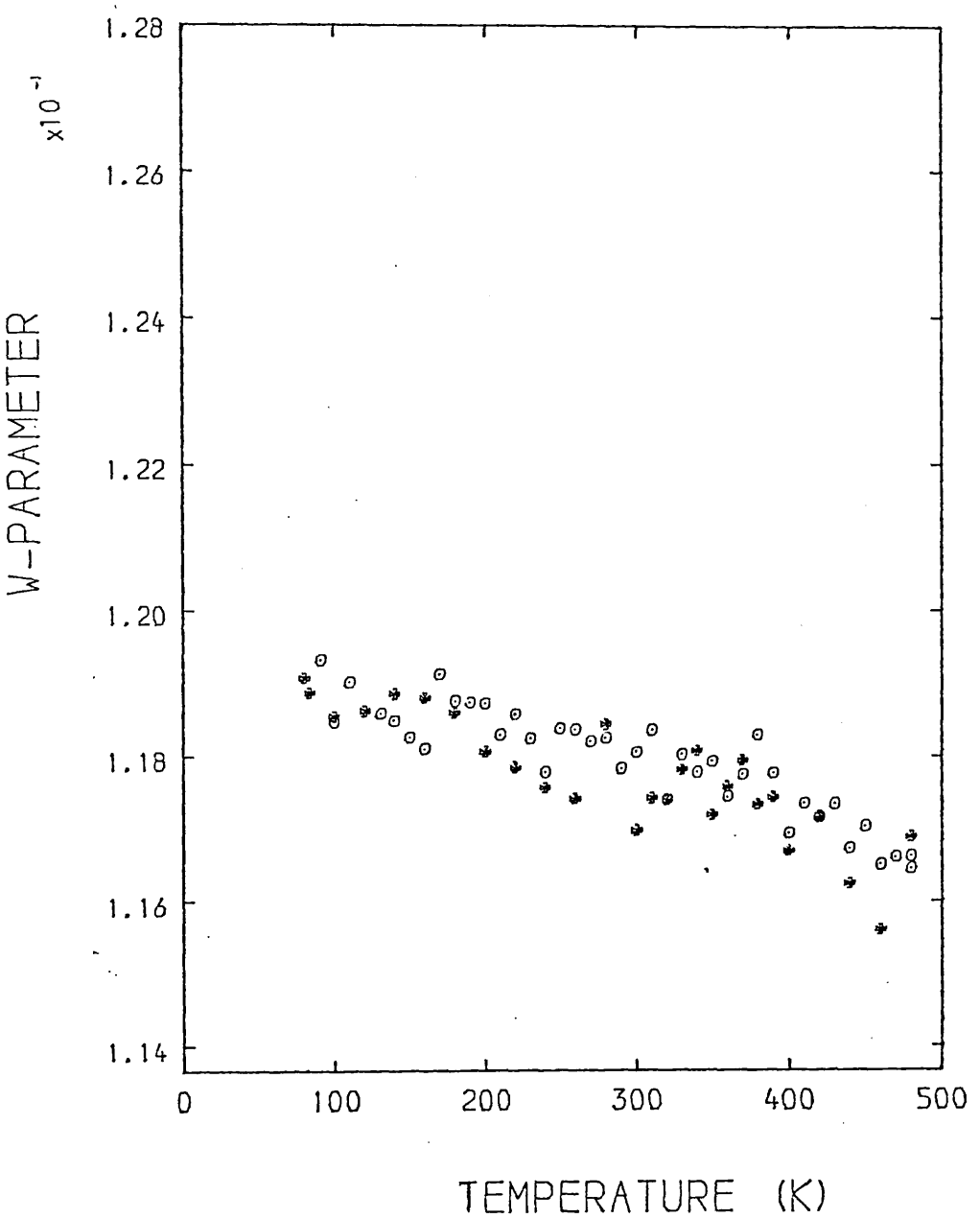

Fig(8.2.2) The variation of W-parameter as function of temperature for selenium sample. The standard deviation of W value is estimated to be $\pm$ 0.0006. Circle is for heating the sample and star is for cooling the sample.

of polycrystalline selenium is fast at high temperatures, (e.g at 220 K the lifetime of τ=322 ps drops to τ=275 ps in less than five minutes). But in 1977 the lifetime of positrons in selenium was reported to be 355 ps by Balogh and Dezise (1977). Later Itoh F. et al (1978) observed that the lifetime of positrons in trigonal selenium is 9% shorter than in amorphous selenium. They suggested that this is because the density of electrons in amorphous selinium is less than in trigonal selenium. But they did not investigate the temperature dependence of positron annihilation in selenium. Recently Vanderbilt and Joannoponlos, (1983), have made some total energy calculations to determine theoretically the structur al configuration of vacancies in selenium. They found a value for the activation energy of 1.3 eV which implies no thermal creation of vacancies below the melting point. This is unlike most other elements. In this experiment the characteristics of positron annihilation in selenium have been investigated as a function of temperature, to search for thermal creation of defects below the melting point.

Method:

The specimen was prepared in this study by the following procedure; two discs of selenium with purity 99.99% supplied by Koch-light Laboratories Ltd were used as the sample. The diameter of pieces was 9.4 mm and thickness 0.4 mm, with trigonal structure. The specimen was used directly to make a source specimen without etching or annealing, since the sample had already been annealed by the company and kept in a vacuum bottle. 200 μCi of a carrier-free ^{22}NaCl solution was then evapourated directly onto the central regions of the two discs, without heating. The two pieces were then put together in a sandwich configuration, and encapsulated in a wrapping of thin aluminium foil. The source sandwich was then mounted in the low

temperature cryostat under vacuum better than 10^{-6} torr and cooled down to liquid nitrogen temperature 77 K. The same system was used for measurement as was described in chapter four. The data was accumulated for 2 hours at each equilibrium temperature with a total counting rate of 810000 counts at the 511 keV peak area. The system stability was about one channel at 4000 counts per second, and the temperature stability was better than 0.5 K for each run. The data was accumulated over the range 77 K to 480 K near melting point of selenium (495 K).

8.2-Line-shape parameter;

The F and W parameters are illustrated as a function of temperature, in figures(8.2.1) and (8.2.2) respectively. Apart from fluctuations, the F-parameter appears flat to about 400 K and rises very gently at about 0.6% above 400 K. It is difficult to believe that this small rise in the F-parameter is due to conventional trapping of positrons in large volume vacancies and voids. The small increase in the F value does not characterize well the behaviour of positrons in selenium as a function of temperature owing to the inherent scatter in the points. Therefore, in order to minimise this scatter, the centroid channels of the peak for the F-parameter (i.e. the integration of the central area of the spectrum) were varied from 15 channels to 12,21,25,29 channels respectively. The result of this change variation made no significant difference to the changes in the F-parameter.

But as is shown in figure(8.2.2) the W-parameter was smoother than the F-parameter and decreased by about 2.4% from the low temperature region with respect to the high temperature region. It remains approximately flat to 200 K and then it begins to decrease slowly with

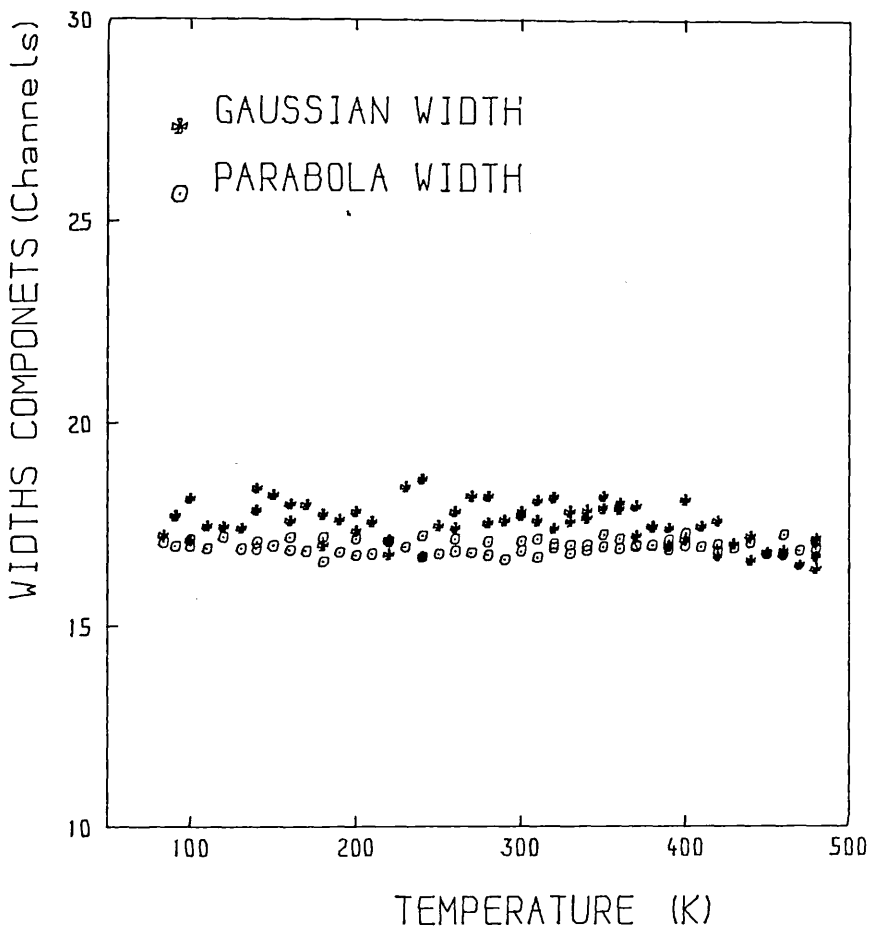

Fig(8.3.1) The variation of the Gaussian and parabolic width components as function of temperature for selenium.

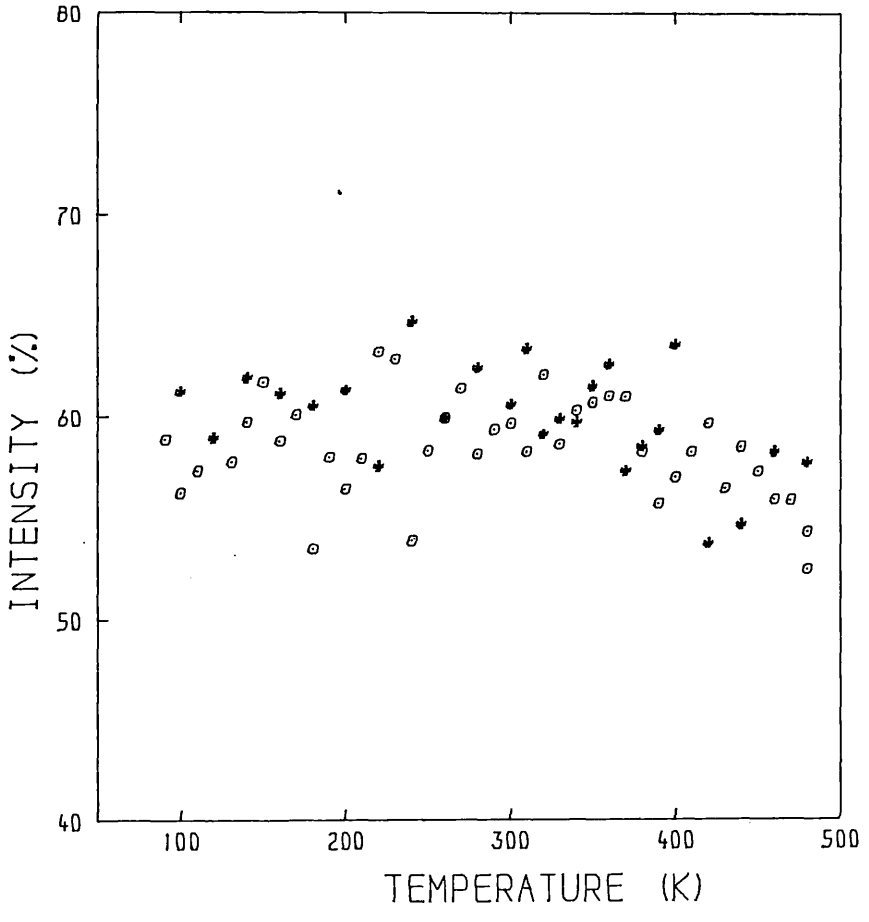

Fig(8.3.2) The variation of parabolic percentage with temperature in selenium, circle is for heating and star is for cooling the sample. The standard deviation is $\pm 2\%$.

a small slope from 200 K up to 350 K which represents thermal expansion as in other metals, and then decreases sharply to near the melting point of the selenium (480 K).

The results showed no sign of trapping of positrons in selenium, unlike metals such as cadmium, lead, indium, etc. where it was observed (Rice-Evans et al 1978b). This tends to confirm the calculation of Vanderbit and Joannopoulos (1983).

8.3-line-shape analysis:

The model dependent convolution technique outlined in section three of chapter five, was used in analysing the selenium data. The Gaussian and parabola widths are shown in figure(8.3.1). It can be seen that the parabola width is not temperature dependent and it is roughly constant with an average of 16.8 channels. The Gaussian width as can be seen in the curve is different and narrower than for metals such as cadmium and tin (see previous chapter). It seems, the core electrons of selenium have low momentum compared with metals. This width decreases approximately 1.0 channel from room temperature to near the melting point temperature. The chi-squared goodness of fit was between 1.8 to 2.4 and is higher than the chi-squared which was found in the case of metals (tin, cadmium) below room temperature. This suggests that perhaps it was not correct to fit the selenium data spectrum with a Gaussian and an inverted parabola. Therefore attempts were made to fit with only two Gaussians, and also two Gaussians plus an inverted parabola, but unfortunately this was found to give a worse chi-squared than the previous value.

The percentage of parabola calculated averaged 62.5% below room temperature which is not in good agreement with 79% by Kusmiss (1965). Figure(8.3.2) illustrates the parabola percentage as a function of

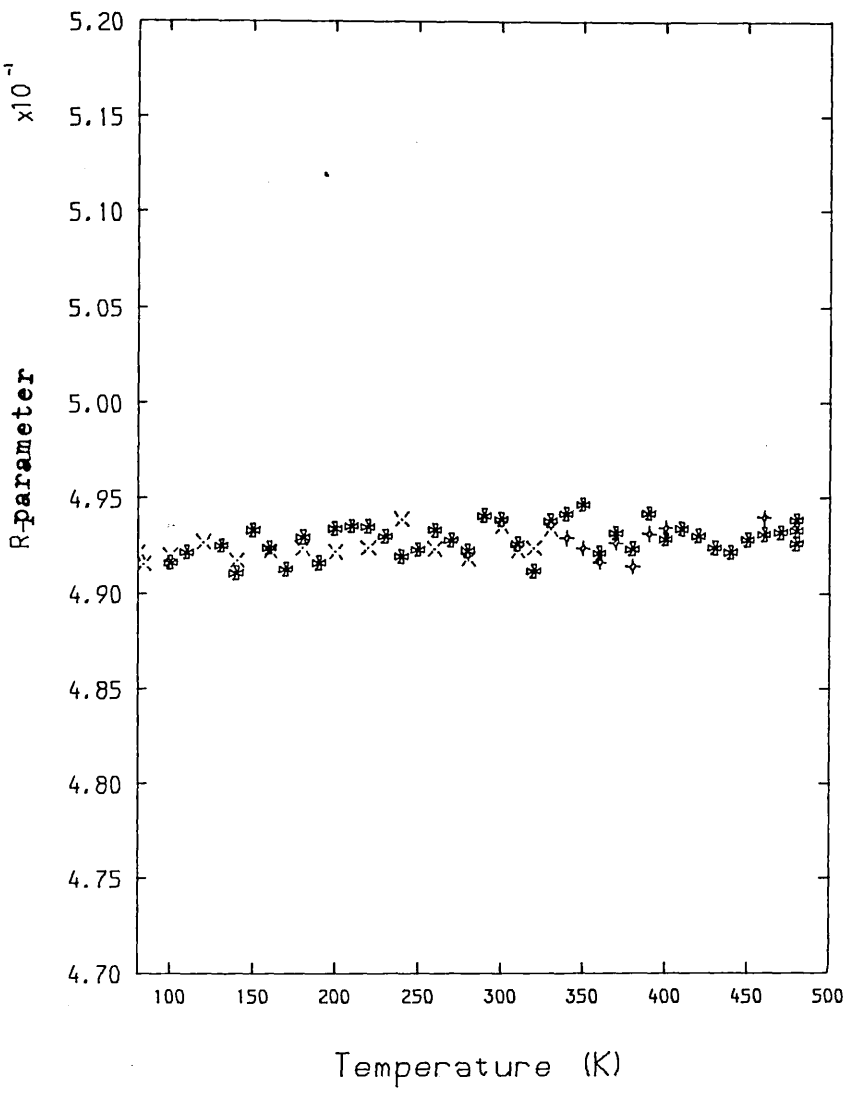

Fig(8.4.1) The varition of R-parameter with temperature for positron annihilation in selenium. The standard deviation of R value is $\pm$ 0.0009.

temperature. It shows, apart from a high fluctuation in points, a small decrease at high temperature. It is difficult to deduce any thing significance from these results. Perhaps the similarity between the Gaussian and parabola widths hides any effects such as the creation of vacancies at high temperature.

8.4-Search for positronium:

If positrons behave in selenium as they do in an insulator which has no free electrons, (Hautojarvi and Jauho 1967), then it is to be expected that positronium will be formed. Therefore the R-parameter (ratio of the total area under the band width in 340 keV region over total area of the pea k) were calculated and plotted as a function of temperature [figure(8.4.1)]. R appears flat as temperature is increased up to near the melting point, indicating there is no change in the creation of positronium. This too is inconclusive for there may be no positronium produced any way. The results agree with the angular correlation measurements of Hautojarvi and Jauho.

8.5-Conclusion:

In this investigation of the F-parameter and from the convolution analysis of the spectrum it is concluded that the F-parameter is weakly temperature dependent. There is no direct evidence to suggest vacancies are created in selenium at high temperature. Vanderbit and Joannopoulos (1983) calculated the total energy of the structural configuration of vacancies in selenium to be 1.3 eV. This implies a high threshold temperature (>600 K) for the creation of a vacancy, a temperature at which in fact selenium melts. This reminds us of Seeger's explanation for tin where he said that it melted too early. To confirm this the spectra w ere also fitted with a single Gaussian to look for any signs of positron trapping in vacancies. The Gaussian

width would increase at high temperatures with the creation of the vacancies because of the broadening in the spectrum induced by zero point motion. The fits show no sign of an increase again confirming that no vacancies are created below selenium melting point.

The small increases in F and the decrease in W parameters as a function of temperature can be attributed to the thermal expansion of the specimen.

Chapter IX Positron annihilation in grafoil

9.1-Introduction and method:

Positron annihilation in metals offers a unique way to observe the momentum distribution of electrons and some other properties of the solid. The gamma-ray spectroscopy result of positron annihilation is one of the ways of studing materials. The techniques used to investigate the spectroscopy result of the annihilation pairs are lifetime, angular correlation, and Doppler broadening measurments.

The behaviour of positrons in the bulk of a solid is different from its behaviour on the surface of the solid. For example the lifetime of the positron in the bulk is ($\tau \sim 0.2$ ns) while the lifetime of the positron on the surface is (~ 0.4 ns) which is two times greater (Jean et al 1984). The low energy positron beam has recently being used as a good technique to investigate the behaviour of positrons on the surface of materials and their surface properties by (Mills Jr 1979), (Mills Jr et al 1983) and (Lynn et al 1985). When the slow positrons are implanted into metal some diffuse back to the surface where they may either become bound or may leave the surface. Most positrons diffus ing back to the surface are not emitted as free positrons or Ps but become bound at the surface in their image correlation potential well, or become weakly bound to the surface by van der Waals force (Platzman and Tzoor 1985). Mills Jr (1979) reported that bound positrons are thermally desorbed from the surface as the temperature is increased to form Ps which is then annihilated, (for more detail see chapter three section three).

The investigation of positron annihilation in graphite and carbon black has been reported by West et al (1979), Shimotonai et al (1981) and Berker et al in 1983. They reported the lifetime of the positron

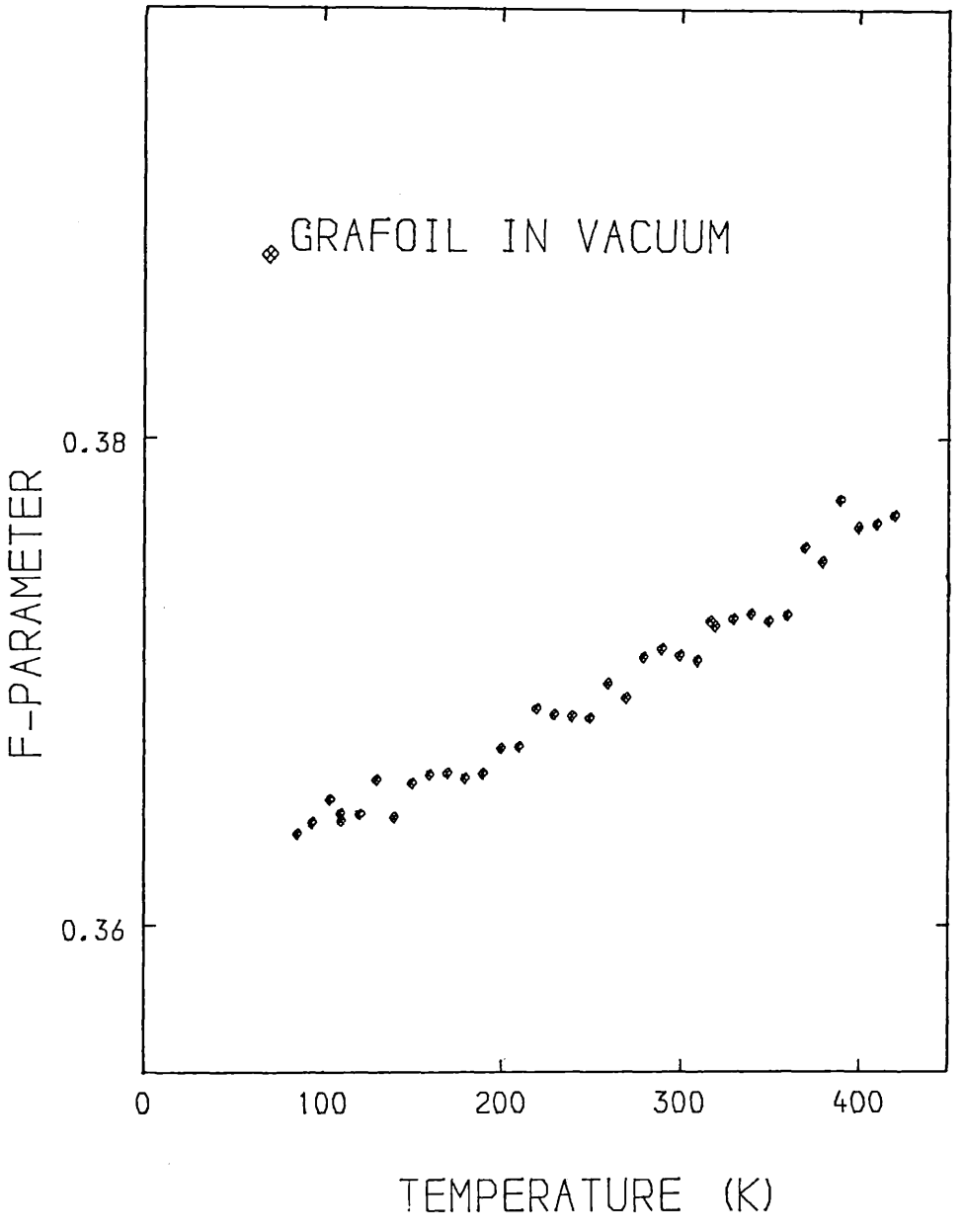

Fig(9.2.1) The variation of F-parameter with temperature for positron annihilation in grafoil, without any background subtractions. The standard deviation of F value is $\pm$ 0.0007.

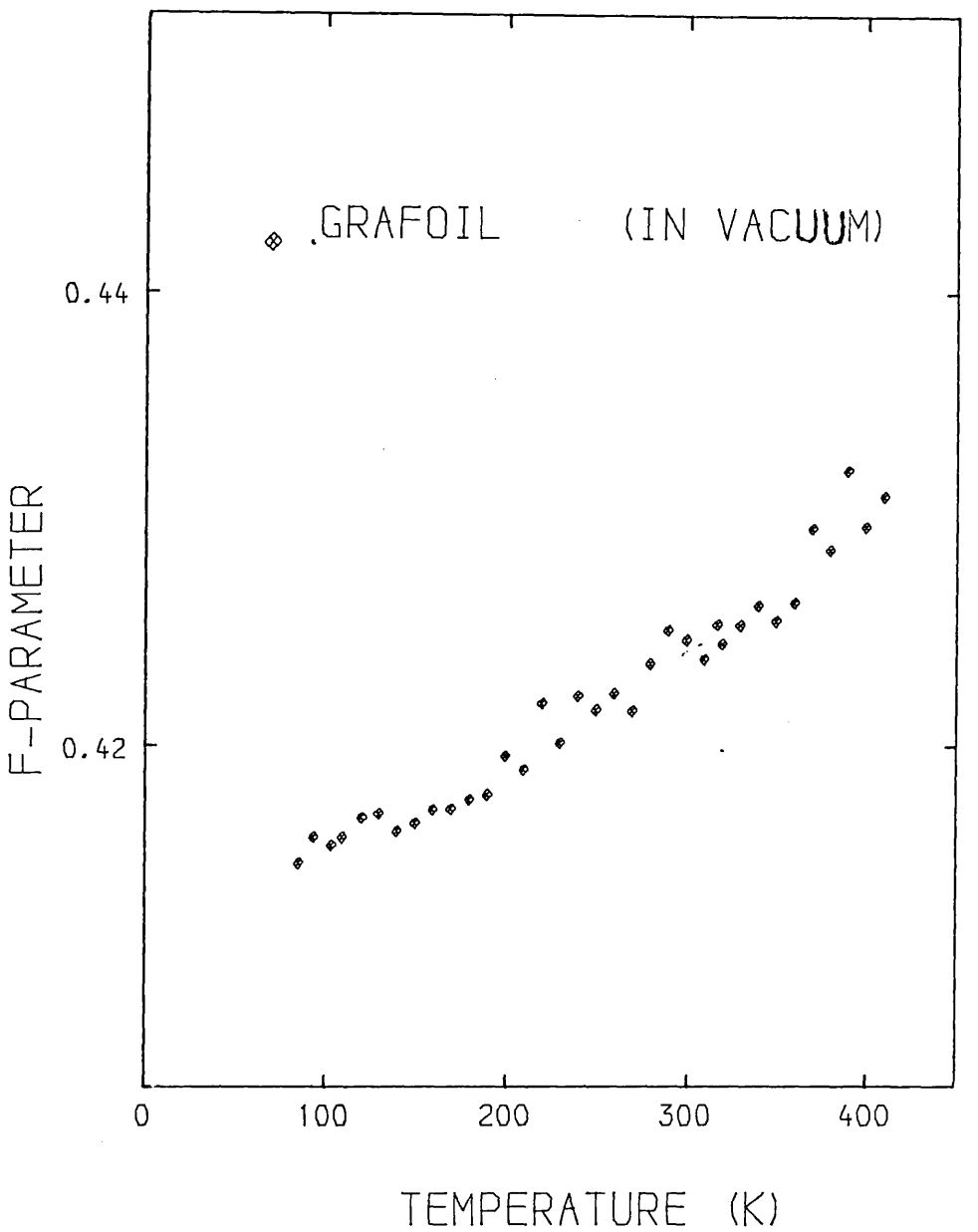

Fig(9.2.2) The variation of F-parameter as function of temperature for positron annihilation in grafoil, with error function background subtraction. The standard deviation for F value is ± 0.0008.

in bulk graphite or carbon to be in the range .19 ns to .28 ns. Shimotonai et al have observed vacancies created in graphite at high temperatures in the range 1575K to 1775K. They also found the lifetime for a free positron annihilation to be 0.2 ns and that of a trapped positron to be 0.37 ns. In 1983 Jean et al observed two aspects of positron annihilation with lifetimes of 0.4 ns and τ_3=2.3 ns in graphite. These long-lived components have been assigned to be positron annihilation on the graphite surface and the interface between crystals. The longer lifetime is annihilation of ortho-positronium (oPs), this lifetime is much smaller than free oPs annihilation (140 ns). They believe that the lifetime of 2.3 ns indicate pick-off annihilation of oPs with electrons from the medium to two photons. The intensity of this component varied between 1.5% at room temperature to 7.5% at 900 K. They also found the activation energy of positronium formation on the surface of the grafoil to be about E_a=0.22 ev. In this chapter we report on our experiment on positron annihilation in grafoil and positronium formation on the clean grafoil surface. The temperature range for investigation was 77 K to 600 K.

Method:

Two pieces of grafoil (exfoliated from graphite of 99.999% purity) each with a density of 0.94 gr/cm^3 were used to prepare the sample. The dimension of each piece was 12X10X.4 mm^3. The positron source was made from a carrier-free solution of ^{22}NaCl with 0.5 mCi specific activity, which was deposited onto the central areas of both pieces of grafoil. The thickness of the sample was not enough to stop all the positrons, since the stopping range of positrons in this sample was found to be 1.9mm (see chapter one). The two pieces of grafoil were then put together in a sandwich configuration and five extra sheets of

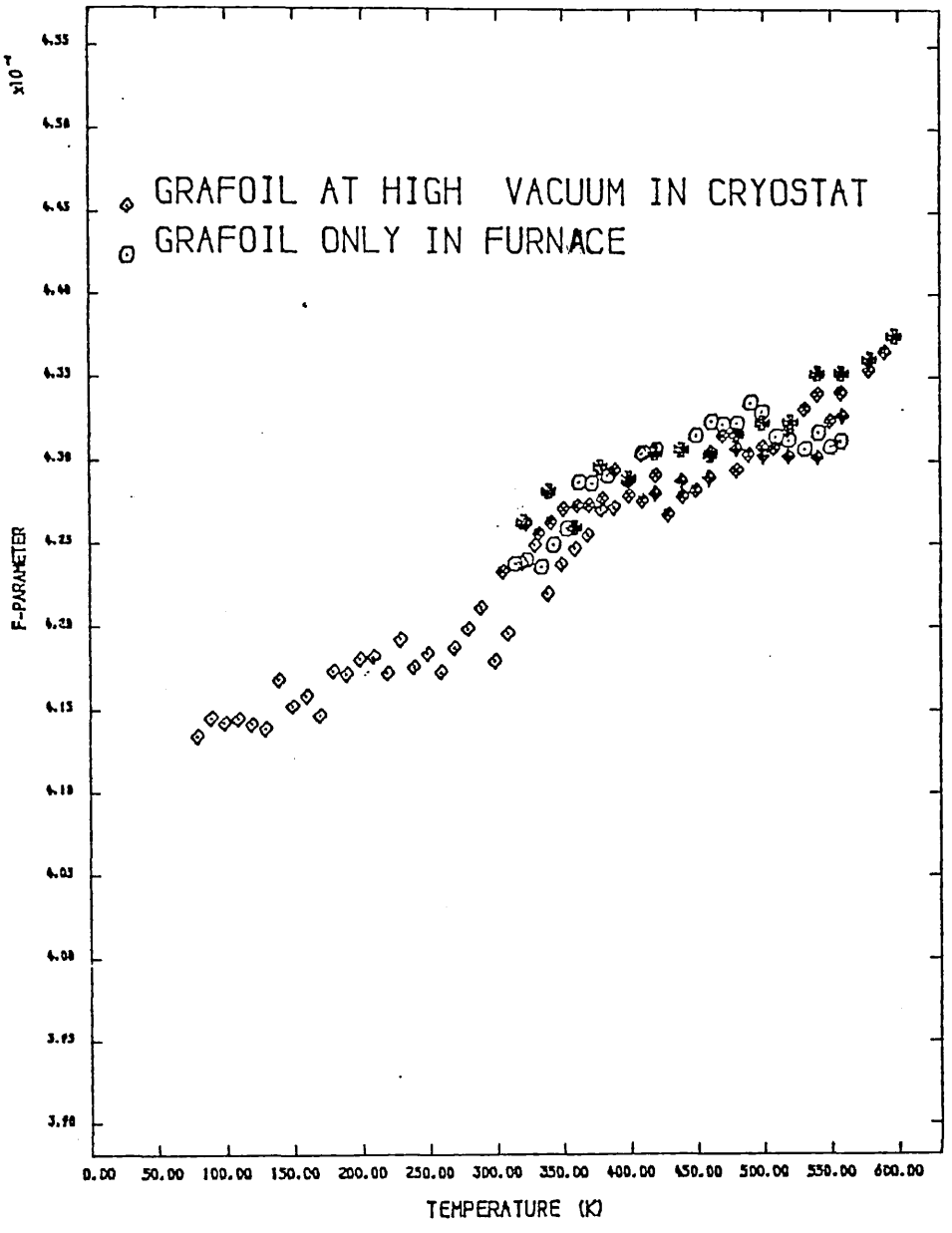

Fig(9.2.3) The variation of F-parameter with temperature for annihilation of positon in garfoil in range 77 K to 600 K, with error function back ground subtraction.

grafoil with the same dimensions were added to each side of the source sandwich and the arrangement wrapped in thin aluminium foil. The specimen was mounted in to the cryostat and evacuated to 10^{-4} torr and cooled down to 77 K. Data was collected from 77 K to 420 K with increments of 10 K and temperature stability of better than 0.5 K. The obtained vacuum was found to be insufficient and therefore the first results were not satifactory. The sample then transferred to a furnace and data accumulated at temperatures varing from room temperature to 600 K, under a vacuum of better than 10^{-6} torr. The total counts over the peack in two hours was approximately 600000 and the temperature stability was better than $\pm$0.5 K. After repair of the cryostat chamber system the sample was transferred back to the cryostat and evacuated to a vacuum of better than 10^{-6} torr. Futher data was collected for temperatures from 80 K to 420 K with an increment of 10 K and with the same temperature stability.

The grafoil sample has a hexagonal structure with $9.1X10^{6}$ m^2/m^3 surface area (equivalent to 9.68 m^2/gr). The number of free electrons in graphite is just about one electron per carbon atom (Ganguli et al 1941).

9.2-Line-shape parameter:

The F-parameter results for both with and without background subtraction are illustrated in figures(9.2.1), and (9.2.2) for temperatures from 77 K to 420 K. It can be seen that the F-parameter is approximately a horizantal line up to 170 K, above which it rises gradually. This increasing of the F-parameter above 170 K is not similar to that for other metals. The increase is due neither to thermal expansion of the sample nor to positron trapping. This is because the former case would be incompatible with the sharp slope of F, and the

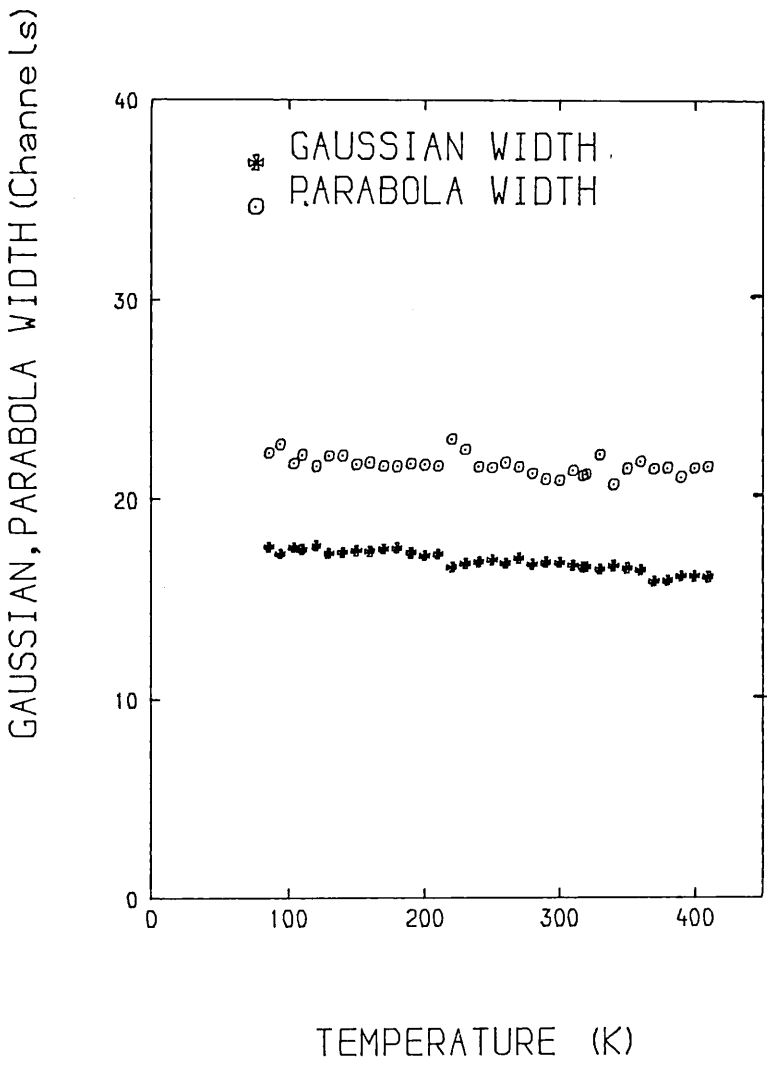

Fig(9.3.1) The Gaussian and parabolic width components as function of temperature for positron annihilation in grafoil.

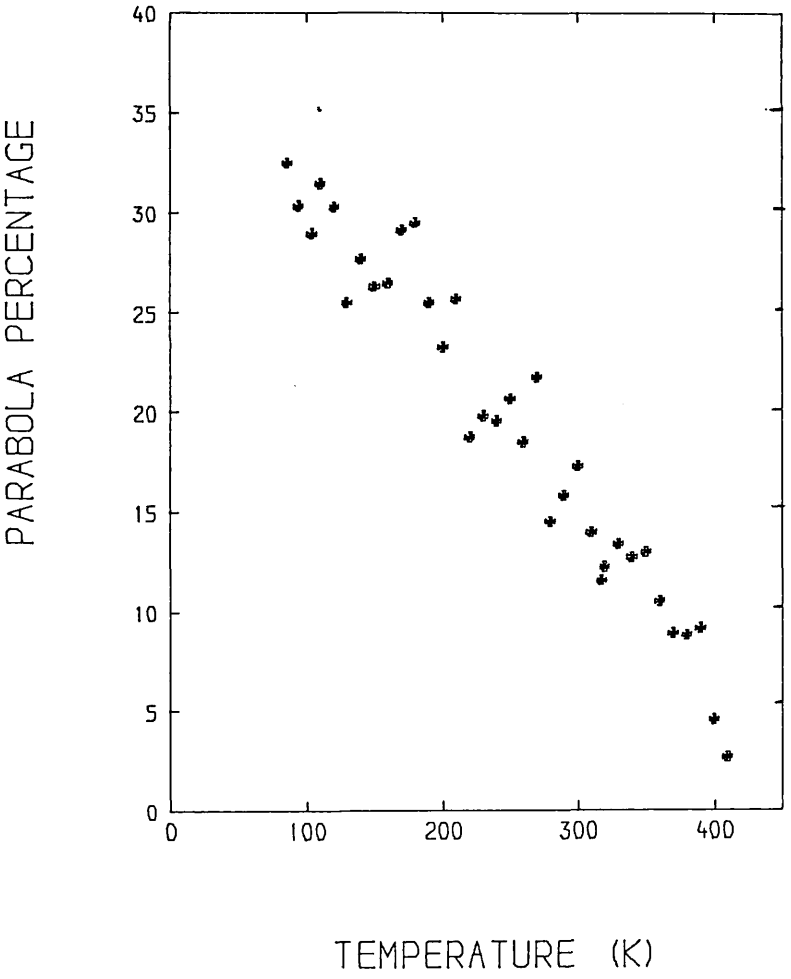

Fig(9.3.2) The variation of parabolic intensity as function of temperature for positron annihilation in grafoil. The standard deviation is estimated as ± 1.7.

later case can occur only at sufficiently high temperatures, at least 1575 K (Shimotomai et al 1983). This rise in F-parameter continues at temperature above 420 K, up to 600 K. At the temperature range between 170 K and 600 K the change in F is about 4.8% which has risen gradually (figure(9.2.3)). Jean et al (1984) reported that the positron lifetime in bulk graphite usually fell in the range of 0.19 to 0.28 ns, but a relatively long lifetime about 0.4 ns occured in various forms of graphite. They also observed a longer lifetime, attributed to the oPs component (Pick-off) whose intensity depended on temperature and surface area of grafoil.

Hence the increase of the F-parameter above 170 K is possibly the annihilation of positrons on the grafoil surface and interfaces between the crystals rather than annihilations in the bulk. The increase can also be attributted to low energy positron interaction with the surface of grafoil, because as mentioned the sample had included, extra sheets of grafoil on each side of the source specimen. Since the end-energy of positrons from the source is 0.54 Mev, they will not stop in the first three or four grafoil sheets, but would be slowed and interact with the other more outer sheets in the way of a a low energy beam. This makes it possible for positrons to penetrate the grafoil sheet and diffuse back to the surface becoming bound at the surface (Mills Jr 1979).

Therefore we can say that the increasing F value above 170 K is due to desorption of positrons from the surface. These positrons can form Ps by capturing an electron during their escape from the surface and then be annihilated. To verify the above argument the R-parameter was also measured. This measurement is explained in the following sections.

9.3-Line-shape analysis:

The spectra were analysed by the convolution method using a least-square minimization method. The result of this analysis is illustrated in figures(9.3.1), and (9.3.2). Figure(9.3.1) shows the parabola and Gaussian width, which are seen to be completly different to th se from positron annihilation in metals such Cd and Sn. The differences are as follow; the observed parabola width is wider than parabola widths in metals while the Gaussian width is narrower. The average parabola width is 22.7 channels which is non temperature dependent and which gives the Fermi energy of 17.6eV for graphite. The Gaussian width does not change much from low temperatures to high temperatures. The change is about 1.2 channels. Hence the momentum of the core electrons in grafoil is less than the equivalent in metals and the wider parabola width represents the high electron Fermi energy.

Figure(9.3.2) shows the parabola percentage which is also observed to be completely different from that of annihilation in metals. Usually parabola percentage is expected to increase when the positron becomes trapped in monovacancies, in metals such as cadmium, zinc, indium (Rice-Evans et al 1978b). This implies that parabola percentage should increase as a function of temperature, but as can be seen in figure(8.3.2) the parabola percentage decreases as a function of temperature for positron annihilation in grafoil. This suggests that the positrons annihilated on the surface of the sample rather than in the bulk. Another possibility is that bound positrons at the surface are desorbed to form Ps as the temperature is increased (Mills Jr 1979). Therefore the Gaussian percentage increase, or equivalently the parabola intensity decrease, represents the annihilation of bound positrons. Therefore it can be further said that this decrease in

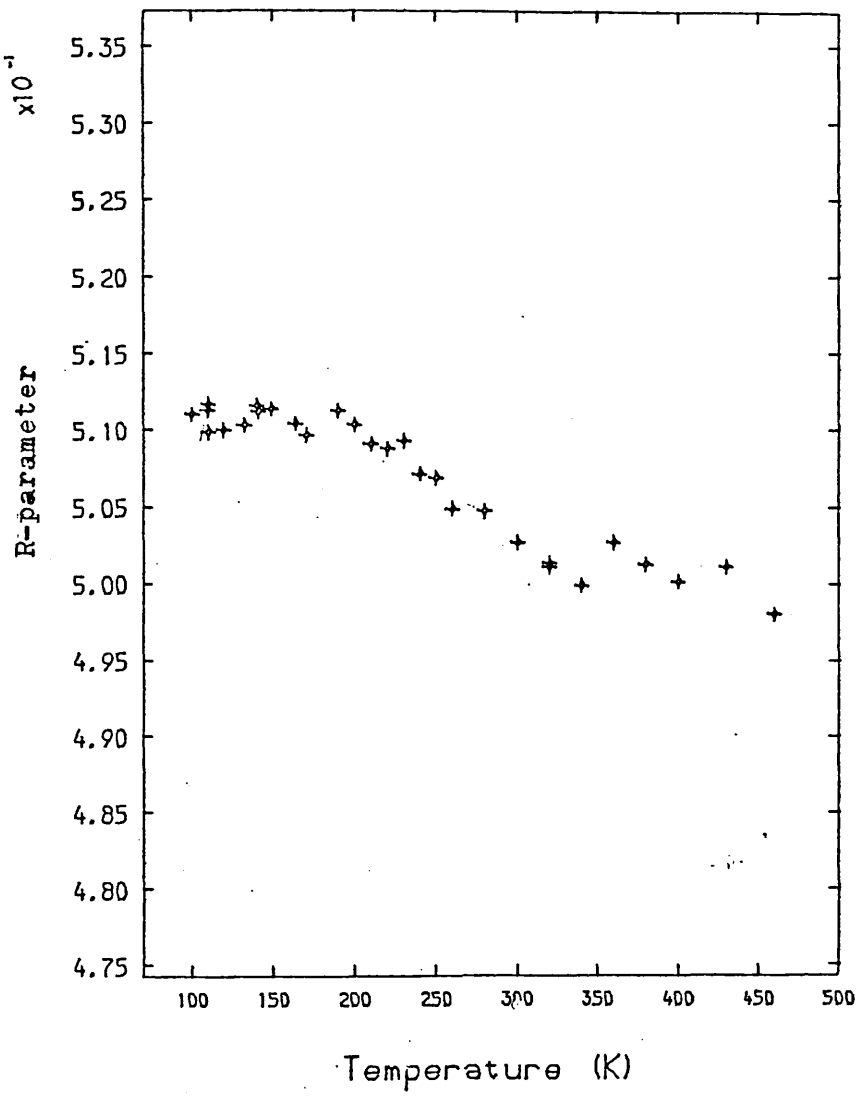

Fig(9.4.1) The variation of R-parameter with temperature for grafoil specimen. The standard deviation for R value is ± 0.001.

parabola intensity from 33% to approximately 3% is proportional to positronium fraction on the surface of grafoil implying that approximately 30% of desorbed positrons form positronium at high temperatures (420 K). The fitting is satisfactory because the chi-squared per degree of freedom lies between .96 and 1.3.

9.4-Positronium fractions:

The R-parameter was introduced in chapter V and gives a measure of the relative change in two photon emissions to three photon emissions. In practice to search for the formation of ortho-positronium, which entails three gamma-rays decays, the counts in the whole 511 keV photo-peak (A) and of a chosen band of channels (B) in the Compton region, corresponding to an energy of about 340keV were used for R. Both A and R(=A/B) will be indicators of the strength of three photon event (oPs) decays (Lynn and Lutz 1980). The resulting R-parameters are shown in figure(9.4.1). It can be seen from the figure that the graph is approximately horizontal below 170 K. As temperature rises above 170 K the R-parameter decreases. This decrease in R as a function of temperature represents increasing oPs formation. In the low temperature region below 170 K positrons are bound on the surface of grafoil and no sign of positronium formation is observed but as the temperature is increased to above 170 K, these positrons are thermally desorbed(Mills Jr 1979) and then form Ps by capturing an electron in the medium during escape from the surface. This process is similar to that observed with low energy positron beams interacting with surfaces (Mills Jr 1979,1980 and Lynn et al 1985).

9.5-Theoretical expression for R-parameter:

Mills, Jr et al found the positrons on the surface thermally active and found the relation between Ps fraction and temperature as;

$$(f-f_o)/(f_\infty-f)=Z(T).\bar{\eta}^{1}$$

where $Z=Z_o(T).\exp(-E_a/kT)$, Z is the rate of ocurrence of the energetically forbidden desorption process. f_o and f_∞ are the low and high temperature limit values of f respectively and η is the annihilation rate of surface bound positrons and is temperature independent. A similar expression was used to fit the R-parameter;

$$R=[R_l+R_h A.\exp(-E_a/kT)]/[1+A.\exp(-E_a/kT)] \qquad (9.5.1)$$

where E_a is the activation energy of positronium and is given as $E_a=E_s+\varphi_- -6.8$ ev. E_s is the binding energy of the positronium atoms on the surface, φ_- is the electron work function, 4eV for graphite, and finally 6.8eV is the positron-electron binding energy. R_l is positronium fraction at the low temperature limit and R_h is positron fraction at the high temperature limit. A is a constant and is given as $A=(8.335X10^{10})/\eta$. The result of the fitting is shown in figure(9.5.1a) and the parameter values given in table(9.5.1b).

$E_a=(0.225\pm0.003)$ ev

$A=(2.47\pm0.6)X10^{4}\ K^{-1}$

$R_l=(0.511\pm0.0003)$

$R_h=(0.501\pm.0005)$

$\frac{\chi^2}{\upsilon}=1.6$

table(9.5.1b)

The activation energy was, worked out using all the points in the fitting of the R-parameter with expression (9.5.1) and was found to be in good agreement with the value which was found by Jean et al as $E_a=(0.23\pm.03)$eV. Jean et al used the simple expression $\Gamma=\upsilon.\exp(-E_a/kT)$ where is frequency of the Ps formation. If we use a

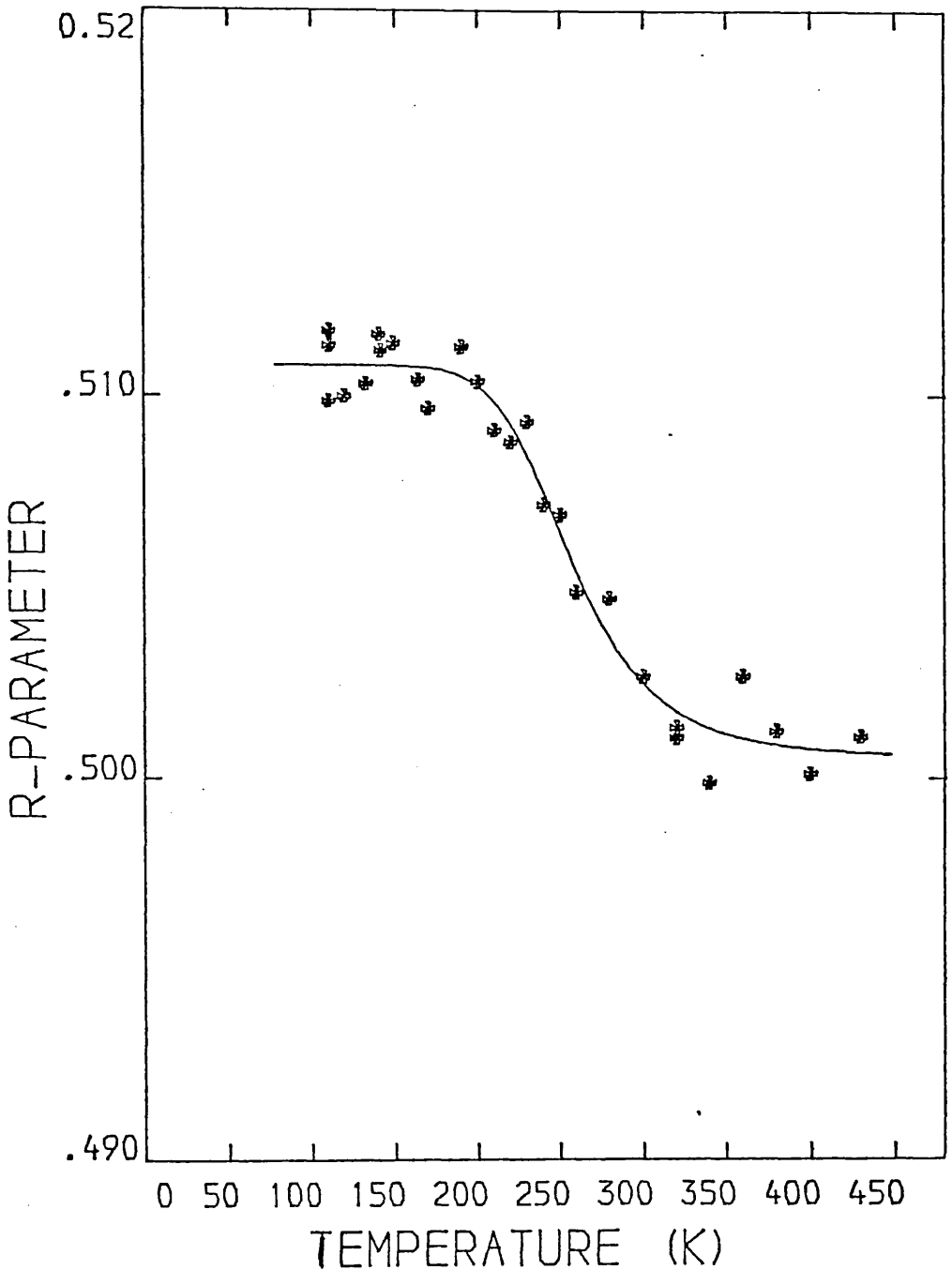

Fig(9.5.1a) Theoretical fitting "expression (9.5.1)" to R-parameter (soild line) as function of temperature for grafoil specimen.

simple expression like $R=R_1+C\ EXP(-E_a/kT)$ which is similar to that of Jean et al (1984), the activation energy would come to $E_a=0.08eV$ which is far from the value found by them. The goodness of fit (chi-squared) in this case is also found to be worse.

The value of the binding energy of Ps atoms with the surface of grafoil was found to be $E_s=(3.02\pm.0005)eV$.

9.6-Geometric orientation of the sample:

The crystal structure of graphite is hexagonal and the electrons are bounded to nuclus as σ-shape and π-shape in the atom (Valence p102). The mobility of electrons in graphite is one electron per carbon atom (Ganguli et al 1941). Having these properties the geometric orientation of the sample may have some effect on the positron annihilation line shape. These effects on the annihilation line shape were first observed by Berko et al (1957) in angular correlation measurements. They found the spectrum of the positron annihilation with σ-bound electrons in a direction perpendicular to the hexagonal plane (c-axis) to be different from positron annihilation with π-bound electrons in a direction parallel to the hexagonal plane. They suggested that the annihilation of positrons with electrons which moved parallel to the c-axis was different to electrons which moved perpendicular to the c-axis. Measurments, from which the F-parameter was found, were made with varing sample orientations, at 80 K, see figure(9.6.1). Apart from the F-parameter value the angle of 90 ; which seems to be due to high scattering of Gamma-rays through the sample holder, the F-parameter reaches a maximum at 70 . This implys that the line-shape spectrum depends on the orientation of the sample. In direction of our measurment (c-axis) the effective mass of the electrons is large which causes the F-parameter to be minimum at

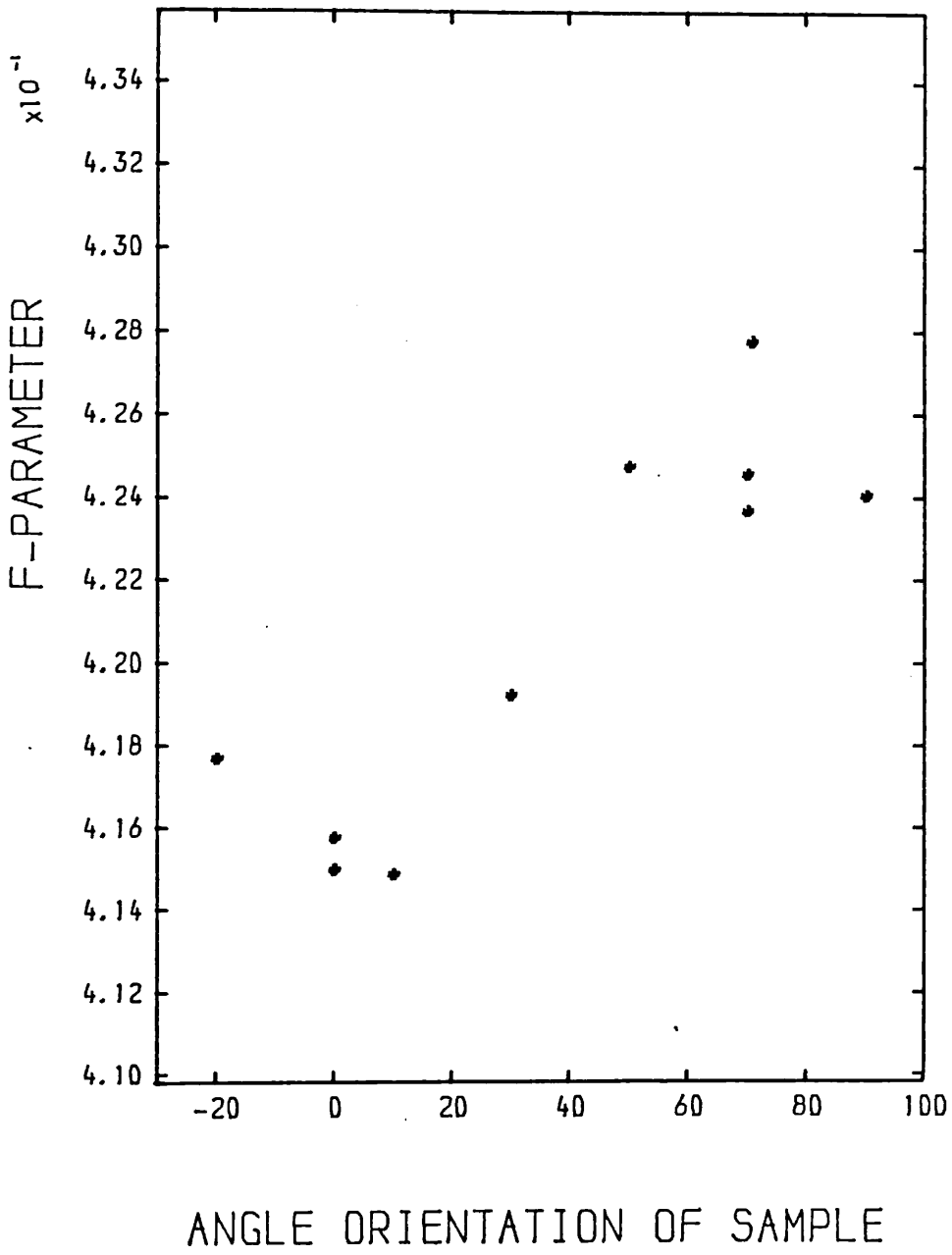

Fig(9.6.1) The variation of F-parameter with geometrical rotation of the sample specimen for positron annihilation in grafoil, at 80 K.

zero angle. This because the σ and π electrons uniformly and yields a momentum density that only slightly extended along the c-axis (Reed et al 1974). The parbola and Gaussian widths of the line-shapes change as the sample orientation is altered. The parabola width changed from 23 channels to 20.3 channels and the Gaussian width from 17.7 channels to 16.8 channels. The parabola percentage also changed from 35% to 15%.

9.7-Conclusion:

The results obtained from the annihilation of positrons with electrons in grafoil are summarised as follow:

1)Positron annihilation in grafoil and Ps formation at the surface of grafoil were observed to be temperature dependent.

2)The F-parameter is temperature dependent. It also depends on the orientation of the sample, because more annihilations of positrons seem to annihilate with electrons moves in c-axis than electrons moves in perpendicular to c-axis.

3)The relative change in both the total area of spectrum and R parameter, was observed and can be attributed to the formation of orthopositronium on the surface of the sample and is temperature dependent. This leads us to conclude that the thermal desorption process of positrons is a surface-trapping mechanism which was proposed in the slow positron method (Lynn 1979, Mills Jr 1978b).

4)The activation energy of positronium formation calculated from expression (9.5.1) comes to $E_a=(0.225\pm.003)$eV which is reasonable agreement to that of Jean et al.

5)The observation of a decreasing parabola percentage is an anomalous effect compared to metals. It can be suggested that positrons desorbed thermally from the surface can form Ps by capturing an

electron of the medium during their escape. Most of this resultant Ps seems to be in the triplet state (oPs) which can decay to three photon (self-annihilation) or can pick-off an electron from the medium and decay into two photons.

6)The parabola widths are greater than the corresponding Gaussian widths which is opposite to that found for metals, this may be due to the high Fermi energy of the grafoil electrons.

The above results are concluded from observing positron annihilation on a clean grafoil surface in a range of temperatures from that of liquid nitrogen to 420 K, 420 K being very far from the melting point of grafoil. The threshold temperature for the creation of monovacancies in the graphite was to be found 1575 K which again is far from the range covered. Therefore the fact that the increase in the F-parameter was found approximately linear is undoubteledly because of annihilation of positrons on the surface which are thermally desorbed and not in monovacancies or dislocations etc.

It is reasonable to study whether the so called positronium formation effect on the clean grafoil surface mentioned in this chapter is also observeable when the sample is exposed to gases. The adsorption of gases on condensed matter is an old subject but the phenomena's study by the positron annihilation method is new, it has been recently observed by Jean et al (1985). In the next chapter we investigate the adsorption of some gases with our grafoil sample as the substrate, by means of the Doppler broadening method.

Chapter X Positron annihilation with argon condensed on grafoil.

10.1-Introduction and method:

The phase transition of gases at low temperature was discussed in chapter three and it was mentioned that the cooling gas molecules are more attractive to cold substrates under van der Waals forces. Argon is one of the noble gases which is adsorbed on the surfaces of a cold substrate such as a metal. In most adsorption experiments graphite is used because of its large and energetically uniform surface area. The adsorption of the gas on the surface of substrate depends on vapour pressure and temperature as was described in chapter three.

There are so far many investigations reported on argon adsorbed on the graphite by many different methods, such as low energy electron diffraction (LEED), neutron diffraction, calorimetric measurments, etc. But, recently, the positron annihilation technique was also used to investigate monolayer adsorption of the gases on the surfaces of matter (Jean and Zhou 1985). They found the monolayer of argon on graphite (exfoliated) at 77K and a pressure of less than 5 torr with amount of 136 CC of argon. They also mentioned that the positron lifetime is increased as a function of coverage up to the maximum at the half coverage, and then is decreased.

In calorimetric measurment at 77K, Rouquerol et al (1977) found that a anomalous effect occured in the vapour-pressure graph of argon on graphite at 12.6 torr. They estimated that the area of each argon molecule which was occupying the surface, to be 12.5 A^{o2}. Later Kjms et al (1980) reported that this anomaly may be due to order-disorder transition of the argon on the surface of grafoil. The transition of argon from solid to liquid and then to gas was observed by Jean and

Zhou (1985) using positron lifetime measurments. Their grafoil sample had a surface area of 21.2 m^2/gr (560 m^2) relative to our sample with a surface area of 9.68 m^2/gr (5. m^2). Therefore it can be estimated that the amount of gas needed for a complete monolayer of argon on the grafoil sample is approximately 1% of the volume they needed. In this chapter we describe the adsorption behaviour of argon on grafoil by use of positron annihilation technique.

Method:

The exfoliated graphite (as grafoil) source specimen which was used in the graphite experiment, was used once again as a substrate. First of all the sample specimen was kept at a temperature of 400 K for a few hours, under vacuum of 10^{-6} torr. Then it wascooled to room temperature, and argon gas with a purity of 99.999% was transfered, from the cylinder, to the chamber under high pressure (note: before doing this, all vacuum pumping lines from the cylinder to the chamber were evacuated to 10^{-6} torr for, at least, one hour). The pressure of the argon was read from the gauges above the chamber to be (1520±10) torr at room temperature and the volume was estimated to be approximately 300 CC. The argon gas was kept in the chamber for at least one night at room temperature to let enough gas diffuse into the sample, for the creation of layers. The sample then was cooled down at liquid nitrogen temperature (from room temperature), and the pressure dropped from 1520 torr to 200 torr where it remained during the rest of the experimental work. According to the results of Jean and Zhou's experiment in agreement with this work only a few CC of the gas was enough for full area coverage. Therefore, the amount of gas which was allowed in was much more than that needed for monolayers creation. The data accumulation started after equilibrium temperature was reached, for 2 hour per run and over

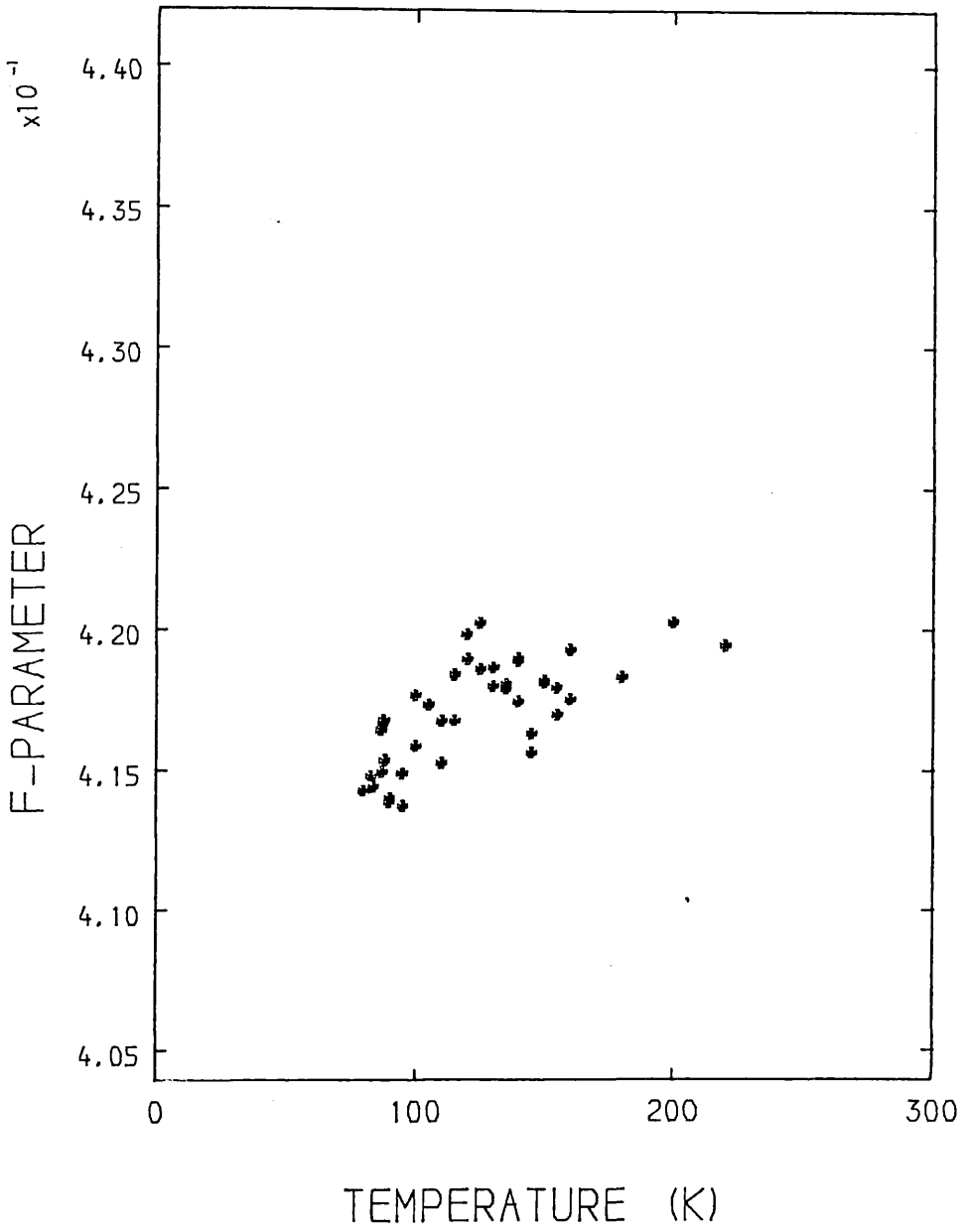

Fig(lo.2.1) F-parameter versus temperature for argon adsorbed on grafoil, with error function background subtraction. The standard deviation of F value is ± 0.0006.

a temperature range of 80-220K with increments of 5 K. The temperature stability was better than ±0.1 K.

10.2-Line-shape parameter:

The line shape parameter (F-parameter) was calculated (using an error-function background subtraction) and is illustrated in figure(10.2.1) as a function of temperature. It can be seen that the F-parameter depends on the temperature and a small increase of about 1% in F is observed approximately at 120 K. Comparison with the F-parameter for positron annihilation on the clean surface of grafoil (chapter nine) shows that this rise at 120 K is undoubtedly due to the positron in argon gas on the surface of the grafoil. The properties of argon gas indicated that it should be fluid above 88 K and therefore it can be expected that a fluid layer will be formed on the grafoil surface at this temperature and pressure since high pressure is associated with high temperature for adsorption (Kjems et al 1976). This increase in F at 120 K suggests that as the substrate is cooling down from the higher temperature (160 K), the argon gas interact with the cooling substrate and a layer builds up. During this process bound positrons capture an electron from a gas molecule at the surface durind their escape to form positronium. The decrease of F below 120 K suggests that it is due to an increasing density of the argon at the surface (multi layers) and as this density increases, the positron lifetime decreases (Tao 1969, Canter and Roellig 1976). Another possiblity for this decrease is that the positron can not diffuse back to surface (Lynn et al 1983). The behaviour of the positron on the surface above 150 K is similar to the positron interaction with the clean surface (chapter nine). This question as to whether the maximum value of F observed at 120 K can be attributed to a monolayer

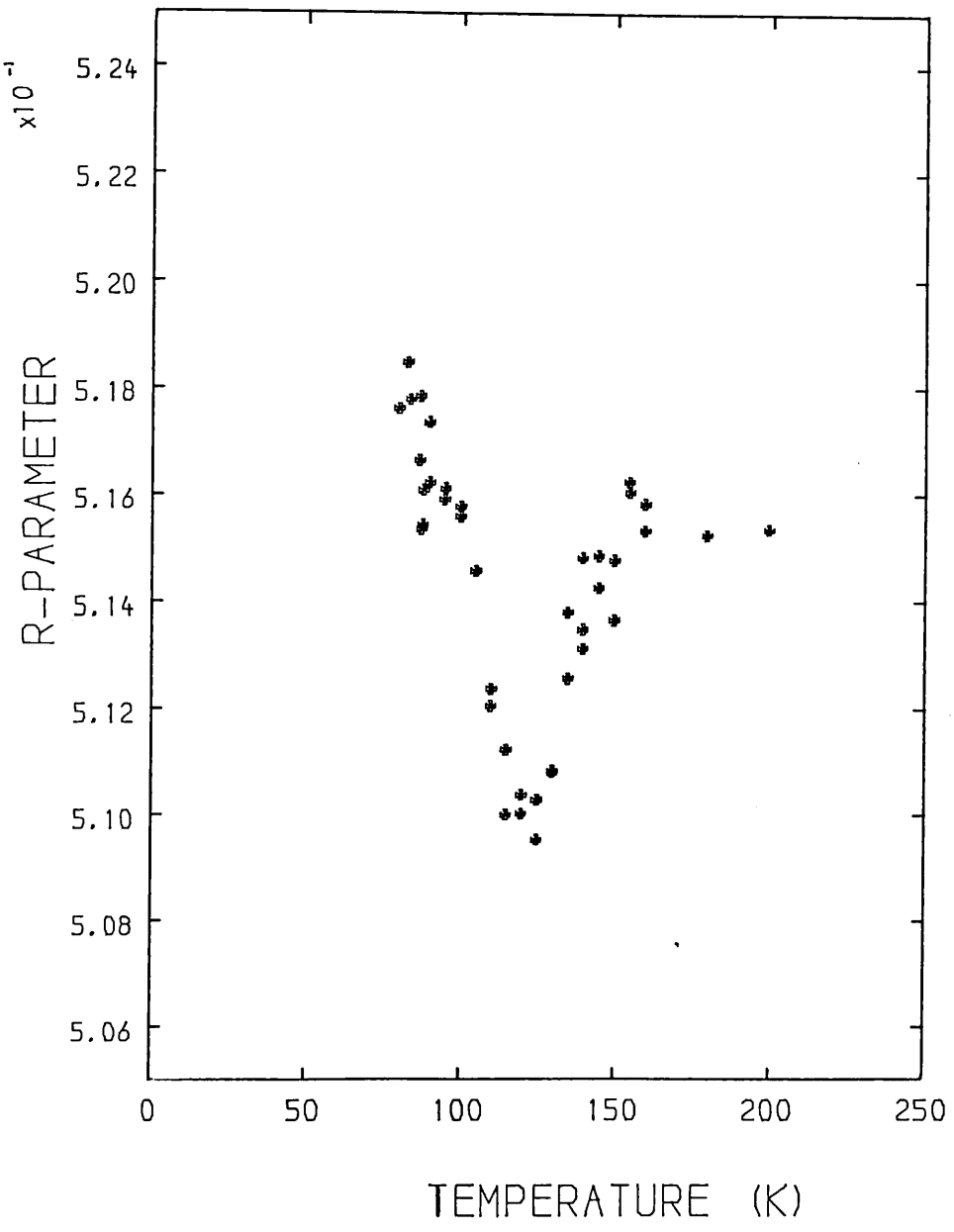

Fig(10.3.1) The variation of the R-parameter as a function of temperature for argon condensed on grafoil. The standard deviation of R value estimated as ± 0.0005.

coverage of argon molecules on the grafoil surface is a fundamental one. Unfortunately there is no immediate answer to this question at this stage with present equipment and experimental conditions. The increase of the F-parameter is due to parapositronium emission or orthopositronium pick-off by an electron of medium. On the other hand oPs decays to three photons, their energies being distributed between zero and $m_o c^2$. Therefore the line-shape spectrum should show changes and it would be expected that the R-parameter gives a clearer result than the correspondig F-parameter (next section).

10.3-Positronium fraction (R-parameter):

The ratio of two photon decays to three photon decays (R-parameter) was calculated and the result is shown in figure(10.3.1). By comparison of this R-parameter with that from the grafoil work, where it is clear that in the range of 80 K to 170 K the value of R is flat (see chapter nine), the value in argon decreases by approximately 2.2% with respect to the lower point at 122 K. This decrease is due to the annihilation of positrons on the surface of grafoil with argon gas. The decrease of R to a minimum value at 122 K is assigned to oPs formation on the surface of the grafoil. The increase of R above 120 K could be due to desorbtion of the argon gas from the surface, and then the behaviour of the positron is that of a positon on a clean surface. The argon is fluid above 85 K and therefore it is possible that positronium bubbles are formed in fluid argon (Varlashkin 1971, and Canter and Roellig 1975). This is another explanation for the minimum point at 120 K. The increase of R below 120 K might be due to increasing gas density on the surface (Canter and Roellig) or because positrons can not diffuse back to the surface due to the creation of multilayers of argon gas (Lynn et al 1983). The bubble formation on

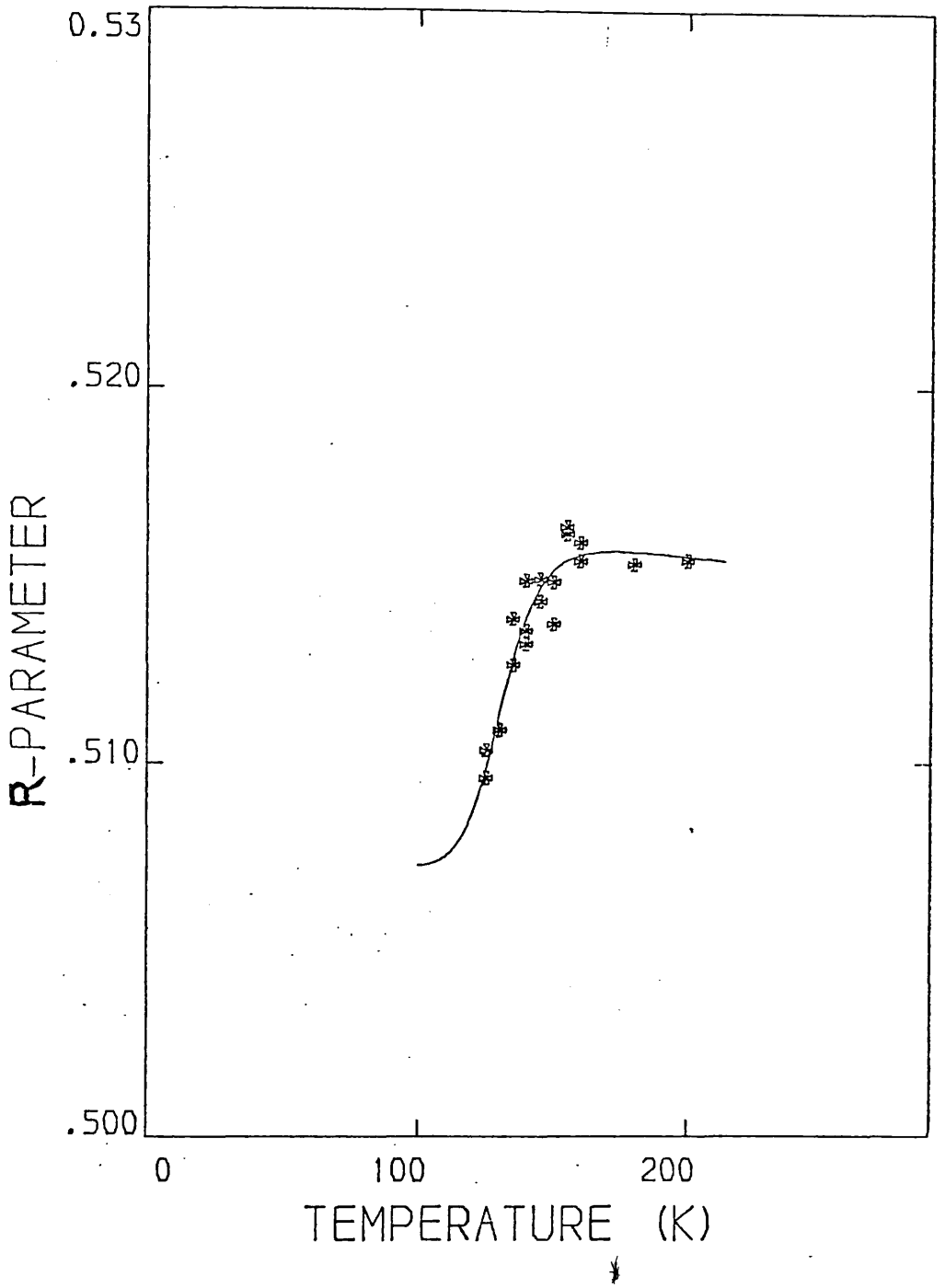

Fig(lo.4.1) shows the R-parameter fitting theoretically by expression (lo.4.2).

the surface of the grafoil, due to condensation of the gas is an other possibility which is also reported by Jean and Zhou for liquid argon with a large lifetime component. Our result is different from that of Jean and Zhou's (1985), because of the different conditions of the experiment. They controlled the amount of the gas that they put in, therefore they observed the transition of the argon gas from solid to liquid and then to gas by observing the increase in the positron lifetime. This effect was not observed in our experiment because the amount of argon could not be as carefully controlled. In conclusion, it seems possible that many layers are created on the surface of grafoil at low temperature.

10.4-Theoretical fitting on the R-parameter:

The expression used by Mills Jr and Lynn for the fitting of the positronium fraction as a function of temperature is

$$f=(f_0+f_\infty.\bar{\nu}^{-1}.Z)/(1+\bar{\nu}^{-1}.Z) \qquad (10.4.a)$$

where $Z=Z_0(T)\exp(-E_a/kT)$, E_a is activation energy of positronium (for more explanation see chapter three), ν is the annihilation rate of surface bound positrons and is temperature independent. A similar expression to the above was used to fit the R-parameter from the minimum point (120 K) to the right of the peak. It was also assumed that the probability of annihilation of a positron with a argon molecule is proportional to the coverage (X) of the gas on the surface of grafoil, then it can be written as;

$$R=[R_h+R_l.X.Z_0.\bar{\nu}^{-1}.\mathrm{Exp}(-E_a/kT)]/[1+X.Z_0.\bar{\nu}^{-1}.\exp(E_a/kT)] \qquad (10.4.b)$$

Where E_a is activation energy and R_l, R_h are the low and high limits value of R-parameter and X is the coverage of the gas on the surface of the sample. The coverage is calculated under two different assumptions. Firstly by assuming that the film's site is fixed, the

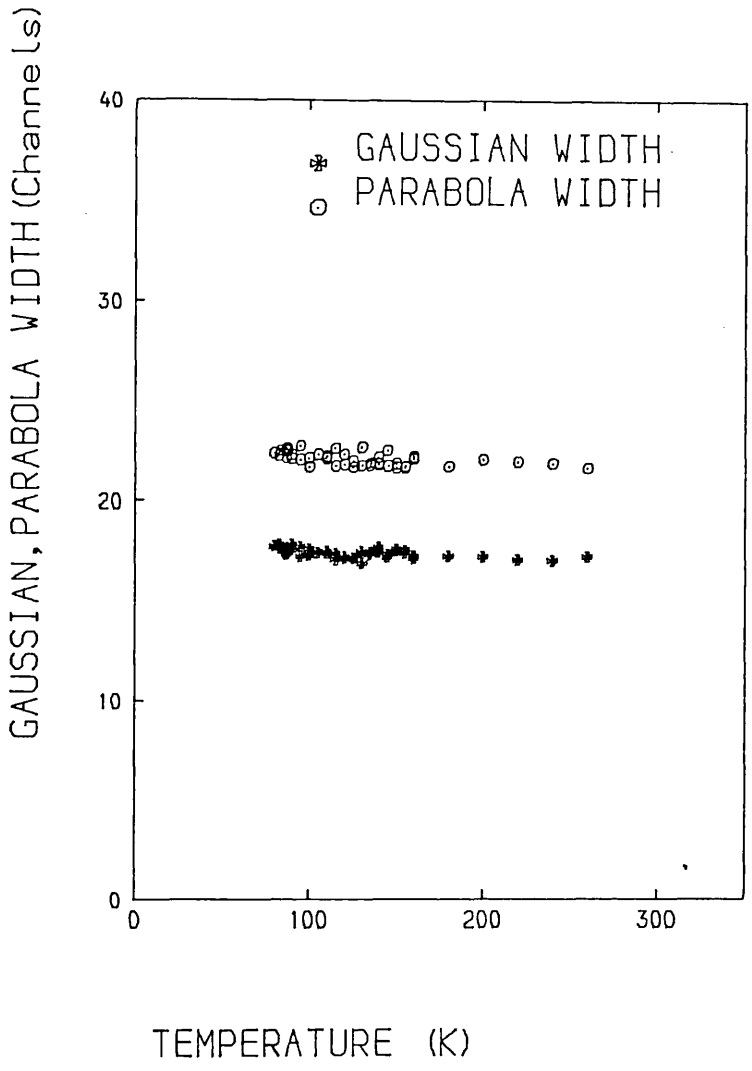

Fig(lo.5.1) shows the parabola and Gaussian width versus temperature of argon adsorption on the grafoil.

Langmiur monolayer formula can then be used. The result of this fitting is given in table (10.4.1a) in two cases 1)Ea=0, 2)Ea≠0.

1)		2)	
	$R_h=(0.516\pm0.0007)$		$E_a=(0.051\pm0.008)$ ev
	$R_l=(0.504\pm0.0006)$		$G=(2.9\pm0.5)\times10^9$
	$\varepsilon_0=(1548\pm98)$ K		$R_l=(0.505\pm0.0003)$
	$X=(0.017\pm0.006)$		$R_h=(0.516\pm0.0003)$
	$\frac{\chi^2}{\upsilon}=5.49$		$X=(0.050\pm0.009)$
			$\varepsilon_0=(2122\pm160)$ K
			$\frac{\chi^2}{\upsilon}=3.69$

Table(10.4.1a)

Where ε_0 is the binding energy of an argon molecule on the surface, and X is the coverage; these were used as the fitting variables. It is expected that the value of X to be equal to 50% (Jean and Zhou). As can be seen from the table(10.4.1a) the value of X is very low and physicaly inconsistent. It has been mentioned that the argon could not be solid at such a temperature and pressure but the fluid state is possible, and therefore the Boltzmann approximation formula is suitable to replace the above expression. The area of an argon molecule occupied on the surface is reported to be 12.5 A^{o2} which is used (Rouquerol et al 1976). Our result is given in table (10.4.1b) for two cases and it is shown in figure(10.4.1).

1)		2)	
	$R_h=(0.516\pm0.0006)$		$Ea=(0.032\pm0.006)$ ev
	$R_l=(0.507\pm0.0007)$		$G=(3.4\pm0.3)\times10^9$
	$\epsilon_o=(1273\pm34)$ K		$R_h=(0.516\pm0.0003)$
	$\frac{\chi^2}{\upsilon}=3.69$		$R_l=(0.503\pm0.0005)$
			$\epsilon_o=(1142\pm28)$ K
			$\frac{\chi^2}{\upsilon}=5.30$

Table(10.4.1b)

The results shown in table(10.4.1b) are more reasonable than those above

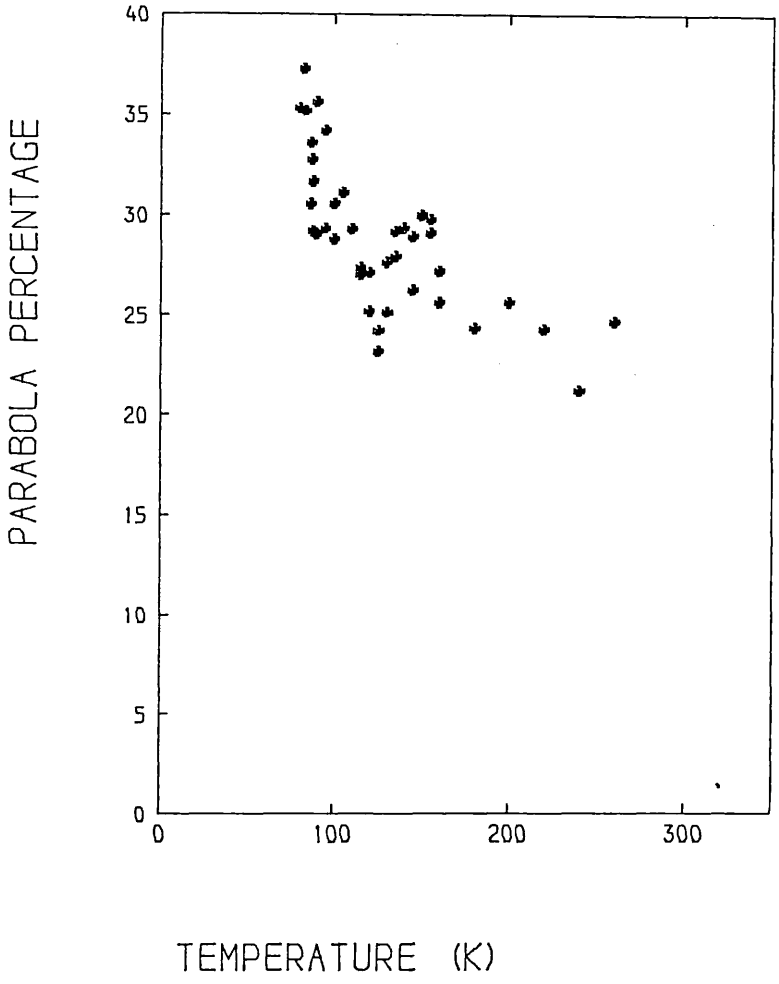

Fig(lo.5.2) The parabola percentage versus temperature of argon adsorption on the grafoil. The standard deviation of parabola percentage is $\pm 2\%$.

and coverage is found to be approximately one for this case which seems reasonable. The average binding energy ϵ_0=(1208±33)K.

10.5-Line-shape analysis:

The line-shape photopeak was fitted by an inverted parabola in conjunction with a Gaussian, both convoluted with the same resolution function, which was used for analysis of spectrum for the other metals (see previous chapters). The result of the fitting by the CURFIT program (appendex(II)), is shown in figures(10.5.1) and (10.5.2) respectively. The goodness of the fitting as measured by the chi-square test is satisfactory, as it varies from 0.98 to 1.27. Figure(10.5.1) shows the parabola and Gaussian widths as a function of temperature. It can be seen from the graph that the parbola and Gaussian width stay approximately constant. The parabola width is an average of 23.3 channels and is much greater than parabola widths in metals such as tin and cadmium. The Gaussian width is an average of 18.5 channels and does not depend on temperature. The parabola percentage is shown in figure(10.5.2) and is temperature dependent. As can be seen from the diagram, the parabola percentage of positrons annihilating in argon condensed on the grafoil surfaces is decreased by about 10% approximately at 120 K compared with that of the clean surface. This difference may be due to the positronium intensity on the surfaces of the grafoil caused by interaction of the positron with argon molecules. The result of the parabola percentage is completly different when compared to that in metals. It seems to be due to the positron interaction on the surface, and the Ps formed should be mostly in the form of oPs since the width of the parabola has not changed (Fig 10.5.1). However a sharp decrease was observed in parabola width for oxygen (see chapter 12).

10.6-Conclusion:

The adsorbtion of the argon molecules on the grafoil sample was observed by positron formation on the surface of the sample. The maximum positronium emission was observed approximately at 120 K from R and F parameter graphs. The R and F parameters were found to be temperature dependent. The decrease below 120 K could be due to an increase of argon atoms on the surface resulting in positrons being unable to diffuse back to the surface to form positronium (Lynn et al 1983). There also seems to be multilayer created below 120 K, and an increasing R value above 120 K denotes the melting of the argon layers on the surface. The behaviour of the positron is similar to that at a clean surface at higher temperatures (over 150 K). This implies that positrons are bound at image potentials or by van der Waals forces on the surface. These results were not the same as isothermal measurements made by Jean and Zhou. They clearly observed the phase transition of the argon gas from solid to liquid and then to gas, but we did not. The reason for that is the different conditions of experiment (the different surface area of sample and amount of argon actually used). Some improvement of the system is necessary for the isothermal experiment to be performed.

The R value was fitted with expression (10.4.b) and the average value of the binding energy of argon on the graphite surface was found to be ϵ_0=(1208±32) K, the resultant activation energy being computed to be Ea=(.032±.005) eV, which is very small. It can be concluded that no thermal desorption of positrons from the surface has occured. The relative change in the value of parabola intensity at 120 K to that of the clean surface analysis is (10±2)% and is assigned to be due to positronium emission from the surface. Unfortunately the system was not complete to measure the coverage at 120 K. The coverage of

monolayer gases depends on pressure and temperature as mentioned by Kjems et al who indicated that the high vapour pressure is associated with high temperature for the same coverage of the gas on the surface of a cold substrate. Therefore it is expected that by changing the pressure, the position of the minimum in the R-parameter also changes. In the next chapter the experiment is performed for nitrogen adsorption on the surface of the sample with different vapour pressures to investigate the changes in the position of the minimum value in R.

Chapter XI Positron annihilation in the nitrogen condesed on the surfaces of grafoil

11.1-Introduction and method:

Adsorption of nitrogen molecules on the grafoil has been investigated for many years by different methods. Most of the measurements were isothermal measurements at low temperature, and very few at liquid nitrogen temperatures. Physisorption is governed by van der waals forces and information on the growth, phase and registration of films as a function of temperature has been acquired from isotherms and calorimetry studies of nitrogen, argon, oxygen etc on graphite Miner et al 1983, and Stolkenberg et al 1980, with neutron diffraction methods Kjems et al 1976, NMR (nuclear magnetic resonance) Cowan 1977 and low energy electron diffraction (LEED) Toney and Fain 1984, and by many other methods.

Recently the interaction of slow positron beams with surfaces has been used to show that positrons are preferentially attracted to the surface and the resulting positron annihilation signals are thus enhaced for surface states. Then Jean and Zhou 1985 observed monolayers of argon and nitrogen on the surfaces of grafoil by using positron lifetime measurements. Because positrons are very senstive to surface contamination, if any atoms or molecules are adsorbed on the surface positron interact with these to form, mostly, positronium. In 1977 Steele found the potential well depth of the nitrogen molecules bound to the surface (binding energy) of the graphite to be 2190 Cal/mol corresponding to 1110 K. In 1975 Bruch again calculated the binding energy of the nitrogen molecule on the grafoil to be ϵ_o=1159 K, Which is different to Steele's value. The difference between these two values is because of the effect of

quadrapole-quadrapole interactions which only Bruch took account of. The other interesting result for nitrogen adsorbed on graphite is the transition of disordered sites into ordered sites of nitrogen molecules (Kjems et al 1975 and Diehl et al 1981). Nitrogen has a solid structure on the cold substrate surfaces below 64.5K, with a transition to a fluid structure above 85 K (Larther 1977), which is before this value 70 K was reported by Dash and Chuge (1974). Recently the tricritical point (coexistence of three phase), of nitrogen on graphite was reported by Miner et al (1983) to occur at 85.37 K. Therefore it will be expected that a monolayer of nitrogen molecules on the cold substrate at the high pressures associated with high temperatures is registered as a fluid monolayer not a solid. Jean and Zhou observed the monolayer of nitrogen on the surface of grafoil at 77 K with 138 CC of nitrogen and vapour pressure of less than 5 torr. The number of molecules per unit area from this amount of nitrogen can be calculated to be about $6.5X10^{18}$ molecules per unit area, This is in good agreement with the value calculated from our experiment (see section 11.4) $n = 6.37X10^{18}$ molecules/m^2.

Method:

The properties of the specimen have been explained in previous chapters. After the argon was pumped out, the sample was kept at room temperature under a vacuum of better than 10^{-6} torr for 48 hours, and then at approximately 400 K for another a few hours, to be sure that the sample area was cleaned of all traces of argon gas. After allowing the sample temperature to drop to room temperature, nitrogen gas of purity 99.99% was let into the sample chamber. (note, all the lines, from the nitrogen cylinder up to the sample chamber were kept under vacuum for a few hours). The free space volume of the sample chamber was found to be approximately 300 CC. Nitrogen gas was

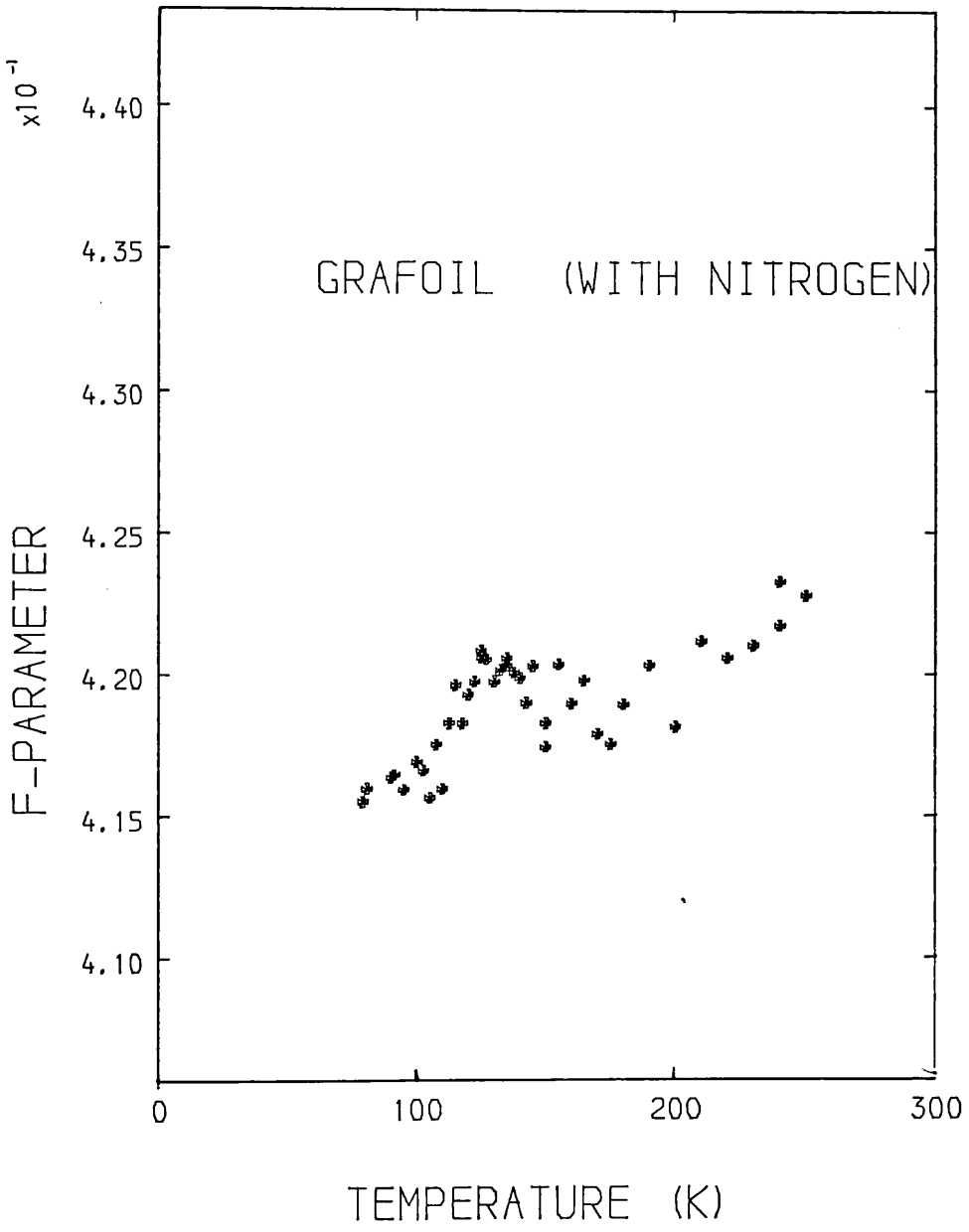

Fig(11.2.1) For nitrogen adsorbed on the grafoil specimen, the change in F-parameter as a function of temperature. The standard deviation of F value is ± 0.001.

inserted into the chamber to a pressure of two atomospheres (1520 torr) at room temperature and the system left over night.

The following morning the cryostat dewars were filled with liquid nitrogen and the sample chamber allowed to drop from room temperature to liquid nitrogen temperature which it did so in approximately 30 min. The pressure was found to drop from 1520 torr to approximately 700 torr. Once an equilibrium temperature had been reached data accumulation was started from 80 K to 250 K with 5 K temperature increments and a temperature stability of better than $\pm$0.5 K. Two sets of runs were collected from forward runs (sample being heated) and backward runs (sample being allowed to cool) with intermediate temperatures being chosen for the backward runs. After a break a new set of runs was started with nitrogen in chamber this time at lower pressure than before (260 torr at 80 K). Then the data was accumulated. Two futher set of measurements were taken with sample chamber pressure reduced by evacuation from the initial 260 torr to 110 torr and then to 18 torr at 80 K. The temperature range for these two sets was 80 K to 170 K. These four measurements concluded the nitrogen experiment.

11.2-Line-shape parameter:

The F-parameter was obtained in the same manner as previously described and is shown in figure(11.2.1) (the second set of measurments are with error function background subtraction). The same effect as was observed in argon is also observed for nitrogen (1.2% increase on F). But as it can be seen the position of the maximum value of F is different, it is at 127.5 K for the second measurements. By comparison of this F-parameter diagram with the F-parameter for positron annihilations on a clean surfaces of grafoil, one see s

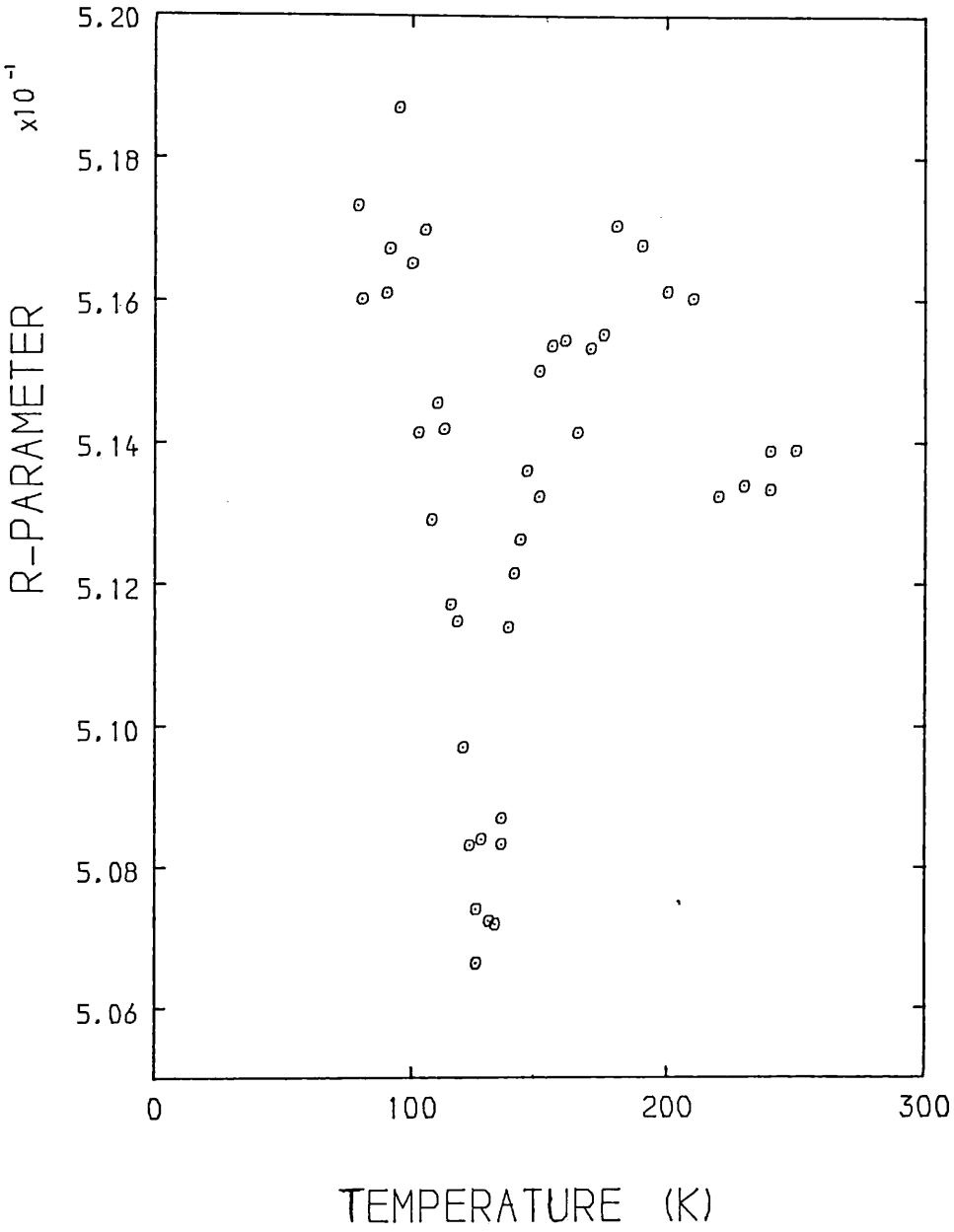

Fig(11.3.1) The variation of R-parameter with temperature for nitrogen adsorbed on the grafoil.The standard deviation of R is ± 0.0006.

that an increases in the F value at 127.5 K, undoubtely occurs because of positron annihilating with nitrogen molecules on the surface of the sample. The position of the peak (maximum point of the F) depends on the pressure of the gas. It is observed that the position of the peak changes from the high temperature of 140 K, associated with the high pressure of 790 torr (at the peak) to low temperatures associated with lower pressures. This is clearly shown by the R-parameter (see next section) on clean surfaces of grafoil (see chapter nine) the F-parameter increases above 170 K and is flat between 80 K and 170 K (apart from the general scatter in the points). The increase above 170 K is attributed due to thermal desorption of positrons or positronium from the surface (Mills Jr 1983). The increase of the F-parameter below 170 K for nitrogen on grafoil as temperature decrease to 127.5 K (maximum value of F) is attributed to positron interactions with nitrogen molecules on the surface and the escape from the surface of the Ps formed by this interaction. At the maximum value of F the monolayer may be complete, this is discribed in later sections. The decline in F-parameter below 127.5 K suggests the increasing of the gas density (multilayer of the gas) and therefore the positrons or Ps being annihilated faster, than being able to escape from the surface. Another explanation is that the positrons can not diffuse back to the surface(Lynn et al 1983). The position of the peak was found to change from 140 K to 127.5 K, to 119 K and then to 105 K as the pressure was reduced from 790 to 290, 130 and then to 30 torr (peaks pressures) respectively.

The change in the position of the maximum value in F-parameter as a function of pressure gives us a certain idea that the nitrogen on the surface of grafoil is fluid and consists of layers. This result is completely different from Jean and Zhou's (1985) result because the

amount of nitrogen that we exposed the grafoil to was more than required for single layer coverages, and also the pressures were higher. Therefore it can not be expected that the transition of nitrogen from solid to liquid or fluid to be observed in this experiment is the same as that in Jean and Zhou's experiment.

11.3-The positron fraction parameter (R-parameter):

The R-parameter which is the ratio of $2\gamma/3\gamma$ decays of positronium was calculated. Any variation in the photopeak spectrum would directly affect the R-parameter. Figure(11.3.1) illustrates the R-parameter versus temperature for one set of data. The minimum value of R shows when the rate of orthopositronium (oPs) emission from the surface of sample is maximum. The peak represents about a 2.2% change in the R-parameter from the low temperature region. The R-parameter shows the interaction of positrons with nitrogen molecules more clearly than F.

The position with respect to temperature of this minimum changes with different nitrogen pressures figure(11.3.2). Figure(11.3.2) shows the R-parameter as a function of temperature for the four different sets of experiments. It clearly shows that the minimum value of R moves from 140 K to 127.5, 119 K and finally to 105 K with respect to pressures at these points of 790, 290, 130, and 30 torr respectively. Nitrogen is fluid above 85 K (Larther 1977) therefore the layers of nitrogen on the grafoil are fluid like not solid like, this is the important difference between our experiment and Jean and Zhou's experiment. However the changing position of the peak in our results shows that layer depends on nitrogen pressures. The temperatures of the minimum values in the R-parameter change according to pressures at these minima . The coverage at this minimum is assumed to be the

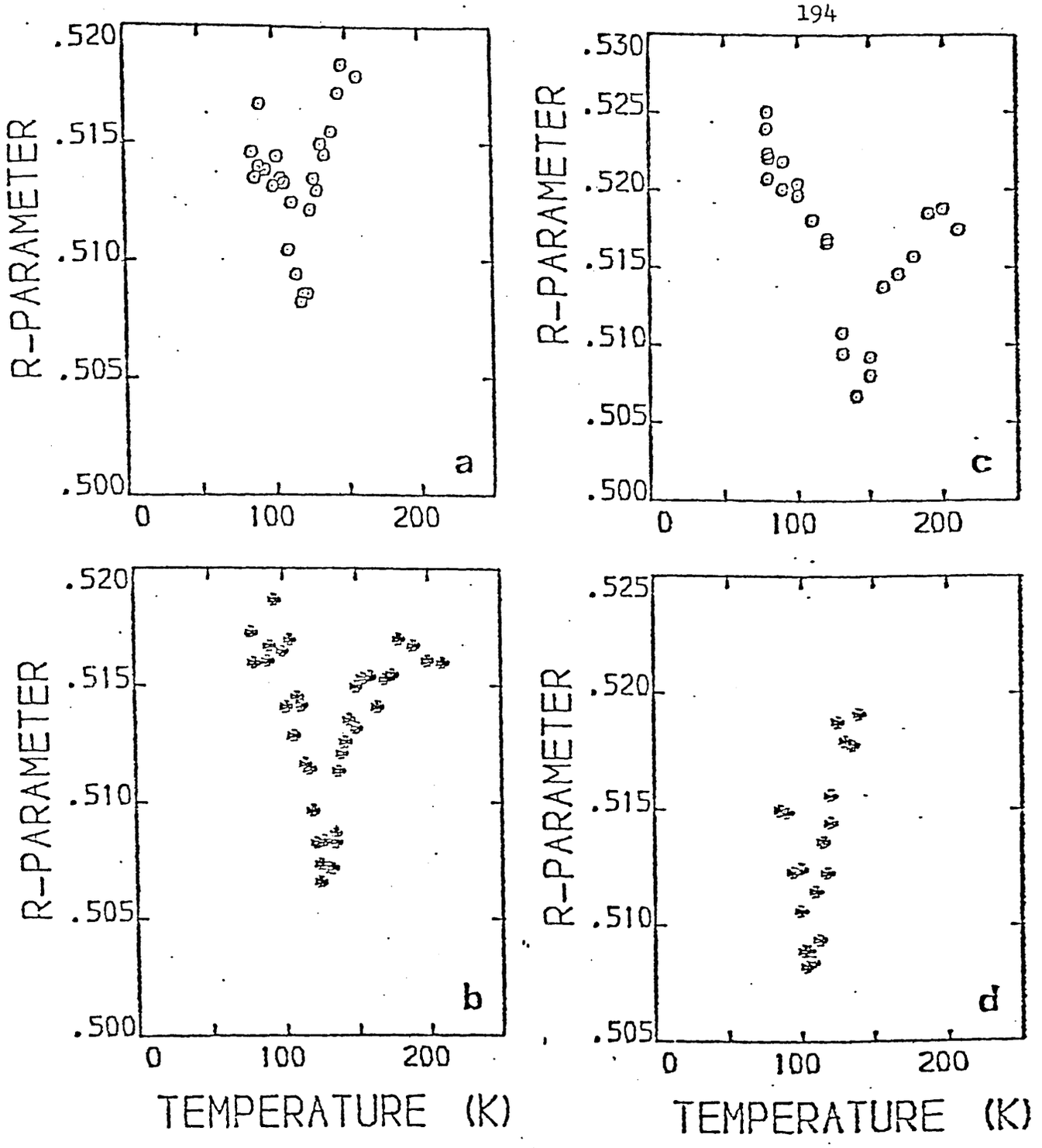

Fig(11.3.2) Formation of orthopositronium: the R-parameter as a function of temperature for nitrogen at pressures of (a) 130 torr, (b) 290 torr, (c) 790 torr, (d) 30 torr, showing the displacement of the peak in Ps formation with pressure.

same for all the cases and this makes it possible to find a theoretical expression for the coverage at the minimum points, and also for the binding energy of the gas molecule on the surface of grafoil. In the next section it is shown how we fitted, by two theroretical expression (Langmuir and Boltzmann), the pressures corresponding to the minima temperatures

11.4-The dependence of coverage on pressure:

As is shown in figure(11.3.2) the position of the minimum in the R-parameter changes as pressure changes. Two theoretical expressions were used to fit this data, first, The pressure versus temperature was fitted by the expression $P=Const.(T)^{5/2}.\exp(-\epsilon_o/kT)[X/(1-X)]$ where X is coverage (the Langmiur monolayer formula). The ϵ_o is the binding energy of nitrogen molecules on the surface. It is assumed that the nitrogen molecule is fixed at sites on the surface. The result of this fitting gives us the value for binding energy of $\epsilon_o=(1186+24)$ which is in reasonable agreement with values of Bruch and others, but this value corresponds to a coverage of 0.5% which is an unbelievable value. The meaningless of this value of X shows that the expression of Langmuir is not useful for this data and is not satisfactory. But, however, nitrogen will be fluid at these temperatures (Larthre 1977) implying that it is unjustified to believe the nitrogen molecule is fixed as solid on the surface of the substrate sites. Therefore the molecules are moving on the substrate surface and the 2-D Boltzmann approximation expression is useful. Assuming the R-parameter minima for nitrogen in figure(11.3.2) correspond to the same coverages n in each case, where n is the numberof the molecules per unit area. The four minima can be fitted by the 2-D adsorption equation $P=A.(T)^{3/2}.\exp(-\epsilon_o/kT)$ where A and ϵ_o are variable parameters and

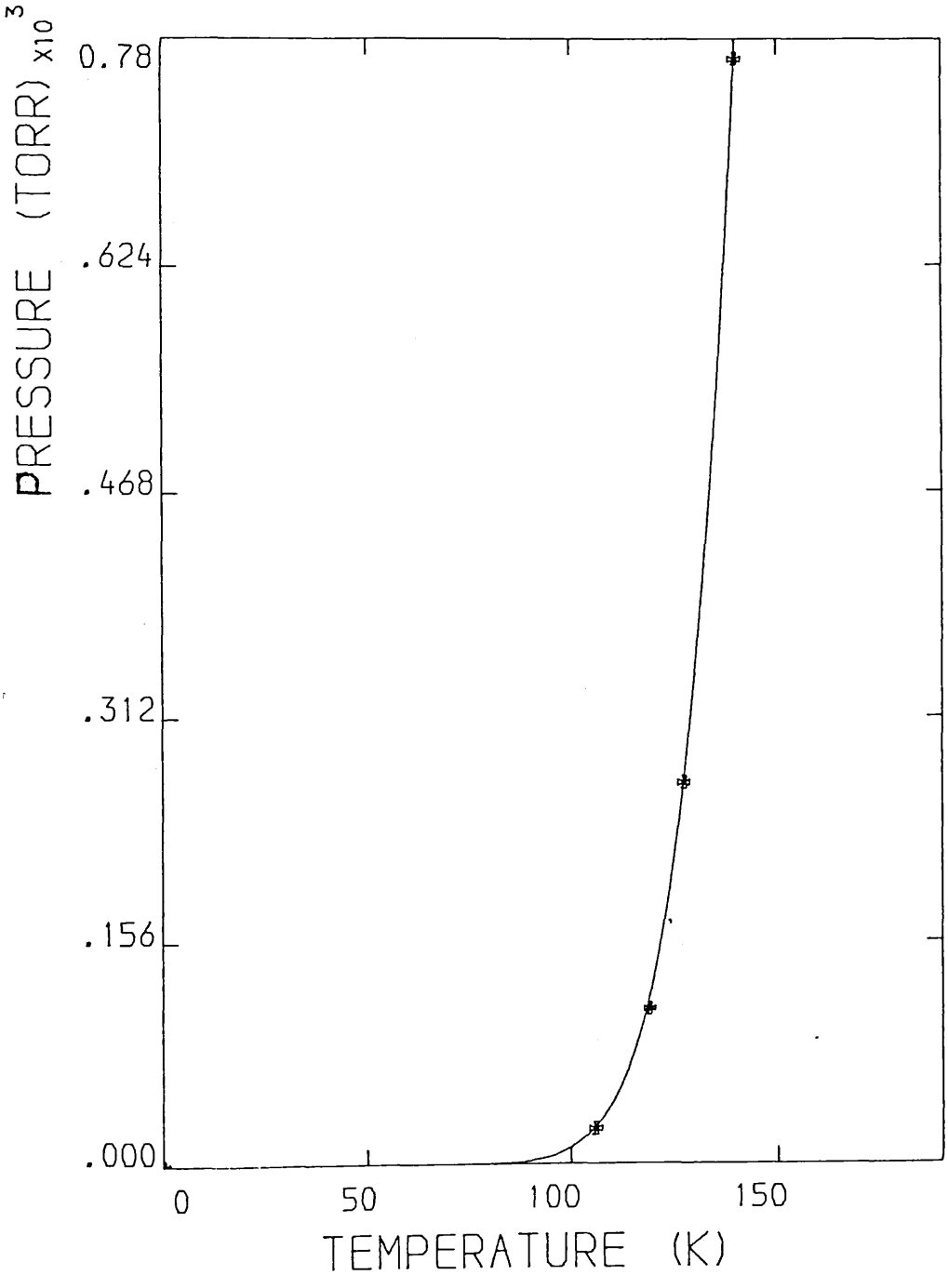

Fig(11.4.1) Boltzmann approximation "expression (3.4.5.5)." is fitted to the displacement of the peak in Ps formation of nitrogen adsorbed on the grafoil, with pressure.

$n = h.A/[(k)^{3/2}(2\pi m)^{1/2}]$ and where h is Plank's constant and m the molecular mass of the gas and k is Boltzmann's constant. The result of fitting yielded the binding energy of the nitrogen molecule on the substrate to be ϵ_o=(1168±11) K which agrees reasonably with theory ϵ_o=1110 K (Steele 1977), ϵ_o=1159 K (Bruch 1983) and calorimetric measurments ϵ_o=1177 K (Rouquerol et al value reported by Steele). The value of n is found from the value of A=(1998.6±134.9) and gives $n = (6.37 \pm 0.43) \times 10^{18}$ mol m^{-2}, which can be compared with an estimated density for 100% coverage. The value n, number of the nitrogen molecules per unit area is in good agreement with that found by Jean and Zhou (1985) and Kjems et al (1975). Assuming the fluid to be "triangularly packed" and taking a value of 4.1 A^o for N_2-N_2 nearest neighbour distance on the surface structure (steele 1977), this n corresponds to a coverage $X = 15.7 \times 10^{-20} .n$. Further taking the area occupied by one nitrogen as 15.7 $\AA^2$ (Jean and Zhou 1985, Roquerol1 et al 1975). The coverage X found X=(1.0±0.01), at the minimum value of R-parameter, which is not in good agreement with Jean and Zhou (1985). They found maximum Ps emission at half coverage, by lifetime measurements of isotherm s at 77 K. But why the positronium emission is maximum at full coverage is a fundamental question which needs to be solved in the future by using a proper pressure gauge and proper volume measurment gauges. In figure(11.4.1) is shown the fit for peak position and pressure at the peak for the four runs.

11.5-R-parameter fitting:

The assumption is made that the positronium fraction probability is proportional to the coverage of the gas on the surface of the substrate. The expression used for the fitting of R (right side) was mentioned in the previous chapter (10.4.b). Theoretically it is

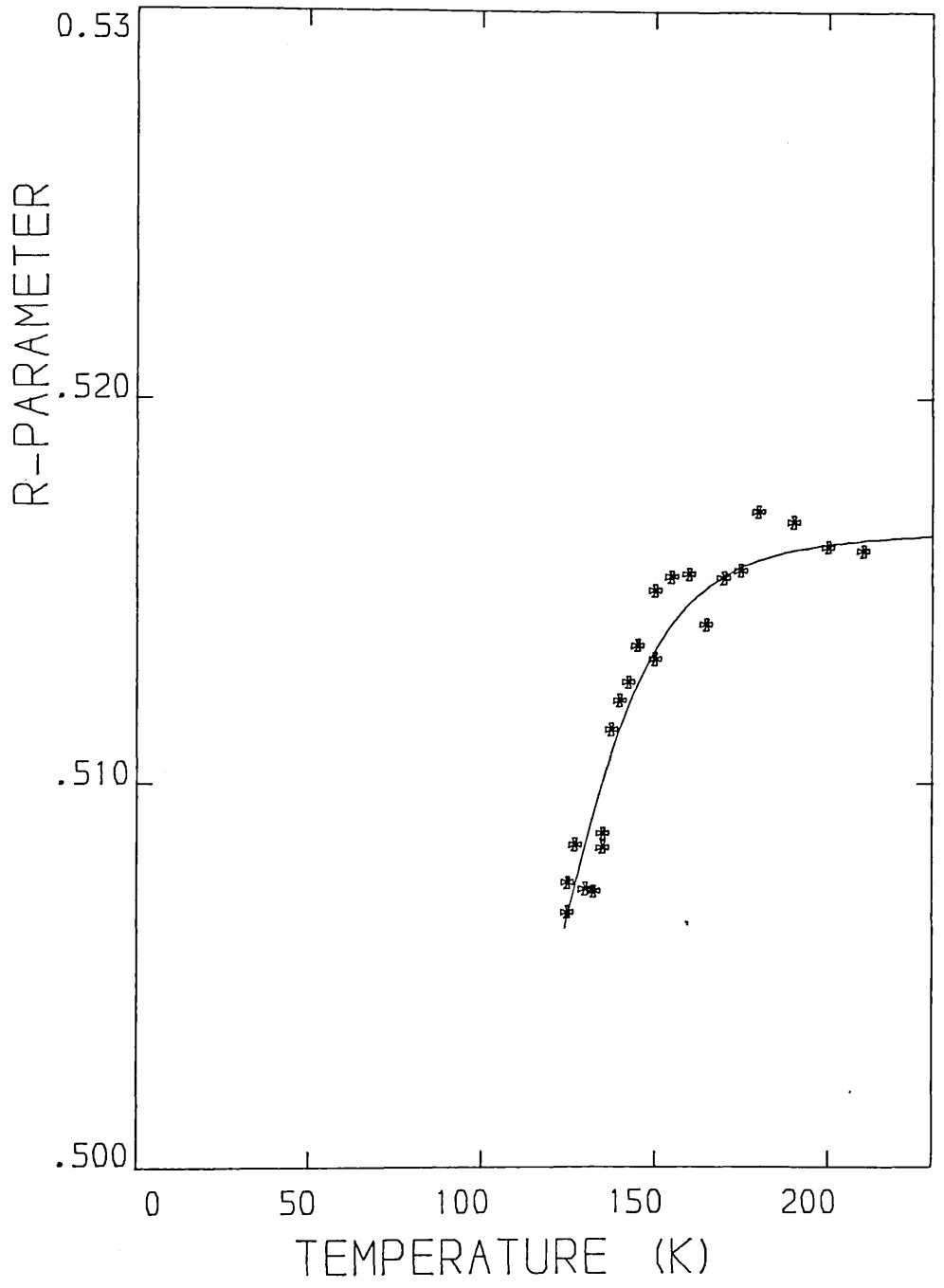

Fig(11.5.1) Theoretical fitting to the right side of R-parameter for second set of nitrogen runs.

possible to apply formula (10.4.b) to fit the individual peaks on the right hand slope of each peak, in which X the coverage is calculated by the Langmiur or Boltzmann formula, and where E_a is the activation energy. In the first try when the Langmiur formula was used for the coverage, parameters without an obvious physical meaning emerged and the binding energy on average come to ϵ_o=1880 K which is very high compared with theory and corresponds to very low coverage. This is expectable because at high temperatures above 85 K the nitrogen must be fluid not solid. The Langmuir formola was then replaced by Boltzmann approximation and the results from fitting the R-parameter, assuming area occupied by a nitrogen molecule 15.7 A^{o2} is given in table(11.4.1a) for two cases on the second (that at 127.5 K) of the experiment. The first case being with E_a set equal to zero and second with E_a as a parameter. These results are justified to be better than the previous result because the average binding energy is much closer to accepted value than before.

1)		2)	
	R_h=(0.516±0.0007)		E_a=(0.012±0.007) ev
	R_l=(0.499±0.0006)		G=(4.30±0.4)X10^9
	ϵ_o=(1181±40) K		R_h=(0.521±0.0009)
	$\frac{\chi^2}{\upsilon}$=3.48		R_l=(0.506±0.0005)
			ϵ_o=(1107±21) K
			$\frac{\chi^2}{\upsilon}$=7.5

Table(11.4.1a)

It is concluded that positronium emission increases as a monolayer builds up and decreases as the bilayer develop s. The decrease at low temperature (80 K) is because the density of the gas has increased (multilayers) and positronium is annihilated before being able to escape. The fitting for the second set of experimental data is shown in figure(10.4.1). The average binding energy calculated by fitting

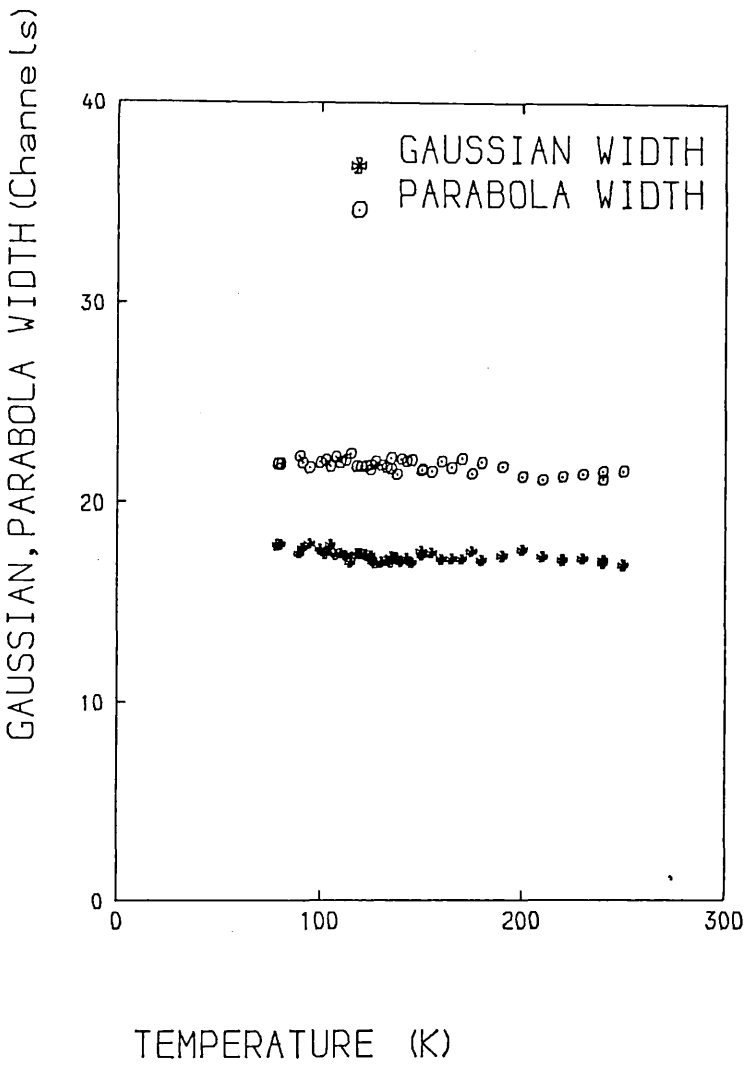

Fig(11.6.1) The variation of the width parameters of the Gaussian and the parabolic components of individual lines for nitrogen adsorbed on the grafoil.

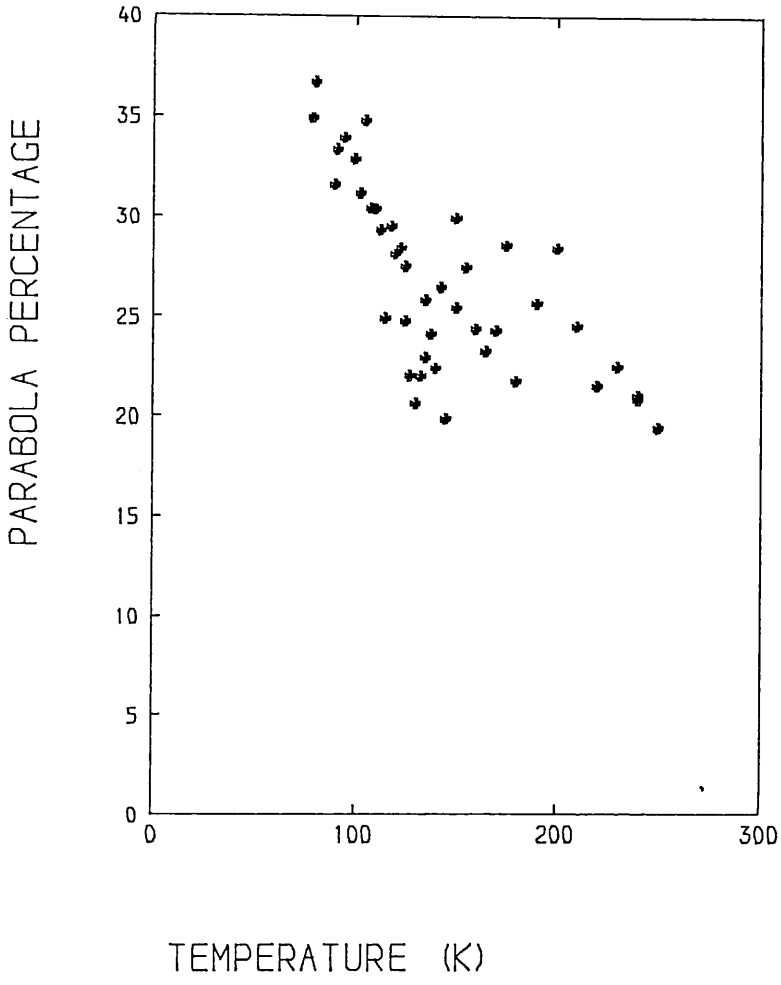

Fig(11.6.2) The change in percentage of parabolic component in nitrogen adsorbed on the grafoil.

the different data was ϵ_o=(1145±24) K and the activation energy E_a=0.035 ev; the small value for the activation energy is attributed to no thermal desorption of positron or Ps.

11.6-Line shape analysis:

The spectrum was again fitted by using a least-squares minimization routine for an inverted parabola and a Gaussian convoluted with the resolution function. The results of this fitting are again parabola and Gaussian widths figure(11.6.1) and parabola percentage figure(11.6.2). It can be seen from figure(11.6.1) that the parabola width and Gaussian width both stay constant against temperature with average values of 22.5 and 18.6 channels, respectively. The parabola percentage changes from 35% to 20% at the peak 127.5K and again increases above 127.5K. The peak position for the four sets of data, in the R and F-parameters correlates to changes in the parabola percentages. The average parabola intensities at peak positions for all the sets of data is different by about 14% compared to the clean surface of the sample (chapter nine). This 14% is attributed to the intensity of the Ps emission, when the nitrogen gas is adsorbed on the surface of grafoil. The chi-squared per degree of freedom lay between 0.98 to 1.23 indicating a good fit to the data. The data was also fitted to two Gaussians only and two Gaussians and one parabola, but the chi-squared was worse than the value above, therefore the best fit accepted was of one Gaussian with an inverted parabola.

11.7-Conclusion:

First of all the vapour pressure of the nitrogen had an important role in our results, because by changing the pressure it was observed that the position of the peak was changed. By using the correct assumptions reported about nitrogen monolayers on graphite (Steele

1977, Bruch 1977, Jean and Zhou 1985,and Kjmin et al 1983) it was found that the coverage of nitrogen at the maximum value of positronium emission was approximately one. Therefore it was concluded that positronium emission increased as the monolayer built up and decreased as the bilayer developed. The binding energy of the nitrogen molecules on the grafoil was found ϵ_o=(1168±18K), to be in good agreement with the value calculated by (Steele 1977, and Bruch 1977). The number of molecules of nitrogen per unit area was calculated to be $6.37X10^{18}$ which is in good agreement with $6.5X10^{18}$ which was found by Jean and Zhou (1985). The nitrogen monolayer (fluid) was observed to form, at different temperatures corresponding to different pressures on the grafoil and characterized by the maximum positronium emission as observed by Doppler broadening method. The results of this experiment including the sample properties compared with other references is shown in table(11.6.1).

Sample	Density [gr/cm^3]	Surface area [m^2]	Molecular No. per unit area [mol m^{-2}]X10^{-20}	Molecule area [m]X10	Coverage (%)
Grafoil	0.904 (a)	1810	6.17	16.4	101
Grafoil	1.11 (b)	570	6.50	15.7 (c)	102
Grafoil	0.940	5.2	6.37	15.7 16.4	100.1 102

table(11.6.1)

(a) Kjems et al (1977)
(b) Jean and Zhou (1985)
(c) Roqurelor et al (1975)

The Fundamental question of why the maximum positronium emission is greatest at a full coverage of monolayer will be answered in the future by more experiments and actual isothermal measurements (eg. at 119 k or 127.5 K etc.). But the system was not complete for this kind of experiment, and needs to be improved. The system needs proper

pressure and volume gauges to measure the pressure and amount of the gas with high accuracy. The 14% change in parabola intensity in going from a clean grafoil surface to monolayer created one can be attributed to the change in positronium emission intensity.

Chapter XII Positron annihilation for oxygen condensed on the surface of grafoil

12.1-Introduction and method:

Oxygen adsorbed on graphite and other substrates has been studied by many different methods for many years. Therefore many properties of oxygen layers on substrates especially graphite have been investigated, such as the transition from solid to liquid at 54.4K. Many other properties such as structure of the solid oxygen layer and its transition on the graphite at very low temperatures and pressures were investigated by MacTangue and Nilson (1976), Stephenes et al (1980), Pan et al (1982) and Marx and Christoffer (1983). Recently the transition in structure from α to β was also observed by Toney and Fain, jr. (1984) at T>18K. These experimental works on the monolayer give useful information about the oxygen adsorbed on the graphite but are far from our measurments in terms of temperature.

In 1982 Patrykiejew et al calculated the minimum depth energy of oxygen molecules on graphite by considering that the gas had an interaction with the homogeneous crystal surface but that there was a negligible interaction between the bulk gas and the condensed phase. The value reported by them is ε_o=1050K, and is the binding energy of the oxygen molecules to the graphite. They also reported the critical temperature of oxygen, above which the layer is liquid as 66.5 K. There are numerous literatures on oxygen monolayers which are adsorbed on graphite at very low temperatures and pressures.

In the positron annihilation field there have been no experiments, so far done on the adsorption of oxygen on grafoil at liquid nitrogen temperatures. But in 1983 Lynn and Lutz reported on the interaction of a positron beam with oxygen which had been chemisorbed. They made two

observations viz: (1) the positronium fraction decreases with the development of overlayers of oxygen on the aluminium surface, and (2) that the positronium is formed as parapositronium rather than ortho-positronium. They claimed that this (point (2)) was because of a spin exchange process occures, they could not detect the difference between the selfannihilation of pPs and of annihilation of positrons trapped in vacancies. Similar effects were also observed in our experiments on positron interaction with oxygen on grafoil, at low temperature.

Method:

The same grafoil source specimen was used as was used for nitrogen and argon. Before the oxygen measurment the source specimen was removed from the cryostat and mounted in the furnace, and with vacuum better than 10^{-6} torr. the temperature was increased from room temperature to 610K (with 10 K steps see chapter nine), then allowed to cool to room temperature. The sample specimen was then removed from the furnace and replaced in the cryostat under high vacuum and left for a few hours at room temperature. After that a cylinder containing oxygen of 99.99% purity was connected to the chamber and the gas feed line evacuated for a few hours. Then the oxygen gas was let in to the chamber at room temperature in pressure of 1520 torr and volume of approximately 300 cc. The system was then left at room temperature over night. While cooling down to 77K the pressure dropped from the 1520 torr to 160 torr which is the vapour pressure of oxygen at 77 K. The pressure remained constant at this value throughout the experiment. When the system had reached equilibrium at 80 K, data collection was started with an accumulation time of 2 hours in steps of 10 K with stability in temperature again better than 0.5 K to a final temperature of 320 K. Cooling down was from 320 K in steps

of 20 K changing at 160 K to steps of 10 K. The experiment was repeated five times in the range 80 K to 170 K by repeatedly heating and cooling the sample. Over the two hours data accumulation time the count at the central of the peak reached 17000.

12.2-Line-shape parameter:

The line shape parameter (F-parameter) which is again the ratio of the integral of 7+1+7 channels of the photopeak center to that of the total area of spectrum after error function back ground subtracted, is illustrated in figure(12.2.1). The F-parameter is very sensitive to variations in line shape caused by positron annihilations with bulk electrons as opposed to free electron. An increase in the F-parameter represents an increase in the rate of annihilations with the free electrons of the medium. The para-positronium self-annihilation, resulting in the production of two gamma-rays each of energy 511 kev, is a component of narrow width in the annihilation spectrum. Consequently the F-parameter will also increase if the positron becomes bound with an electron to form para-positronium. Thus one can expect an increase in the F-parameter with the parapositronium fraction.

The F-parameter increases at 90K see figure(12.2.1) suggesting that an increase in the positronium fraction, that is in the annihilation of the positron with oxygen on the surface of the grafoil. The increase appears to be due to the transition of the oxygen layers to vapour. The decreasing F value below 90K suggests the exposure of the surface to oxygen (multilayers completely filled with liquid) similar to the chemisorbed oxygen on aluminium (Lynn and Lutz 1980) who reported a reduction in the positronium fraction for overlayers due to exposure of the aluminium to oxygen at room temperature, and a spin-exchange

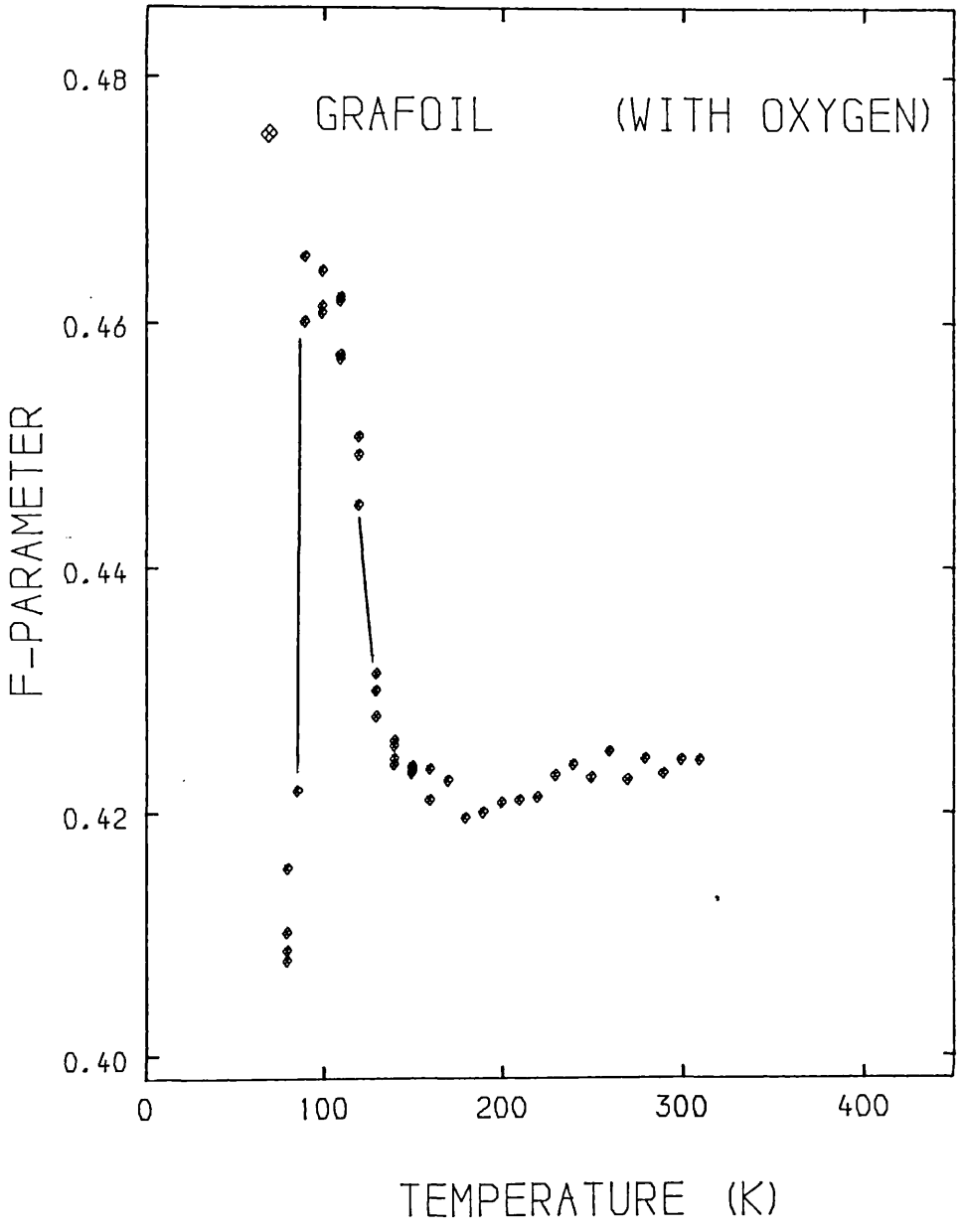

Fig(12.2.1) the F-parameter variation as function of temperature for oxygen condensed on the surfaces of grafoil. The standard deviation of F value estimated ±0.0005.

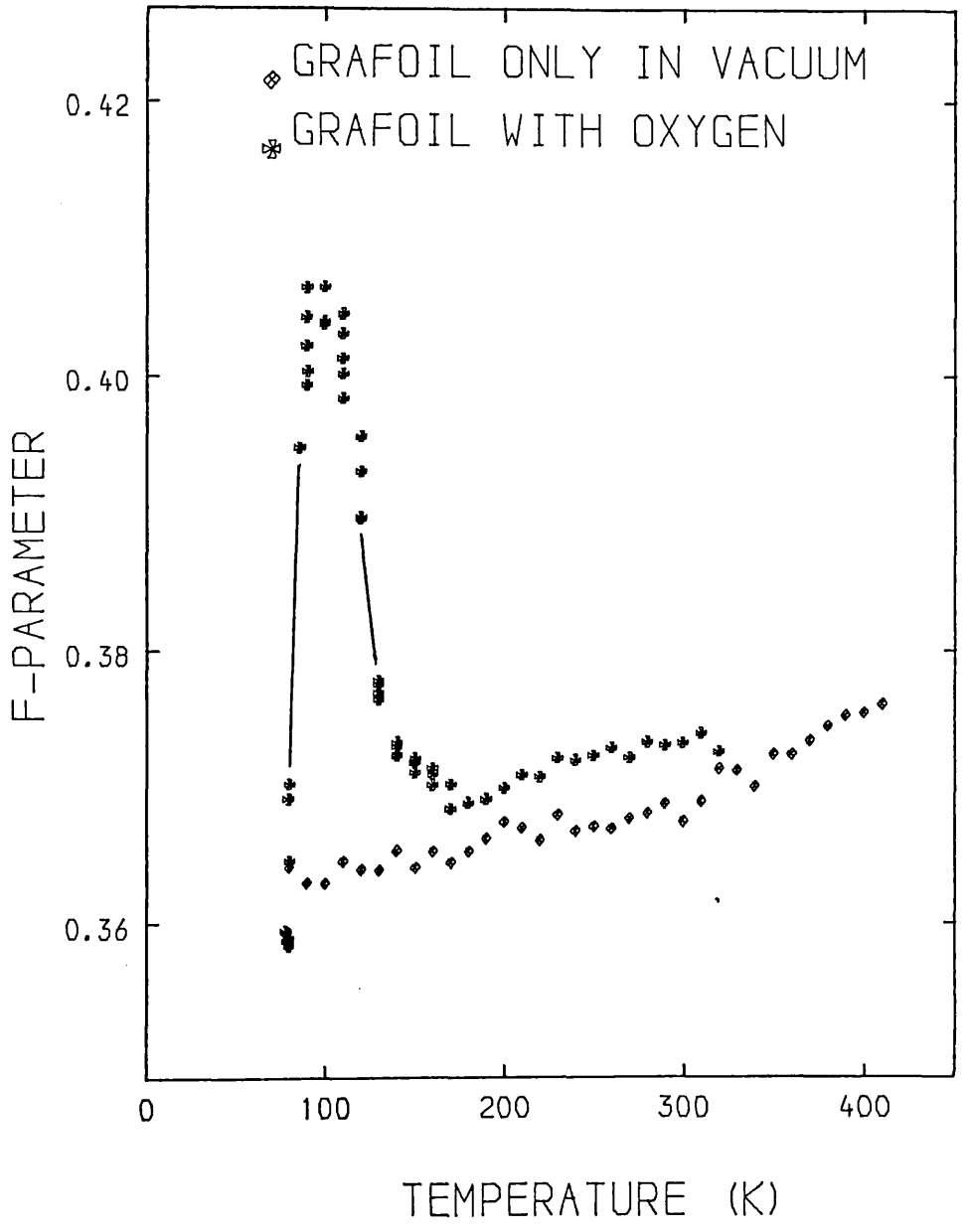

Fig(12.2.2) the F-parameter versus temperature (without background subtracted) of oxygen on the grafoil surfaces (star) compared with grafoil only (square).

process leading to parapositronium decays. This sharp increase in F was not observed in the other two gases (argon and nitrogen); the oxygen result on the surface of grafoil is merely due to the spin exchange process which changes the triplet state ($^3S_1$) to singlet state ($^0S_1$). Brimheill and Pase (1965) also mentioned that since the triplet state is largely quenched in oxygen via conversion to the singlet state (which decays some 10^3 times faster) essentially all the decay of positronium is observed by emission of two photons. This is in good agreement with our experiment at 90K and 100K, all the ortho-positronium is converted to para-positronium.

Above 150K the F-parameter as can be seen is slightly higher with respect to the F value for grafoil in vacuum figure(12.2.2). This figure shows the different effects of the positron annihilation with oxygen on the surface of grafoil compared with positron annihilation with grafoil in vacuum. The oxygen may completly escape from the surface of the grafoil, above 300 K, because the F value appears the same as that resulting from positron annihilation in the grafoil alone.

12.3-Line-shape analysis:

Another interesting result of the positron interaction of oxygen molecules on the surface of grafoil is the width of the inverted parabola fitted to the spectra. First the spectrum was analysed with an inverted parabola and Gaussian convoluted with the resolution function in the same manner as before, and gave a resonable chi-square per degree of freedom of between 0.94 and 1.3. The parabola width and parabola intensity of oxygen adsorbtion on the grafoil spectrum was completly different with respect to the width and parabola intensity of metals (see cadmium and tin analysis). The parabola width was

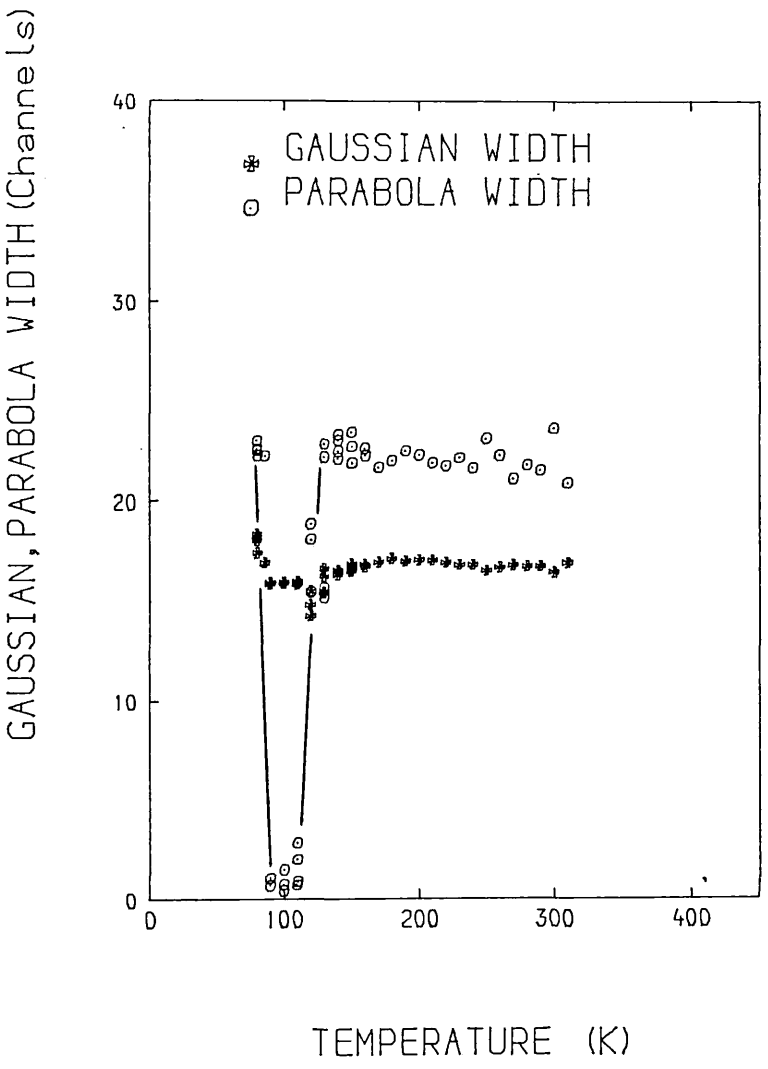

Fig(12.3.1) shows the Gaussian and parabola width versus temperature of positron interaction with oxygen adsorption on the grafoil surfaces.

found to drop sharply at 90K from a width of 23.4 channels to approximately 2 channels, there was also a small change in the Gaussian width figure(12.3.1). The original rise in the F-parameter is due to the appearance of sharp spike of a width that is only a few channels in the Doppler spectrum. This width increases again at 120 K, and 130 K to 15 channels, then up to the 23.4 channels, as the sharp component disappears. This shows that the parabola width is very sensitive to the narrow component in the Doppler spectrum, and gives us a hint that the increase in the F-parameter is due to the self-annihilation of the para-positronium (electron positron bound in oxygen).

The parabola percentage decreases sharply from approximately 35% to 6-7% at 90 K or 100 K and increases to 15% above 120 K and finally to 20% above 140 K, the decrease of parabola intensity above 200 K was also observed on the clean surface of grafoil figure(12.3.2). The decrease in the parabola intensity which was observed in the argon and nitrogen experiments suggests the formation of positronium. These parabola widths and percentages were found to be a very important factor in showing that the positronium forms on the surface and in the gas molecules on the surface of the sample. The parabola intensities and widths together with Gaussian widths, from grafoil with oxygen and from grafoil in vacuum are compared in figurs(12.3.3). As is clear in fig(12.3.3) the parabola intensity drops from 35% at 90 K to approximately 7% implying that 28% of the positrons annihilate with oxygen molecules on the surface of the grafoil.

In fact the narrow width of the parabola is not the width of the narrow component on the Doppler spectrum, and thus a second Gaussian was introduced. The data was then fitted with one parabola plus one narrow gaussian and one wide Gaussian (in the region 80 K to 170 K).

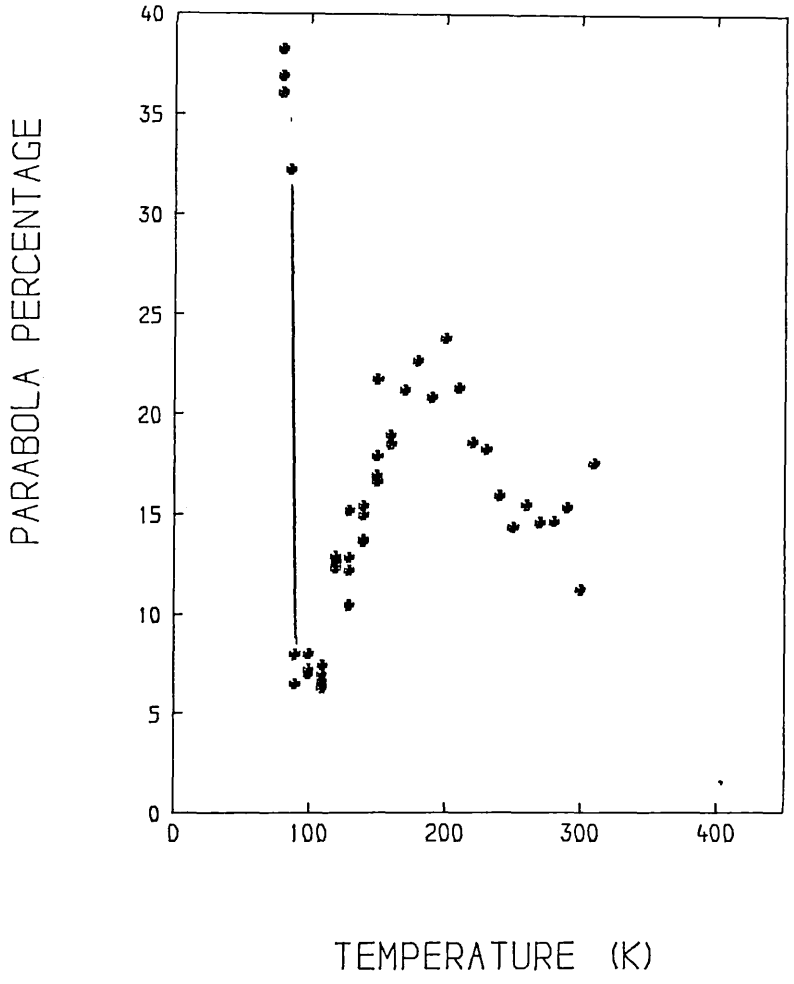

Fig(12.3.2) the parabola percentage of positron interaction with oxygen adsorption on the grafoil surfaces as the function of temperature. The standard deviation of parabola percentage is calculated $\pm$2.3%.

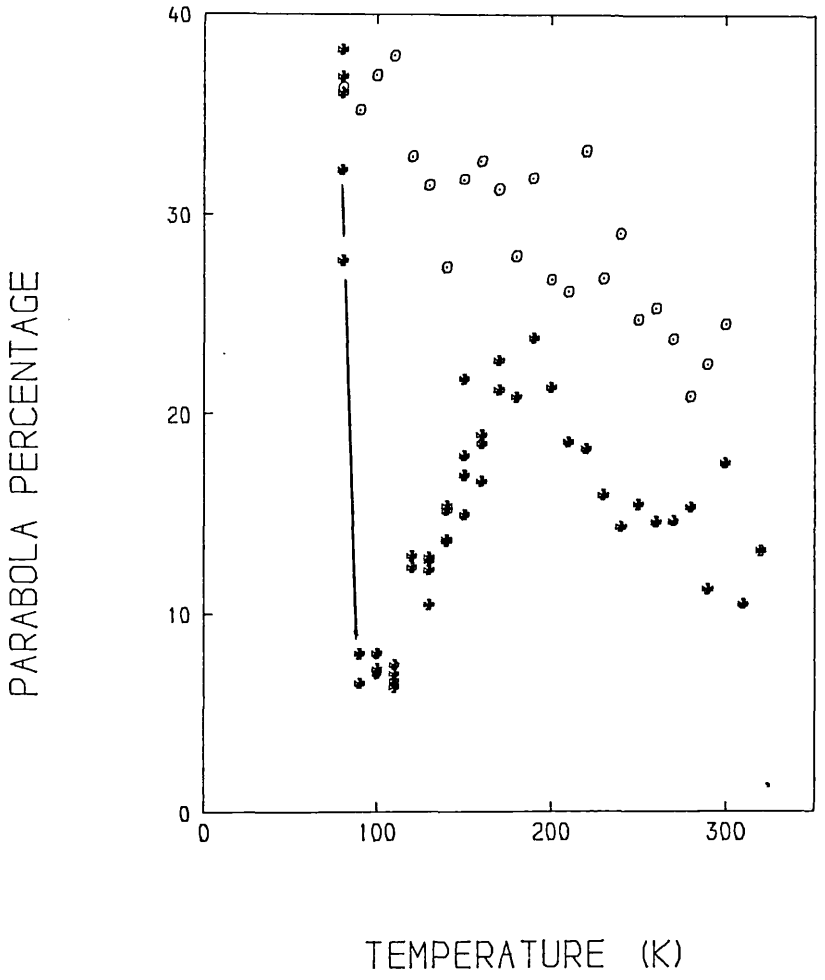

Fig(12.3.3) shows the parabola percentage of positron interaction with oxygen adsorption on the grafoil surfaces as function of temperature (star) compare with parabola percentage of positron interaction with grafoil only (circle).

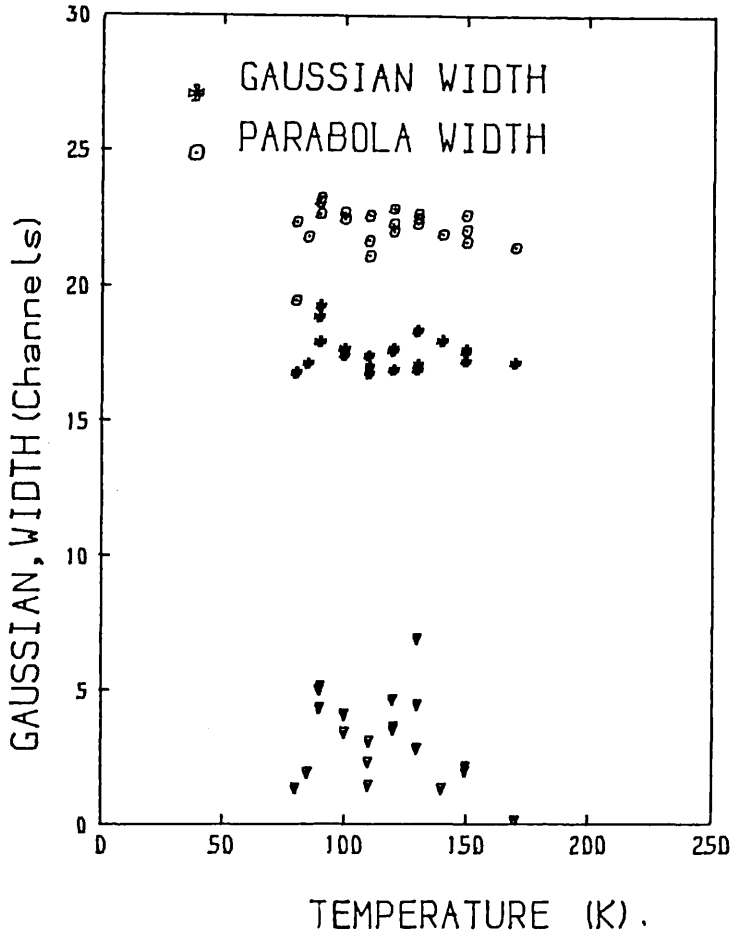

Fig(12.3.5) shows the parabola and two Gaussian Width, one is wider (star), and another is narrower (triangle) of positron interaction with oxygen adsorption on the surface of grafoil as a function of temperature, for range (80-170 K).

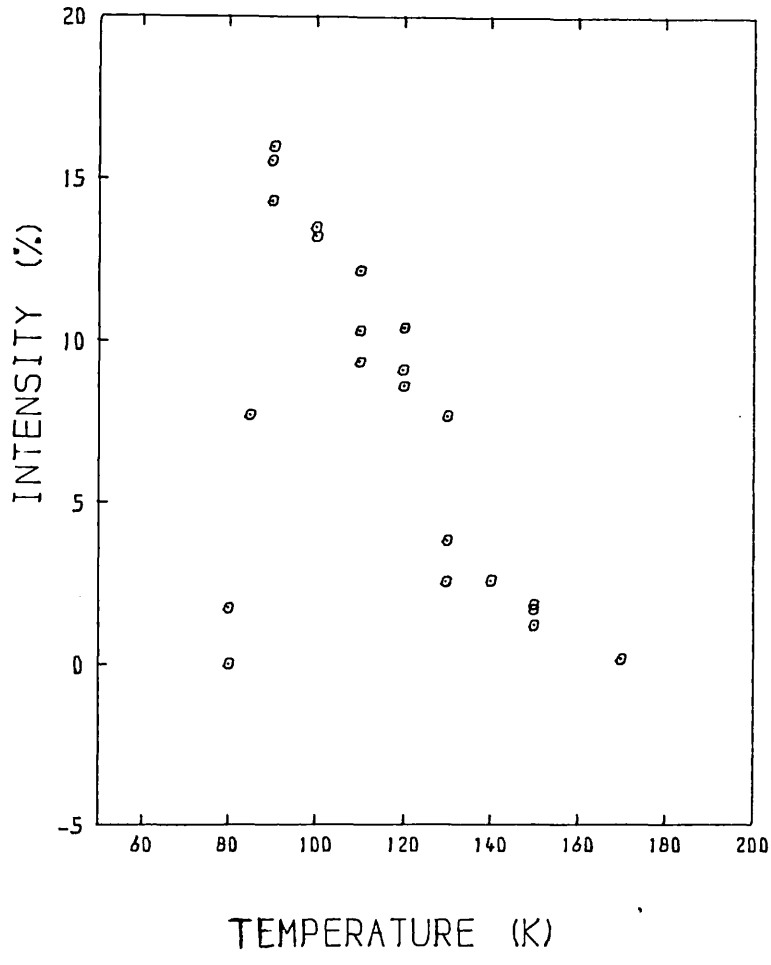

Fig(12.3.6) The narrow Gaussian percentage as a function of temperature for positron annihilation in oxygen condensed on the grafoil. The standard deviation is estimated to be $\pm 1.5\%$.

The change in the width of the parabola back to the 23.4 channels as the positrons annihilate in grafoil only, and the narrow Gaussian width (4.0±1.0 channels), is illustrated in figure(12.3.5) and figure(12.3.6) which are showing clearly the correlation of the this narrow Gaussian and F-parameter. The maximum value (16+2)% at the 90 K shows the maximum rate of the Ps emission. The chi-squared was slightly reduced from its previous value. The full width of the half maximum (FWHM) of the narrow component is given from the narrow Gaussian width to be approximately 6.8 channels.

12.4-Fitting the F-parameter:

We assume the positronium fraction is proportional to the coverage of oxygen on the surface of grafoil, and as such use both coverage formulae of Langmuir and Boltzmann, plus Mill,Jr's expression for positronium activation energy (used in chapter ten equation (10.3.b)), to fit the F-parameter. In the first try we used the Langmuir coverage formula and for three cases of the fitting the values found are given in table (12.4.a).

1)	2)	3)
F_l =(0.464±0.0007)	E_a=(0.058±0.008) ev	E_a=(0.23±0.05) ev
F_h =(0.417±0.0006)	G=(43.7±3.3)X10^6	G=(29.8±2.6)
ϵ_0=(1734±40) K	F_l =(0.464±0.0003)	F_l =(0.461±0.0008)
β =(8.3±0.7)X10^{-4}	F_h =(0.422±0.0005)	F_h =(0.420±0.0006)
$\frac{\chi^2}{\upsilon}$=2.25	ϵ_0=(1843±50) K	β=(3.17±0.24)X10^{-4}
	$\frac{\chi^2}{\upsilon}$=3.93	$\frac{\chi^2}{\upsilon}$=3.33

Table(12.4.a)

The value found for the of binding energy is much greater than that reported by Palrskijew et al (1982). The result obtained by using the Boltzmann approximation for covearage are given in table (12.4.b). The binding energy of the oxygen on the grafoil as calculated in this

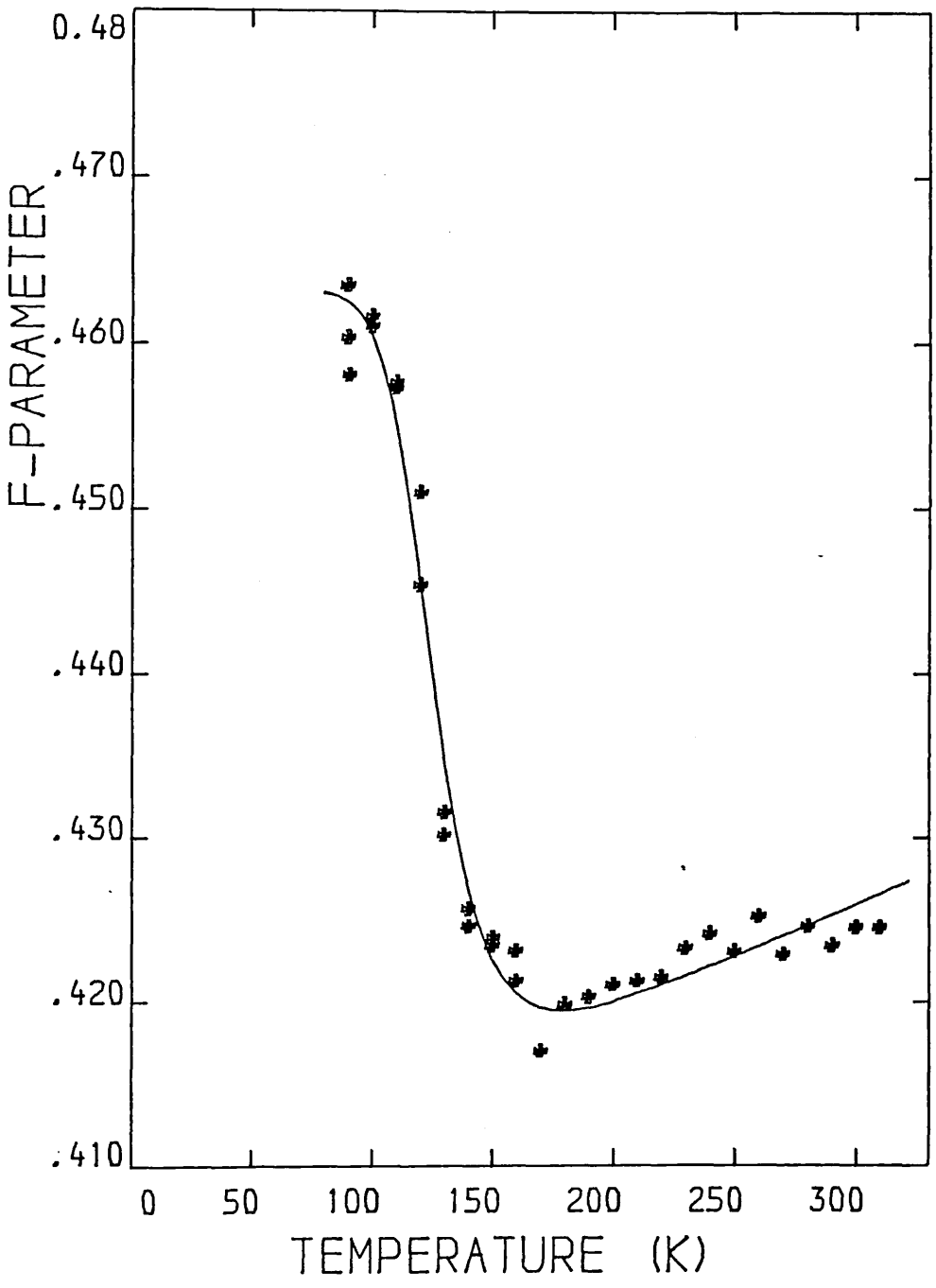

Fig(12.4.1) The theoretical fitting to F-parameter with temperature for positron annihilation in oxygen adsorbed on grafoil specimen.

case is (1250±70) K which is almost that found by other groups. This value corresponds to a coverage of one at 110<T<120 (using all data points for fitting).

1) $F_l = (0.467 \pm 0.0003)$

$F_h = (0.405 \pm 0.0006)$

$A = (0.153 \pm 0.062) \times 10^{-3}$

$\varepsilon_o = (1250 \pm 70)$ K

$\frac{\chi^2}{\upsilon} = 8.39$

Table(12.4.b)

The binding energy and chi-squared, both decreased when the F-parameter was fitted from data points starting of 100 K,110 K and 120 K to 300 K, the fits giving corresponding values of ϵ_0 =1226,1185 and 946 K and chi-squa red 6.4,5.8 and 3.7 respectively. For all these fitting cases the coverage came to one when temperature range was 110<T<120. From this it may concluded that ϵ_o has an average value of between 1188 and 946 K corresponding to monolayer coverage between 110<T<120. The average binding energy is $\epsilon_0 = (1064 \pm 10)$ K, which is resoanable agreement with others. Fig(12.4.1) shows the F-parameter together with the fit generated from equation (10.4.b) of chapter 10.

12.5 Positron annihilation for helium on the grafoil surface

12.5.1-Introduction and method

Generally the density of gases ought to increase as temperature decreases. In the case of dense fluids, positronium bubbls are created due to exchange of repulsive force between positronium and gas atoms. The positronium bubble was observed in liquid and solid helium by Hernaber and Choi (1969) and also in liquid argon, krypton and xenon by Varlashkin (1970) at low temperatures. In the positronium bubble state the orthopositronium lifetime reaches about 100 ns since the overlap of the trapped particle with the bulk fluid is very small (Hautojarvi and Vehamen 1979). Three components of positron lifetime in helium were reported by Paul and Graham (1956) at very low temperature with the long lifetime attributed to oPs pick-off or conversion to two photon emission processes. All measurments were reported for very low temperatures.

At sufficiently low temperature peculiar phenomena have been seen in noble gases especially helium. Both positron and positronium may exist in localized states. The attractive polarization forces between a positron and helium atom induce droplet formation around positrons when their kinetic energy is sufficiently low (Canter et al 1975).

The adsorption of helium on graphite has been investigated by many different methods at very low temperatures and sufficiently low pressures. Dash mentioned that there is no experimetal work to show the adsorption of helium on the cold substrate above 100K (1974). In this chapter our experimental work for observation of positronium emissions regarding helium atoms on the surface of grafoil at liquid nitrogen temperatures and high pressures is presented.

Method:

Before insertion of the helium gas in the chamber, the sample specimen was kept at a high temperature (400 K) for a few hours. After which it was allowed to cool to room temperature, at which point helium of purity 96% was let in. The pressure at 300K was taken to two atomospheres (1520 torr) and on cooling to 80 K dropped to 690 torr. Data was collected over two hour periods between 80 K and 180 K by heating and then from 180 K down, in steps of 10 K. After this set of measurements, the helium was pumped out and the sample temperature raised to 400 K under high vacuum and kept there for a few hours. The sample then again allowed to cool to 80 K and helium gas of purity 99.999% was let in to the chamber. Unfortunately the pressure in the feeding cylinder was not high enough to obtain the same pressure. The final pressure was 350 torr at 80 K. The conditions of the experiment were thus different and therefore we should not expect to observe the same results as in the previous experiment.

12.5.2-Line-shape parameter results:

The F-parameter is shown in figure(12.5.2.1). It can be seen from this figure that the F value is increased approximately by 2.3% from the lower points. The F-parameter was gradually increased after at least ten hours at 80 K which is different from the other gases such as oxygen, nitrogen and argon. The value of F is then decreased as the temperature is raised and then dropped to its original value for annihilations on the clean surface of grafoil at 170 K. After cooling down from 170 K the F value agian increased to a maximum value at 80 K. This observation of increasing F at 80 K suggests that the interaction of positrons with gas atoms on the surface and the emission of positronium. Unfortunately this effect may have been due to the helium gas on the cold substrate not being of good purity

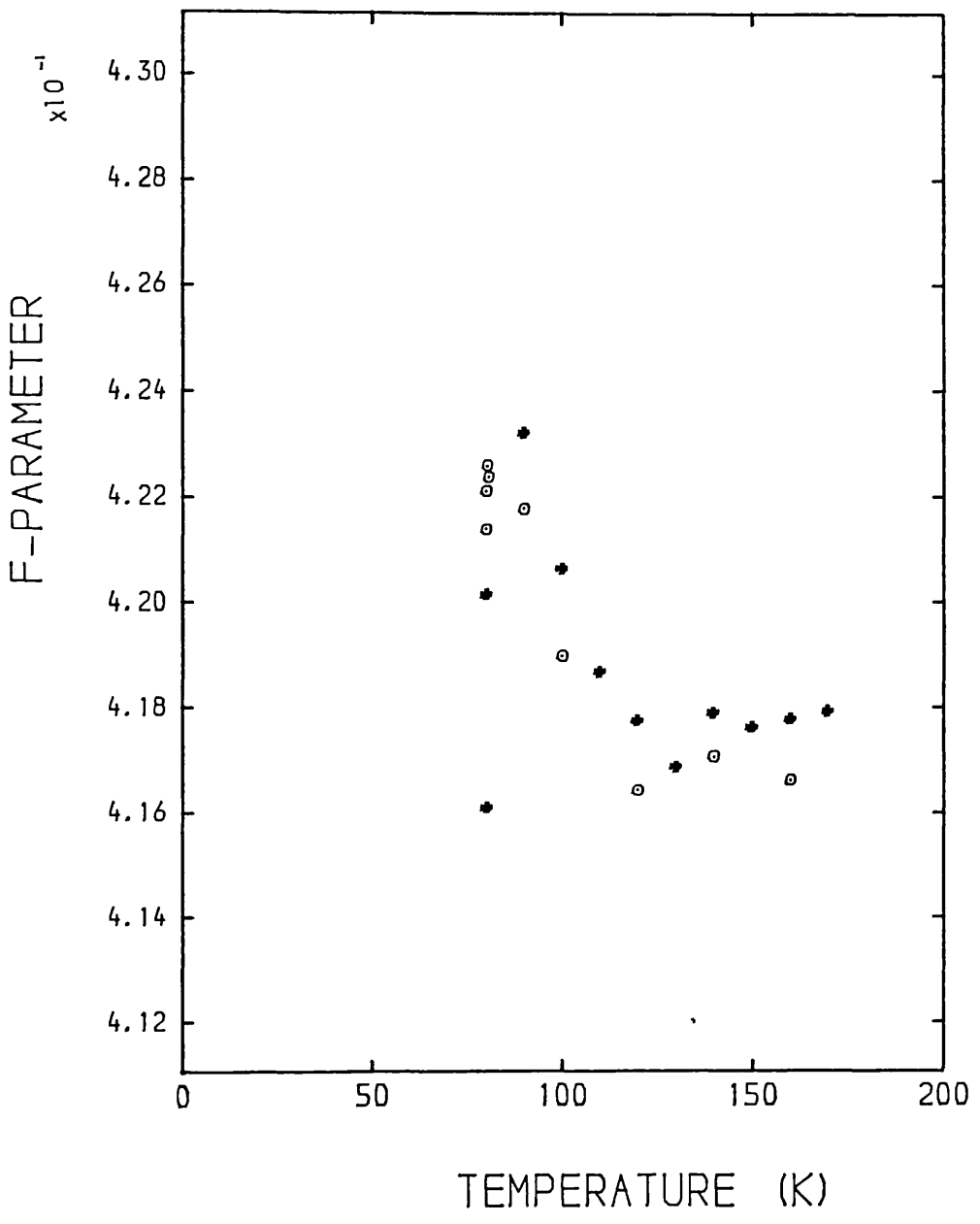

Fig(12.5.2.1) The variation of F-parameter with temperature for helium condensed on the grafoil specimen, star is for heating and circle is for cooling the sample. The error function background subtracted and standard deviation is estimated as $\pm$0.0008.

because impurity would play an important role. Because of this, the higher purity of helium gas was used, where results are shown in figure(12.5.2.2). At first the F-parameter did not shown an increase for consecutive runs at 80 K, nor when the temperature was raised from the 80 K to 170 K, but in cooling down from 170 K it showed an increase for runs at 80 K. This effect is very strange at this temperature and such a pressure. It might be attributed to the interaction of helium on the surface of grafoil as results of which positronium emission from the surface occurs and the F-parameter increases. However this later experiment, with the high purity gas, dose not show any greater effect. This may be because of the lower gas pressure (350 torr as opposed to 690 torr). To draw further conclusions, more experiments are needed to be preformed at liquid nitrogen temperature and below if possible.

Unfortunately our equipment was not set up to contin ue the experiment at lower temperatures below 77 K and it was not possible to observe the monolayer or bilayer of helium on the grafoil surface, as we were able to do so for the other gases. Although our equipment is based a helium cryostat, the system is not suitable for low temperature adsorption measurements because it is not possible to keep the temperature low and stable. The liquid helium coolant boils off very fast during runs (owing to increased heat transfer by the gas under investigation); also because of the condensed sample chamber gas, it is very difficult to obtain the stable temperature.

12.5.3-R-parameter:

In the case of the 99.999% pure helium (second experiment) the R-parameter was also measured and it is shown in figures(12.5.3.1). It can be seen that the R value is decreased at 78 K, showing the rate

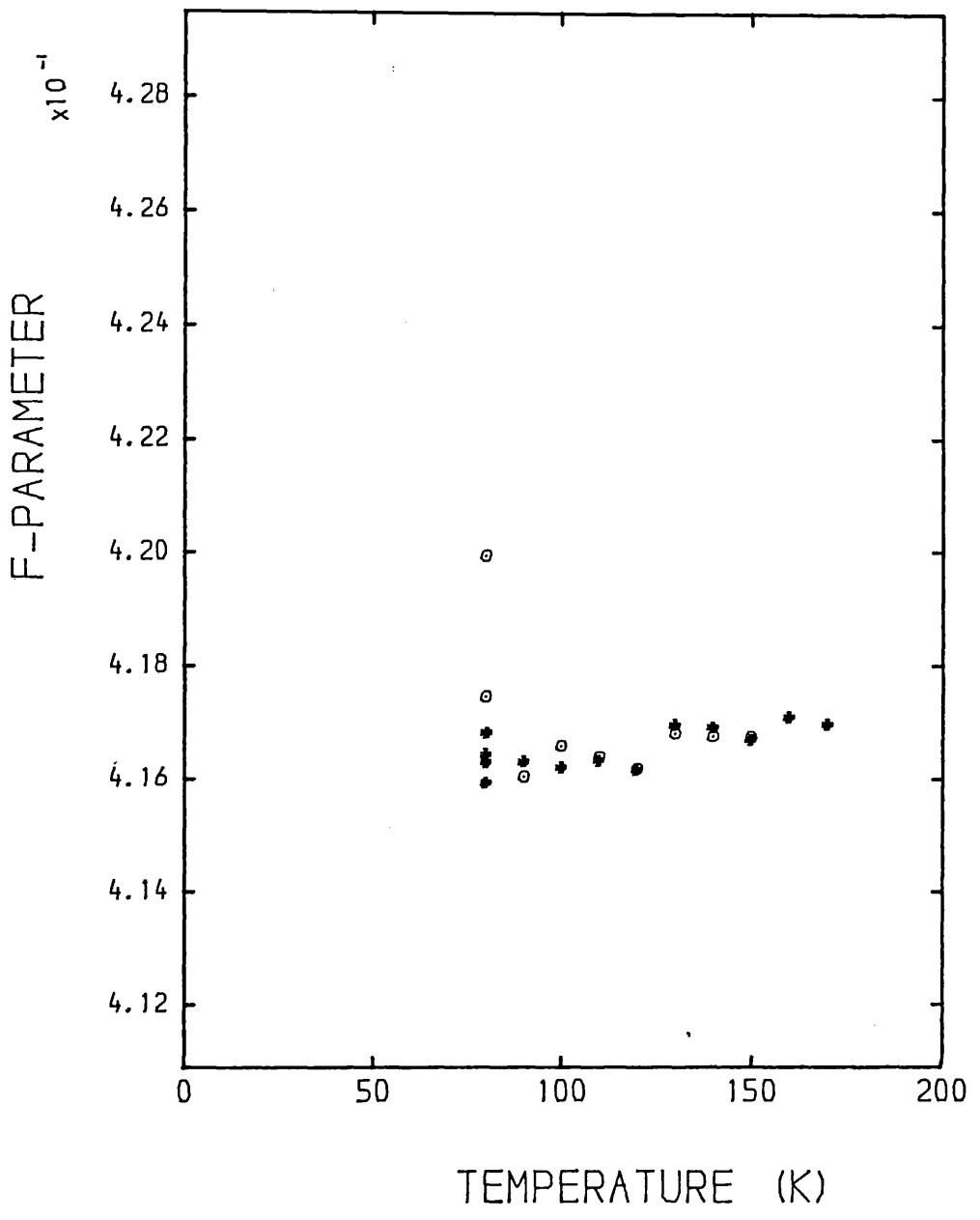

Fig(12.5.2.2) The variation of F-parameter with temperature for pure helium condensed on the grafoil specimen, star is for heating and circle is for cooling the sample. The standard deviation is estimated as $\pm$ 0.0007.

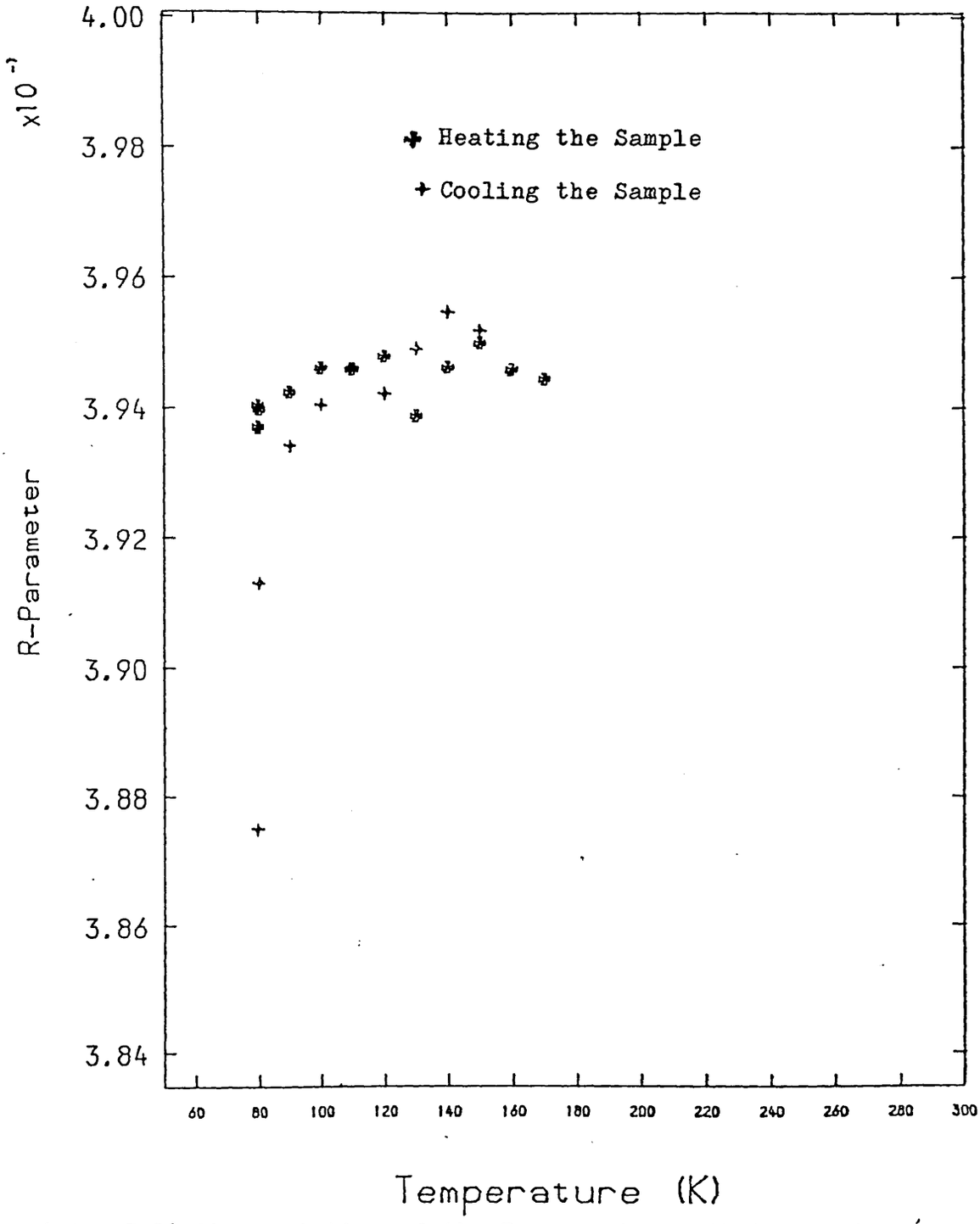

Fig(12.5.3.1) The variation of the R-parameter with temperature for pure helium condensed on grafoil. The standard deviation for R value is $\pm$(0.0006).

of oPs emission to increase. This may be due to an interaction of the helium gas with the grafoil surface (when the surface is cold enough) producin positronium which then escapes to form oPs. The possibilities of that a positronium bubbles or adsorption of the helium on the surface of grafoil are unrealistic because at such temperatures the helium is a vapour but not fluid. At temperature of 80 K and sufficiently high pressures, interaction between the gas is possible with positrons being trapped at surface of grafoil and then escape from the surface to form Ps as witnessed by the increase in F and decline in R. Although we know that adsorption of the light gases on the surface of metals is possible at high pressure and temperature but the possibility of occuring such an effect in our experiment is difficult to be concluded.

12.5.4-Line-shape analysis:

The line-shapes were again fitted by an inverted parabola and a Gaussian. The results are shown in figure(12.5.4.1) and (12.5.4.2). The parabola as we would expect, decreases as positronium is emmitted from the surface of grafoil. But the parabola and Gaussian widths remaine constant at mean values of 22.3 and 18.5 channels, respectively against temperature. The parabola width not changing in contrast to the oxygen runs, implies that no spin exchange processes occur converting three photon emission to two photon emission. However Pick-off of oPs is still possible. The goodness of the fit is shown by the chi-square, which was satisfactory at around one. The parabola percentage change shows that 8% positronium is emitted at (80 K).

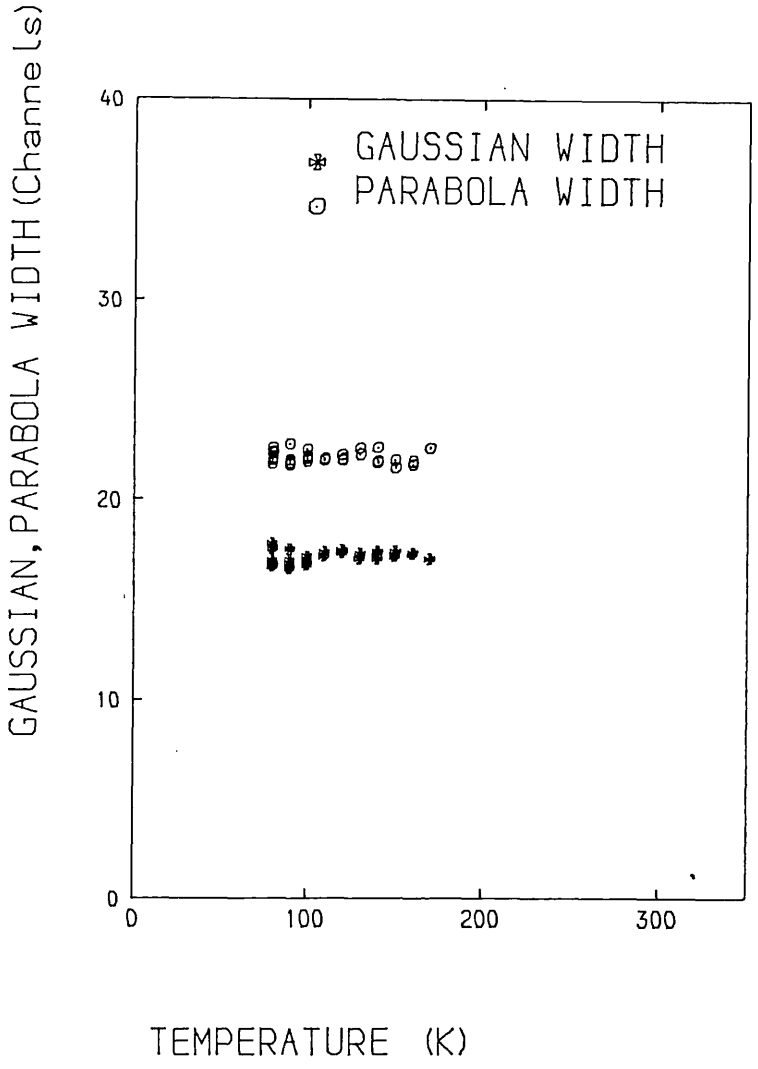

Fig(12.5.4.1) The variation of the Gaussian and parabolic width components with temperature for pure helium condensed on grafoil.

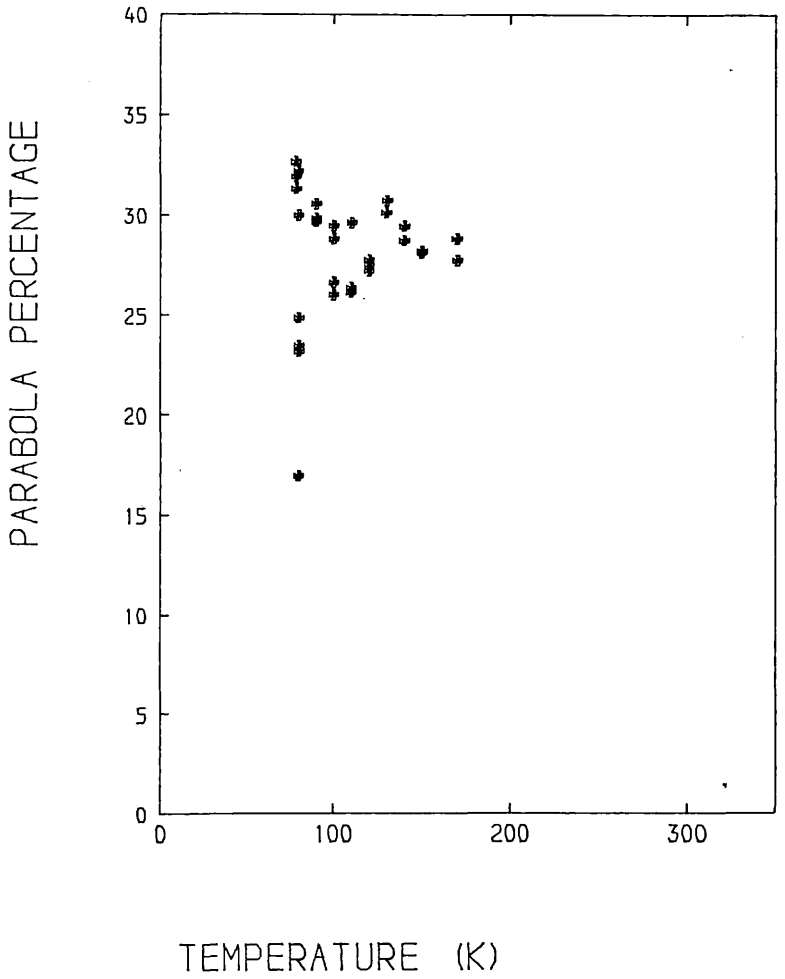

Fig(12.5.4.2) The temperature dependence of the parabolic percentage for positron annihilation in pure helium condensed on garfoil. The standard deviation is estimated to be $\pm$ 1.8%.

12.6-Conclusion:

From the results of the gas adsorption on the surface of grafoil experiments the following summary and conclusions are drawn:

1)Maximum positronium emission was observed at approximately monolayer coverages of nitrogen and of argon, fluid monolayers being created for both gases. The maximum in positronium emission was indicated by the R and F parameters. The position of temperature corresponding to the minimum value of R and maximum value of F changed as a function of pressure for the series of the nitrogen runs. Therefore the fluid monolayer builds up at temperatures associated with a certain pressures, leading to maximum Ps emission, which then decreases when a bilayer or multilayer builds up. The decline with increasing coverage is attributed to the increase in the density of the adsorbate on the surface disabling the positron or Ps from diffusing back to the surface. Thus in this instant annihilation occurs before escape from the surface. Another explanation is that of Ps bubbles in fluid gas (Canter et al 1977). The Ps bubbles exist from the balance between an outward pressure due to the zero point motion of the trapped particle and a shrinking force due to surface tension and external pressure. As a results the lifetime of Ps increases (the overlap between Ps atom and fluid atom wavefunction is less) at minimum in R. The decrease in R with bilayer build up is probably due to the increase in density of the monolayers and disabling the creation of Ps bubbles it means the overlap of Ps atom and fluid atom wavefuction becomes large and Ps annihilates faster.

2)From the variation in pea k position with pressure the binding energy of the nitrogen to the grafoil surface was found to be ϵ_0 =(1168±11) K which is in good agreement with that found by other groups.

3)Oxygen somehow is a special case for which the F-parameter shows a clear increase at the boiling point (at 90.1 K the transition from liquid to vapour). The increase is attributed to decreasing oxygen density leading to high parapositronium (Pps) emission. The Pps emission is the result of a spin exchange process in which the triplet state ($^3S_1$) is converted to a singlet state ($^1S_0$) which decays via two photons (sharp increase in the F-parameter).

4)This spin exchange process induces a narrow component in the spectrum photopeak. The observation of a sharp decrease in parabola width for oxygen is attributed to this narrow component (the result of the conversion of three photon to two photon decay.

5)The intensity change of about 28% in parabola percentage between the clean sample surface and that with oxygen adsorbed is assigned to percentage of positron interaction in oxygen molecules at the surface of the sample.

6)The decrease in the F-parameter in oxygen below 9o K is attributed to the exposure of the surface to liquid oxygen stop the Ps emission from the surface and positron diffusion back to the surface as also reported by Lynn et al (1983) for an aluminium surface at room temperature.

7)There was also an increase in Ps emission at low temperatures (80 K) for the case of grafoil with helium. However the experiment was incomplete and it would be necessary to modify a system to study the effect of helium on the surface of grafoil before driving further conclusion.

****

12.6-Conclusion:

From the results of the gas adsorption on the surface of grafoil experiments the following summary and conclusions are drawn:

1)Maximum positronium emission was observed at approximately monolayer coverages of nitrogen and of argon, fluid monolayers being created for both gases. The maximum in positronium emission was indicated by the R and F parameters. The position of temperature corresponding to the minimum value of R and maximum value of F changed as a function of pressure for the series of the nitrogene runs. Therefore the fluid monolayer builds up at temperatures associated with a certain pressures, leading to maximum Ps emission, which then decreases when bilayer or multilayer build up. The decline with increasing coverage is attributed to the increase in the density of the adsorbate on the surface disabling the positron or Ps from diffusing back to the surface. thus in this instant annihilation occurs before escape from the surface. Another explanation is that of a Ps bubbles in fluid gas (Canter et al 1977). The Ps bubbles exists from the balance between an outward pressure due to the zero point motion of the trapped particle and a shrinking force due to surface tension and external pressure. As a results the lifetime of Ps increases (the overlap between Ps atom and fluid atom wavefunction is less) at minimum in R. The decrease in R with bilayer build up is probably due to the increase in density of the monolayers and disabling the creation of Ps bubbles it means the overlap of Ps atom and fluid atom becomes large and Ps annihilate faster.

2)From the variation in peack position with pressure the binding energy of the nitrogen to the grafoil surface was found to be ϵ_0 =(1168±11) K which is in good agreement with that found by other groups.

3)Oxygen somehow is a special case for which the F-parameter shows a clear increase at the boiling point (at 90.1 K the transition from liquid to vapour). The increase is attributed to decreasing oxygen density leading to high parapositronium (Pps) emission. The Pps emission is the result of a spin exchange process in which the triplet state ($^3S_1$) is converted to a singlet state ($^1S_0$) which decays via two photons (sharp increase in the F-parameter).

4)This spin exchange process induces a narrow component in the spectrum photopeak. The observation of a sharp decrease in parabola width for oxygen is attributed to this narrow component (the result of the conversion of three photon to two photons decay.

5)The intensity change of about 28% in parabola percentage between the clean sample surface and that with oxygen adsorbed is assigned to percentage of positron interaction in oxygen molecules at the surface of the sample.

6)The decrease in the F-parameter in oxygen below 9o K is attributed to the exposure of the surface to liquid oxygen stop the Ps emission from the surface and positron diffusion back to the surface as also reported by Lynn et al (1983) for an aluminium surface at room temperature.

7)There was also an increase in Ps emission at low temperatures (80 K) for the case of grafoil with helium. However the experiment was incomplete and it would be necessary to modify a system to study the effect of helium on the surface of grafoil before driving further conclusion.

****

APPENDIX I

The first law of thermodynamic is

$$dE=dQ-\sum_m X_m dX_m$$

where E is enternal energy and q is external heat exchange in system and X_m denoted to pressure, volume, area, etc. From the Helmholtz free energy we can write

$$SdT+dF+TdS=dQ-\sum_m X_m dX_m$$

or

$$dF=-SdT-\sum_m X_m dX_m$$

here $X_m dX_m=PdV+VdP+\varphi dA+Ad\varphi$. The partial derivation of abve expression give

$$P=-(dF/dV)_{T,A} \quad \text{and} \quad \varphi=-(dF/dA)_{T,V}$$

where P is vapour pressure and V is volum, A is surfauce area and φ is films pressure on the surface.

In the real adsorption system the seperation between films and vapours are not exact, the assumptions are summerise as

a)The vapour volume relative to whole volume of system is so small in range of surface films.

b)The volume of the adsorption films is so small fraction of the whole system volume.

c)any distrotion or deformation on the substrate directly effected on the films. All the measuring must be measured in equilibrium state.

Consider on isolate adsorption system with total fixed energy E, volume V, adsorption area A, and number of the particle N. So the total entropy and energy are

$$E=E_s+E_a=\text{Constant}, \qquad S=S_s+S_a=\text{Constant}$$

where $S=S_s+S_a$ that films and vapour entropies. AT equilibrium system temperature of the substrate is equal with temperature of the adsorber $T_s=T_a$.

The maximum entropy exchange in the system is constant therefore $(dS_s/dE_s)_{N,V,A}=0$, and also $(dS_a/dE_a)_{N,V,A}=0$.

Now we consider the excahnge of particles between film and vapour at equilibrium the entropy is a maximum, so that $(dS/dN_f)_{E,V,A}=0$. Therefore the partial derivation of that is given

$$(dS_f/dN_f)_{E,N_s,A,N_v}+(dS/dN_f)_{E,N_s,A,N_v}-(dS/dN_f)_{E,N_f,A,N_s}$$

According to assumption (c) any changing on second term of expression above actually embedded in the first term, (dS/dN). Therefore by ignoring second term we have the fundamental equation of vapour-film equlibrium,

$$(dS_f/dN_f)_{E,N_s,A}=(dS_v/dN_f)_{E,N_s,A,N_v}$$

This equation involve with chemical potential of film and vapour. From previous formola for differentionls of E and F can be write

$$dE=T(dS_f+dS_v+dS_s)-\varphi\, dA-PdV+\mu_f dN_f+\mu_s dN_s+\mu_v dN_v$$

Then it can easily find out the chemical potential is partial derivations of the energies and entropies as

$$\mu_f=(dE_f/dN_f)_{S,A,N_v,N_s}=T(dS_f/dN_f)_{E,A,N_v,N_s}$$

$$\mu_s=(dE_s/dN_s)_{S,A,N_v,N_f}=T(dS_s/dN_s)_{E,A,N_f,N_v}$$

$$\mu_v=(dE_v/dN_v)_{S,A,N_s,N_f}=T(dS_v/dN_v)_{E,A,N_f,N_s}$$

The helmholtz and Gibbs free energies and also the enthalpy from the therodynamic laws for the arbitary system are

$$F=E-TS$$

$$G=F+\sum_m X_m dX_m$$

$$H=E+\sum_m X_m dX_m$$

By differentiating each state and substituting the dE we can write

$$dF=-SdT-\varphi\, dA-PdV+\sum_m X_m dX_m$$

$$dG=-SdT-Ad\varphi-VdP+\sum_m X_m dX_m$$

$$dH=TdS+Ad\varphi+VdP+\sum_m X_m dX_m$$

These are also proved that the chemical potential of the three states

related to partial differential function of Helmholtz, Gibbs, and ethalpy with respect to N_i, therefore can be write

$$\mu_f = (dF/dN_i)_{T,A,V,N_{i\neq j}} = (dG/dN_i)_{S,\varphi,A,N_{i\neq j}} = (dH/dN_i)_{T,\varphi,P,N_{i\neq j}}$$

Now by the assuming that the substrate has homogeneity surface, then in equilibrium stat $\mu_f = \mu_v$. Apart from substrate intraction if we assuming that the vapour behave like the ideal gas. The Helmholtz free energy of an ideal classical gas is given by

$$F_v = -N_v kTLn(e^{3/2} V/N_v \lambda^3)$$

where, $\lambda = h/(2\pi mkT)^{1/2}$ is thermal De Broglie wavelength. Simply it can carried out the entropy of the vapour, vapour pressure and chemical potential as

$$S_v = -(dF_v/dT)_{N_v,V} = N\ kLn(e^{5/2} V/N_v \lambda^3)$$

$$P = -(dF_v/dV)_{T,N_v} = N_v kT/V$$

$$\mu_v = (dF_v/dN_v)_{T,V} = -kTLn(V/N_v \lambda^3) = -kTLn(kT/P_v \lambda^3)$$

APPENDIX II

GRAFOIL AT HIGH VACUUM RUN#=33GHE 12/3/85
12/ 3/85
TIME NOW 16:49:38 SINCE START, 1:59:28
RUN#=33
DTC SET TO 6.206MV
DTC=6.208MV TEMP=399.97K TEMP REQ=400.0K
399.97

LIVE TIME	6717
PRESET LIVE TIME	0
REAL TIME	7200
PRESET REAL TIME	7200
ELAPSED TIME	0
CYCLE	0

CENTRE CHANNEL	INTEGRAL
3547	592263

3360	589	590	533	572	589
3365	576	598	540	559	572
3370	579	528	573	539	572
3375	591	580	541	583	539
3380	561	560	619	583	606
3385	592	555	583	579	552
3390	545	574	553	578	564
3395	607	559	559	582	599
3400	542	555	515	565	576
3405	591	574	586	584	569
3410	579	609	588	589	568
3415	566	575	554	553	573
3420	614	615	585	544	601
3425	576	563	583	601	543
3430	560	585	588	610	590
3435	632	626	615	639	665
3440	630	612	636	660	738
3445	711	769	870	999	1118
3450	1279	1553	1868	2195	2359
3455	2829	2985	3135	3303	3205
3460	3114	2831	2389	2106	1782
3465	1433	1250	1087	886	845
3470	714	725	639	586	595
3475	632	624	593	612	559
3480	596	623	639	602	573
3485	639	602	602	552	625
3490	629	566	624	585	556
3495	628	593	599	574	601
3500	579	614	603	542	614
3505	626	579	586	562	575
3510	595	595	616	590	619
3515	547	578	567	605	608

3520	626	595	594	614	570
3525	569	627	585	646	629
3530	661	651	647	578	620
3535	668	627	656	624	662
3540	644	697	641	637	670
3545	645	658	667	643	674
3550	667	703	680	702	734
3555	820	762	750	735	765
3560	848	846	836	839	921
3565	914	956	889	948	1079
3570	1142	1173	1217	1393	1430
3575	1547	1647	1839	2013	2160
3580	2343	2648	2988	3337	3847
3585	4212	4753	5198	5847	6395
3590	7070	7739	8630	9242	9850
3595	10641	11366	12058	12915	13524
3600	14021	14739	15346	15758	15996
3605	16353	16609	16781	16738	16473
3610	16307	16345	15813	15469	15000
3615	14184	13617	12990	12357	11594
3620	10723	10148	9464	8589	7795
3625	7193	6335	5758	5111	4624
3630	4063	3604	3076	2787	2488
3635	2184	1970	1737	1512	1320
3640	1307	1079	1021	1017	891
3645	833	838	749	747	643
3650	658	652	634	606	567
3655	600	538	585	560	534
3660	514	474	518	498	487
3665	516	447	463	443	463
3670	464	478	456	451	467
3675	423	450	431	467	434
3680	412	390	418	432	393
3685	447	427	406	449	445
3690	458	406	405	400	427
3695	421	396	407	390	405
3700	406	392	402	408	420
3705	433	370	398	380	373
3710	403	422	393	402	385

3

APPENDIX III

PROGRAM CURFIT

This program employes the NAG subroutine E04FCF (based and Haorwell routine) to make a function non-linear fit by least squares fitting method. The certain parameters are given as input including the data, and after minimization the ajustable parameters are given as output. After minimization complete the standard deviation of the output parameters also calculated by program.

```
POGRAM CURFIT
DIMENSION (VARIABLES) (the correct dimension must be given)
EXTERNAL FUNCTIONS
READING THE INPUT DATA
CALCULATING THE WEIGHT
CALL THE NAG E04FCF(X,Y,....)
CREATED A FILE FOR OUTPUT PARAMETERS
CALCULATED THE CHI-SQUARED
STANDARD DEVIATION CALCULATION
STOP
END
```

THE FUNCTION REQUIRED

The user has to supply a FORTRAN function to calculated the y value on the curve for given x. This should have the real function.

```
REAL FUNCTION VALUE(N,PAR,X)
DIMENSION PAR(N) n is number of the variable parameters
VALUE= NON-LINEAR FUNCTION USED
RETURN
END
```

The input data are 1) N number of the variable parameters 2) M the number of the data points 3) the initial guess for parameters 4)

variable x, y, and weight for each data points. After successful convergence it should print IFAIL=0 and then the gives the values of the parameters after minimization with standard deviation erorr.

The function value for analysis of spectrum of Gaussian and inverted parabola convoluted with resolution function is

```
      REAL FUNCTION VALUE(N,PAR,X)
      DIMENSION PAR(N),R(200),C(200)
C     R is the response functio array
C     C is the are of spectrum data points
      DATA IN (for resolution function  Sr)
      I=IFIX(X+.05)
      IF(MC.EQ.1)GO TO 888
    2 S=0
      DO 6 K=1,M
      J=IBAR+I-K [IBAR is centroid of the resolution function]
      IF(J.LT.1)J=1
      IF(J.GT.M)J=M
    6 S=S+R(J)*C(K)
      COUNTS=S+BACKGROUND [polynomial or erorr function]
      MC=MC+1
      GO TO 999
  888 DO 4 J=1,M
      T=PAR(1)-FLOAT(J) [PAR(1) is peak center]
      GW=T*T/PAR(3)/PAR(3) [PAR(3) is Gaussian width]
      PW=T*T/PAR(5)/PAR(5) [PAR(5) is Parabola width]
      PARA=0
      GUASS=0
      IF(GW.LT.200)GUASS=PARA(2)*EXP(-GW)  [PAR(2)  is  Gaussian
hieght]
```

```
      IF(PW.LE.1.)PARA=PARA(4)*[1.-PW] [PAR(4) is Parabola hieght]
    4 C(J)=GUASS+PARA
      GO TO 2
  999 VALUE=COUNTS
      RETURN
      END
```

The extra Gaussian or any other function can be added to this preogram to minimise.

****

PHILOSOPHICAL MAGAZINE A, 1985, VOL. 52, NO. 4, 431–439

Positron annihilation study of lattice defects and phase transitions in tin

By P. C. RICE-EVANS, M. MOUSSAVI-MADANI, F. A. R. EL KHANGI and K. U. RAO

Department of Physics, Bedford and Royal Holloway Colleges (University of London), Regent's Park, London NW1 4NS, England

[*Received 2 January 1985 and accepted 15 March 1985*]

ABSTRACT

Positron annihilation in tin has been studied as a function of temperature. The Doppler broadening of the 511 keV line has been measured with a germanium photon detector system. For annealed white tin the positron parameters show only a small increase on approach to melting. For the tin sample plastically deformed at 77 K, the grey–white phase transitions are strikingly manifested at 240 and 300 K.

§ 1. INTRODUCTION

This study concerns positron annihilation in tin. Measurements on annealed tin are reported which shed light on the creation of lattice vacancies as temperatures approach the melting point, and measurements on plastically deformed tin are reported which illuminate the nature of the phase transitions from white to grey to white tin as the temperature is varied.

It is well known that the Doppler broadening of the 511 keV photon line arising from positron annihilation is a sensitive indicator of characteristics of the site of a positron at the instant of its annihilation (West 1979, Brandt and Dupasquier 1983). The technique reveals information about the momentum distributions of electrons selected for annihilation, which in turn can yield information on the nature of the lattice, and on the existence or creation of defects such as vacancies, dislocations and voids. Parameters such as the vacancy formation enthalpies and entropies may be determined with some confidence.

§ 2. DOPPLER BROADENING METHOD

The shape of the 511 keV photopeak measured with a high-resolution germanium detector can indicate the relative proportions of conduction and core electrons that participate in the annihilations. The geometry of a typical experiment is to sandwich a carrier-free positron-emitting radioactive source such as ^{22}NaCl between two specimen metal plates. The energetic positrons are rapidly thermalized within the metal in about 10^{-12} s, which is short compared with the typical positron lifetime of about 10^{-10} s. A consequence is that, compared with the electron velocities, the positron has a negligible speed; hence any Doppler broadening arising from the motion of the centre-of-mass of the e^+e^- pair is mainly attributable to the electron velocity.

Figure 1 shows the line shapes corresponding to positron annihilation in deformed tin at two different temperatures, together with the line shape for the monochromatic 514 keV gamma ray from ^{85}Sr which indicates the intrinsic resolution of the system. The Doppler broadening of the line is easily visible and it can be reasonably expressed

Fig. 1

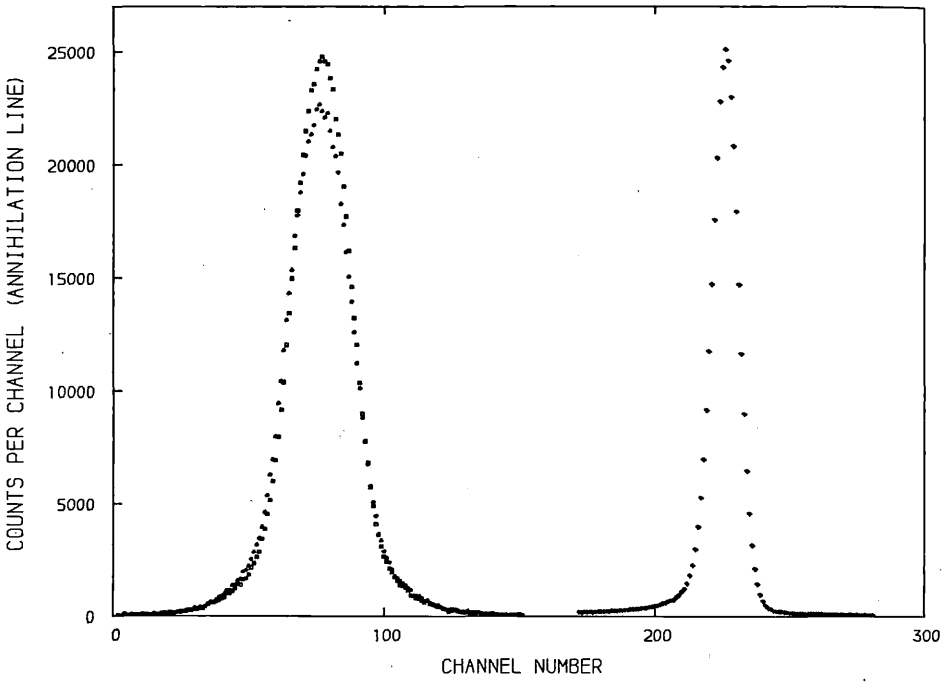

Examples of line shapes. To the right is the response of the photon detector to a monochromatic gamma ray at 514 keV. To the left are two Doppler-broadened 511 keV lines for white tin and grey tin.

as the sum of two components, a parabolic curve representing annihilations with free conduction electrons, and a Gaussian representing essentially annihilations with bound core electrons in the metal. The observed curve is given by these components convoluted with the resolution function (Rice-Evans, Chaglar and El Khangi 1981)

$$f(x)=A\int_{-\infty}^{+\infty}\exp[-(x'-\bar{x})^2/2\sigma_g^2]R(x-x')\,dx'$$

$$+B\int_{-\sigma_p\sqrt{2}}^{\sigma_p\sqrt{2}}[1-(x'-\bar{x})^2/2\sigma_p^2]R(x-x')\,dx.$$

The simplest linear parameter which can be used to characterize changes in the line shape is the line-height parameter F (some physicists use S), the ratio of the counts in a selected band of channels in the centre of the line to the counts in the whole line. Thus, an increase in F indicates a narrowing of the line, which usually signifies an increase in the proportion of the parabolic component.

In the present experiments the annealed sample consisted of two $15\times15\times1\,\text{mm}^3$ pieces of 99·999% pure tin, supplied by Metals Research Ltd., which were spark cut and then etched in a mixture of nitric acid and alcohol. After direct deposition of the source within a central circle of diameter 3 mm, and composition into a sandwich, the sample was annealed at 450 K in a vacuum of 3×10^{-6} mbar for 15 hours and allowed to cool slowly to room temperature over 8 hours. It was then transferred to a vacuum cryostat, the temperature of which could be accurately controlled in the range 4·2–430 K. The

higher temperature range (300–500 K) was studied by placing the sample in a vacuum furnace.

The plastically deformed specimen was two $10 \times 10 \times 2\,\text{mm}^3$ pieces of the same tin. After production of the radioactive sandwich, the whole sample was placed in a bath of liquid nitrogen which lay between the jaws of a hydraulic press. The application of 10 tons pressure resulted in a reduction of sample thickness at 77 K from 2 mm to 1 mm. The sample was immediately transferred to the cryostat at 77 K during which operation the temperature was monitored and seen not to rise above 90 K.

§ 3. Positron trapping by lattice defects

Defects such as vacancies appear as attractive potential wells that trap slow positrons diffusing through a lattice. Positrons annihilating in traps experience an electron environment that differs from the bulk lattice and hence a different F parameter signature is likely to result: This has been exploited in the so-called trapping model, on which several excellent reviews have been written (see for example, West 1979, Brandt and Dupasquier 1983). The model has been especially successful in monitoring the creation of vacancies as the sample temperature is raised. Furthermore, the dimensions and depths of the wells vary according to the type of defect (vacancy, dislocation, void, etc.) and thus in many cases the F parameter may distinguish them.

The concentration of thermally created vacancies as the temperature of the crystal is raised is given by

$$C_v = \exp(S_v/k)\exp(-H_v/kT),$$

where S_v and H_v are the entropy and enthalpy of vacancy formation.

The parameter F may indicate linearly the proportion of positrons trapped

$$F = F_f P_f + F_v P_v,$$

where F_f corresponds to $P_f = 1$, that is 100% of positrons annihilating in the free state, and F_v corresponds to P_v, that is, 100% trapping; $P_f + P_v = 1$. F_v is expected to exceed F_f because positrons trapped in vacancies will be more likely to annihilate with conduction electrons.

It follows (Rice-Evans *et al.* 1978 that

$$\frac{F - F_f}{F_v - F} = (\sigma\tau_f)\exp(S_v/kT)\exp(-H_v/kT),$$

where σ is the trapping rate, and τ_f is the lifetime of the free positron in the lattice. This expression may be fitted to data to yield values of H_v and S_v.

In practice it is observed that in the temperature region below the onset of vacancy production, the F parameter exhibits an approximately linear 'prevacancy rise'. This is naturally associated with the thermal expansion of the lattice; however, it remains to be properly explained (see, for example, Stott and West 1978 on lattice vibrations; Rice-Evans, Chaglar, Khangi and Berry 1981 on orientational effects; and Smedskjaer 1983 on positron detrapping). In any event, it is customary to write $F_f = F_f^\circ(1 + \beta T)$ and extrapolate it into the vacancy region; in other words, to fit the data to

$$F = \frac{F_f^\circ(1 + \beta T) + F_v A \exp(-H_v/kT)}{1 + A\exp(-H_v/kT)}.$$

The positron annihilation signature has also been exploited in elucidating the nature of annealing processes as a function of rising temperature, for example the migration of vacancies to form clusters in quenched samples (West 1979, Nieminen and Manninen 1979). Also, studies on a variety of plastically deformed metals in the temperature range 4–400 K have revealed a number of distinctive features associated with altering defect distributions (Rice-Evans *et al.* 1978 b).

The wavefunction of a positron trapped in a well is localized and the uncertainty principle therefore leads to some zero-point motion. This motion causes an extra Doppler broadening of the shape of the 511 keV photopeak. Jackman, Schulte, Campbell, Lichtenberger, MacKenzie and Wormald (1974) have shown that trapping in deep wells can be accommodated by fitting with an extra Gaussian broadening term, and this has also been achieved by Rice-Evans *et al.* (1981) with cadmium.

§4. Phase transitions in tin

The first scientific report of a low-temperature phase of tin was given by Erdman in 1851. For more than a century, extensive studies were conducted on the transformations leading to this non-metallic grey (α phase) tin from the commonly known white (β phase) tin, and these have been summarized by Busch and Kern (1960). The α phase, which is stable below 286·4 K, forms spontaneously if metallic β tin is kept below this temperature for sufficiently long periods (days to years). The transformation is accompanied by a 27% increase in volume, and a piece of white tin becomes a powdery mass of grey tin. Typically, after a certain incubation period, the transformation starts at one or several points on or near the surface and spreads out spherically until the whole piece is transformed, although there are indications that a small percentage remains untransformed (Burgers and Groen 1957). Grey tin converts back to white tin in a shorter time if it rises above the equilibrium temperature. Alpha tin has a diamond structure with a density of 5·76 g cm^{-3} and the β phase has a body-centred tetragonal structure with a density of 7·29 g cm^{-3}.

It has been accepted (Busch and Kern 1960) that the transition from β to α requires two processes: an incubation period in which α nuclei are formed, followed by a period of spherical growth at a linear rate. Various factors influence the processes, for example impurities or previous treatments such as cold-working and annealing. The atomic mechanism for the β to α transition has not been established, but some observations indicate that the α to β process is of the diffusionless or martensitic type.

Traditionally, quantitative information on the transformations has been obtained (*a*) by dilatometric measurements on the change of volume, and (*b*) by direct observation of the motion of the phase boundary; but recently more modern techniques have been used to study the phases, such as X-ray crystallography (Burgers and Groen 1957) and Mössbauer isomeric shifts (Nikolaev, Mar'in, Panayishkin and Pavlynkov 1973). The phases of tin have also been studied with annihilating positrons. Badoux, Heinrich and Kallmeyer (1967) used the angular correlation method to establish the different momentum distributions of the electron participating in the annihilations for α and β samples and Puff, Mascher, Kindl and Sormann (1983) used positron lifetime measurements to indicate that the β to α transformation occurred at 230 K.

Fig. 2

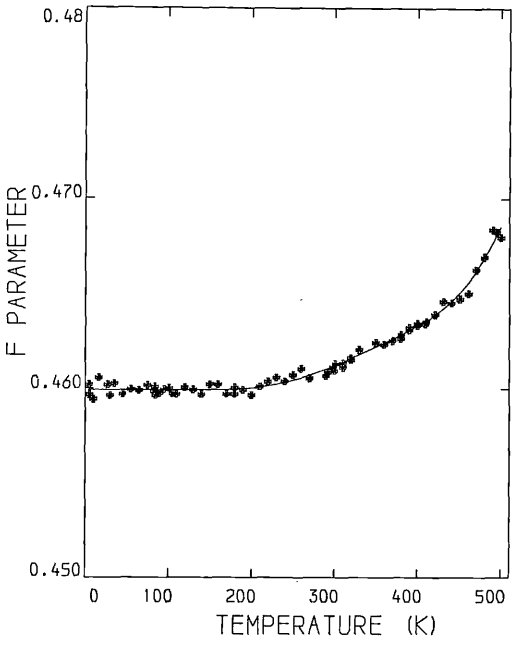

The variation of the F parameter as a function of temperature for annealed tin, showing only a modest rise at high temperatures resulting from the creation of vacancies.

§ 5. Results and discussion

5.1. *Results for annealed tin*

Figure 2 shows the curve of F parameter versus temperature plotted over the range 4·2 K to the melting point. Each point corresponds to a run of 2 hours with intervals of 30 min for adjusting and stabilizing the temperature.

The curve appears flat up to 200 K, then rises apparently linearly between 200 and 400 K with what is presumably the customary prevacancy rise. Thereafter the curve rises more steeply, corresponding, one assumes, to the trapping of positrons in an increasing concentration of thermally produced point vacancies. In contrast with many other metals, there is little evidence of a saturation pattern (i.e. a plateau) as the melting point at 509 K is approached.

The curve has been fitted with the expressions outlined in § 3. When the prevacancy rise is fitted with a straight line from 200 K upwards and extrapolated into the vacancy region (>450 K) the value obtained for the vacancy formation enthalpy (H_v) is $0{\cdot}56 \pm 0{\cdot}01$ eV. The slope (β) of the prevacancy rise is $(28{\cdot}0 \pm 4) \times 10^{-6}$. When the analysis includes self-trapping the value of H_v reduces to $0{\cdot}52 \pm 0{\cdot}02$ eV. It is estimated that the proportions of positrons trapped at 500 K are 67% and 63% for the two cases, respectively (El Khangi 1980).

5.2. *Results for deformed tin*

Figure 3 shows the line-height parameter (F) plotted as a function of temperature, the sequence of measurements being indicated alphabetically. The white tin sample was compressed at 77 K and the 2 hour runs started, as indicated at A. No change is seen for

Fig. 3

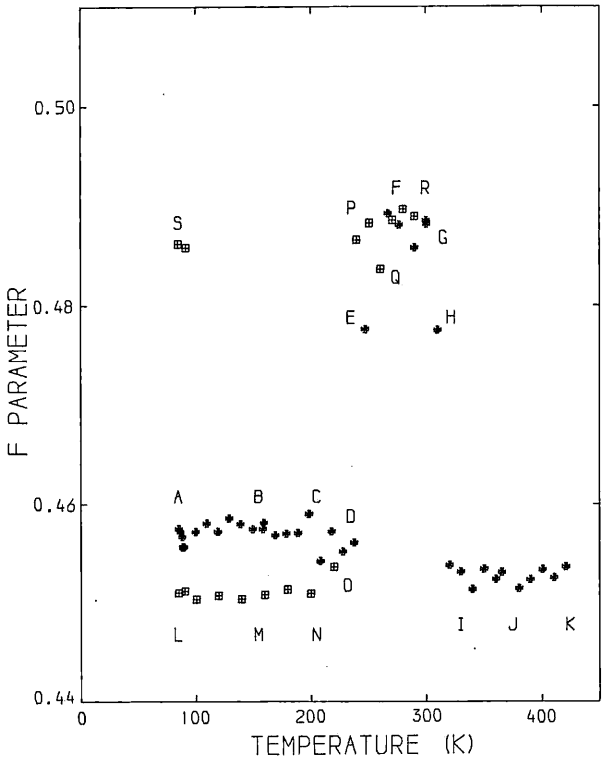

The variation of the F parameter as a function of temperature for tin plastically deformed at 77 K. The measurements are indicated sequentially A to S. The high values ($\approx$0·48) indicate grey tin; the low values ($\approx$0·46) correspond to white tin.

A–B–C–D, but after 235 K F suddenly increases (D–E–F). This demonstrates the rapid transition from white to grey tin which corresponds to the reduced metallic density. The sample remains grey until 300 K (F) when it quickly reverts (G–H–I) to white tin. The sample was further raised in temperature (I–J–K) during which a thorough annealing must have occurred, the melting temperature being 505 K.

The sample was reduced again to 77 K and a similar sequence of measurement started. It may be seen in the figure that the F values for annealed white tin (L–M–N–O) are significantly lower than (A–B–C). This can be ascribed to the high concentration of defects in the early life of the sample. These defects, introduced by the compression, act as traps for the positrons and produce higher values in F; but just as tin is unusual in yielding small values of F_v for saturation trapping in vacancies at high temperatures (§ 3), so too the change in F corresponding to high concentrations of defects at low temperatures is also small, say, compared with cadmium (Rice-Evans *et al.* 1978).

The white tin transforms to grey once more (O–P) at about 230 K and remains so until 290 K (P–Q–R). The experiment was concluded at 290 K (R) by lowering the temperature of the sample to 80 K, at which temperature two more runs were taken (S). The high F values at S indicate that the sample remained in the grey tin state.

Finally, the sample was extracted from the cryostat and the metal was discovered to have been reduced to a fine powder.

5.3. *Defects in tin*

In his model of the positron trapping process at vacancies, applying the Schrödinger equation to an effective potential well, Hodges (1970) did not discern any anomalous results for positrons in tin. Whereas he found a trapping potential of 5·2 eV and a positron binding energy of 1·4 eV for traps in tin, he found virtually the same values (4·9 and 1·4 eV) for indium which is known to exhibit a large trapping effect (see, for example, Rice-Evans, Hlaing and Chaglar 1977).

Both indium and white tin have a body-centred tetragonal structure and their valences are 3 and 4, respectively. In his discussion of the curious case of tin, Seeger (1973) points out that although the higher valence of β-Sn should favour positron trapping, three other features militate against it. The radius of the Sn^{4+} ion is 0·71Å (Pauling 1968), which is small compared with half the interatomic distances (1·4 Å and 1·51Å). Thus, in spite of its $4d^{10}$ core, β-Sn must be considered as a metal with narrow cores, and hence likely to have shallower traps. Furthermore, inward relaxation of the atoms surrounding a vacancy may seriously reduce the trapping probability at such a site. The value of the tracer self-diffusion coefficient of $5 \times 10^{-11}\,cm^2\,s^{-1}$ (Nachtrieb and Coston 1965) leads to a very low value of 0·25 for the monovacancy formation volume in tin (cf. 0·45 in indium, 0·8 in copper), and this should result in a smaller potential well to attract the positrons. Finally, Seeger contrasts the above self-diffusion coefficient for tin with typical values of 10^{-8}–$10^{-7}\,cm^2\,s^{-1}$ for most other metals and, assuming that the mobility of vacancies near the melting point of tin is similar to other metals, he estimates that the melting point vacancy concentration in β-Sn is three orders of magnitude less than in many other metals; tin melts too early, judged by the equilibrium concentration of vacancies.

The values of F for deformed white tin at low temperatures (fig. 3) (A–B–C) are 3·5% higher than the values for samples when annealed (L–M–N). This may be compared with the rise of 0·8% when the annealed specimen was taken to high temperatures (fig 1). In cadmium, where saturation trapping is seen at high temperatures, the equivalent figures are 6·6% and 7·0%, respectively (Rice-Evans *et al.* 1978). The present authors are not aware of any arguments that would link a low concentration of vacancies at the highest temperatures with a low frozen defect concentration in deformed states at low temperatures; one might imagine them to be independent of each other. In this event one would expect ΔF to be much greater in the case of frozen traps. Thus we do not find the arguments from positron annihilation for a low C_v on approach to the melting point conclusive.

However, evidence of another sort comes from the comparison of macroscopic thermal expansion with X-ray measurements of lattice expansion. Balzer and Sigvaldason (1979) found them indistinguishable in tin, from which they concluded that the vacancy concentration at the melting temperature was low: less than 3×10^{-5}. Nevertheless the result might have other explanations, such as the possibility of displaced atoms becoming interstitials.

The findings for $\bar{H}_v$ (§ 5.1) agree reasonably with results from other laboratories: 0·57 eV (MacKenzie and Fabian 1980); 0·51 eV (Dedoussis, Charalambous and Chardalas 1977); 0·58 eV (Puff *et al.* 1983); 0·51 eV (Shah and Catz 1984); 0·54 eV (Segers, Dorikens-Vanpraet and Dorikens 1980). The curve concurs with the results of MacKenzie and Fabian who observed that the ratio of the threshold temperature for trapping by vacancies (450 K) to the temperature of melting is 0·88, in contrast with the value of 0·63 found for most close-packed metals.

Puff *et al.* (1983), on the basis of lifetime measurements, believed they could

distinguish two regions in the prevacancy rise; the first, 230–370 K, being attributable to thermal expansion and the second, 380–450 K, which is steeper, corresponding to a temporary localization of positrons in dilation zones of the lattice. The present results do not indicate this distinction of two regions, and in accord with our previous findings (see, for example, Rice-Evans *et al.* 1981) in the present authors' opinion the major theoretical question of the origin of the prevacancy rise remains unresolved.

5.4. *Discussion on phase transitions in tin*

Whereas the annealed sample showed no signs of the α–β phase transition as the temperatures were varied, it is clear from the results on the deformed specimen that a high concentration of defects promotes the transitions. Assuming the overall effect corresponds to a 100% transition, it is seen that approximately 85% of the white tin is transformed to grey in 2 hours (O–P), the F parameter being a linear indicator. Similarly the grey to white transition (G–H–I) is seen to occur in 4·5 hours, with 61% transforming in about 2 hours (H–I). Thus, the positron annihilation method can indicate the phase transition rates and transition temperatures for tin rather accurately, and possibly uniquely. The method could be further refined by conducting a series of measurements with various degrees of plastic deformation and correlating defect concentrations with rates of phase transition.

Acknowledgments

It is a pleasure to thank Dr J. H. Evans of AERE, Harwell, and Dr Ian Butler of the Tin Research Institute for valuable discussions; and the Science and Engineering Research Council for its financial support.

Note added in proof

W. Puff, P. Mascher, P. Kindl and H. Sormann reported observations in the phase transitions in tin at the Seventh International Conference on Positron Annihilation in Delhi, January 1985. Their results are to be published.

References

Badoux, F., Heinrich, F., and Kallmeyer, G., 1967, *Helv. phys. Acta*, **40,** 815.
Balzer, R., and Sigvaldason, H., 1979, *Phy. Stat. Sol.* (b), **92,** 143.
Brandt, E., and Dupasquier, A., (editors), 1983, *Positron Solid State Physics* (*Fermi School, Varenna*) (Amsterdam: North-Holland).
Burgers, W. G., and Groen, L. J., 1957, *Discuss. Faraday Soc.*, **23,** 183.
Busch, G. A., and Kern, R., 1960, *Solid St. Phys.*, **11,** 1.
Dedoussis, S., Charalambous, S., and Chardalas, M., 1977, *Phys. Lett.* A, 359.
El Khangi, F. A. R., 1980, Ph.D Thesis, University of London.
Erdmann, O. L., 1851, *J. prakt. Chem.*, **52,** 428.
Hodges, C. H., 1970, *Phys. Rev., Lett.*, **25,** 284.
Jackman, T. E., Schulte, C. W., Campbell, J. L., Lichtenberger, P. C., MacKenzie, I. K., and Wormald, M. R., 1974, *J. Phys.* F, **4,** L1.
MacKenzie, I. K., and Fabian, J., 1980, *Can. J. Phys.*, **58,** 1635.
Nachtrieb, N. H., and Coston, C., 1965, *Physics of Solids at High Pressure*, edited by C. T. Tomizuko and R. M. Emrick (Academic Press: New York), pp. 336–48.
Nieminen, R. M., and Manninen, M. J., 1979, *Positrons in Solids*, edited by P. Hautojärvi (Berlin: Springer-Verlag) pp. 145–196.
Nikolaev, I. N., Mar'in, V. P., Panyishkin, V. N., and Pavlynkov, L. S., 1973, *Sov. Phys. solid St.*, **14,** 2022.
Pauling, L., 1968, *Die Natur der Chemischen Bindung*, Vol. 3 (Weinheim/Bergstrasse: Verlag Chemie), p. 479.

PUFF, W., MASCHER, P., KINDL, P., and SORMANN, H., 1983, *Appl. Phys.* A, **32,** 183.
RICE-EVANS, P., CHAGLER, I., EL KHANGI, F. A. R., 1978 a, *Phil. Mag.*, **38,** 543; 1978 b, *Phys. Rev. Lett.*, **40,** 716; 1981, *Phys. Lett.* A, **81,** 480.
RICE-EVANS, P., CHAGLAR, I., EL KHANGI, F. A. R., and BERRY, A. A., 1981, *Phys. Rev. Lett.*, **47,** 271.
RICE-EVANS, P., HLAING, T., and CHAGLER, I., 1977, *Phys. Lett*, A, **60,** 368.
SEEGER, A., 1973, *J. Phys.* F, **3,** 248.
SEGERS, D., DORIKENS-VANPRAET, L., and DORIKINS, M., 1980, *Phys. Stat. Sol.* (a), **59,** 543.
SHAH, N., and CATZ, A. L., 1984, *Phys. Rev.* B, **30,** 2498.
SMEDSKJAER, L. C., 1983, *Positron Solid-State Physics*, edited by W. Brandt and A. Dupasquier (Amsterdam: North Holland) pp. 597–608.
STOTT, M. J., and WEST, R. N., 1978, *J. Phys.* F, **8,** 635.
WEST, R. N., 1979, *Positrons in Solids*, edited by P. Hautojärvi (Berlin: Springer-Verlag), pp. 89–145.

POSITRON ANNIHILATION
edited by P. C. Jain, R. M. Singru & K. P. Gopinathan

SEARCH FOR A MONOLAYER SURFACE OF OXYGEN ON EXFOLIATED GRAPHITE AT LOW TEMPERATURES

P.C. Rice-Evans, M. Moussavi-Madani, K.U. Rao and B.P. Cowan

Department of Physics, Bedford College,
Regent's Park, London NW1 4NS, England.

The results are presented of a pilot study devised to demonstrate the growth of a monolayer surface of oxygen due to van der Waals forces. Exfoliation of graphite involves the formation of intercalation complexes within layer-structured crystals, and subsequent heating which explodes the layers apart. It forms a uniform substrate with a large area/volume ratio [9.1 x 10^6 m^2/m^3].

A standard sandwich sample containing $^{22}NaCl$ was prepared and placed in a cryostat and the annihilation radiation studied with the Bedford Doppler spectrometer. An orthodox graph of the line-height parameter was obtained with temperature when the sample chamber was evacuated. The introduction of oxygen allows the formation of a monolayer on the substrate at appropriate low temperatures, and this is clearly indicated with the line-height values. Further line-shape analysis suggests the formation of positronium at the monolayer, although some features remain unexplained.

Positrons have been valuable probes in Solid State Physics for many years. They have enabled important advances to be made in our knowledge of the bulk properties of solids including Fermi surface studies and in the investigation of lattice-defects such as vacancies, voids, dislocations (Hautojärvi, 1979) etc. Recently the techniques of positron annihilation have been extended to surfaces with the development of beams of low energy positrons, and rich pastures remain to be grazed (Brandt and Dupasquier, 1983).

However, low energy positron beams require high vacuum, usually ultra high vacuum. This fact militates against some types of surface investigation. In cases where the surface condition is in equilibrium with gas at a relatively high pressure a beam of positrons with energies of the order of 1 eV could not easily be transported to the surface.

In this paper we report initial work on a system which allows surfaces to be studied, without the use of a beam. We have exploited the special properties of exfoliated graphite (known as grafoil, commercially available from Union Carbide) namely a huge surface area, in the expectation that a large proportion of positrons may be induced to interact with a monolayer surface of oxygen laid down at low temperature.

Exfoliation of graphite involves the formation of intercalation complexes within layer-structured crystals, and subsequent heating which explodes the layers apart. It forms a uniform substrate with a large area/volume ratio of 9.1 x 10^6 m^2/m^3. Its use is an extension of the idea of using powder samples as a means of enhancing the area/volume ratio.

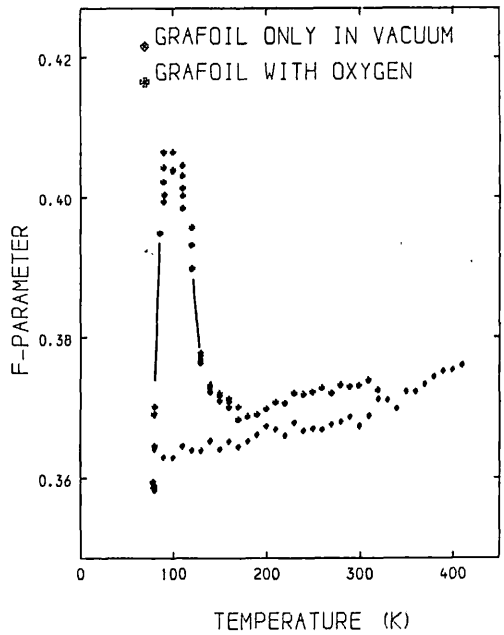

Fig.1. Variation of the line-height parameter F, as a function of temperature, for grafoil in vacuum and in oxygen.

A conventional sandwich sample containing $^{22}NaCl$ was prepared. Because of the low density (0.94 gm cm^{-3}) of grafoil the source

was deposited directly at the centre of a stack of 12 pieces of grafoil, each 1 x 1 x 0.07 cm^3, the number being determined by the need to stop all the positrons. After preparation the sample was transferred to a cryostat capable of maintaining controlled temperatures in the range 77-430K and the annihilation radiation studied with the Bedford photon spectrometer (Rice-Evans et al, 1978). Shimotomai et al (1983) have already studied Doppler effects in pure graphite as a function of crystal orientation.

For the preliminary analysis, we have employed the usual Doppler line-height parameter, F, defined in our case as the contents of the central 15 channels in the 511 keV peak normalised to the total area of the peak. It is assumed that the positrons will rapidly thermalise in the carbon, and the Doppler-broadening will be a consequence of the motion of the annihilating electron. Figure 1 shows the response of the annihilation line to varying sample temperatures. For graphite in high vacuum of about 10^{-6} Torr, the points display a not unexpected gentle rise in temperature, that is commonly seen with many materials and often associated with thermal expansion and other prevacancy effects.

The graph also shows the effects of introducing oxygen into the sample chamber. The procedure adopted was to insert the

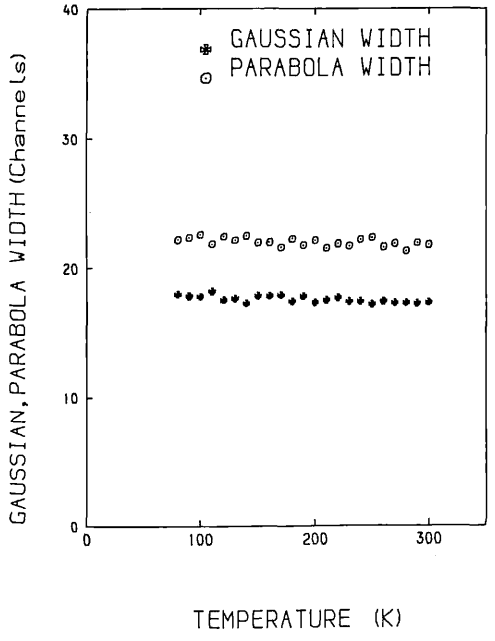

Fig.2. Results of analysis of annihilation peak for grafoil only.

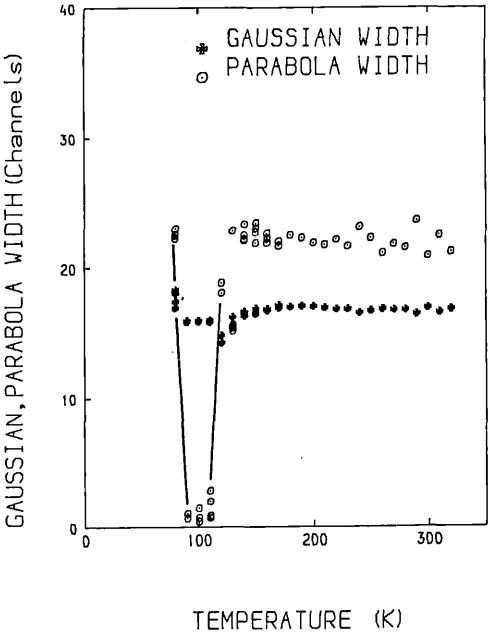

Fig.3. Results of analysis of annihilation peak for grafoil in the presence of oxygen.

oxygen at room temperature; after which the cryostat was cooled, so that the wall of the sample chamber itself was reduced to 77K by contact with liquid nitrogen. The effect of this was to reduce the oxygen pressure to 160 Torr, the expected equilibrium vapour pressure for oxygen at 77K and it remained constant throughout the experiment. In the graph, for sample temperatures above 160K, it is seen that the F parameter values for oxygen lie slightly above the values for carbon indicating a fraction of positrons annihilating in the oxygen gas between the graphite layers.

As the temperature decreases we expect physisorption of the gas to commence, initially with an increasing monolayer coverage (Dash, 1975). We are not certain at what temperature bilayers and more could be laid down, but below the boiling point of oxygen (90.1K) we assume that the crevices within the grafoil will be completely filled with liquid oxygen.

In Fig.1 we see that below 160K, with oxygen present, the value of F rises sharply, but further reduction below 90K causes a sharp diminution of F. It seems sensible to associate the rise with the physisorption of a monolayer of oxygen.

To examine the origin of the magnified value of F between 90 and 150K we analysed the

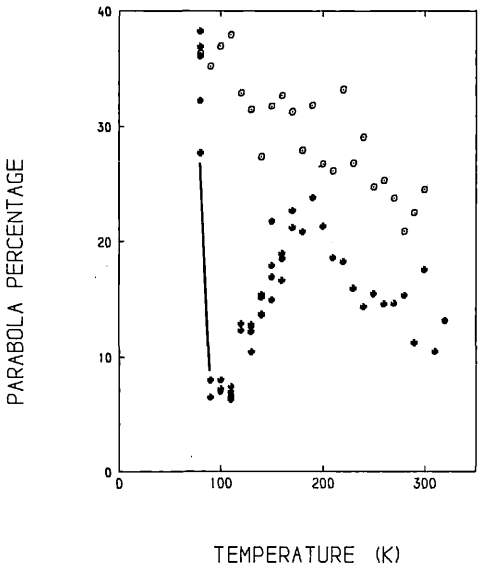

Fig.4. Results of analysis: open circles refer to grafoil only, stars to grafoil in presence of oxygen.

annihilation peaks into a parabolic and a Gaussian component (Rice-Evans et al, 1981). This relies on convoluting the intrinsic resolution (R) of the system determined with the ^{85}Sr gamma line at 514 keV and fitting with the expression

$$f(x) = A \int_{-\infty}^{+\infty} \exp[-(x'-\bar{x})^2/2\sigma_g]R(x-x')dx' + B \int_{-\sigma_p\sqrt{2}}^{\sigma_p\sqrt{2}} [1-(x'-\bar{x})^2/2\sigma_p]R(x-x')dx'.$$

Figs. 2, 3 and 4 show the results of this analysis. In Fig.2 one finds rather steady values for the Gaussian and parabolic widths throughout the temperature range for grafoil in vacuum. The usual interpretation for metals is that the parabolic component corresponds to annihilation with conduction electrons and the Gaussian to core electrons. In graphite there is one free electron per carbon atom [Ganguli and Krishnan, 1940]. Normal to the basal plane, and in the direction of our detected photons, the effective mass of the electrons is large and one therefore cannot justify theoretically the use of a parabola. For our purposes it may be that any curve would actually suffice - and a parabola is convenient.

Below 130K, in the presence of oxygen, one sees a sharp reduction in the width of the parabola to a mere couple of channels, while the Gaussian width remains unaltered. This narrow component we suggest indicates preferential formation of positronium at the monolayer surface. Fig.4 shows that the intensity (6-7%) of this positronium peak at 100K not negligible. Below 90K, the narrow component disappears and the fittings indicate a return to the wider parabola. From this we conclude that the formation of positronium is inhibited either by relatively thick adsorbed oxygen layers or by the total elimination of empty space between the graphite surfaces. The fits are all reasonable with reduced χ^2/ν between 0.9 and 1.3.

These studies complement those of Lyn and Lutz (1980, 1983) who observed positronium fractions emitted from aluminium surfaces, after exposure to various levels of oxygen at 300K, using a low energy positron beam. They detected ortho positronium by observing the 3-photon region of the spectrum. Our results below 90K - i.e. the disappearance of the positronium - coincide with Lyn's finding that the positronium fraction declines with large oxygen exposures. Nevertheless, in view of several unexplained features, our conclusions must be only tentative at this stage, and obviously further work is called for.

Acknowledgement

We wish to thank the Science and Engineering Research Council for their support.

References

1. P.Hautojarvi (Ed), Positrons in Solids, Topics in Current Phys. 12, (Springer, Heidelberg, 1979).
2. W. Brandt and A. Dupasquier (Eds), Positron Solid State Physics (North-Holland, Amsterdam, 1983).
3. P.Rice-Evans, I. Chaglar and F.A.R. El Khangi, Phys.Rev.Lett. 40 716 1978.
4. M. Shimotamai, T. Iwata, T. Takahashi and M. Doyama, J.Phys.Soc.Japan, 52 694 1983.
5. J.G. Dash, Films on Solid Surfaces (Academic Press, New York, 1975).
6. P. Rice-Evans, I. Chaglar and F.A.R. El Khangi, Phys.Lett. 81A 480 1981.
7. N. Ganguli and K.S. Krishnan, Proc.Roy. Soc.(Lond), A177 168 1941.
8. K.G.Lynn and H. Lutz, Phys.Rev.B, 22 4143 1980.
9. K.G.Lynn - chapter in reference (2) 1983.

POSITRON ANNIHILATION
edited by P. C. Jain, R. M. Singru & K. P. Gopinathan

POSITRON ANNIHILATION IN THE SEMICONDUCTING ALLOY $Pb_{.93}Ge_{.07}Te$

P.C. Rice-Evans*, K.U. Rao*, M. Moussavi-Madani*, He Yusheng**, and A.D.C. Grassie***

* Department of Physics, Bedford and Royal Holloway Colleges, Regent's Park, London, NW1 4NS, England.

** Department of Physics, Tsinghua University, Peking, China.

*** Department of Physics, Sussex University, Brighton, England.

(PbGe)Te is a narrow gap chalcogenide semiconductor material that is of interest technologically because it is easily obtained in the crystalline state and because it has a structural phase transition with a transition temperature that is dependent on the carrier concentration and the germanium composition. The Doppler-broadening of the 511 keV radiation arising from positrons annihilating in the semiconductor has been studied as a function of temperature. The results failed to show any indication of the phase transition, expected to occur at about 150 K, but the role of the defect structures was signified as the temperature was varied. A detrapping phenomenon was seen in the region 77K - 300K, and a slow clustering of shallow defects commenced at 300 K, reached a maximum at 450 K, after which annealing was evident.

The chalcogenide (Pb,Ge)Te is a narrow gap semiconductor. It is of considerable interest in the physics and technology of semiconductors due to the fact that it is easily obtained in the crystalline state, and that it has a structural phase transition with a transition temperature that is dependent on carrier concentration and germanium composition. Positron annihilation measurements have already proved to be a valuable approach to this class of semiconductors (1,2) and they might be expected to yield information on phase transitions, on trapping sites and on defect concentrations.

Mokrushin et al (1) undertook lifetime and angular correlation studies on various chalcogenides (e.g. $As_{42}Te_{58}$ and $Ge_{15}Te_{85}$) in both crystalline and glassy states. They observed a single lifetime component, $\tau = 0.35 \pm .03$ ns, for all compounds and both states. The angular distributions indicated a predominance of positron annihilation with chalcogen atoms; and the authors concluded that the annihilation was essentially of positrons bound in vacancy defects.

The polycrystalline sample for the present study, made in Sussex from a melt with weighed proportions of pure (5N) elements, was $Pb_{1-x}Ge_xTe$ with x = 0.07; after melting in an rf-furnace, the sample was quenched in iced water. Figure 1 shows a resistivity measurement on the material. The anomalous peak at 150K is taken to indicate a ferroelectric phase transition,

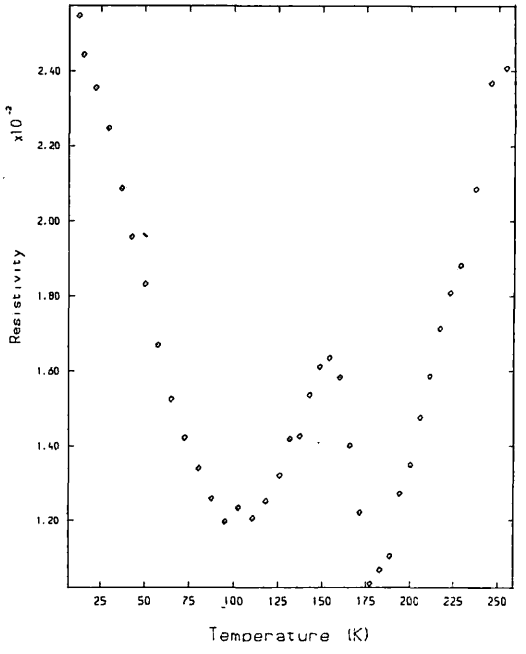

Fig.1. The resistivity of the sample of (Pb,Ge)Te plotted as a function of temperature.

from a rhombohedral to a cubic structure, associated with a decrease in the relaxation time of the free carrier. The sample had lain for several years at room temperature prior to this experiment; hence any defects initially present at 77K would be those that

could survive at 300K.

Positron annihilation in the semiconductors has been investigated with the Bedford-Doppler-broadening spectrometer. Two 1 mm. thick slices sandwiched 100 μc of $^{22}NaCl$, and the sample was subjected to temperatures ranging from 77-400K in a cryostat and 300-600K in a vacuum furnace. The germanium photon detector recorded 511 keV line shapes, with two hours for each temperature. The intrinsic resolution of the system was 1.05 keV at 514 keV. Each spectrum was accumulated in two hours.

The method relies on assessing the shape of the 511 keV photon annihilation line. Energetic positrons from the radioactive source are assumed to be rapidly thermalised to negligible velocities and the Doppler-broadening is mainly due to the electron momentum of the e^+e^- pair. The conventional line-height parameter F has been employed which is taken essentially to indicate changing proportions of annihilations with outer (lower momentum) and inner (higher momentum) electrons. F is defined as the accumulated number of counts in the central region of the 511 keV peak, normalised to the total peak area (3). The underlying background below the peak has not been subtracted. The conventional trapping model has been used to analyse the results (see (4)).

The results of a sequence of measurements, indicated alphabetically A→S, are shown in Fig.2. Initially the sample was placed in the cryostat and the temperature reduced to 77K. The runs A → C → E were recorded, after which the sample was allowed to cool again to 77K where a further measurement was made (F). We take the fact that the F-parameter is the same at both E and F to suggest that the positron trapping rate is independent of temperature for deep traps on the assumption that the traps at E and F are identical (i.e. frozen at F). The decline in F, from A → B → C (350K) appears to be a rare example of detrapping from shallow traps (5). The rise C → D → E (370-430K) is taken to indicate the clustering of shallow defects to create deeper traps, possibly vacancies (see (6)).

On transfer to the furnace, commencing at 300K the rise G → H → I occurs. This rise is surprising. It rather suggests the clustering was not complete at E, but continued to occur at a relatively slow rate over the same temperature range in the furnace.

The decline in F from I → J → K → L we take to represent the annealing of the defects.

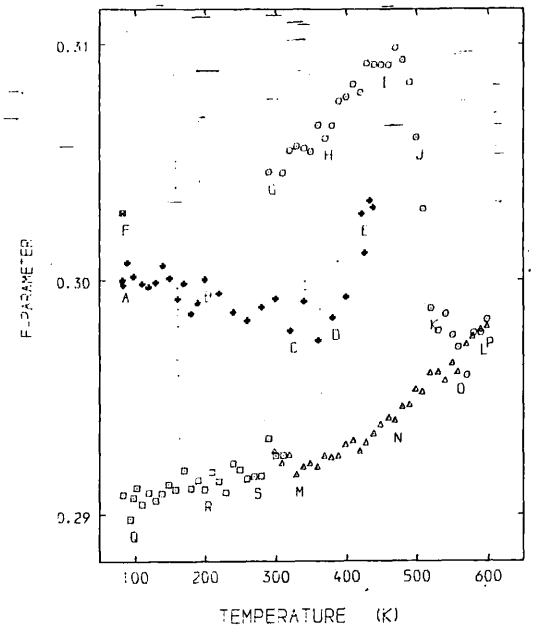

Fig.2. The positron annihilation Doppler line-height parameter F plotted as a function of temperature. The sequence of measurements is indicated alphabetically.

This is confirmed by taking the sample down to 300K and taking points MNOP which have the characteristic appearance of results for an annealed crystal.

The annealed crystal was replaced in the cryostat and the range Q → R → S studied. The absence of any significant feature at about 150K means the phase transition is not observable although the scatter of points might hide a small effect.

References

1. Mokrushin A., Prokop'ev E., Minaev V., Kisekka B., and Kupriyanova R., Sov. Phys.Semicond. 14, 751 (1980).
2. Kobrin B., Shantarovich V., Mikhailov M., Tukina E., Physica Scripta 29, 276 (1984)
3. Rice-Evans P., Chaglar I., and El Khangi F., Phil.Mag. 38, 543 (1978).
4. Brandt W. and Dupasquier A., (Ed) Positron Solid-State Physics [Fermi School, Varenna]. North Holland, Amsterdam, 1983.
5. Smedskjaer L.C., Manninen M., and Fluss M.J., J.Phys.F. 10, 2237 (1980).
6. Petersen K., chapter in ref.(4).

Acknowledgement

The authors thank the Science & Engineering Research Council for its financial support.

PHYSICAL REVIEW B VOLUME 34, NUMBER 9 1 NOVEMBER 1986

Positronium formation at physisorbed monolayer surfaces of argon, nitrogen, and oxygen on graphite

P. Rice-Evans, M. Moussavi-Madani, K. U. Rao, D. T. Britton, and B. P. Cowan
Department of Physics, Royal Holloway & Bedford New College (University of London), Egham, Surrey, England
(Received 4 June 1986)

Photon spectra arising from positrons annihilating at surfaces in exfoliated graphite have been measured over a range of temperatures. The role in the annihilation process of physisorbed equilibrium layers of argon, nitrogen, and oxygen has been observed. With argon and nitrogen the formation of orthopositronium is indicated by a three-to-two γ ray ratio; for nitrogen maximum o-Ps was found to occur on completion of one monolayer. In contrast, a Doppler analysis shows that oxygen yields parapositronium. In the case of nitrogen, the results allow the estimation of the coverage, the binding energy of the molecule to the carbon substrate, and the activation energy for the process of Ps emission from the surface traps.

MS code no. LH3136B 1986 PACS number(s): 71.60.+z, 68.45.−v

The invention of monochromatic low-energy positron beams[1–3] has been important, and early advances are being made in our knowledge of positron interactions at solid surfaces.[4] For example, the fact that positrons may be trapped in surface states has been confirmed by the observations of enhanced thermally desorbed positronium at increasing temperatures.[2,3] However, the theory of the positron surface state is still incomplete; indeed, recently reported 2γ angular correlation results[5] on an aluminium surface indicating an isotropic momentum distribution have not been consistent with either a positron bound by its "image correlation potential"[6,7] or a positronium atom weakly bound to the surface.[8] It is clear that more evidence on the behavior of positrons under a variety of surface conditions is needed to resolve the theoretical uncertainties. One such condition is the two-dimensional layer of gas condensed on a known substrate for which positron trapping sites are, in principle, capable of being well characterized. In this paper we show that positrons respond sensitively to monolayer coverages of argon, nitrogen, and oxygen on graphite.

Physisorption is governed by van der Waals forces and information on the growth, phases, and registration of thin films[9] as a function of temperature has been acquired from isotherm and calorimetry studies[10,11] neutron diffraction,[12] NMR,[13] and low-energy electron diffraction[14] methods amongst others. It remains to be seen whether annihilating positrons will provide new insights into the thermodynamics of low-dimensional systems.

Beam studies require UHV to facilitate positron transport and ensure uncontaminated surfaces. Equilibrium monolayer systems are more easily investigated by thermalizing fast positrons within a solid substrate and relying on a large surface-to-volume ratio to ensure that positrons have a high probability of annihilating at the surface. High ratios are possible in powder samples, but they are also obtained in graphite that has been exfoliated—a process that involves the formation of intercalation complexes within layer-structured crystals, and subsequent heating which explodes the layers apart, to form a uniform substrate of large area. Furthermore, surface oxidation of carbon does not arise.

To study the role of positrons at physisorbed two-dimensional structures on Grafoil,[15] we have measured the annihilation photon spectrum with a germanium detector as a function of sample temperature. A conventional sandwich containing 100 μ Ci ^{22}NaCl was prepared. Because of the low density (0.94 g cm^{-3}) of Grafoil, the source was deposited directly at the center of a stack of 12 pieces of Grafoil, each $1\times1\times0.04$ cm^3, the number needed to stop all the positrons. After preparation the sample was transferred to a cryostat capable of maintaining controlled temperatures in the range 77—460 K.

The specimen chamber was made of brass which lay in a Dewar of liquid nitrogen. The oxygen and argon gases were introduced in sufficient amounts to ensure they condensed into liquid pools at the bottom of the chamber: hence their equilibrium pressures at 77 K prevailed for all measurements; i.e., 156 and 190 Torr, respectively. The suspended Grafoil sample was maintained at a range of temperatures and the gases were physisorbed on the carbon substrate under equilibrium conditions at the prevailing pressure. In the case of nitrogen four sets of measurements were taken at different pressures.

We have analyzed the spectra in several ways. Specifically, to seek the formation of orthopositronium, which entails 3γ decays, we have recorded the contents of the whole 511-keV photopeak (A) and also of a band of channels (B) in the Compton region corresponding to an energy band at 190—200 keV. Both A and Y ($=A/B$) will be indicators of the strength of 3γ events, i.e., orthopositronium decay.[16] The Doppler broadening is illustrated with the line-height parameter F, defined as the ratio of the contents of the central 15 channels in the 511-keV photopeak to A; and in the analysis of the peaks into parabolic and Gaussian components[17] by convoluting the intrinsic resolution (r) of the system determined with the ^{85}Sr line at 514 keV and fitting the expression:

$$f(x)=a\int_{-\infty}^{+\infty}\exp[(-x'-\bar{x})^2/2\sigma_G^2]r(x-x')dx'$$

$$+b\int_{-\sigma_P\sqrt{2}}^{\sigma_P\sqrt{2}}[1-(x'-\bar{x})^2/2\sigma_P^2]r(x-x')dx' ,$$

from which the widths (σ_G,σ_P) and the relative intensity of the parabolic component (if $>2-3\%$) can be obtained. It has also been valuable on occasion to analyze instead for two Gaussian components.

Prior to the physisorption measurements we studied the positron-annihilation characteristics of Grafoil in vacuum. Figure 1, which shows the gentle trends of the parameters as a function of temperature, is presented to provide contrast with the physisorption experiments. The only comparable work on such a system has been on positron lifetimes,[18] which found essentially three components, 200, 410, and 1800 ps, interpreted as annihilations in the bulk, in surface-trapped states or quasi-Ps states bound on the surface, and as orthopositronium. We can note that in Fig. 1(b), a declining Y indicates a slow increase in the formation of positronium as the temperature rises above 200 K.

Figure 2(a) shows the results with argon in the chamber; the Y parameter shows a very distinctive minimum at 120 K indicating a maximum of orthopositronium. Figures 2(b) 2(c), 2(d), and 2(e) show the results for nitrogen at equilibrium pressures of 30, 130, 290, 790 Torr, respectively. Sharp minima are again observed, implying maximum o-Ps at 105, 119, 127, and 140 K. For both argon and nitrogen only slight variations were observed in the other parameters.

Oxygen is a different case. In Fig. 3(b) the dip in A (Ref. 19) indicates only a modest increase in o-Ps at low temperatures. However, the corresponding values of F rise sharply as the temperature declines below 140 K,

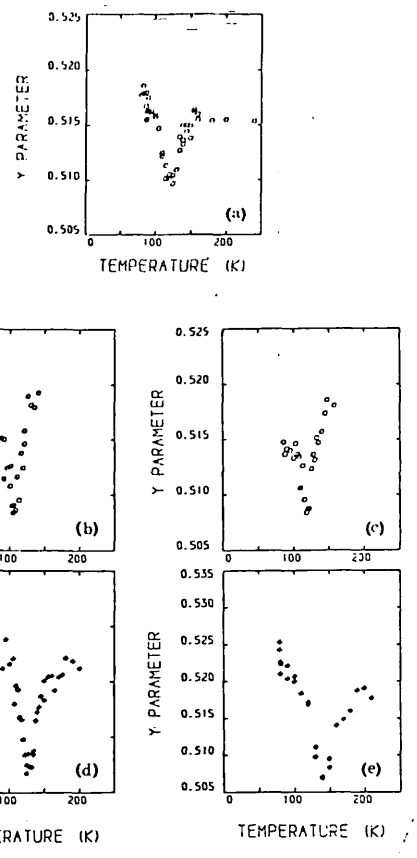

FIG. 2. Formation of orthopositronium: The Y parameter as a function of temperature for (a) Grafoil in argon at 190 Torr; and (b), (c), (d), and (e) Grafoil in nitrogen at 30, 130, 290, and 790 Torr, respectively, showing the displacement of the peak in Ps formation with pressure.

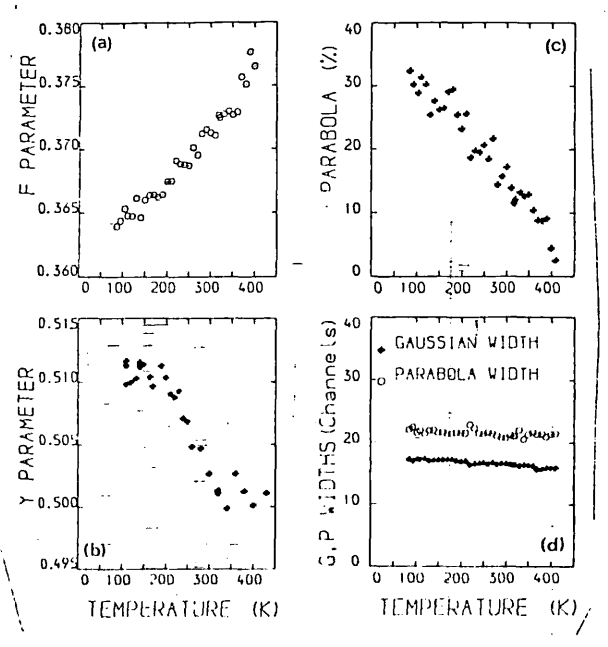

FIG. 1. Grafoil in vacuum: analysis of annihilation photon

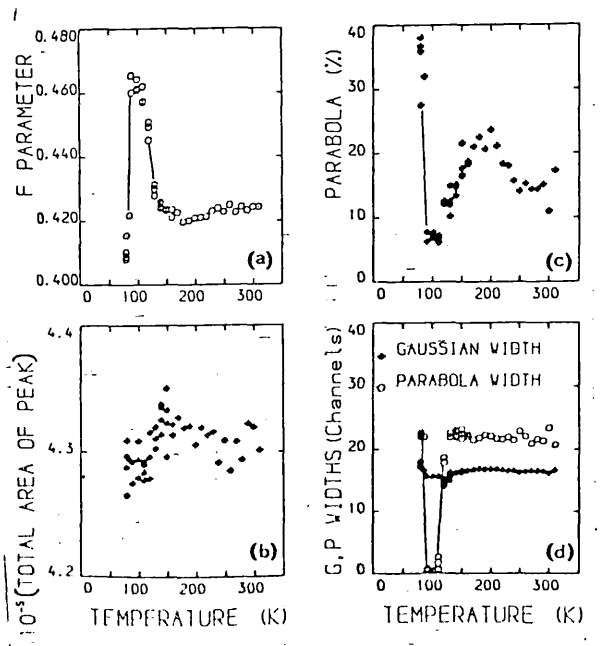

reaching a maximum at 100 K, only to drop again at 90 K. The origin of this rise is seen in Fig. 3(d), where a sharp spike of width of only about two channels appears in the Doppler spectrum. This must be parapositronium decaying via 2γ, implying a strong quenching of o-Ps by the oxygen, either in a condensed layer or in the gas. We attribute the disappearance of the 2γ spike at 90° to the suppression of Ps formation by multiple overlayers of oxygen. The 2γ spike is reminiscent of the finding[16] of a reduction in the 3γ fraction for overlayers of chemisorbed oxygen on aluminium and a spin-exchange process leading to p-Ps.

The results must be mainly associated with the condensation of gas; it is inconceivable that the temperature alone could affect so discretely the interactions of positrons or the formation of positronium. Although an extensive literature exists on monolayers, the vast majority concerns layers laid down at very low temperatures with low pressures; very little appears comparable with our measurements in a context of high equilibrium pressures.

In the case of graphite in vacuum, the decline in Y at high temperatures suggests positrons in relatively deep traps on the carbon surface emerging as Ps. Assuming Ps emission is a thermal process,[2,3] fitting Fig. 1(b) with $Y=C\exp(-E_a/kt)$ yields a value for the activation energy E_a of 0.07 eV, which is lower than the 0.23 eV proposed in Ref. 18. If $E_a=E_b+\phi_- -6.8$ eV, where $\phi_-=5.0$ eV is the electron work function for carbon,[20] then the positron binding energy E_b is 1.87 eV which is lower than for most metals.[2]

For argon the simplest explanation is that the decline in Y for temperatures 160→120 K corresponds to enhanced Ps formation as a condensed monolayer develops, and that the rise for 120→80 K coincides with further condensation inhibiting Ps creation. Nitrogen is similar. With oxygen, however, rather than a sharp maximum in Ps production, a plateau appears in the F-parameter curve [Fig. 3(a)] which disappears only at 90 K, suggesting that multilayers fill the spaces within the Grafoil and stop all Ps formation at this temperature.

For a fluid monolayer, bound to a substrate and in equilibrium with the adjacent gas, the ideal two-dimensional gas model with the Boltzmann approximation may be applied.[9] The relation between coverage (n molecules m^{-2}) and pressure (P) is $P=(nkT/\lambda)\exp(-\varepsilon_0/kT)$, if $n\lambda^2\ll 1$ and where $\lambda=h/(2\pi mkT)^{1/2}$ and ε_0 is the binding energy of the molecule to the substrate. The equation can be applied to nitrogen which is fluid above 85 K for near-monolayer coverages.[10,12]

Assuming the Y-parameter minima for nitrogen in Fig. 2 correspond to the same physical state, i.e., the same value of n_m, in each case, one can fit the four minima to the two-dimensional (2D) gas equation to yield ε_0 and n_m. The fitting was most satisfactory: the optimum value of ε_0 was 1170 K which agrees reasonably with theory, 1070 K,[21] 1159 K,[22] and for calorimetric measurements, 1177 K.[23]

The best $n_m=(7.1\pm1.2)\times10^{18}$ molecules m^{-2}, which can be compared with an estimated density for 100% coverage. Assuming the fluid is "triangularly packed," and taking a value of 4.1 Å for the N_2-N_2 nearest-neighbor distance on a structureless surface,[21] this n_m corresponds to a coverage of (103±17%). We think the alternative view that the positron traps are at a maximum at 50% coverage[24] in unlikely in view of the strong mutual repulsion of the N_2 molecules at smaller separations. We therefore conclude that positronium emission increases as the monolayer builds up, but decreases as the bilayer develops.

It is possible to apply the trapping model formula[2,3] to fit individual peaks on the right-hand slope, i.e.,

$$Y^{-1}=\frac{Y_0^{-1}-Y_\infty^{-1}Z\gamma^{-1}\exp(-E_a/kT)}{1-Z\gamma^{-1}\exp(-E_a/kT)},$$

in which allowance is made for thermal promotion of Ps emission from traps with an activation energy E_a, and where it is assumed that the rate Z is proportional to coverage n at temperatures above the minimum in Y. Fair fits were achieved; our values averaged at $E_a=0.035\pm0.015$ eV for nitrogen.

We conclude that Ps is emitted from trapped states determined by physisorbed monolayers of atoms or molecules on a regular substrate, and that the finding represents an advance in our prospects of characterizing surface traps for positrons. Furthermore, we show the positron method enables one to explore the creation of fluid monolayers at high temperatures and high pressures.

We thank the Science and Engineering Research Council and Professor Y. C. Jean for sending us a copy of his paper,[24] and M. Fardis and M. A. Husain for their advice.

[1]W. Cherry, Ph. D. thesis, Princeton University, 1958.
[2]A. P. Mills, Jr., in *Positron Solid State Physics*, edited by W. Brandt and A. Dupasquier (North-Holland, Amsterdam, 1983), p. 432 and references therein.
[3]K. G. Lynn in *Positron Solid State Physics*, Ref. 2, p. 609 and references therein.
[4]R. M. Nieminen and J. Oliva, Phys. Rev. B 22, 2226 (1980).
[5]K. G. Lynn, A. P. Mills, Jr., R. N. West, S. Berko, K. F. Canter, and L. O. Roellig, Phys. Rev. Lett. 54, 1702 (1985).
[6]C. H. Hodges and M. J. Stott, Solid State Commun. 12, 1153 (1985).
[7]R. M. Nieminen and M. Manninen, Solid State Commun. 15, 403 (1974).
[8]P. M. Platzman and N. Tzoar, in *Positron Annihilation* edited by P. C. Jain, R. M. Singru, and K. P. Gopinathan (World Scientific, Singapore, 1985), p. 941.
[9]AUTHOR'S NAME, JOURNAL TITLE *xx*, xxxx (19xx).
[10]K. D. Miner, M. H. W. Chan, and A. D. Migone, Phys. Rev. Lett. 51, 1465 (1983).
[11]J. Stolkenberg and O. E. Vilches, Phys. Rev. B 22, 2920 (1980).
[12]J. K. Kjems, L. Passell, H. Taub, J. G. Dash, and A. D. Novaco, Phys. Rev. B 13, 1446 (1976).
[13]B. P. Cowan, M. G. Richards, A. L. Thomson, and W. J. Mullin, Phys. Rev. Lett. 38, 165 (1977).
[14]M. F. Toney and S. C. Fain, Jr., Phys. Rev. B 30, 1115 (1984).

[15]Grafoil is the commercially available form of exfoliated graphite produced by the Union Carbine Corp., New York.
[16]K. G. Lynn and H. Lutz, Phys. Rev. B 22, 4143 (1980).
[17]P. Rice-Evans, I. Chaglar, and F. A. R. El Khangi, Phys. Lett. 81A, 480 (1981).
[18]Y. C. JEan, K. Venkateswaran, E. Parsai, and K. L. Chang, Appl. Phys. A 35, 169 (1984).
[19]For technical reasons B was not recorded, but A and Y behave similarly.
[20]*Handbook of Chemistry and Physics*, 63rd ed. (CRC, Boca Raton, Florida, 1982–83).
[21]W. A. Steele, J. Phys. (Paris) Colloq. 38, C4-xx (1977).
[22]L. W. Bruch, J. Chem. Phys. 79, 3148 (1983).
[23]J. Rouquerol, value reported in Ref. 21.
[24]C. Yu, N. Zhou, and Y. C. Jean, in *Positron Annihilation* edited by P. C. Jain, R. M. Singru, and K. P. Gopinathan (World Scientific, Singapore, 1985), p. 669.

REFERENCES

Anderson C.D; Phys. Rev. Vol.43 P491 (1933).

Badoux Von F, Heinrich F and Kallmeyer G; Helvetica Phys. Acta. Vol.40 P815 (1967).

Baller R and Sigraldosen H; Phys. state Sol. (B) Vol.92 P143 (1979).

Baskova K.A, Dzhelepov B.S and Komissaroua Z.A; Sovite Phys. JETP Vol.13 No.4 P703 (1961).

Bennett A.J, Mc´Carroll B and Messmer P; Phys. Rev. B Vol.3 No.4 P1397 (1971).

Berestetskii V.B, Lifshitz E.M and Pitaevskii L.P; (Relativistic Quantum Theory) (1971) Pergamon, Oxford).

Bergersen B and Taylor D.W; Can. J. Phys Vol.52 P1594 (1974).

Beringer R and Montgomery C.G; Phys. Rev. Vol.16 P222 (1942)

Berko S and Plaskett J.S; Phys. Rev. Vol.112 P1877 (1958).

Berko S and Mader J; Appl. Phys. Vol.5 P287 (1975).

Berry A; PhD Thesis Bedfrod College (University of london) (1982).

Bourdon A, Marti C and Thorel P; Phys. Rev. Lett. Vol.35 No.8 P544 (1975).

Brandt W; "Positron Solid-State Physics" (1983).

Brandt W and Orenland M; Phys. Lett. A Vol.57 NO.4 P387 (1976).

Bruch L.W; J. Chem. Phys. Vol.79 No.6 P3148 (1983).

Burgers W.G and Groen L.J; Discussion Faraday Soc. Vol.23 P138 (1957).

Bush G.A and Kern; Phys. Solid State Vol.11 P1 (1970).

Campbell J.L, Schulte C.W and Jackman T.E; J. Phys. F: Metal Phys. Vol.7 P1985 (1977).

Canter K.F, Mills Jr A.P and Berko S; phys. Rev. Lett. Vol.33 P7 (1974).

Canter K.F and Roellig L.O; phys. Rev. A Vol.12 No.2 P386 (1975).

Canter K.F, Mcnutt J.D and Roellig L.O; phys. Rev. A
Vol.12 P375 (1974).

Chaglar I; PhD Thesis Bedfrod College (University of london) (1978).

Chaglar I, Rice-Evans P, El Khangie E.A.R and Berry A;
Neuclear Instr. and Met. Vol.187 P581 (1981).

Cherry W; PhD Thesis Dessertation princeton university (1985).

Chu S, Marray C.A and Mills Jr A.P Phys. Rev. B Vol.23 P2060 (1981).

Cohen and Van Eyk Z; Phys. Chem. Vol.30 P601 (1899).

Coleman C.F; Appl. Phys. Vol.19 P87 (1979).

Connors D.S and Crisp V.H.C and West R.N;;Phys. Lett. A
Vol.33 P180 (1971).

Connors D.S and West R.N; Phys. Lett. A Vol.30 P24 (1969).

Costello D.E, Groce D.E, Herring D.F and Mc´Gowan J.W; Phys. Rev. B
Vol.5 P1433 (1972).

Coulson C.A "Valence" published by OUP (1961).

Dash J.G; Sci. Ame. Vol.228 No.5 P30 (1973)

Dash J.G; Films adsorption on solid (1974).

Dash J.G; Phys. Today/December (1985).

De Benedetti S, Covan C.E, Konneker W.R and Primakoff H; Phys. Rev.
Vol.77 P205 (1950).

De Blonde G, Chuang S.Y, Hogg B.G, Kerr D.P and Miller C.M;
Can. J. Phys. Vol.50 P1619 (1972).

De Doussis S.P, Charalambous Stef and Chardlas; Phys. Lett. A
Vol.62 No.5 P359 (1977).

Diehl R.D, Toney M.F and Fain Jr F.C; Phys. Rev. Lett. Vol.48
No.3 P177 (1982).

Dirac P A M; Proc. Camb. Phil. Sco. Vol.26 P361 (1930).

Doyama Masao Prog. 5th Inf. Conf. (Positron electron
annihilation) (Japon 1979).

Fuselier C.R, Gillis N.S and Raich J.C Solid State Commu. Vol.25 P747 (1978).

Gainotti A, Germognoli E, Schianchi G and Zecchina L;Phys. Lett. Vol.13 P9 (1964).

Gol´danskii V.I and Prokopev E.P; Sovit. Phys. Solid State Vol.6 P264 (1965).

Groce D.E, Costello P.G, Griffith T.C and Herring D.F; Bull Am. Phys. Soc. Vol.13 P1397 (1968).

Hautojoarvi "Positron in Solids" P17 Spinger-Verlag Berlin Heidelberg New York (1979).

Hautojoarvi P; Soild State Commun. Vol.11 P1049 (1972)

Hautojarvi P and Jauho P; Acta Polytech. Scand. Phys. Incl. Nucleon Ser. Vol.98 P1 (1973).

Hautojarvi P, Judin T, Vehaness A, Yli-Kauppila J, Johansson, J, Verdone J and Moser P; Solid State Commun. Vol.29 P855 (1979).

Hodges C.H and Trinkaus H; Solid State Commun. Vol.18 P857 (1976).

Hodges C.H; Phys. Rev. Lett. Vol.25 P284 (1970).

Hodges C.H and Stott M J; Phys. Rev. B Vol.7 P73 (1973).

Hotz H.P, Mathiesen J.M and Harley J.P; Phys. Rev. Vol.170 P351 (1968).

Jackman T.E, Lichtenberger P.C, and Schulte C.W; Appl. Phys. Vol.5 P259 (1974).

Jackman T.E, Schulte C.W, Campbell J.L, Lichtenberger P.C, Mackenzie I.K and Wormald M.R; J. Phys. F: Metal Phys. Vol.4 P(11) (1974).

Jean Y.C, Venkateswaran K, Parsai E and Cheng K.L; Appl. Phys. A Vol.35 P169 (1984)

Jean Y.C, Yu C and Zhou D.M; Phys. Rev. B vol.32 No.7 P4313 (1985)

Itoh Fumitake, Matsuura M, Suzuki K, Miyata Y and Noguchi S; J. Phys. Soc. Japon Vol.45 No.5 P1622 (1978).

Kerr D.D; Can. J. Phys. Vol.52 P935 (1974).

Khangi F.A; PhD Thesis Bedfrod College (University of london) (1980).

KirKegaord P and Eldrip M; computer Phys. commun. Vol.3
P240 (1972) and Vol.7 P401 (1974).

Kjems J.K, Passel L, Taub H, Dash J.G and Novaco A.D; Phys.
Rev. B Voll.3 No.4 P1446 (1976).

Kusmiss J; PhD Thesis Dissertation, University of North Carolina,
Chaple Hill (1965).

Larher Y; J. Chem. Phys. Vol.68 No,5 P2257 (1978).

Lichtenberger P.C, Schlte C.w and Mac´Kenzie I.K Appl.
Phys. Vol.6 P305 (1975).

Leung C.H, Mc´Mullen T and Stott M.J J. Phys. F: Vol.6
Metal Phys. P1063 (1976).

Leventhal M; Astrophys. J Vol.183 P(L147) (1973).

Lohberg V.K and Presche P; Z. Metallkde Vol.59 P74 (1968).

Lynn K.G and Lutz H; Phys. Rev. Vol.22 No.9 P4143 (1980).

Lynn K.G; Phys. Rev. Lett. Vol.43 P391 (1979).

Lynn K.G, Mills Jr A.P, West R.N, Berko S, Canter K.F and Roelling
L.O; Phys. Rev. Lett. Vol.54 No.15 P1702 (1985).

Mackenzie I.K; Phys. Lett. A Vol.30 P115 (1969).

Mackenzie I.K, Eady J.A and Gingerich R.R; Phys. Lett. A
Vol.33 P729 (1970).

Mackenzie I.K and Fabian J; Can. J. Phys. Vol.58 P1635 (1980).

Madansky L and Rosetti F; phys. Rev. Vol.79 p397 (1950).

Madey J.M.J; Phys. Rev. Lett. Vol.22 P784 (1969).

Max R and Chirstoffer B; Phys. Rev. Lett. Vol.51 No.9 P790 (1983).

Mc´Kee B.T.A, Stewart A.T, Stott M,J and Triftshouser W; SEcond
Int. Conf. on positron annihilation KIngston Ontorio P49 (19).

Mc´Kee B.T.A, Triftshauser W and Stewart A.T;Phy. Rev. Lett. Vol.28 P358 (1972).

Mc´Tague J.P and Nielsen M; Phys Rev. Lett. Vol.37 No.10 P596 (1976).

Mills Jr A.P; phys. Rev. Lett. Vol.41 P1828 (1978b).

Mills Jr A.P; Solid State Commum. Vol.31 P623 (1979).

Mills Jr A.P; "Positron solid state physics" (1983)

Mills Jr A.P; phys. Rev. Lett. Vol.46 P717 (1981).

Mills Jr A.P,Pfeiffer L, and Platzman P.M; phys. Rev. Lett. Vol.51 No.12 P1085 (1983b).

Mills Jr A.P,Platzman P.M and Brown B.L; phys. Rev. Lett. Vol.41 P1076 (1978a).

Mills Jr A.P and Welech D.O; Phys. Rev. B Vol.22 P99 (1980).

Miner K.D, Chan M.H and Migone A.D; Phys. Rev. Lett. Vol.51 No.16 P1464 (1983).

Mouritsen O.G and Berlinsky A.J; Phys Rev. Lett. Vol.48 No.3 P181 (1982).

Muirhead H; "The Physics of Elementary Particles" (Pergamon Press, Oxford 1965)

Nieminen R.M (positron solid state physics); P392 (1983).

Nikoloev I.N, Marin V.P, Panjushkin V.N and Pavliyukov L.S; Soviet. Phys. Solid State Vol.14 No.8 P143 (1973).

Novaco A.D and Mc´Tague J.P; Phys. Rev. B Vol.20 No.6 P2469 (1979).

Ore A and Powell J.L; Phys Rev Vol75 p1695 (1949).

Platzman P.M and Tzoar N; Int. conf. of "Positron annihilation" India, Dlhie (1985).

Pan R.P, Etters R.D and Kobashi K; J. Chem. Phys. Vol.77 No.2 P1035 (1982).

Panyashkin V.N; Soviet Phys. Solid State Vol.10 No.6 P1515 (1968).

Patrykiejew A, and Jaroniec M; Thin Solid Films Vol.70 p363 (1980).

Patrykiejew A, Jaroniec M and Marczewski A.W; Chemica, Scripta Vol.22 P136 (1983).

Puff W and Mascher P; J. Phys. F: Metal Phys. Vol.14 P(L231) (1984).

Puff W, Mascher P, Kindl P, and Sormann H; Appl. Phys. A Vol.32 P183 (1983).

Rice-Evans P, Chaglar I, El Khangi A.R F; Phys. Lett. A Vol.64 P450 (1978a).

Rice-Evans P, Chaglar I and El Khangi A.R F; Phil. Maga. A Vol.38 No.5 P543 (1978).

Rice-Evans P, Chaglar I, El Khangi A.R F; Phys. Rev. Lett. A Vol.40 P716 (1978b).

Rice-Evans P, Chaglar I and El Khangi A.R F; (positron annihilation) Proc. 5th Intr. Conf. (Japon 1979).

Rice-Evans P, Moussavi-Madani M and Ruo O; Phil. Maga. A Vol.38 No.5 P543. (1985).

Rouquerol J, Partyka S and Rouquerol F; J. Chem.Soc. Faraday Trans. I Vol.73 P306 (1976).

Schultz P.J, Lynn K.G, Mackenzie J.K, Jean U.C and Snead C.L; Phys. Rev. Lett. Vol.44 P1629 (1980).

Seeger A; J. Phys. F: metal Phys. Vol.3 P248 (1973).

Seeger A; Appl. Phys. Vol.7 P85 (1975).

Seeger A; Phys. Lett. A Vol.40 P135 (1972).

Segers D, Dorikens-Vanpralt L and Dorikens M Phys. state Sol. (A) Vol.59 P543 (1980).

Seguin J.L, Suzanne J, Bienfaint M, Dash J.G and Venables J.A; Phys. Rev. Lett. Vol.51 No.2 P122 (1982).

Shah N.C and Catz A.L; Phys. Rev. B Vol.30 No.5 P2498 (1984).

Shinotomai M, Takahashi T, Fukushima H and Douama M; J. Phys. Soc. Japon Vol.52 P694 (1983).

Siegal R.W; Mater. Sci. Vol.10 P393 (1980).

Sieng Wei M and Bruch L.W; J. Chem. Phys. Vol.75 No.8 P4130 (1981).

Sokolowski S; J. Chem. Soc. Faraday Trans. II Vol.78 P255 (1982).

Steele W.A; Journal De Physioue (paris) Vol.38 No.10 P(C4-61) (1978).

Stephens P.W, Heiney P.A and Birgereau R.J; Phys. Rev. Lett. Vol.45 No.24 P1959 (1980).

Sumi A and Toyozaway J; J. Phys. Soc. Japon Vol.35 P137 (1973).

Tague J.P and Nielson M; Phys. Rev. Lett. Vol.37 No.10 p596 (1976).

Tao S.J; Phys. Rev. A Vol.1 No.4 P1257 (1969)

Toney F.T and Fain Jr S.C; Phys. Rev. B Vol.30 No.2 P1115 (1984).

Vanderbit D and Joannopoules J.D; (paper II) Phys. Rev. B Vol.27 No.10 P6302 (1982).

Varlashkin P.G; Phys. Rev. A Vol.3 No.4 P1230 (1971).

Waite T.R; Phys. Rev. Vol.107 P463 (1975).

Wallace P.R; Solid State Phys. Vol.10 P1 (1960).

West R.N; Positron Study Of Condensed Matter (1973).

Yang C.N; Phys. Rev. Vol.77 P242 (1950).